Artificial Tissue Binding Models: Development and Comparative Evaluation of High -Throughput Lipophilicity Assays and their Use for PET Tracer Optimization

INAUGURALDISSERTATION

zur

Erlangung der Würde eines Doktors der Philosophie

vorgelegt der

Philosophisch-Naturwissenschaftlichen Fakultät

der Universität Basel

von

Frauke Assmus

aus Dessau, Deutschland

Basel 2015

Genehmigt von der Philosophisch-Naturwissenschaftlichen Fakultät auf Antrag von

Prof. Dr. Anna Seelig
Prof. Dr. Beat Ernst

Prof. Dr. Jörg Schibler, Dekan

Basel, den 26.Februar 2013

Abstract

The purpose of this thesis was to increase the efficiency of the Positron Emission Tomography (PET) tracer development process. Since many neuroimaging agents fail due to undesirably high non-specific binding (NSB) to brain tissue, we aimed at estimating the extent of NSB as early as possible, preferably before radioactive labeling and extensive animal testing. To this purpose we have developed, optimized and evaluated several *in vitro* assays with respect to their ability to predict brain tissue binding and, in particular, NSB in PET. A major goal of this thesis was the implementation of a miniaturized assay for the prediction of NSB in order to meet the demand for maximal efficiency, i.e. high throughput and minimal consumption of reagents, samples and animal tissue. Since octanol/water distribution coefficients ($\log D_{oct}$) are routinely measured in almost every research organization, we investigated whether $\log D_{oct}$ is also useful for the prediction of brain tissue binding. In this context, we have developed a filter-based $\log D_{oct}$ assay (Carrier Mediated Distribution System=CAMDIS) to overcome the drawbacks of the traditional shake flask technique, i.e. tedious phase separation and high consumption of reagents. Strategies have been developed to correct for drug adsorption to the assay construct in order to warrant both high throughput and high quality of the data. Even though the CAMDIS $\log D_{oct}$ values were in excellent agreement with literature shake flask data, our results indicated that octanol is only a poor surrogate for tissue binding, as shown by the poor correlation between $\log D_{oct}$ and the unbound fraction of drug in brain ($f_{u,brain}$) available through equilibrium dialysis. The latter is the current industrial standard method for the measurement of tissue binding, however the technique is hampered by high consumption of animal tissue and low throughput. Apart from $\log D_{oct}$, another, more complex membrane surrogate system, namely the Parallel Artificial Membrane Permeation Assay (PAMPA), has found entry into many laboratories. We investigated whether the fraction of drug retained by the PAMPA barrier proves useful for the prediction of tissue binding. Since the default PAMPA setup at Roche was inappropriate in this respect, we optimized PAMPA towards better predictive power and compatibility with mass spectrometric analysis. Provided that PAMPA was conducted under optimized conditions (pH 7.4, brain polar lipids, without solubilizers), the membrane fraction was in much better agreement with tissue binding as compared to $\log D_{oct}$. Nevertheless, the predictive power was still unsatisfactory reflecting the fact that reverse micelles rather than

lipid bilayers constitute the permeation barrier as revealed by NMR experiments. Since neither CAMDIS nor PAMPA yielded sufficiently reliable NSB - estimates, we developed a miniaturized label-free Lipid Membrane Binding Assay (LIMBA) allowing for the measurement of brain tissue/water distribution coefficients at minimal consumption of brain homogenate. LIMBA was highly predictive for the binding of drugs and molecular imaging probes to brain tissue and therefore provides a viable alternative to the equilibrium dialysis technique. LIMBA thus allows for more efficient optimization of potential PET tracers and should reduce the attrition rate in the late and particularly expensive stages in the PET tracer development process.

Keywords: Tissue distribution, Non-specific binding, Equilibrium dialysis, PET tracer, Octanol/water distribution coefficient

Table of Contents

List of Abbreviations

AD	Alzheimer's Disease
ACN	Acetonitrile
A_D	Cross sectional area
ADME	Absorption, Distributions, Metabolism, Elimination
B_{avail}	Receptor density which is available for drug binding
BBB	Blood-brain barrier
$B_{\max}$	Total receptor density
BLM	Black lipid membrane
BP	Binding potential
BPL	Brain polar lipids
BTL	Brain total lipids
C	Concentration
C_{ND}	Concentration of free plus non-specifically bound tracer
C_S	Concentration of tracer bound specifically to receptors
C_p	Concentration of unmetabolized tracer in plasma
CAMDIS	Carrier Mediated Distribution System
CE	Capillary electrophoresis
CHAPS	Na· 3-[(3-Cholamidopropyl) dimethylammonio]-1-propanesulfonate
CPI	Critical Path Initiative
CT	Computer tomography
CTAB	Cetyltrimethylammonium bromide
D2 receptor	Dopamine D2 receptor
DMPK	Drug Metabolism and Pharmacokinetics
DMSO	Dimethyl sulfoxide
ESI	Electrospray ionization source
FaSSIF	Simulated gastrointestinal fluid in the fasted state
FDA	Food and Drug Administration
FDG	2-(F-18)Fluoro-2-Deoxy-D-Glucose
FeSSIF	Simulated gastrointestinal fluid in the fed state

f_{ND}	Free fraction of drug in brain (PET nomenclature)
f_p	Free fraction of drug in plasma (PET nomenclature)
$f_{u,brain}$	Unbound fraction of drug in brain
GCA	Glycocholic acid
HP - β - CD	Hydroxypropyl-β-cyclodextrine
HPLC	High performance liquid chromatography
IND	Investigational new drug
K_1, k_2	Rate constants governing the transfer of a PET tracer from plasma into tissue and vice versa
k_3, k_4	Rate constants governing receptor association and receptor dissociation of a PET tracer
Kp_u	Tissue/plasma water partition coefficient
LIMBA	Lipid Membrane Binding Assay
$LogBB$	Brain/blood distribution coefficient
$LogD_{brain}$	Brain tissue/water distribution coefficient
$LogD_{oct}$	Octanol/water distribution coefficient
$LogD_{PAMPA}$	PAMPA-lipid/water distribution coefficient
MRI	Magnetic resonance imaging
ms	Manuscript
MS	Mass spectrometry
NCE	New chemical entity
NMP	N-methyl-2-pyrrolidone
NMR	Nuclear magnetic resonance
NSB	Non-specific binding
PAMPA	Parallel Artificial Membrane Permeability Assay
PBPK modeling	Physiologically based pharmacokinetic modeling
P_e	Effective permeability
PE	Phosphatidylethanolamine
PET	Positron Emission Tomography
PFGNMR	Pulsed field gradient NMR
PG	Propylene glycol
P-gp	P-glycoprotein

PK/PD	Pharmacodynamic/pharmacokinetic
pK_a	Negative logarithm of the acid dissociation constant
POPC	1-Palmitoyl-2-oleoyl-phosphatidylcholine
PTFE	Polytetrafluorethylene = Teflon
PVDF	Polyvinylidendifluorid
QSAR	Quantitative structure/activity relationship
R&D	Research and Development
R_{REF}	Reference region in autoradiography or PET
RO	Receptor occupancy
ROI	Region of interest in autoradiography or PET
RP	Reversed phase
SDS	Sodium dodecyl sulfate
TAC	Time-activity curve
TB	Total binding
TC	Taurocholic acid
TCM	Tissue compartment model
V_{ND}	Volume of distribution in the non-displaceable compartment
V_S	Volume of distribution (specific binding at the receptor site)
V_{aq}, V_{oct}	Volume of the aqueous phase and volume of the octanol phase
$V_T(ROI), V_{ND}(R_{REF})$	Total volume of distribution as in the region of interest and in the reference region
$1/K_D$	Receptor affinity
18F, 11C, 15O, 13N	Fluorine-18, cabone-11, oxygen-15, nitrogen-13
5-HT receptor	Serotonin receptor

1 Introduction

1.1 The Traditional Drug Discovery Process

Advances in genomics and systems biology [1] in addition to the evolutions in automation and information technology had been expected to result in a vast number of potential drug candidates that could be used in clinics for the treatment of human disease [2]. However, for the past two decades the pharmaceutical research and development is facing a crisis in productivity. The number of new chemical entities (NCE) approved by the FDA has neither met expectations nor the demand for potent and selective drug compounds acting at novel targets [3].

The traditional process in drug discovery is a lengthy enterprise and traditionally proceeds linearly across the preclinical milestones and the clinical phases I-IV. Structural optimization of hit series is heavily based on *in vitro* models for the selection of promising lead candidates which are subsequently tested in animals prior to human subjects [4]. It takes on average 12-15 years to bring a drug to the market and the cost for the process has reached the order of US$2 billion (2010 [5]). Only 1-2 compounds out of ten thousand enter the clinical phase and the success rate of those which have reached entry into human is only approximately 11% [6]. The vast majority of attrition occurs in the full development clinical phases (IIb and III) and it goes without saying that failing at this stage is costly. The major reasons for attrition, i.e. lack of efficacy and safety (each contributing to 30 % of the failures) [6], are even more prominent when novel targets are concerned for which biological mechanisms might be insufficiently explored [7, 8] and therapeutical needs are unmet [1].

The development of drug compounds for the treatment of human mental disorders is exceptionally challenging and the chance that clinical candidates reach the market is as low as 8 % [6]. Neuropsychiatric diseases such as depression, bipolar disorder and schizophrenia are far from being entirely understood and animal models are at best approximations thereof [9]. In addition, drug molecules targeting the central nervous system (CNS) have to be delivered across the blood brain barrier (BBB) which essentially acts as a neuroprotective barrier and hinders large or hydrophilic compounds from entering the brain [10]. As a consequence, considerable discrepancies between plasma and biophase concentrations may arise and pharmacokinetic - pharmacodynamic (PK/PD) modeling approaches based on plasma pharmacokinetics likely become invalid [11].

1.2 The FDA's Critical Path Initiative

The limitations of developing drugs (particularly CNS-active drugs) along the milestones in the traditional discovery and development process are apparent and the realization has grown that the drug development process needs to be modernized in order to translate the advances of basic research into new marketed therapies. In 2004, the U.S. Food and Drug Administration (FDA) launched a Critical Path Initiative (CPI) diagnosing and addressing the reasons for the productivity decline in pharmaceutical research and development (R&D) [12]. The landmark 2004 report drew the conclusion that the technologies applied for the prediction of the clinical performance of promising drug candidates have not kept pace with the development of basic scientific innovation. While cutting edge technologies have found entry in drug discovery and lead optimization, pre-clinical and clinical trials in animals and humans appear to be based on trial and error rather than on evidenced-based research. A better product development toolkit is urgently needed to "get fundamentally better answers about how the safety and effectiveness of new products can be demonstrated, in faster time frames, with more certainty, and at lower costs" [12]. i) The development and utilization of biomarkers, i.e. surrogate markers for disease progression, drug effectiveness and drug safety and ii) the streamlining of clinical trials by using biomarkers have been uncovered as the most important areas for improving medical product development [13, 14].

1.3 Molecular Imaging with PET

Modernizing the critical path according to the abovementioned strategies requires innovative technologies to support the claimed objectives. The FDA has stressed the great potential of imaging technologies, especially molecular imaging tools, in contributing to new biomarkers (imaging biomarkers) and providing valuable insights into the distribution, binding and pharmacological effect of new chemical entities (NCE) [13, 14]. However, it has also been recognized that the application of imaging tools within the drug development process requires efforts invested in developing them specifically for this purpose.

The basic concept of molecular imaging may be summarized as the visualization, characterization and quantification of biological processes in living organisms at the cellular or molecular level [15, 16]. In contrast to primarily morphological imaging methods (e.g. magnetic resonance imaging, MRI), the primarily molecular imaging methods permit to study disease models and the effect of drug treatment prior to the manifestation of anatomical

changes (e.g. tumor growth) [15]. Owing to its high sensitivity[1][17] and the large number of compounds to which the technique is applicable [18], particularly positron emission tomography (PET) holds much promise to bridge the gap between preclinical and clinical research, especially in the field of neurodegenerative and neuropsychiatric disorders [19]. The principles and applications of PET in addition to the requirements posed upon the molecular imaging probes are summarized in the following.

1.3.1 Principles of PET

PET is a non-invasive technique that provides three-dimensional images of physiological functions (e.g. cerebral blood flow, brain metabolism) and molecular targets (receptors, transporters or proteins) in intact living subjects (animals, humans). The technique exploits molecular imaging probes which are labeled with short-living positron - emitting radionuclides such as fluorine-18 (half-life, $t_{1/2}$ = 110 min), carbon-11 ($t_{1/2}$ = 20 min), nitrogen-13 ($t_{1/2}$ = 10 min) and oxygen-15 ($t_{1/2}$ = 2 min) [18]. The radionuclides are produced by nuclear reactions (bombardment of stable isotopes with protons or deuterons) within a cyclotron before they are incorporated in the molecules of interest by radiosynthesis [20, 21]. Since many molecules of interest (drugs; biomolecules, e.g water and glucose) contain e.g. carbon, labeling is possible without considerably changing the biological activity of the probes (fluorine-18 may replace hydrogen in biomolecules) [18]. Tracer concentrations (picomolar amounts) of the radioligand are injected intravenously into the test organism in question and the temporal and spatial distribution of the radioligand is monitored by means of a PET camera (for details see Fig. 1).

[1] PET is 1-2 orders of magnitude more sensitive as compared to SPECT

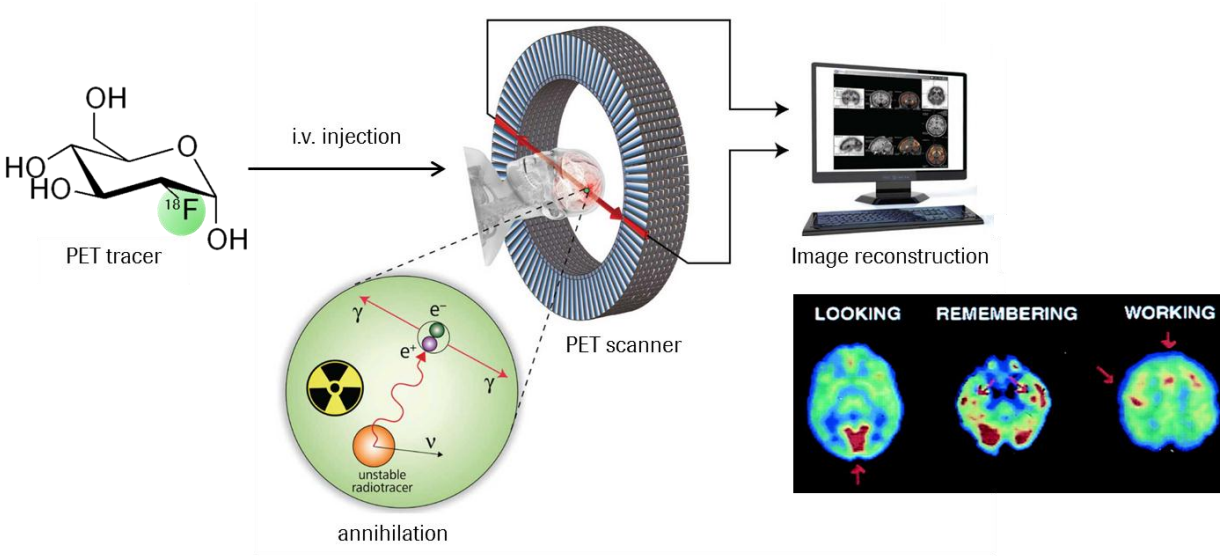

Figure 1 Schematic representation of the principles of PET. A biologically active molecule labeled with a positron-emitting radionuclide (e.g. 2-(F-18) Fluoro-2-Deoxy-D-Glucose) is injected into a patient. The radionuclide decays by emission of a positron which collides with a nearby electron in the tissue. Positrons and electrons are matter and antimatter, and their collision produces two gamma rays (511 keV) that move in opposite direction throughout the body. These are detected by the PET camera comprised of scintillator units arranged in circuit around the test organism. Only photons which arrive simultaneously (in coincidence) at two detectors located opposite to each other are transformed into the image finally observed. The image reflects a three-dimensional map of the tracer distribution in a time and location-resolved manner. PET images are shown at the example of glucose metabolism to map a human brain's response in performing different tasks (highest metabolic rates are in red); adapted from [22].

The PET scanner yields dynamic images of the tracer distribution (Fig. 2A) which need to be translated into truly quantitative biological outcome measures such as receptor density, ligand affinity, or the rate of transport through a molecular pathway [23]. Since the PET scanner cannot differentiate between the chemical forms or environments in which the radioactivity resides [24], the time activity curve (TAC) in a region of interest (ROI, e.g. the striatum, Fig. 2B) represents a composite of free and bound, parent and metabolized radioligand in plasma and in tissue.

In order to isolate the signal emerging from the specific binding to the target site, a mathematical model is required which relates the radioactivity delivered by plasma (plasma input function) to the radioactivity accumulated at the target site in tissue (tissue response function). To this pursuit, the principles of compartmental modeling are frequently applied which characterize a radioligand's fate in terms of rate constants governing the transfer between predefined compartments [25, 26]. Target binding and brain uptake, for example,

enter the model as a combination of rate constants which are to be estimated by fitting the model to the observed PET data.

In many cases, a three-compartment model (Fig. 2C) is appropriate for describing the kinetics of radiotracer delivery from plasma (compartment 1) into the brain, where the tracer either binds non-specifically to tissue environment (brain compartment 1) or specifically to the target (brain compartment 2) [26]. However, the parameterization of the plasma input function requires continuous blood sampling including tedious HPLC-based determination of parent and metabolized tracer and the quantification of the unbound fraction in plasma. An alternative approach, which avoids blood sampling, relies on using a reference tissue essentially devoid of receptors as input function for the TAC observed in the ROI. In simple terms, the specific binding to the target corresponds to the difference between the radioactivity in the receptor-rich region (ROI) and the receptor - free reference region. The higher the specific binding and the lower the non-specific binding (NSB), the higher the sensitivity of PET to monitor radioligand interactions with the target site. Since the number of available binding sites (B_{avail}) and a radioligand's affinity to that binding site ($1/K_D$) cannot be inferred separately, a PET scan seeks to derive the binding potential, (BP), corresponding to the product of receptor density and affinity[2] [27]. Changes in the binding potential can be interpreted in terms of disease progression or drug-target interaction. For example, the reduction of the binding potential in the striatum may be related to the degeneration of dopaminergic neurons in Morbus Parkinson or to the percentage of dopamine receptors occupied after treatment with dopamine agonists [28].

[2] If the reference tissue model is used for data analysis, the unbound fraction of tracer in the brain, f_{ND}, is not accessible for quantification. Therefore, the binding capacity is expressed as $BP_{ND} = f_{ND} \cdot B_{\max} / K_D$.

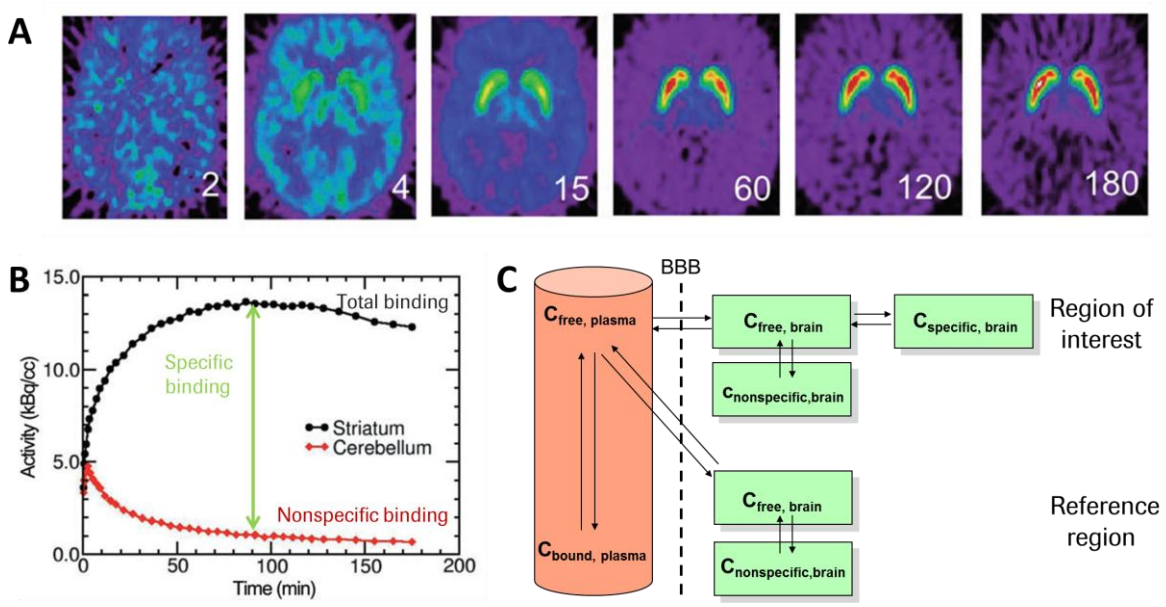

Figure 2 The time course of the uptake, binding and washout of [^{18}F]-fallypride (dopamine D2/3 receptor antagonist) in the brain of a healthy human subject. **A:** Examples of images from the 180 min scan and **B:** the associated time activity curves in the region of interest (striatum) rich in dopamine receptors and in the reference region (cerebellum) devoid of dopamine receptors (approximation), adapted from [29]. **C:** Three-compartment model (two-tissue compartment model) taking into account the tracer concentrations in plasma (free and non-specifically bound in plasma), the passage across the blood-brain barrier, the distribution into the non-displaceable compartment (free and non-specifically bound tracer in brain) and the binding to the target site (specifically bound). Free and non-specifically bound tracer concentrations are lumped together into one compartment, based on the assumption that equilibration between the two states is rapid as compared to receptor binding. The free fraction in brain, f_{ND}, denotes the fraction of tracer in the non-displaceable compartment in the unbound state. It is assumed that only the unbound concentration is available for receptor binding and similarly that only the free fraction in plasma (f_p) can cross the blood brain barrier. The rate constants K_1, k_2, k_3 and k_4 describe the transport into and out of the brain and the association and dissociation at the target site, respectively. In the reference region, a two-compartment model is sufficient due to the assumed absence of dopamine receptors.

1.3.2 The Value of PET in the Drug Discovery and Development Process

As outlined above, PET is a powerful non-invasive tool, able to provide dynamic, quantifiable measures of e.g. brain uptake and drug-target interaction in healthy and diseased animals and humans [28]. Due to the high sensitivity of PET, picomolar concentrations of a radioligand can be determined with high accuracy and without disturbing the biological process of interest. The outcome measures of PET are of relevance in all preclinical and clinical stages (Fig. 3) including the following areas of application [30,31]: i) Pharmacokinetic studies with the labeled drug, to confirm that the drug reaches the target. ii)

RO studies with the cold drug and a target-specific radioligand, to answer the questions whether the drug binds to the target and how much receptors are occupied. iii) Proof-of-mechanism studies with imaging biomarkers reflecting changes in metabolism (e.g. glucose consumption), physiology (e.g. blood perfusion) and/or biology (receptor density), to answer the question whether the application of the drug is related to a pharmacodynamic response. iv). Proof-of-concept studies with imaging biomarkers for pathophysiology, to answer the question whether the drug has a clinical benefit. The results from clinical studies on pathophysiology and response after treatment can also be back-translated to characterize the target expression in different species [8] and to assess the scope, limitations and possible refinements of preclinical animal models [32]. This advocates PET as a valuable translational tool to bridge the gap between pre-clinical research and clinical application [8].

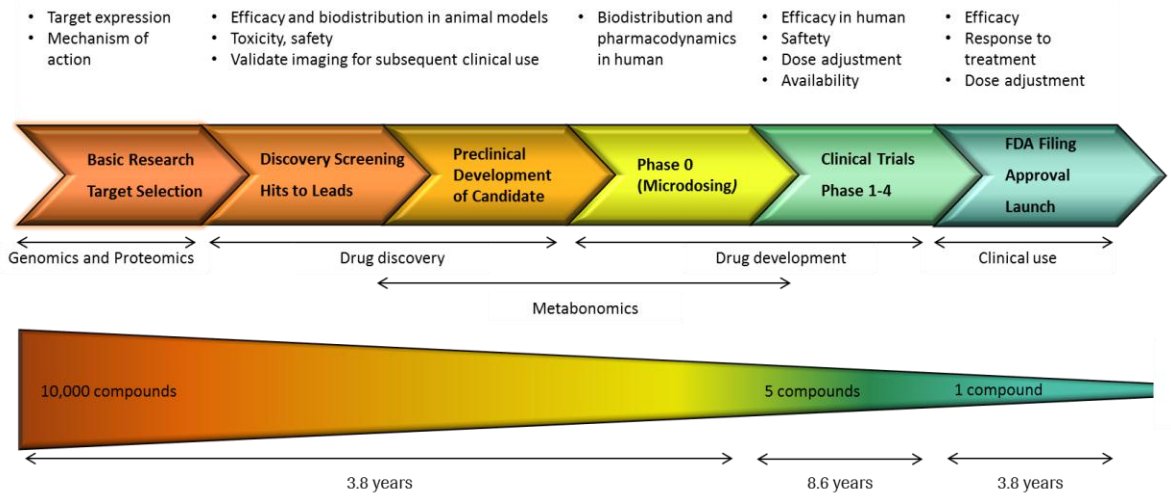

Figure 3 The drug discovery and development process and key aspects that can be studied with PET. (adapted from [9, 31] .

1.3.2.1 Studying Disease Pathophysiology

The FDA has particularly recognized the great potential of PET in providing imaging biomarkers for neurocognitive disorders and depression [1]. Much progress has been made, for example, in the development of PET tracers ([^{18}F]FDDNP, [^{11}C]PIB) that bind to amyloid plaques in Alzheimer's disease (AD, Fig. 4) [33]. Apart from these target-specific radioligands, also functional imaging with 2-(^{18}F)Fluoro-2-Deoxy-D-Glucose (FDG) as a measure of glucose metabolism has the capability to allow earlier diagnosis of subtle changes in pathophysiology [12]. Prevention trials and therapeutic intervention prior to the manifestation of clinical symptoms thus become feasible. Monitoring disease progression

after treatment with an investigational new drug (IND) could moreover provide a new, more precise way for demonstrating drug efficiency. It is also worth noting that diagnostic biomarkers hold promise to streamline clinical trials by identifying patient populations which would benefit most from drug treatment. Apart from Alzheimer's disease, radioligands for the quantitative assessment of inflammatory response in multiple sclerosis [34], for the degeneration of dopaminergic neurons in Morbus Parkinson and for other disease-related changes in pathophysiology have also been developed [18].

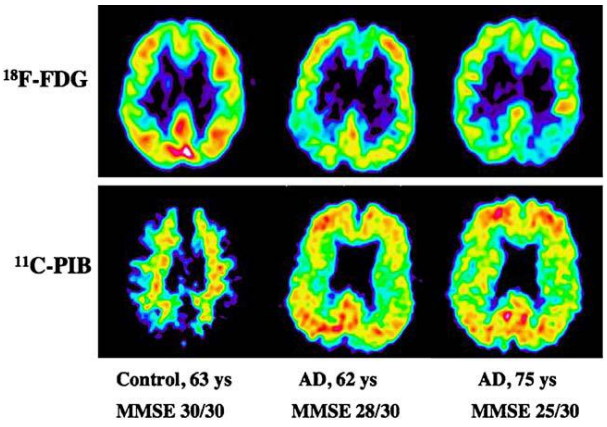

Figure 4 "Cerebral glucose metabolism (^{18}F-FDG) and ^{11}C-PIB amyloid imaging in two AD patients and one healthy control. The PET scans show ^{18}F-FDG and ^{11}C-PIB at a saggital section. Red indicates high, yellow medium, blue low ^{11}C-PIB retention. MMSE Mini-Mental- State-Examination, ys. years. Courtesy of Uppsala PET centre/ Imanet and Karolinska University Hospital Huddinge" [33].

1.3.2.2 Pharmacokinetic Studies

PET has evolved as a valuable tool to characterize the pharmacokinetic profile of radioactively labeled drug candidates by following their distribution throughout the body. The demonstration of drug entry into the target tissue confirms exposure for efficiency [16] and similarly the (unwanted) accumulation of drug candidates in other organs can be used for safety assessment. Biodistribution studies in living human subjects are of particular interest for drug candidates directing the brain where i) biopsies are not suitable to confirm passage across the highly restrictive BBB and ii) significant species differences in the expression of efflux transporters (e.g. P-glycoprotein, P-gp) may confound the extrapolation from animal models to humans [10].

The high sensitivity of PET allows conducting 'microdosing' studies early in phase I, initiated by the FDA/EMEA to accelerate the pace of first-entry-into-human studies [35]. Since microdosing is based on the application of sub-pharmacological doses (< 100th of the dose required for a pharmacologic effect), the potential risk of toxic effects is relatively low and regulatory requirements accordingly moderate. The information which PET provides on drug availability, delivery, clearance, tissue binding and target interaction may help

concentrate resources for clinical studies on the most promising drug candidates while compounds with a high probability to fail could be eliminated prior to the enrollment of large numbers of patients.

1.3.2.3 Receptor Occupancy Studies and Pharmacodynamics

RO studies are aimed to relate the dose, plasma and/or tissue concentration of a drug candidate to the percentage of the target site occupied. To this pursuit, competition studies are conducted, based on the visualization of receptor densities with a target-specific radioligand (tracer doses), before and after application of the unlabeled drug candidate (pharmacological dose) [36].

Dose-RO relationships have the capability i) to de-risk clinical trials by assisting in dosing selection [23] and ii) to differentiate between under-dosing (too low RO) and lack of efficiency (proof-of-concept) [31, 37]. Insight into mechanistic aspects of drug action can be gained by combining radioligand studies of drug occupancy with radiotracer studies of tissue markers expected to change after treatment, e.g. downstream cellular pathways, metabolism, glucose consumption, cell trafficking and gene expression. Radioligands acting at specific targets can also provide biomarkers for drug safety and efficiency as the following example shows: the treatment of schizophrenia requires 65-80% occupancy of dopamine D2-receptors while higher levels aggravate extrapyramidal side effects without additional therapeutic benefit [8]. The link between RO and clinical endpoint, however, still needs to be validated.

1.3.2.4 Summary of Major Achievements in Brain PET

As outlined above, PET has a tremendous potential for streamlining the drug discovery process and many imaging agents have found application in such relevant research areas like oncology (tumor diagnosis with e.g. FDG), cardiology (diagnosis of coronary heart disease) and neurology [11].

PET is of particular value in CNS research due to the severely restricted accessibility of the tissue and possible discrepancies that may arise between plasma and tissue pharmacokinetics as to the presence of the BBB. Jones et al. summarized that “brain PET has made its greatest advances in quantifying metabolism and G-protein coupled receptors in various disease states and after treatment” [23]. Historically, many efforts for treating neurological disorders (schizophrenia, Parkinson’s disease) have been directed at dopamine and serotonine receptors, resulting in a large portfolio of drug candidates; some of which have become successful PET tracers. Notably, “improved tracers for subtypes of serotonin, cannabinoid, and metabotropic glutamate receptors, as well as noradrenaline transporters, amyloid-β and

neuroinflammatory changes" [19] are important breakthroughs of the recent years which have expanded the scope of PET to new questions. Examples of successful PET tracers for imaging physiological processes and specific target sites are presented in Table 1, along with an example of a labeled drug, zolmitriptan, whose pharmacokinetic profile had been characterized with PET.

Table 1 Radiotracers and ligands used in PET studies of neuropharmacology. Table adapted from [30].

Physiological Process/Molecular Target	Radiotracer/Ligand
Metabolic or physiologic biomarkers	
Blood flow	$H_2{}^{15}O$
Oxygen consumption	$^{15}O_2$
Oxidative metabolism	^{18}F-FDG
Radioligands for known targets and radiolabeled drugs	
L-DOPA decarboxylase activity (Parkinson's disease)	^{18}F-6-fluorodopa (F-DOPA)
Amyloid deposits (Alzheimer's disease)	^{11}C-PiB and ^{18}F-FDDNP
Dopamine transporter	^{11}C- and ^{18}F-CFT
Dopamine D1 receptors	^{11}C-SCH23390
Dopamine D2 receptors	^{11}C-raclopride
Serotonin transporter	^{11}C-DASB
Serotonin 5-HT1A receptor	^{11}C-WAY100635
Serotonin 5-HT2A receptor	^{18}F-altanserin
Muscarinic acetylcholine receptors	^{11}C-(+)3-MPB
Nicotinic acetylcholine receptors	^{11}C- and ^{18}F-A-85380
Opioid μ, κ, e, δ receptors	^{11}C-diprenorphine, ^{11}C-buprenorphine
Opioid μ receptor	^{11}C-carfentenil
Opioid δ receptors	N1'-(^{11}C-methyl)naltrindole
Central benzodiazepine receptor (GABA)	^{11}C-flumazenil
Substance P/NK1 receptor	^{18}F-FE-SPA-RQ
Radiolabeled drug	
Pharmacokinetics	^{18}C-Zolmitriptan

1.3.2.5 Suggestions for Future Research in Brain PET

The brain is the most studied and the most complex tissue, but also the one least understood [23]. In view of the burden of suffering due to the manifestation of mental disorders, and especially with the ever growing relevance of Alzheimer's disease, Morbus Parkinson, cancer and stroke in an aging society, the conceivable future applications of PET are manifold. Jones et al. recently suggested the following relevant biological processes that require imaging agents (Table 2) [23]:

Table 2 Suggested future research areas of brain PET.

	"Future suggestions of relevant biological processes that require robust imaging agents [...] include:
i	Downstream effector pathways coupled to neuroreceptors
ii	Neuroimmunity/inflammation as a factor in brain disease and the role of astrocytes and their associated chemokines
iii	Transient opening of the BBB as a factor in brain inflammation
iv	Enhancing the delivery of drugs across the BBB
v	Specific imaging markers of neuronal and glial subtypes
vi	Progenitor stem cell activity and their chemokines for repairing brain damage
vii	Glioma stem cell activity
viii	Brain viral and bacterial infections (e.g., herpes encephalitis and tuberculosis)
ix	Brain plasticity, e.g., in stroke recovery
x	The neurochemical components underlying memory, learning, maturation, ageing cognitive decline/enhancement, and personality"[23]

1.3.3 Shortcomings and Challenges of Developing New PET Tracers

Despite the wealth of information PET could provide for accelerating the development of novel CNS-active drugs, it appears that its full potential has not been exploited yet [23]. The lack of access to sophisticated methodologies (cyclotron) and the high cost of PET as compared to other imaging methodologies (e.g. MRI) have been identified as major hindrances for the further advancement of PET [23, 38].

Moreover, the expansion of PET for use in basic research and clinical application is heavily dependent on the availability of innovative PET tracers [39]. Even though many target-specific imaging radioligands are available (especially for D2/3 and 5 - HT receptors), the development of drug candidates binding to novel targets requires in-parallel development of novel PET tracers. The more imaging agents are developed, the more physiological processes and targets in healthy and diseased brain can be explored and the higher is the impact of PET for drug discovery. However, the lack of innovative PET tracers has contributed to the fact that PET has not evolved as extensively as expected [23].

1.3.3.1 The PET Tracer Development Process

The development of novel PET tracers poses a major challenge which is almost as time-and resource-intensive as the development of novel drugs (8-10 years for imaging agents, 10-15 years for drugs [40]). In view of the fact that a radioligand's success is directly dependent on the success of a drug candidate and vice versa, the synchronous development of both is particularly ambitious and potential pitfalls are numerous. Special technical facilities (cyclotron, PET camera, modeling and image reconstruction) and the expert knowledge of a radiotracer imaging team are required for developing PET tracers, however, there are many analogies to the drug development process (Fig.5).

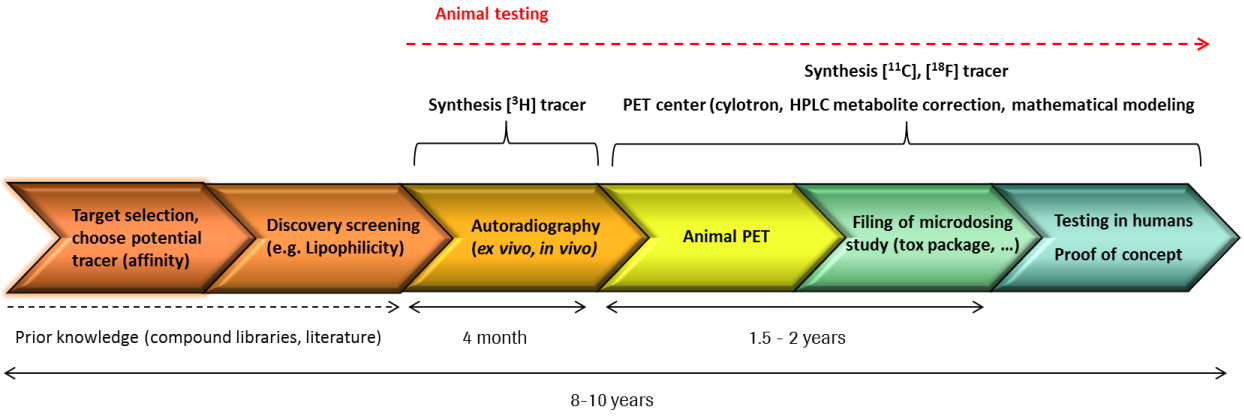

Figure 5 The PET tracer discovery and development process. The details for the timeframe of developing an imaging agent up to the Filing for microdosing studies are based on experience within Roche (personal communication, unpublished). The estimation of the timeframe for the whole development process (8-10 years) was obtained from literature [40].

After selecting a target of interest, high affinity ligands with suitable physicochemical properties (see below) are tritium-labeled for further experiments in rodents. Labeling with

Tritium (long half - life) opens the possibility to measure radioligands at tracer concentrations without the need for sophisticated PET facilities (cyclotron). The long half-life is of practical importance since *in vitro* and *ex vivo* studies (*in vivo* is not possible) can be performed over a period of several month using the same batch [23]. Autoradiography performed as *in vitro* or *ex vivo* tissue binding study (incubation of the PET tracer with tissue slices) allows for quantification of tracer specific binding, non-specific binding and the regional distribution thereof in various tissue sections [41, 42]. *In vivo* autoradiography (injection of tracer and sacrifice of animal thereafter) provides additional information about pharmacokinetic aspects before the tracer is finally tested in living man. The last stage, the actual PET experiment, is the most elaborate since incorporation of a positron - emitting radionuclide is required.

Predictive, less resource demanding assays are therefore of utmost importance in order to concentrate resources on the most promising candidates and to eliminate inappropriate molecules as early as possible. Notably, the requirements placed upon successful PET tracers and drugs are not necessarily the same and several aspects important for a good image quality in PET need to be considered. As will be outlined below, the list of requirements is long and balancing of physicochemical properties necessary [43] which might contribute to the current lack of innovate PET tracers.

1.3.3.2 Relationships between PET Tracer Properties and Image Quality

1.3.3.2.1 Target Density, Target Affinity, Selectivity and Specific Radioactivity

First and foremost, the target needs to be identified and a measureable number of target sites should be present in the tissue of interest, e.g. the brain. Since the concentration of many neuroreceptors (B_{max}) is rather low (nano to femtomoles per mg tissue range), the affinity ($1/K_D$) of the tracer candidates should be sufficiently high, i.e. in the nanomolar to sub-nanomolar range [44, 45]. It goes without saying that a lower target density requires a higher affinity of the radioligand [43]. An ideal tracer should also be selective, although non-selectivity is no criterion for exclusion provided that target and non-target sites are anatomically separated. To achieve high levels of sensitivity it is important to prepare tracer candidates with high specific radioactivity and with sufficient yield. A low specific activity would require higher doses which may lead to saturation of available binding sites making assumptions on tracer kinetic modeling invalid and undesired toxic and pharmacological effects probable. The radiosynthesis should be rapid and feasible in a few steps due to the short half - lives of the commonly used positron - emitting radioisotopes (fluorine-18:

$t_{1/2}$ = 110 min, carbon-11, $t_{1/2}$ = 20 min) [18]. At a given specific radioactivity, the receptor concentration/affinity ratio (B_{max}/K_D) displays the maximum possible specific signal which can be obtained from a radiotracer. However, it should be noted that optimizing compounds exclusively towards higher affinity may be misleading if other aspects like toxicity, scanning duration, radiotracer delivery (brain uptake), metabolism and non-specific binding are disregarded [43].

1.3.3.2.2 Toxcicity

A prerequisite for any application of radioligands in living human subjects is non-toxicity and the absence of adverse pharmacological effects [24]. The advantage of PET in this respect is certainly the fact that only tracer doses are applied, in a few patients and in a limited number of experiments. The safety requirements for FDA approval are therefore less stringent than for the entry of drug candidates into the clinical phase. Nevertheless a limited safety package is required based on single dose acute toxicology studies in two animal species [46].

1.3.3.2.3 Affinity and Tracer Kinetic Modeling

A very high affinity may leads to a situation that obviates the interpretation of PET scans in terms of processes at the target site, namely when the distribution of the radiotracer becomes dependent on the blood flow rather than on the rate of target binding [43]. In addition, high affinity prolongs the time until specifically bound radioligand is equilibrated, i.e. when the rate of ligand-receptor association equals the rate of dissociation. This equilibrium state is succeeded by a washout phase as the radiotracer is being cleared from brain and plasma. Extracting the relevant outcome measures (related to B_{max}/K_D) from a series of PET scans requires capturing the washout phase which explains that high affinity also prolongs the scanning duration. In view of the short half - lives of commonly used PET tracers, it becomes clear that exceedingly long scanning times and very high affinity radioligands are incompatible with PET. Furthermore, it has been recognized that ligands with very high affinity are unsuited because the modeling approaches used for data analysis can only handle reversible and irreversible binding, but not the states in between [44].

1.3.3.2.4 Plasma Protein Binding and Plasma Clearance

A low plasma protein binding of the radiotracer is advantageous since only the unbound fraction of radioligand in plasma is available for entering the brain [43]. Moreover, a lower protein binding gives rise to a higher plasma clearance which in turn is associated with a shorter time to reach steady state. Accordingly, the minimal scan duration decreases for the

benefit of a higher sensitivity and the possibility to use higher affinity radioligands. Generally, a moderate-to-high clearance is desirable to improve the image quality and the likely development success of a PET tracer. In addition, lower protein binding assures more reliability of the image analysis since the unbound fraction can be quantified with higher accuracy. The consideration thereof is crucial for assuring that changes in the binding potential are related to changes at the target site rather than to intersubject differences in plasma protein binding.

1.3.3.2.5 Blood - Brain Barrier Permeability

The BBB functions to protect the CNS from natural xenobiotics and to maintain cerebral homeostasis. Unlike peripheral permeation barriers, the tight endothelium constituting the BBB lacks fenestrations and contains tight junctions which prevent paracellular diffusion [10]. The highly protective function of the membrane is reinforced by ABC transporters such as P-gp and multidrug resistance associated proteins [10]. The size and charge restrictions for entering the brain are therefore particularly conservative and only small (cross sectional area, $A_D < 70$ Å^2) and low-to moderately charged molecules are able to pass the BBB by passive diffusion [47]. Radiotracers targeting receptors in the CNS should readily cross the BBB and they should preferably be non-P-gp substrates [45].

1.3.3.2.6 Metabolism

An additional quality criterion is the resistance of the tracer to rapid metabolism including the absence of brain penetrant radiolabeled metabolites which would complicate the unambiguous interpretation of radioactivity-time curves. This requirement is an implication from the inability of a PET camera to distinguish between the parent radioligand and radiolabeled metabolites [45].

1.3.3.2.7 Non-specific Brain Tissue Binding and the Role of Lipophilicity

Provided that the unmetabolized radioligand reaches its target, the signal obtained is still lower than what is hoped for according to the receptor density/affinity ratio, B_{max} / K_D. Apart from specific binding to the target site, radioligands also bind non-specifically to non-saturable brain components (membrane structures) [18]. NSB can be understood in terms of a background noise from which the specific binding needs to be distinguished. A high NSB reduces the signal contrast in PET and thus the sensitivity to explore changes in the binding capacity due to physiological, pathophysiological or pharmaceutical processes. Undesirably high NSB is one of the main reasons why PET tracers undergo attrition *in vivo*. More

precisely it is an unsuitably low ratio between specific binding and non-specific binding which makes a radioligand likely to fail *in vivo* [28].

As a rule of thumb it is assumed that higher lipophilicity goes along with higher NSB but also with higher affinity for the target site [43]. Balancing lipophilicity is therefore crucial, not only to ensure a good image quality, but also to warrant brain permeability. It has been recognized that successful PET tracers are characterized by $\log P_{oct}$ values < 3, most of them are in the range of $\log P_{oct} = 2.5$ [20]. However, there are exceptions to the rule which raise the question as to the ability of octanol to predict NSB of radioligands in brain tissue.

2 Rationale and Aims of Research

As described in the introductory chapter, PET provides the unique opportunity to monitor disease progression and drug efficiency on a cellular, subcellular and molecular level in living subjects at an early stage in drug development. PET therefore holds great promise to aid the optimization of potential drug candidates and to reduce the attrition rate in the later and cost-intensive clinical phases. The expansion of PET for use in basic research and clinical application is heavily dependent on the availability of innovative PET tracers [39]. However, the number of approved radioligands considerably lags behind the number of receptors, especially neuroreceptors, which could potentially be visualized and targeted to treat human disease [48]. Many radioligands fail due to an unfavorably high NSB to lipid membranes and non-target proteins which attenuate the signal arising from specific binding at the target site [43]. In order to enhance the confidence in the likely development success of a PET tracer it is desirable to estimate the extent of NSB as early as possible, preferably before labeling of the molecular probe. The unbound fraction of drug in brain ($f_{u,brain}$) is considered a reliable NSB-surrogate for PET tracers targeting receptors in the CNS [49]. However, the measurement of $f_{u,brain}$ requires laborious equilibrium dialysis hampered by the requirement for large quantities of animal tissue [50].

Therefore, the main purpose of this thesis was to devise and to evaluate a strategy for estimating the NSB of neuroimaging agents in an assay which works with unlabeled compounds and which requires fewer animals as compared to equilibrium dialysis. In a broader sense, we were interested whether an *in vitro* NSB-estimate can be used as decision criterion for the selection or rejection of potential PET tracers. This raised the question upon the existence of a NSB limit above which the failure of a PET tracer is more probable than its success. The expected benefit of an *in vitro* NSB - estimate for the PET tracer development process is obvious: Either tracer candidates with inappropriately high NSB can be rejected prior to labeling, or, more desirable, the optimization towards balanced lipophilicity can be accelerated.

There are several possibilities conceivable for estimating the NSB of neuroimaging tracers in a manner that is consistent with our ambition to replace or reduce animal testing. For obvious ethical reasons, the use of artificial surrogate systems would be preferable. We considered i) octanol worth to evaluate since opinions about the quality of which as membrane-mimicking system diverge substantially. Previous comparisons between $\log D_{oct}$ and tissue binding in

general [51], and between $\log D_{oct}$ and NSB [43] in particular, relied on rather small datasets limiting the explanatory power of these studies. Moreover, correlations between NSB and chromatographically derived $\log D_{oct}$ values [52] are ambiguous: using a model (reversed phase in chromatography) of a model ($\log D_{oct}$) introduces scatter to the data and leaves questions unanswered as to the value of octanol itself. For the measurement of $\log D_{oct}$, we have developed a novel assay, referred to as CArrier-Mediated DIStribution System (CAMDIS, see below). Similar to octanol, it has recently become common practice within Roche (Basel) to use the membrane fraction in the Parallel Artificial Membrane Permeability Assay (PAMPA) as a primary indicator for NSB (in-house, unpublished results). Yet, a systematic comparison between tissue binding and PAMPA-membrane retention has been pending ever since the introduction of PAMPA in 1998 [53]. Hence, we addressed the question whether ii) the fraction of drug retained in the PAMPA membrane represents a meaningful surrogate for NSB. In addition, iii), we aimed to develop an *in vitro* assay for assessing the binding of drugs and drug-like molecules to brain homogenate and to predict the NSB of PET tracer candidates. The assay will in the following be referred to as LIpid Membrane Binding Assay (LIMBA). The decision to develop LIMBA in a miniaturized format was driven by the aim for accurate NSB-estimates at low expenses of animals. We were specifically interested whether LIMBA, in comparison with the artificial-membrane mimicking systems mentioned above, provides significant advantages that justify favoring animal tissue over artificial models for the prediction of NSB.

A comparative evaluation of the different surrogate systems required first and foremost a thorough validation of the individual assays (CAMDIS, PAMPA, LIMBA) to ensure the accuracy of the respective assay read-outs. The first objective of this thesis was the development, optimization and implementation of the novel $\log D_{oct}$ assay, CAMDIS, which is described in *manuscript 1*. What was the driving force for developing CAMDIS after thousands of $\log D_{oct}$ values have been measured with the traditional shake flask technique? The question can be answered with i) the tedious and time-consuming phase separation encountered in the traditional shake flask method which on top of that is prone to error due to emulsification [54] and incomplete phase separation [55]; and ii) the lack of suitable alternatives with respect to direct lipophilicity assays. As a strategy to overcome the difficulties of the shake flask technique, a filter was used in CAMDIS as support for octanol, yet the basic concept of shaking, separating and then analyzing two immiscible solvents for the distributed solute (octanol/water) was maintained.

It is important to note that CAMDIS was developed as a miniaturized high-throughput assay in order to meet the demand for cost-effective profiling of a large number of compounds in a short time. However, miniaturization in general goes along with an increase in the relative proportion of boundary layers to which a solute could adsorb or penetrate. Nominal and actual drug concentrations may then not necessarily be the same and, as a result, experimental artifacts are likely to arise. This drawback of miniaturized screening assays is particularly important when measuring $\log D_{oct}$ since two interfaces need to be considered, i.e. the filter-supported octanol/water interface and the interface formed between water and the well plate. However, neither have adsorption-related artifacts been estimated before in a quantitative manner, nor have methods been proposed to correct for erroneous $\log D_{oct}$ values. For the sake of more reliable $\log D_{oct}$ values, we addressed the question under which experimental conditions (e.g. solute concentration, phase volume ratio) adsorption does not significantly compromise the accuracy of $\log D_{oct}$. Aiming to predict and eventually prevent adsorption-related artifacts, we also raised the question which physicochemical properties make compounds susceptible to adsorption.

Within this scope, we first studied the adsorption to the filter-supported octanol/water interface (*manuscript 1*). Specifically we were interested whether interfacial drug adsorption actually manifests itself as an error in $\log D_{oct}$. Moreover we were interested whether this error must be attributed to the adsorption to the liquid/liquid interface, the adsorption to the filter support or both. To resolve this question, we compared the CAMDIS-$\log D_{oct}$ values with $\log D_{oct}$ values derived from a conventional, miniaturized shake flask experiment (no filter) using the example of a cationic, an anionic and a non-ionic drug.

If and how adsorption to the well plate affects the accuracy of $\log D_{oct}$ was investigated separately in *manuscript 2*. We chose Teflon as the well plate material of interest since it is widely used and preliminary studies in our lab were not in line with the often supposed inertness to adsorption. First, we characterized the sorption profile of 24 structurally diverse drugs by means of HPLC-UV, and we then parameterized a model which incorporates both, Teflon adsorption and octanol/water distribution. The predictive power of the model was tested by comparing $\log D_{oct}$ values derived with a miniaturized (CAMDIS) assay and with a large-scaled (1L glass flask) shake flask experiment considering the latter the gold standard for the following reasons: i) both phases were accessible for concentration analysis and ii) the surface to volume ratio was much smaller as compared to a miniaturized assay.

During the course of our investigation it became clear that drug-well plate interactions significantly falsify $\log D_{oct}$ values whenever sticky, hydrophilic or sparingly soluble compounds are concerned which likely precipitate. For such instances, we aimed to correct erroneous $\log D_{oct}$ values by recovering adsorbent or aggregated drugs from the Teflon plate. Excipients such as detergents [56], cyclodextrines [57], organic solvents [58] and bovine serum albumin [59] have proven useful for the recovery from drug adsorption to polypropylene and polystyrol. Yet, studies on the minimization of drug loss to Teflon are missing due to the uncritical use of the polymer. In addition, most of the knowledge concerning excipient-aided drug recovery has been gained from case studies rather than from designed experiments on a structurally diverse data set. In screening assays such as CAMDIS it is however crucial to lean on excipients which work for a large variety of compounds and which moreover do not interfere with the detection method for the analyte. HPLC coupled with electrospray ionization/mass spectrometry (HPLC - ESI/MS) was used for concentration analysis in CAMDIS since the method is more sensitive and better selective as compared to UV spectroscopy. Hence, in *manuscript 3* we not only tested the desorbing efficiency of various excipients (detergents, cyclodextrines, organic solvents) on a structurally diverse dataset (n=26) but also evaluated the excipients in terms of compatibility with HPLC - ESI/MS. In this regard, it is worth noting that excipients can disturb the concentration analysis with HPLC-MS by suppressing an analyte's ionization efficiency (matrix effect) [60]. Among the excipients tested, 2-propanol was the only agent which was both effective and compatible with MS. The question as to whether 2-propanol also proves useful for correcting erroneous $\log D_{oct}$ values was then addressed in *manuscript 2* within the framework of the $\log D_{oct}$ - adsorption study.

Only after having shown how to avoid, identify and correct experimental artifacts, respectively, we were able to validate CAMDIS on an extended dataset in *manuscript 1*. To this purpose, the literature was searched for compounds with known shake flask $\log D_{oct}$ values serving as gold standard for $\log D_{oct}$. Stringent quality criteria were applied for the inclusion of compounds in the validation dataset (n = 52) in order to enable an unambiguous comparison of the methods.

Recall that our ultimate purpose was the comparative evaluation of various membrane-mimicking systems (octanol, PAMPA lipid, brain homogenate) with respect to their predictive ability for NSB. Accordingly, the next major objective of this thesis was the alignment of PAMPA with the basic requirements for a sensitive, specific and predictive

assay which moreover can be interpreted on a molecular level. To the pursuit of our objective, we used the Roche PAMPA setup as starting point for our own optimization purposes. By default, a solubilizer (glycocholic acid) is used in the Roche setup to accomplish the detection of sparingly soluble compounds, however, also other excipients are frequently applied in PAMPA as model formulation agents (N-methyl-1-pyrrolidone [NMP], hydroxypropy-β-cyclodextrine [HP-β-CD], propylene glycol [PG], taurocholic acid [TC] as one component of the FaSSIF/FeSSIF media) [61]. Since matrix-related excipient effects may disturb the concentration analysis with ESI/MS (see above), we addressed the following questions in *manuscript 4*: i) which of the excipients used in PAMPA cause matrix effects ii) is it possible to predict the presence of matrix effects, iii) do matrix effects manifest themselves as erroneous assay read-outs (permeability, membrane retention) and if so, iii), how does the experimental setup need to be modified towards MS compatibility. There is a certain overlap between the dosing vehicles which have already been evaluated in terms of matrix effects [62, 63] and the excipients tested within the scope of this thesis. However, the literature lacks information on matrix effects in presence of the FaSSIF/FeSSIF media, GCA and NMP. In addition, the studies published on excipient-related matrix effects pertain to the excipients levels in plasma which are typically encountered in a Drug Metabolism and Pharmacokinetics (DMPK) study. In contrast, we studied excipient concentrations relevant in PAMPA and required for effective solubilization.

Apart from these analytical objectives, we aimed at shedding light on the lipid organization in the PAMPA barrier by means of different NMR techniques. Although there are different speculative models [64], the structure of the PAMPA barrier has never been characterized before at the molecular level. For example, the wide - spread assumption that bilayers are formed was based on electrochemical experiments with a filter-lipid-solvent system different from that actually used in PAMPA [65]. It is far from clear whether the results can be applied to PAMPA and therefore we dedicated a chapter of this thesis (*manuscript 5*) to that question. Specifically we were interested whether or not the term bilayer membrane and PAMPA membrane can be used synonymously. Knowledge about the lipid organization in PAMPA is not only of academic interest, but also of utmost importance to assess the scope and limitation of the membrane-mimicking system [10, 66, 67]. Ultimately it is essential for understanding the relationship between the structure of a test compound and the extent of membrane retention, which is in turn fundamental for guiding the structural optimization of test compounds.

The next major objective of thesis was the development of LIMBA, a novel miniaturized *in vitro* assay for estimating the binding of drugs and drug-like molecules to brain homogenate. The concept of LIMBA was inspired by PAMPA and CAMDIS in terms of using a filter device as support for the membrane-mimicking system. In contrast to CAMDIS and PAMPA, brain homogenate instead of an artificial lipid-solvent mixture was coated on the filter in order to remain as close as possible to the *in vivo* situation.

In *manuscript 6* we aimed at evaluating all assays, CAMDIS, PAMPA and LIMBA, in a comparative way with respect to their predictive ability for NSB. The following strategy was pursued: The literature was searched for drugs which had been characterized with equilibrium dialysis. The corresponding $f_{u,brain}$-estimates were considered the gold standards for tissue binding allowing for comparative evaluation with the various surrogate systems investigated. Even though the $f_{u,brain}$-estimates themselves are only approximations of the NSB *in vivo*, for validation purposes we abstained from using *in vivo* data for the following reasons: i) the number of compounds characterized with PET was much smaller than that measured with equilibrium dialysis and ii) active transport processes may complicate the interpretation of the PET data. In *manuscript 6* we aimed to identify the *in vitro* assay which was best to predict $f_{u,brain}$. In *manuscript 7*, we finally tested whether that assay, i.e. LIMBA, is also useful for the prediction of NSB in autoradiography and in a PET study. The research plan is summarized in Fig. 6.

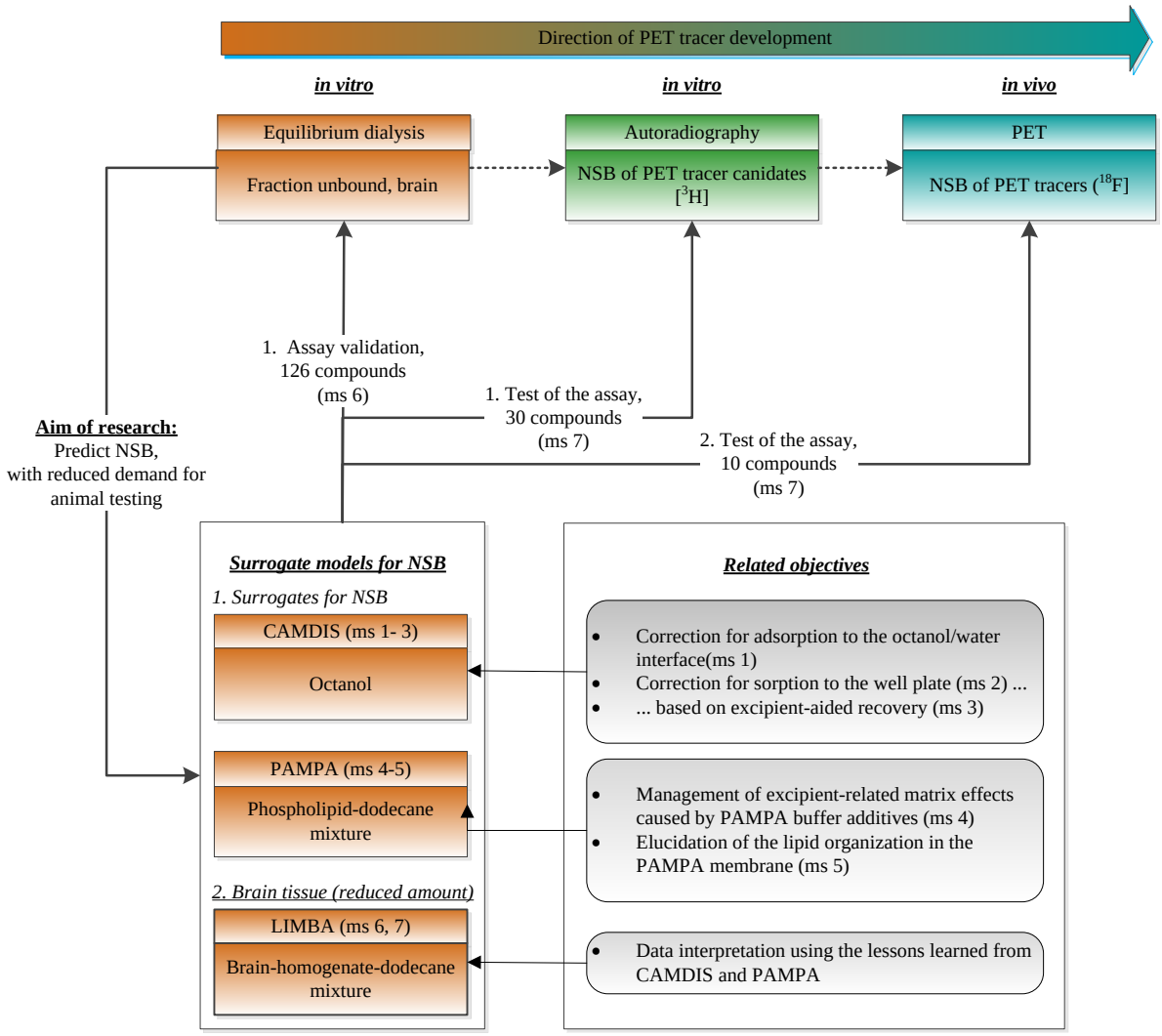

Figure 6 Research plan.

References

1. Pammolli, F., L. Magazzini, and M. Riccaboni, *The productivity crisis in pharmaceutical R&D.* Nat. Rev. Drug Discovery, 2011. **10**(6): p. 428-438.
2. Kennedy, T., *Managing the drug/discovery interface.* Drug discovery today, 1997. **2**(10).
3. Gleeson, M.P., et al., *Probing the links between in vitro potency, ADMET and physicochemical parameters.* Nat. Rev. Drug Discovery, 2011. **10**(3): p. 197-208.
4. Gee, A.D., *Neuropharmacology and drug development.* Br. Med. Bull., 2003. **65**: p. 169-177.
5. EvaluatePharma2011.
6. Kola, I. and J. Landis, *Can the pharmaceutical industry reduce attrition rates?* Nat Rev Drug Discov, 2004. **3**(8): p. 711-5.
7. Farde, L., *The advantage of using positron emission tomography in drug research.* Trends Neurosci., 1996. **19**(6): p. 211-214.
8. Lee, C.-M. and L. Farde, *Using positron emission tomography to facilitate CNS drug development.* Trends Pharmacol. Sci., 2006. **27**(6): p. 310-316.
9. Nestler, E.J. and S.E. Hyman, *Animal models of neuropsychiatric disorders.* Nat. Neurosci., 2010. **13**(10): p. 1161-1169.
10. Seelig, A., *The role of size and charge for blood-brain barrier permeation of drugs and fatty acids.* J. Mol. Neurosci., 2007. **33**(1): p. 32-41.
11. Uppoor, R.S., et al., *The Use of Imaging in the Early Development of Neuropharmacological Drugs: A Survey of Approved NDAs.* Clin. Pharmacol. Ther. (N. Y., NY, U. S.), 2008. **84**(1): p. 69-74.
12. FDA, *Challenge and opportunity on the critical path to new medical technologies.* 2004.
13. FDA, *Critical path opportunities list.* 2006.
14. FDA, *Critical path opportunities report.* 2006.
15. Willmann, J.K., et al., *Molecular imaging in drug development.* Nat. Rev. Drug Discovery, 2008. **7**(7): p. 591-607.
16. Massoud, T.F. and S.S. Gambhir, *Molecular imaging in living subjects: seeing fundamental biological processes in a new light.* Genes Dev., 2003. **17**(5): p. 545-580.
17. Zhang, L. and A. Villalobos, *Recent advances in the development of PET and SPECT tracers for brain imaging.* Annu. Rep. Med. Chem., 2012. **47**: p. 105-119.
18. Miller, P.W., et al., *Synthesis of 11C, 18F, 15O, and 13N radiolabels for positron emission tomography.* Angew. Chem., Int. Ed., 2008. **47**(47): p. 8998-9033.
19. Virdee, K., et al., *Applications of positron emission tomography in animal models of neurological and neuropsychiatric disorders.* Neurosci Biobehav Rev, 2012. **36**(4): p. 1188-216.
20. Cherry, S.R., *The 2006 henry N. wagner lecture: of mice and men (and positrons)-advances in PET imaging technology.* J. Nucl. Med., 2006. **47**(11): p. 1735-1745.
21. Paans, A.M.J., et al., *Positron emission tomography: the conceptual idea using a multidisciplinary approach.* Methods (San Diego, CA, U. S.) 2002. **27**(3): p. 195-207.
22. Phelps, M.E., *Positron emission tomography provides molecular imaging of biological processes.* Proc. Natl. Acad. Sci. U. S. A., 2000. **97**(16): p. 9226-9233.
23. Jones, T. and E.A. Rabiner, *The development, past achievements, and future directions of brain PET.* J. Cereb. Blood Flow Metab., 2012. **32**(7): p. 1426-1454.
24. Pike, V.W., *Positron-emitting radioligands for studies in vivo. Probes for human psychopharmacology.* J. Psychopharmacol. (Oxford), 1993. **7**(2): p. 139-58.

25. Gunn, R.N., et al., *Positron Emission Tomography Compartmental Models: A Basis Pursuit Strategy for Kinetic Modeling.* J. Cereb. Blood Flow Metab., 2002. **22**(12): p. 1425-1439.
26. Slifstein, M. and M. Laruelle, *Models and methods for derivation of in vivo neuroreceptor parameters with PET and SPECT reversible radiotracers.* Nucl. Med. Biol. , 2001. **28**(5): p. 595-608.
27. Mintun, M.A., et al., *A quantitative model for the in vivo assessment of drug binding sites with positron emission tomography.* Ann. Neurol., 1984. **15**(3): p. 217-27.
28. Seneca, N., *Recent advances in positron emission tomography imaging of brain.* Drugs Future, 2011. **36**(8): p. 601-613.
29. Cumming, P., D. Caprioli, and J.W. Dalley, *What have positron emission tomography and "Zippy" told us about the neuropharmacology of drug addiction?* Br. J. Pharmacol., 2011. **163**(8): p. 1586-1604.
30. Fernandes, E., et al., *Positron emitting tracers in pre-clinical drug development.* Curr. Radiopharm., 2012. **5**(2): p. 90-98.
31. Patel, S. and R. Gibson, *In vivo site-directed radiotracers: a mini-review.* Nucl. Med. Biol., 2008. **35**(8): p. 805-815.
32. Cherry, S.R. and S.S. Gambhir, *Use of positron emission tomography in animal research.* ILAR J 2001. **42**(3): p. 219-32.
33. Nordberg, A., *Amyloid plaque imaging in vivo: current achievement and future prospects.* Eur J Nucl Med Mol Imaging, 2008. **35 Suppl 1**: p. S46-50.
34. Wong, D.F., J. Tauscher, and G. Grunder, *The Role of Imaging in Proof of Concept for CNS Drug Discovery and Development.* Neuropsychopharmacology, 2009. **34**(1): p. 187-203.
35. FDA, *Guidance for industry, investigators, and reviewers. Exploratory IND studies.* 2006.
36. Cunningham, V.J., et al., *PET studies in drug development: methodological considerations.* Drug Discovery Today: Technol., 2005. **2**(4): p. 311-315.
37. Marik, J., et al., *New imaging paradigms in drug development: the PET imaging approach.* Drug Discovery Today: Technol., 2011. **8**(2-4): p. e63-e69.
38. Nunn, A.D., *Update: Molecular Imaging and Personalized Medicine: An Uncertain Future.* Cancer Biother. Radiopharm., 2007. **22**(6): p. 722-739.
39. Schwaiger, M. and H.-J. Wester, *How many PET tracers do we need?* J. Nucl. Med., 2011. **52**(Suppl. 2): p. 36S-41S.
40. Nunn Adrian, D., *The cost of developing imaging agents for routine clinical use.* Invest Radiol, 2006. **41**(3): p. 206-12.
41. Patel, S., et al., *Screening cascade and development of potential Positron Emission Tomography radiotracers for mGluR5: in vitro and in vivo characterization.* Mol Imaging Biol, 2005. **7**(4): p. 314-23.
42. Patel, S., et al., *An in vitro assay for predicting successful imaging radiotracers.* Mol Imaging Biol, 2003. **5**(2): p. 65-71.
43. Laruelle, M., M. Slifstein, and Y. Huang, *Relationships between radiotracer properties and image quality in molecular imaging of the brain with positron emission tomography.* Mol Imaging Biol, 2003. **5**(6): p. 363-75.
44. Wong Dean, F. and G. Pomper Martin, *Predicting the success of a radiopharmaceutical for in vivo imaging of central nervous system neuroreceptor systems.* Mol Imaging Biol, 2003. **5**(6): p. 350-62.
45. Ametamey, S.M. and P.A. Schubiger, *PET radiopharmaceuticals for neuroreceptor imaging.* Nucl. Sci. Tech., 2006. **17**(3): p. 143-147.

46. McCarthy, D.J., et al., *Discovery of novel positron emission tomography tracers.* Annu. Rep. Med. Chem., 2009. **44**: p. 501-513, 2 plates.
47. Fischer, H., R. Gottschlich, and A. Seelig, *Blood-brain barrier permeation: molecular parameters governing passive diffusion.* J. Membr. Biol., 1998. **165**(3): p. 201-211.
48. Hopkins, A.L. and C.R. Groom, *Opinion: The druggable genome.* Nat. Rev. Drug Discovery, 2002. **1**(9): p. 727-730.
49. Guo, Q., M. Brady, and R.N. Gunn, *A biomathematical modeling approach to central nervous system radioligand discovery and development.* J. Nucl. Med., 2009. **50**(10): p. 1715-1723.
50. Kalvass, J.C. and T.S. Maurer, *Influence of nonspecific brain and plasma binding on CNS exposure: implications for rational drug discovery.* Biopharm. Drug Dispos., 2002. **23**(8): p. 327-338.
51. Wan, H., et al., *High-throughput screening of drug-brain tissue binding and in silico prediction for assessment of central nervous system drug delivery.* J. Med. Chem., 2007. **50**(19): p. 4606-4615.
52. Jiang, Z., et al., *A rapid vesicle electrokinetic chromatography method for the in vitro prediction of non-specific binding for potential PET ligands.* J. Pharm. Biomed. Anal., 2011. **54**(4): p. 722-729.
53. Kansy, M., F. Senner, and K. Gubernator, *Physicochemical High Throughput Screening: Parallel Artificial Membrane Permeation Assay in the Description of Passive Absorption Processes.* J. Med. Chem., 1998. **41**(7): p. 1007-1010.
54. Leo, A., C. Hansch, and D. Elkins, *Partition coefficients and their uses.* Chem. Rev., 1971. **71**(6): p. 525-616.
55. Yamashita, T., E. Yamamoto, and I. Kushida, *Frozen water phase method for logD measurement using a 96-well plate.* Talanta, 2011. **84**(3): p. 809-13.
56. Ji, A.J., et al., *Challenges in urine bioanalytical assays: overcoming nonspecific binding.* Bioanalysis, 2010. **2**(9): p. 1573-1586.
57. Sun, L. and J.A. Stenken, *The effect of β-cyclodextrin on liquid chromatography/electrospray-mass spectrometry analysis of hydrophobic drug molecules.* J. Chromatogr., A 2007. **1161**(1-2): p. 261-268.
58. Fukazawa, T., Y. Yamazaki, and Y. Miyamoto, *Reduction of non-specific adsorption of drugs to plastic containers used in bioassays or analyses.* J. Pharmacol. Toxicol. Methods, 2010. **61**(3): p. 329-333.
59. Song, D., L.-F. Hsu, and J.L.S. Au, *Binding of Taxol to Plastic and Glass Containers and Protein under in Vitro Conditions.* J. Pharm. Sci., 1996. **85**(1): p. 29-31.
60. Taylor, P.J., *Matrix effects: the Achilles heel of quantitative high-performance liquid chromatography-electrospray-tandem mass spectrometry.* Clin. Biochem., 2005. **38**(4): p. 328-334.
61. Bendels, S., et al., *PAMPA-Excipient Classification Gradient Map.* Pharm. Res. , 2006. **23**(11): p. 2525-2535.
62. Tong, X.S., et al., *Effect of Signal Interference from Dosing Excipients on Pharmacokinetic Screening of Drug Candidates by Liquid Chromatography/Mass Spectrometry.* Anal. Chem., 2002. **74**(24): p. 6305-6313.
63. Shou, W.Z. and N. Weng, *Post-column infusion study of the "dosing vehicle effect" in the liquid chromatography/tandem mass spectrometric analysis of discovery pharmacokinetic samples.* Rapid Commun. Mass Spectrom., 2003. **17**(6): p. 589-597.
64. Avdeef, A., *Absorption and drug development: solubility, permeability, and charge state*2012: Wiley.

65. Thompson, M., U.J. Krull, and P.J. Worsfold, *The structure and electrochemical properties of a polymer-supported lipid biosensor.* Anal. Chim. Acta, 1980. **117**: p. 133-45.
66. Balon, K., B.U. Riebesehl, and B.W. Muller, *Drug liposome partitioning as a tool for the prediction of human passive intestinal absorption.* Pharm. Res., 1999. **16**(6): p. 882-888.
67. Gobas, F.A.P.C., et al., *A novel method for measuring membrane-water partition coefficients of hydrophobic organic chemicals: comparison with 1-octanol-water partitioning.* J. Pharm. Sci., 1988. **77**(3): p. 265-72.

3 Capsules

3.1 Carrier Mediated Distribution System (CAMDIS): A Novel Approach for the Measurement of Octanol/Water Distribution Coefficients

Background:

The octanol/water distribution coefficient, $\log D_{oct}$, has found ever growing interest in the drug development process as a key parameter for the prediction of a compound's pharmacokinetic, toxicokinetic and pharmacodynamic profile. To overcome the difficulties of the traditional shake flask method, arising from time - consuming and possibly incomplete phase separation, we have developed and validated a novel filter-based $\log D_{oct}$ assay (CAMDIS).

Results:

The use of a hydrophobic filter support for octanol enabled fast, convenient and complete phase separation. CAMDIS was applicable for compounds of all charge classes yielding highly reproducible $\log D_{oct}$ values in excellent agreement with the literature shake flask data (valid $\log D_{oct}$ range: -0.5 - maximal 4.2). The miniaturized assay requires correction for adsorption which will be discussed in *our accompanying manuscripts 2 and 3*.

Conclusion:

CAMDIS enables the precise measurement of $\log D_{oct}$ at lower sample consumption and reduced net manpower hours as compared to the traditional shake flask technique.

Significance:

CAMDIS bridges the gap between the requirement for high quality AND rapid $\log D_{oct}$ assessment and may thus aid the optimization of potential drug candidates in the earliest phase of the drug development process.

3.2 The Impact of Drug Adsorption to Microtiter Plates on the Accuracy of $LogD_{oct}$

Background:

Miniaturization and automation of high - throughput screening assays, such as CAMDIS, have created a situation where compound aggregation and adsorption to the labware (e.g. Teflon well plate) may remain undetected, but likely lead to experimental artifacts. Therefore, the impact of drug loss to a Teflon microtiter plate on the accuracy of $\log D_{oct}$ was studied.

Results:

Drug loss to Teflon manifests itself as underestimation in $\log D_{oct}$ i) for compounds with low affinity for octanol (hydrophilic) but a high affinity for Teflon (typical for planar drugs with many hydrogen bond donors, e.g. doxorubicin) and ii) for compounds precipitating during the time course of the distribution assay. Experimental errors could be minimized by increasing the drug concentration and/or the volume of octanol (applicable to the 1st case) or by recovering adsorbed drug with 2-propanol (applicable to the 2nd case). The validity of using 2-propanol as a desorbing agent will be demonstrated in *our accompanying manuscript 3*.

Conclusion:

Although lipophilic compounds are prone to adsorption to Teflon, accurate $\log D_{oct}$ values are obtained, provided that only one drug layer adsorbs to the Teflon surface. Then, the distribution equilibrium is shifted towards drug dissolved in the octanol phase and drug adsorption to the well plate can be neglected. In contrast, drug precipitation/aggregation in the well plate may lead to an underestimation of $\log D_{oct}$, which is the more pronounced the lower the lipophilicity of a compound.

Significance:

The identification of compounds with a high propensity for erroneous $\log D_{oct}$ values and the possibility to correct them provides higher data reliability, avoids misinterpretations, and thus helps guiding lead compound optimization in a reasonable way.

3.3 Drug Adsorption to Teflon and Excipient-Aided Drug Recovery

Background:

Non-specific binding of potential drug candidates to microtiter plates has recently been recognized as the source of experimental artifacts, but only scarce information is available for how to correct for adsorption. The proper choice of excipients (i.e. surfactants, cyclodextrines, organic solvents) for drug recovery was investigated for a structurally diverse dataset and the compatibility of these excipients for data analysis with HPLC-ESI/MS was tested.

Results:

Micellar concentrations of SDS (anionic) enabled the recovery of all adsorbent drugs whereas Brij 35 (non-ionic) and CTAB (cationic) were less efficient for the bases chlorpromazine and doxorubicin. Almost complete recovery except for doxorubicin (required acidification) was achieved by addition of 2,6-di-O-methyl-β-cyclodextrin and organic solvents (acetonitrile, DMSO, 2-propanol). All excipients, except for 2-propanol, caused ion suppression in ESI - MS.

Conclusions:

The superior detergency of SDS for cationic drugs indicates that electrostatic repulsion between surfactant residing at the Teflon surface and mixed SDS-drug micelles free in solution plays an important role in excipient-aided drug recovery. We recommend using SDS if UV is the selected analytical technique while 2-propanol is preferable for ESI-MS.

Significance:

The proposed guideline for excipient-aided drug recovery may be applied for the correction of potentially erroneous results in high-throughput assays to avoid misinterpretations and achieve higher certainty in the data of interest.

3.4 Evaluation and Management of Excipient-Related Matrix Effects in HPLC - ESI/MS Analysis of PAMPA-Permeability

Background:

The presence of solubilizers and model formulation agents in the parallel artificial membrane permeability assay (PAMPA) may suppress the ionization efficiency in ESI-MS (matrix effect) resulting in reduced analyte sensitivity and possibly incorrect outcome measures. Therefore we tested whether the excipients commonly used in PAMPA cause matrix effects in HPLC - ESI/MS and if so, to what extent this affects the accuracy of observed permeabilities. In addition, we evaluated strategies to manage excipient-related matrix effects.

Results:

Pronounced matrix effects were observed for excipients favoring the air-water interface (glycocholic acid, FaSSIF/FeSSIF media), forming multiply-charged ions (hydroxypropyl-β-cyclodextrin) and/or carrying a proton acceptor in the form of nitrogen (1 - methyl - 2 - pyrrolidone). Propylene glycol showed the weakest matrix effect. The presence of ion-suppressing solubilizers (tested here: glycocholic acid) in the PAMPA donor invalidated mass balancing and disregard thereof resulted in overestimated permeability.

Conclusion

Excipients distributed non-uniformly in the PAMPA donor and acceptor during the permeation process should be adjusted to the same level before concentration analysis with HPLC-MS. If the use of excipients aims to increase compound solubility rather than to investigate a specific excipient-effect, replacement of the frequently used glycocholic acid by propylene glycol is suggested for the sake of better sensitivity.

Significance

Management of excipient-related matrix effects in PAMPA is crucial when using HPLC - ESI/MS as an alternative detection mode to UV. The proposed strategies may aid in the generation of accurate outcome measures, i.e. permeability and membrane retention.

3.5 ^{31}P and ^{1}H-NMR Studies on the Molecular Organization of Lipids in the PAMPA Permeation Barrier

Background:

The structure forming the permeation barrier in PAMPA (lipid-dodecane-filter system) has never been characterized experimentally. To shed light in the black box we investigated the molecular organization of lipids in the PAMPA barrier by means different nuclear magnetic resonance (NMR) techniques. To deduce the relationship between barrier structure and function we also measured PAMPA-barrier/water distribution coefficient for structurally diverse drugs as a function of drug and lipid concentration.

Results:

Dodecane in large excess over lipid induced the lamellar-to-isotropic phase transition, irrespective of whether or not a filter (PVDF) support was used. The isotropic phase corresponded to lipid aggregates (diameter approximately 5 nm). The PAMPA-barrier/buffer distribution coefficients increased with a rise in the lipid content, a decrease of drug concentration (only for amphiphilic cationic drugs) and, roughly, a rise in the octanol/water partition coefficient.

Conclusion:

The data suggests that the binding to and, in turn, the permeation across the PAMPA barrier is facilitated by the presence of reversed egg lecithin micelles which act as carriers rather than as barriers for the transport of particularly cationic amphiphilic drugs. This distinguishes PAMPA from biological membranes. The size cutoff, arising from attenuated insertion into densely packed biological membranes, is not observed in PAMPA.

Significance

Knowledge about the organization of the PAMPA barrier may aid in the interpretation of the relevant assay read-outs, i.e. passive permeability and membrane retention. The scopes but also the limitations of using a non-bilayer system as a model for a biological bilayer membrane should always be kept in mind in order to allow for a rational optimization of potential drug candidates.

3.6 Evaluation of a Novel Lipid Membrane Binding Assay (LIMBA) for the Assessment of Brain Tissue Binding

Background:

Existing methods for estimating the unbound fraction of drug in brain ($f_{u,brain}$) yield sufficiently accurate results but low throughput (brain slice uptake technique) and high tissue consumption (homogenate dialysis) hamper their application for earlyADME profiling. Therefore we have developed a miniaturized Lipid Membrane Binding Assay (LIMBA) based on the immobilization of minute amounts of brain homogenate (1.2 µL) on a filter support which allows for assessing brain tissue/water distribution coefficients ($\log D_{brain}$) in a high-throughput manner. In particular, we were interested whether $\log D_{brain}$ is in better agreement with $f_{u,brain}$ as compared to $\log D_{oct}$, $\log P$ and the fraction of drug retained in the permeation barrier of the Parallel Artificial Membrane Permeability Assay ($\log D_{PAMPA}$).

Results:

The classical lipophilicity scales, $\log D_{oct}$ and $\log P$, were inappropriate in describing $f_{u,brain}$ at a sufficient statistical certainty level (r^2 ($\log D_{oct}$) = 0.23, r^2($\log P$) = 0.49). Provided that PAMPA was optimized in terms of lipid composition and nature of the buffer, the membrane fraction was satisfactorily predictive for $f_{u,brain}$ (r^2 = 0.61). Using LIMBA the best agreement with $f_{u,brain}$ was obtained (r^2 = 0.74).

Conclusion:

LIMBA allows estimating drug distribution into brain tissue with sufficient accuracy and at considerably reduced tissue consumption and at higher throughput as compared to the homogenate dialysis method.

Significance

LIMBA may aid in the selection of lead compounds with an appropriate pharmacokinetic profile and moreover it can be used to estimate unbound drug concentrations in brain. In addition there is great potential to estimate the non-specific binding or radioligands in Positron Emission Tomography (*accompanying manuscript 7*).

3.7 Label-Free Assay for the Assessment of Non-specific Binding of Positron Emission Tomography Tracer Candidates

Background:

High non-specific binding (NSB) of radiotracers to membranes and non-target proteins affects the accuracy with which receptor occupancy at the target site can be measured by means of positron emission tomography (PET). To enhance the confidence in the likely development success of a PET tracer it is desirable to estimate NSB as early as possible, preferably before labeling of the ligand. Since neither $\log D_{oct}$ nor $\log P$ is predictive for NSB, and homogenate dialysis is hampered by low throughput and high tissue consumption, we validated the ability of the novel high-throughput tissue binding assay, LIMBA, to predict the NSB of potential PET tracers.

Results:

In summary, we could show that brain tissue / water distribution coefficients ($\log D_{brain}$) measured with LIMBA are highly predictive for NSB observed by *in vitro* autoradiography. Moreover, $\log D_{brain}$ is a good surrogate for NSB in PET, provided that non - Pgp-substrates are concerned.

Conclusion:

Since LIMBA works without labeling and the tissue consumption per compound is very low (1.2 µL), estimates of NSB can be obtained with considerably higher throughput than with the homogenate dialysis technique or with autoradiography.

Significance

LIMBA may accelerate the selection of PET tracers with appropriate NSB characteristics and the rejection of compounds with undesirable high background noise. Ultimately, this may enhance the confidence in the likely development success of a PET tracer.

4 Manuscripts

4.1 Carrier Mediated Distribution System (CAMDIS): A New Approach for the Measurement of Octanol/Water Distribution Coefficients

Frauke Assmus/Bjoern Wagner, Holger Fischer, Manfred Kansy, Anna Seelig

Author's Contributions:

Frauke Assmus	• Performing experiments • Development of the model for interfacial drug adsorption and experimental verification thereof • Writing the manuscript
Björn Wagner	• Idea of using filter plates for the facilitated measurement of $\log D_{oct}$ • Performing experiments • Valuable discussions and reviewing the manuscript
Manfred Kansy	• Design of the DIFI tubes
Holger Fischer	• Supervision of the work • Idea of using DIFI tubes as filter support for octanol • Valuable discussions and reviewing the manuscript
Anna Seelig	• Supervison of the work • Valuable discussions • Support in writing the manuscript and reviewing the manuscript

ABSTRACT

We present an improved method for the fast and reliable measurement of octanol/water distribution coefficients ($\log D_{oct}$). The new assay, referred to as carrier - mediated distribution system (CAMDIS), utilizes a filter support for octanol which facilitates the phase separation from water. This overcomes inconveniences of the traditional shake flask method, i.e. laborious phase separation and propensity to emulsion formation. A guideline for the best practice of CAMDIS is derived describing a strategy to manage drug adsorption at the filter-supported octanol/buffer interface. We validated the assay on a set of 52 structurally diverse drugs with known shake flask $\log D_{oct}$ values. Excellent agreement with literature data ($r^2 = 0.996$, standard error of estimate, SEE = 0.111), high reproducibility (standard deviation, SD < 0.1 $\log D_{oct}$ units), minimal sample consumption (10 µL of 100 µM DMSO stock solution) and a broad analytical range ($\log D_{oct}$ range = - 0.5 - 4.2) make CAMDIS a valuable tool for the high - throughput assessment of $\log D_{oct}$.

KEYWORDS

Octanol/water distribution coefficient, Octanol/water partition coefficient, Filter support, CAMDIS, pH dependence, Concentration dependence, Drug Adsorption to Plastic.

1. Introduction

Lipophilicity has emerged as one of the key physicochemical parameters in the drug development process to predict a compound's ADME/Tox profile [1, 2] and its likely biological activity [1, 3-5]. The most frequently used lipophilicity parameter is the octanol/water distribution coefficient ($\log D_{oct}$) or, when referring to non - ionized species, the octanol/water partition coefficient ($\log P_{oct}$). This is mainly due to the vast amount of published $\log P_{oct}$ ($\log D_{oct}$) data [6], the good interlaboratory reproducibility and, as a result, the availability of a growing number of $\log P_{oct}$ prediction packages [7, 8]. In the light of the non - trivial task to cope with the presence of charges, ion - pairing, conformational changes and the lack of parameterization for certain fragments, it is not surprising that *in silico* predictions can only give an initial estimate of $\log D_{oct}$ [9], and as a consequence, the requirement for accurately measured $\log D_{oct}$ values is still high.

The traditional approach to determine $\log D_{oct}$ values using the shake flask technique is tedious, wasteful [10] and, in turn, cannot accomplish the demand for high - throughput screening. Although the concept of shaking and separating two immiscible solvents in order to analyze the concentration ratio of a distributed solute seems simple, phase separation is a time consuming step and, more importantly, is prone to artifacts. Amphiphilic compounds tend to enrich at the interface between two immiscible solvents and to form stable emulsions [6, 11] which sometimes cannot be dispersed by centrifugation. In addition, compounds with high lipophilicity will preferentially distribute into the octanol phase while leaving very small amounts in the aqueous phase. Even minimal contamination of the aqueous phase with octanol will then have a significant effect on the accuracy of $\log D_{oct}$ [12].

Several strategies have been proposed to overcome the difficulties of phase separation and to translate the manual shake flask technique into an automated 96 - well plate format. One example is the frozen water phase method [12]. It involves freezing the aqueous phase in liquid nitrogen and removing liquid octanol from the top. Considering the similar freezing points of water and octanol (0 °C vs. -15 °C [13]), the possible time window for the incubation with liquid nitrogen is quite narrow. Moreover, high-throughput automation is impaired by additional washing steps required to remove octanol remaining on the frozen aqueous phase [12]. Another strategy is to directly inject the liquid into an LC or LC/MS system without separating the phases in advance [14]. Therefore specially developed HPLC

injection programs have been advocated based on the repellant effect of a water plug aspirated before piercing through the octanol layer. However, accumulation of sparingly soluble drugs at the capillary tip weakens the repellant effect and may falsify the results [15].

The inconveniences associated with the conventional or modified shake flask assays have resulted in the development of several other direct or indirect techniques for the assessment of lipophilicity. Despite distinct benefits, none of the alternative methods is without difficulties [16, 17] and the classical shake flask technique is still considered the gold standard. Alternative methods that make use of octanol as a bulk phase are not yet amenable to high - throughput (dialysis tubing [18]) and/or are only applicable to compounds with ionizable groups (filter probe [19], potentiometric method [20]). Concerning the widely used chromatographic methods, disadvantages such as the need for external calibration, restricted column lifetime, nonlinear co - solvent behavior and limited applicability range are well known [10, 16, 21, 22].

An apparatus for the measurement of octanol/water distribution coefficients based on the immobilization of octanol on a filter probe has been proposed by Cantwell [23] and was later improved by Tomlinson [24]. Unfortunately, the apparatus was large scale, and therefore not meeting the demands for high - throughput analysis. In the framework of a permeability assessment across an artificial lipid - mimicking systems [25], Camenisch immobilized octanol on a filter (hydrophobic PVDF). A miniaturized adaptation of the system named PAMPA (Parallel Artificial Membrane Permeability Assay) was later used by Faller to derive $\log P_{oct}$ by estimating the effect of membrane (octanol) retention on the apparent permeability of the neutral species $\log P_{aN}$ [26]. Unfortunately, the PAMPA - octanol assay suffers from reduced accuracy in the $\log P_{oct}$ range $0 - 2$ (the variation of $\log P_{aN}$ with $\log P_{oct}$ flattens [26]) and requires knowledge of the pK_a.

In the present study, we translated the idea of using a filter support for octanol into the development of a novel miniaturized high - throughput $\log D_{oct}$ assay, which will in the following be referred to as CArrier Mediated DIstribution System (CAMDIS [27]). The design of the plate as well as the setup of the assay is described in Fig. 1.

Fig. 1

Rather than relying on variations of permeability with $\log P_{oct}$, the design of CAMDIS was intended to directly measure a solute's concentration ratio in the octanol/water system. In this

sense, CAMDIS retains the straightforwardness of the traditional shake flask method as a direct lipophilicity measure while facilitating time intensive phase separation. As octanol support, we used a PVDF filter attached to the bottom of the customized and commercially available Diffusion - Filtration (DIFI) tubes (Fig. 1 A [28]). The filter surface and the core (PVDF fibers) may constitute an additional compartment, at which an amphiphilic compound may adsorb and to which it may penetrate, respectively. Therefore we investigated under which experimental conditions adsorption of drug at/into the filter becomes negligible compared to the distribution into octanol. To provide an assay yielding accurate data despite miniaturization we assessed the optimal equilibration time, phase volume ratios, drug concentrations and calibration procedure.

2. Theoretical Basis

The octanol/water distribution coefficient is defined as the equilibrium ratio of the drug concentration in octanol, C_{oct}^{eq} , and in the aqueous phase, C_{aq}^{eq} , according to [21]:

$$\log D_{oct} = \log\left(C_{oct}^{eq} / C_{aq}^{eq}\right). \quad (1)$$

The most straightforward way to obtain the distribution ratio is the direct concentration analysis in both solvents. Unfortunately, very lipophilic compounds demand the use of minute amounts of octanol (e.g. 1 µL) which are inaccessible for direct analysis [11]. Even if sufficient octanol is recovered, possible shifts in the absorption spectra, ion suppression in mass spectrometry, difficulties in liquid handling and evaporative loss still complicate the analysis of both phases. Therefore, solute concentrations in octanol are usually obtained from mass balance, i.e. from the difference between initial, C_{aq}^{0}, and equilibrium aqueous drug concentrations, C_{aq}^{eq}. In the following, mass - balance derived distribution coefficients are defined as $\log D_{oct}^{'}$ whereas distribution coefficients relying on the analysis of both phases (eq.1) are indicated as $\log D_{oct}$. As a direct measure, $\log D_{oct}$ is not affected by the presence of the PDVF filter used in CAMDIS and will therefore be considered the gold standard. If, however, only the aqueous phase is assayed, any amount of solute at the filter or at the filter - supported interface, n_{fi}^{eq}, would wrongly be attributed to the octanol phase. Overestimating the solute concentration in octanol by n_{fi}^{eq} may manifest itself as an erroneously high $\log D_{oct}^{'}$, according to (for derivation of eq. 2 see Supporting Information):

$$\log D_{oct}^{'} = \log\left(\frac{\left(C_{aq}^{0} - C_{aq}^{eq}\right)\cdot V_{aq} + n_{fi}^{eq}}{C_{aq}^{eq}\cdot V_{oct}}\right), \quad (2)$$

where V_{aq} and V_{oct} are the volumes of the aqueous and the octanol phase, respectively. In the ideal case, solute adsorption to filter becomes negligible compared to the distribution into octanol ($\left(C_{aq}^{0} - C_{aq}^{eq}\right)\cdot V_{aq} >> n_{fi}^{eq}$) and eq.2 simplifies to:

$$\log D'_{oct} \approx \log D_{oct} = \log\left(\frac{\left(C^0_{aq} - C^{eq}_{aq}\right)\cdot V_{aq}}{C^{eq}_{aq}\cdot V_{oct}}\right). \quad (3)$$

Experimental conditions where the adsorption to the filter can be neglected are highly desirable because in eq. 3 all parameters are either known (V_{aq}, V_{oct}) or can easily be measured (C^0_{aq}, C^{eq}_{aq}). A viable option to increase the amount of drug in octanol in order to outcompete the filter - adsorbed drug is to increase the volume of octanol ($C^0_{aq} - C^{eq}_{aq}$ increases). If saturable binding at the filter occurs, a rise of the total drug concentration, C^0_{aq}, will likewise diminish the influence of the filter and of n^{eq}_{fi}.

An estimate of n^{eq}_{fi} and the true $\log D_{oct}$ can be obtained by measuring the $\log D'_{oct}$ - C^0_{aq} profiles and fitting eq. 4 to the experimental data (see Supporting Information for derivation of eq. 4):

$$\log D'_{oct} = \log\left(\frac{C^0_{aq} - \left(C^0_{aq} / \left(10^{\log D_{oct}}\cdot V_{oct}/V_{aq} + 1\right)\right)\cdot V_{aq} + n^{eq}_{fi}}{C^0_{aq} / (10^{\log D_{oct}}\cdot V_{oct}/V_{aq} + 1)\cdot V_{oct}}\right). \quad (4)$$

3. Materials and Methods

3.1. Drugs and Chemicals

Most of the drugs, chemicals and solutes were obtained from commercial sources (Acros, Aldrich, Alexis, Dayang, Fluka, Gardena, Merck, Molekula, Sigma, Sirius) and were used as received. Amitriptyline, chloramphenical, desipramine · HCl, dexamethasone, diazepam, fentanyl, meprobamate, mesoridazine, metronidazole, prednisolone and primidone were available through our in - house Compound Depository Group as proprietary compounds. Formic acid, water and acetonitril were supplied from Merck (Darmstadt, Germany) and were of HPLC - grade.

3.2. Determination of Distribution Coefficients (n - Octanol/Buffer) with CAMDIS

3.2.1. Assay Protocol (Validation Setup)

Prior to the distribution experiment, octanol and phosphate buffer (25 mM) were mutually saturated at room temperature. Drug compounds were introduced into the pre - saturated phosphate buffer as DMSO stock solutions (10 mM) resulting in a 100 µM sample solution (1200 µL, DMSO content 1 %, v/v). The solutions were filtered (Millipore Multiscreen Filter Plate, MDRLN 0410) into a 96 - deep well receiver plate (Nunc, 278752) and diluted with pre - saturated phosphate buffer (200 µL). The secondary dilution was performed to minimize the risk of delayed drug precipitation during the distribution experiment. Aliquots of the filtrate (V_{aq} = 150 µL) were transferred into an in - house made Teflon plate and covered with the DIFI tubes (Weidmann Plastics Technology AG, Rapperswill, Switzerland, 23358) which were pre - coated with octanol (V_{oct} = 1µL and 15µL, respectively; n = 3 for each volume). Use of an automated liquid handling system (Beckmann Coulter, Bio RAPTER FRD, Microfluidic workstation) permitted fast, reproducible and accurate dispensing of octanol (SD < 3 %). The assay kit was sealed and allowed to shake at room temperature until distribution equilibrium was achieved (16 - 22 h). After disassembly of the DIFI tubes from top of the Teflon plate, the equilibrium drug concentrations in the aqueous phase, C_{aq}^{eq} , were analyzed with HPLC - UV/MS. In parallel, a reference experiment was carried out in the same plate but without octanol to obtain the initial aqueous drug concentrations, C_{aq}^{o}. One of the reference wells contained 1 : 5 diluted filtrate to provide a calibration check. Unless otherwise stated, the equilibrium drug concentrations in octanol, C_{oct}^{eq} , were not measured

directly but obtained by mass balance. The apparent distribution coefficient, $\log D'_{oct}$, was then calculated according to eq. 3. In some cases, octanol residing in the DIFI tubes was analyzed directly after centrifugation (1000 rpm, 5 min) of the octanol phase into a PCR receiver plate (Eppendorf, $\log D_{oct}$). Due to the fact, that all UV measurements were carried out under the same conditions, the concentration terms were replaced by the analyte responses in UV or MS. The commonly non - linear mass response was accounted for by performing an internal calibration series (see Section 3.6).

3.2.2. Time- and Concentration Dependence of Distribution Coefficients

The time- and concentration dependencies at pH 7.4 were performed in octanol - saturated buffer (50 mM Tris/114 mM NaCl, pH 7.4, we only decided after a perusal of the published shake flask data, preferentially obtained in phosphate buffer, to change the buffer system to phosphate for the final assay validation). The concentration dependent measurements at different pH values were performed in octanol - saturated sodium formiate (pH 3; 4), sodium acetate (pH 5), BisTris (pH 6;7), Tris (pH 8;9) and universal buffer (Sirius, pH 10), each at constant ionic strength (I = 0.05 M). The analyte - spiked aqueous solutions were manually prepared in glass vials by diluting a DMSO stock solution with octanol - saturated assay buffer to the desired solute concentration, thereby keeping the DMSO content constant (1 %, v/v). The time dependent measurements were performed at 100 µM rolipram. The concentration dependence at pH 7.4 was obtained at 5; 12.5; 25; 100; 200; 300 µM using rolipram, buspiron and propranolol as test analytes. The $\log D_{oct}$ ($\log D'_{oct}$) - pH profiles of zolpidem were obtained at 12.5 µM and 100 µM, respectively. The time on the shaker was 6 h for the 1 µL setup and min. 24 h for the 15 µL setup (achievement of equilibrium was verified). Only UV data was used for concentration analysis. At least 3 measurements were performed for each incubation time, concentration and pH and mean $\log D_{oct}$ and $\log D'_{oct}$ values were reported.

3.3. Determination of Distribution Coefficients with the Shake Flask Method

Octanol (1 µL and 15 µL) was directly delivered into the assay plate (96 - well PCR plate) using the abovementioned Beckman dispenser. Afterwards, octanol - saturated assay buffer spiked with analyte was distributed on top of the octanol layer. Concentrations and phase volumes were matching the experimental conditions in CAMDIS. The PCR plate was sealed and inversed 100 times followed by overnight shaking at room temperature. After

centrifugation of the PCR plate (1500 rpm, 20 min, Eppendorf, Centrifuge 5810R), the aqueous phase was directly injected onto the HPLC. The injection needle was programmed to pierce through the octanol layer and aspire only the aqueous phase. A contamination of the aqueous phase by octanol cannot be excluded. However, the compounds analysed by the shake flask method were of intermediate lipophilicity for which contamination with octanol should play only a minor role.

3.4. Detection of Precipitation and of Drug Adsorption to the Well Plate

Test compounds (olanzapine, chlorpromazine, Ro - 1) were dissolved in DMSO (50 mM) and 11 consecutive dilutions in DMSO were prepared (0.1 mM - 50 mM). An aliquot of each stock solution (1.5 µL) was transferred into an in - house made Teflon plate and diluted 1 : 100 with octanol - saturated buffer (50 mM Tris, 114 mM NaCl, pH 7.4) resulting in 1 - 500 µM analyte solutions. The Teflon plate was sealed and allowed to shake for 18 h at room temperature. Then, the sample solutions were injected onto an HPLC system and the peak areas were recorded at appropriate wavelength (n = 2). Deviation from a straight line when plotting the absorbance vs. initial aqueous drug concentrations was used to detect drug adsorption to the well plate and drug precipitation.

3.5. Selection of the Validation Dataset

A set of 52 drugs with known shake flask $\log D_{oct}$ values was compiled from literature in order to validate CAMDIS. Starting from a search in the MedChem Database, all original references were carefully inspected and only values retrieved at ambient temperature (20 - 25°C) with the traditional or a miniaturized shake flask method were included. Data from adapted shake flask procedures (interface extraction [29], three - phase titration [30]) was not considered. With respect to ionizable compounds, only $\log D_{oct}$ values obtained at pH 7.4 were included, while no pH constraint was applied to neutral compounds. Generally, only distribution coefficients measured in the octanol - phosphate - buffer system were included. Even if not always stated, we assumed that the two phases were mutually saturated. However, for some compounds we encountered high variability among literature data and in these cases we gave preference to reports leaving no uncertainties about phase saturation. Entries in the MedChem Database of unpublished data (‘private communication’) were only included when confirmed to be of high quality ($\log P_{oct}$ - star value). However, when violating one of the abovementioned criteria, the value was neglected. For validation, the

average literature value was taken and compared with the average $\log D'_{oct}$ value derived from CAMDIS (n = 3).

3.6. HPLC/MS Instrumentation and Chromatographic Conditions

Drug concentrations were quantified using an Agilent 1200 HPLC - MS system (Agilent Technologies, CA, USA) equipped with a degasser, auto - sampler, column oven, binary pump, DAD detector and API single quadrupole mass spectrometer (Agilent 6140). If not otherwise mentioned, a 5 µL aliquot of each sample was injected onto a Kinetex 2.6 µm, 2.1 x 50 mm analytical column (Phenomenex, Germany) operated at 60 °C. The mobile phase consisted of A (water) and B (acetonitril), both containing 0.1 % (V/V) formic acid. The gradient elution on the Agilent 1200 system was performed as follows: initial 40 % B (1.5 mL/min), 0.1 - 0.15 min 40 % B (linear decrease of the flow rate to 1 mL/min), 0.15 - 0.35 min linear gradient from 40 % B to 95 % B (1 mL/min), 0.35 min - 0.9 min 95 % B (1 mL/min). After passing the DAD detector, the eluent was introduced into the electrospray interface maintaining the following source settings: capillary voltage + 4 kV, drying gas flow (N_2) 13 L/min, drying gas temperature 350 °C, nebulizer pressure 60psi, dwell time 50 ms. Electrospray was initiated with a time delay of 0.4 min to prevent extensive entry of DMSO and buffer salts into the API source. The integral of the pseudo - molecular ion intensity, $[M+H]^+$, was aquired in single reaction monitoring mode (SRM). Internal calibration for MS data analysis was accomplished by injection of 1, 3, and 5 µL of the sample solution. If UV sensitivity was sufficient, peak areas at appropriate wavelength were used for the calculation of $\log D'_{oct}$.

4. Results

4.1. Assay Development

Assessment of the optimal assay conditions was an essential element for the successful validation of CAMDIS on an extended dataset. For the assay development we selected compounds with moderate lipophilicity (Fig. 2) to grant the accessibility of $\log D_{oct}$ ($\log D'_{oct}$) values with two phase volume ratios (V_{aq} was kept constant; V_{oct} = 1 µL and 15 µL). Each drug was measured well below its critical micellar concentration, CMC_D (assessed by surface activity measurements [31], data not shown).

Fig. 2

4.1.1. Equilibration Time

For evaluating the optimal shaking time, rolipram (Fig. 2) was selected as a test compound of intermediate lipophilicity. We used an in - house shake flask $\log D'_{oct}$ value obtained after 100 inversions and overnight shaking to provide a reference. Fig. 3 shows that distribution equilibrium was achieved after 6 h in the 1 µL octanol setup and after 16 h in the 15 µL octanol setup. After this time, CAMDIS $\log D'_{oct}$ values were comparable with the reference shake flask values. The slight decrease of 0.2 $\log D'_{oct}$ units after 16 h shaking in the 1 µL CAMDIS setup can be traced back to the preceding evaporation of octanol (approximately 0.2 µL). From a practical point of view, overnight shaking (16 - 22 h) is most feasible in the laboratory routine because it allows for the assessment of CAMDIS $\log D'_{oct}$ at sufficient accuracy for both phase volume ratios.

Fig. 3

4.1.2. Optimal Drug Concentrations and Phase Volume Ratios

As indicated in the Theoretical Section, the validity of estimating distribution coefficients with the simplified mass balance equation (eq. 3) heavily depends on the experimental

conditions. In order to retrieve the boundary conditions at which a possible adsorption to the filter can be neglected and the 'true' $\log D_{oct}$ is approximated (eq. 3), we varied two key parameters in CAMDIS: i) the phase volume ratio (V_{oct} = 15 µL and 1µL; V_{aq} = 130 µL) and ii) the initial aqueous drug concentration (C_{aq}^{0} = 12.5 µM and100 µM). As a reference, we used the traditional shake flask $\log D_{oct}^{'}$ values and attributed potential discrepancies between CAMDIS and shake flask data to the presence of the filter (all other parameters like buffer, drug concentrations, phase volume ratios etc. were identical). In addition, we conducted CAMDIS at V_{oct} = 15 µL and both, the octanol and the buffer phase, were assayed for the distributed drug. We consider these $\log D_{oct}$ values as the 'true' values (gold standard) because assumptions of mass balance were not necessary and adsorption of compounds to the filter can be neglected. Therefore, the $\log D_{oct}$ values can be used as a reference to prove the accuracy of the $\log D_{oct}^{'}$ values (CAMDIS and shake flask) that were derived from analysis of the initial and the equilibrium aqueous concentrations. To render the study meaningful for a wide range of lipophilicity and different ionization states, we measured the distribution coefficients for a weak base, zolpidem, (pK_a = 6.47), a weak acid, phenytoin (pK_a = 8.18), and a neutral compound, rolipram, over a wide pH range (pH 3 - 10). The investigated lipophilicity range is determined by the intrinsic lipophilicity of the non-ionized drug, $\log P_{oct}$, reduced by the fraction of ionized drug at a particular pH (see eq. S8 and S9 [9], Supporting Information).

Fig. 4 shows the fraction of the basic compound zolpidem in its non - ionized form (Fig. 4A) in association with the lipophilicity - pH profiles obtained from different setups: i) the 'true' CAMDIS $\log D_{oct}$ - pH profile (Fig. 4B), ii) the CAMDIS $\log D_{oct}^{'}$ - pH profile (Fig. 4C) and iii) the shake flask $\log D_{oct}^{'}$ - pH profile (Fig. 4D).

Fig. 4

Irrespective of which setup was used, the variation of distribution coefficients with C_{aq}^{0} or V_{oct} was minimal when the non - ionized species predominated (pH > pK_a). However, with a decrease in pH, mass - balance derived CAMDIS $\log D_{oct}^{'}$ values showed the following trend (Fig. 4C): Low concentrations and, particularly, low volumes of octanol resulted in an

overestimation of $\log D'_{oct}$ which reflects an additional drug adsorption to the filter. Ion pairing as a mechanism leading to higher $\log D'_{oct}$ values can be excluded, because the gold standard $\log D_{oct}$ (Fig. 4B) was independent of variations in drug concentration (the same buffer was used). The overestimation in CAMDIS $\log D'_{oct}$ (Fig. 4C) became the more pronounced the higher the ionization degree, paralleling the drop in lipophilicity. With respect to the shake flask profile, the same, but much less pronounced trend was observed at pH 3 (Fig. 4D). Because adsorption to the filter could be excluded, the erroneously high shake flask $\log D'_{oct}$ (pH 3) must be traced back to an enrichment of amphiphilic zolpidem at the octanol/buffer interface (see Discussion). A comparison of the mass balanced $\log D'_{oct}$ - pH profiles (CAMDIS, Fig. 4C; shake flask Fig. 4D) with the per - definition 'true' $\log D_{oct}$ - pH profiles (Fig. 4B) revealed agreement over the whole pH range when high drug concentrations (100 µM) in combination with high volumes of octanol (V_{oct} = 15 µL) were used. The example of $\log D'_{oct}$ at pH 4 shows that, with this optimal setup, excellent agreement of CAMDIS and shake flask data was achieved (Table 1).

Table 1

The CAMDIS $\log D'_{oct}$ - pH profiles for the acid, phenytoin, and the neutral compound, rolipram, are shown in Fig. 5A and Fig. 5B, respectively. In contrast to zolpidem, neither for phenytoin nor for rolipram a variation of $\log D'_{oct}$ with drug concentration was observed which indicates that no or only negligible adsorption to the filter occured. We confirmed this by comparing CAMDIS $\log D'_{oct}$ with shake flask $\log D'_{oct}$ values, for which perfect agreement was found (data not shown). Because no discrepancy in CAMDIS $\log D'_{oct}$ at different concentrations was observed for the most critical case, i.e. at 1 µL octanol, we did not perform the experiment with 15 µL octanol.

Fig. 5

4.1.3. Drug Adsorption to the Filter for Different Cationic Compounds

In the next step we tested whether i) adsorption of drug to the filter is a general trend for cationic compounds, ii) the resulting overestimation in $\log D'_{oct}$ relates to the degree of ionization, and iii) an increase of C^0_{aq} and/or V_{oct} may be used as a general strategy for avoiding an overestimation in $\log D'_{oct}$. For these purposes, we measured the CAMDIS $\log D'_{oct}$ values (pH 7.4) for structurally unrelated compounds with different ionization degrees and covered a wide concentration range (C^0_{aq} = 5 - 300 µM) and two phase volume ratios (V_{oct} = 1 µL and 15 µL, respectively).

Fig. 6A-C shows the C^0_{aq} - CAMDIS $\log D'_{oct}$ (pH 7.4) profiles for rolipram (non-charged, Fig. 6A), buspiron (61.9 % positive charge at pH 7.4, Fig. 6B) and propranolol (99.2 % positive charge at pH 7.4, Fig. 6C), given in the order of increasing positive ionization.

Fig. 6

As expected, the non - charged rolipram corresponded to the ideal case in which the $\log D'_{oct}$ was independent of variations in C^0_{aq} and V_{oct} (Fig. 6A). In contrast, the $\log D'_{oct}$ values of the bases, buspiron and propranolol, obtained with 1 µL octanol dropped exponentially with increasing drug concentration up to approximately 25 µM (buspiron, Fig. 6B) and 100 µM (propranolol, Fig. 6C), respectively, where a plateau was reached. The difference between $\log D'_{oct}$ at infinite dilution and infinite concentration (extrapolated) was higher for propranolol, which is also the compound with the higher ionization degree and the lower lipophilicity ($\Delta \log D'_{oct}$ 0.22 vs. $\Delta \log D'_{oct}$ 0.08 for buspiron). At propranolol concentrations exceeding 100 µM, the measured $\log D'_{oct}$ obtained with 1 µL octanol approached the $\log D'_{oct}$ derived with the 15 µL setup (Fig. 6C). We compared the CAMDIS $\log D'_{oct}$ values for propranolol (Fig. 6 C) with the corresponding shake flask $\log D'_{oct}$ values (Fig. 6 D) and an excellent agreement was observed at 15 µL octanol, and also at 1 µL octanol provided that C^0_{aq} > 100 µM. At lower drug concentrations, the CAMDIS $\log D'_{oct}$ values (1 µL setup) were overestimated with respect to the shake flask data corresponding to an enrichment of drug at the PVDF filter. Similarly, the shake flask data showed slight concentration dependence with the same trend towards overestimated $\log D'_{oct}$ values at lower concentrations. This again

points to the fact that interfacial enrichment also takes place in shake flask. In summary, positively charged compounds tend to adsorb to the PVDF filter or the filter - supported boundary layer leading to an overestimation of $\log D'_{oct}$, which can be counteracted by a rise in C^0_{aq} and/or V_{oct}.

4.1.4. Quantification of Drug Adsorption to the Filter

Estimates for the amount of drug at the solvent boundary layer, n^{eq}_{fi}, (with filter in CAMDIS and without filter in shake flask) were obtained by fitting eq. 4 to the experimental data in Fig. 6B - D. The number of layers at the filter, N_{layer}, could be assessed from n^{eq}_{fi} according to eq. S10 (Supporting Information). Table 2 shows a summary of the fitting parameters for each compound and setup including the correlation statistics as well as the estimates for the 'true' $\log D_{oct}$, n^{eq}_{fi} and N_{layer}.

Table 2

The fitted estimates for the 'true' $\log D_{oct}$ were in excellent agreement with the apparent (observed) $\log D'_{oct}$ values at high drug concentrations. We found approximately two layers of drug sticking to the filter, irrespective of which compound was used. A possible interpretation is that each side of the membrane, i.e. the side towards the aqueous and towards the octanol phase, respectively, was covered by one layer of drug. Assuming the same interfacial area, we gained a slightly smaller estimate for the number of layers (N_{layer} = 1.7) in the 15 µL shake flask experiment. Only approx. $1/5^{th}$ of this estimate was found for the 1 µL shake flask setup. The simple reason therefore is that due to the small volume of octanol, which is not forced to spread throughout the filter area, the contact area with the buffer phase was only approx. $1/5^{th}$ of the filter area. The n^{eq}_{fi} estimates in shake flask assay were less precise than in CAMDIS due to less pronounced concentration dependence of $\log D'_{oct}$.

4.1.5. Diagnosis and Handling of Precipitation and Drug Adsorption to the Well Plate

A simple proof of whether precipitation or drug adsorption to the well plate occurs during the assay time can be gained from a calibration check. Fig. 7 shows the calibration curves for test solutions of olanzapine (Fig. 7A), chlorpromazine (Fig. 7B) and a Roche compound (Fig. 7C)

obtained after 18 h storage in a Teflon plate (the total drug concentration ranged from 1 - 100 µM).

Fig. 7

Olanzapine is an example of the ideal case where a plot of UV response vs. drug concentration yielded a straight line indicating that neither drug adsorption to the well plate nor precipitation occurred (Fig. 7A). In contrast, the increase (chlorpromazine, Fig. 7B) and the decrease (Ro - 1, Fig. 7C) in analyte response at high drug concentrations were clear indicators of saturable plastic sorption and drug precipitation, respectively. Within the framework of a HT $\log D_{oct}$ assay, it is impractical to obtain a complete calibration curve. However, a two - point check with the initial aqueous drug solution (C_{aq}^{0} = 100 µM, reference 1) and a 1 : 5 dilution thereof (reference 2) is feasible. Both should be treated in the same way as the aqueous solutions used for the distribution experiment, however, without addition of octanol. When the linearly extrapolated 1 : 5 dilution yields a predicted UV response above (below) that observed with the 100 µM reference, saturable drug adsorption to the well plate (precipitation) occurs (like in Fig. 7 B, C, respectively). Drug precipitation occurs most likely in the reference experiment because the concentration in the aqueous phase is not reduced by the presence of octanol. In contrast, adsorption to the well plate plays a major role in the distribution experiment (with octanol) because saturation of the Teflon surface in the reference might be achieved.

4.1.6. Guideline for CAMDIS

The implications drawn from the calibration check and the filter - related adsorption are summarized in the flow chart in Fig. 8. It is intended as guideline to avoid artifacts possibly arising when the calculation of distribution coefficients relies on mass balance (eq.3).

Fig. 8

For high-throughput purposes, we recommend performing measurements generally at high initial drug concentrations (C_{aq}^{0} =100 µM) and at two phase volume ratios (V_{oct} = 15 µL and 1 µL; V_{aq} = 150 µL). To yield the initial aqueous drug concentration, C_{aq}^{0} , two aqueous drug

solutions without octanol should be prepared, one at C^0_{aq} =100 µM (reference 1) and a 1:5 dilution thereof ($C^0_{aq,1:5}$ =20 µM, reference 2).

The actual analysis should start with i) the calibration check: If neither aggregation/precipitation nor sorption to the well plate occurs, reference 1(100 µM) and the extrapolated value of reference 2 (5*20 µM) should yield the same value, with the average of it reflecting C^0_{aq}. In case of precipitation (reference 1(100 µM) < 5*reference 2(20 µM) it is evident that the extrapolated UV response of the 20 µM reference should be used as a measure of C^0_{aq}. In contrast, when saturable adsorption to the well plate occurs (reference 1(100 µM) > 5*reference 2(20 µM)), we recommend considering the undiluted 100 µM reference as C^0_{aq} . Although the violation in the mass balance equation due to drug adsorption to the well plate cannot be corrected in this way, the error in $\log D'_{oct}$ is in most cases negligible. Experimental evidence will be published (*accompanying manuscript 2*).

ii) After defining which reference to use, the $\log D'_{oct}$ values obtained with 1 µL and 15 µL octanol should be compared. Anionic and electrically neutral compounds do not adsorb to Teflon and therefore the $\log D'_{oct}$ values obtained from the two setups should agree. For cationic compounds, overestimation in $\log D'_{oct}$ due to filter adsorption was observed ($\log D'_{oct}$(1µL) > $\log D'_{oct}$(15µL). To correct for adsorption, it is not only essential to perform measurements at high initial drug concentrations (100 µM); in addition, the $\log D'_{oct}$ for hydrophilic ($\log D_{oct}$ < 2.5), cationic compounds should be estimated from the 15 µL octanol setup. For very lipophilic compounds ($\log D_{oct}$ > 2.5), low volumes of octanol (1 µL) are advisable because otherwise hardly any drug is left in the aqueous phase for concentration analysis. The solute dissolved in octanol will in case of lipophilic drugs be much higher than the solute bound by the filter yielding still valid results for $\log D'_{oct}$ (for exact range see Discussion).

4.2. Assay Validation

A set of 52 drugs with known shake flask $\log D_{oct}$ (pH 7.4) values was compiled from literature in order to validate the novel CAMDIS assay. We applied stringent selection criteria to the literature reports (see Section 3.5) and entries in the Pomona College MedChem Database to ensure the highest possible consistency among the data. As an

additional quality parameter we calculated the standard deviation across the various literature reports. The standard deviation was still considerable for some compounds and not linked to the magnitude of $\log D_{oct}$. The final dataset was structurally diverse and covered a broad range of physicochemical properties (Table 3).

Table 3

All compounds along with their literature $\log D'_{oct}$ values, corresponding original literature references and measured CAMDIS $\log D'_{oct}$ values are listed in Table 4.

Table 4

We retrieved the CAMDIS $\log D'_{oct}$ values by strictly following the flow chart in Fig. 8. Compounds which showed strong signs of precipitation (astemizole, felodipine, ketoconazole, loratadine) were excluded from the dataset. Three drugs, notably only phenothiazines (*values in Table 4), adsorbed to the Teflon well plate but were still considered in the correlation statistics. The standard deviation among the CAMDIS data was generally very low (SD < 0.1 $\log D'_{oct}$ units). Fig. 9A shows the correlation line of literature shake flask vs. the CAMDIS log D_{oct}' values yielding the following statistics:

Shake flask $\log D_{oct}$ (or $\log D'_{oct}$) = 0.960 * CAMDIS $\log D'_{oct}$ +0.025 (12)

r^2=0.996, SEE 0.111, n=52

The slope close to 1 and the intercept close to 0 indicate excellent correlation statistics which show that the classical shake flask method and the novel CAMDIS method are directly comparable. An inspection of the residuals plot (Fig. 9B) indicates a generally low error in $\log D'_{oct}$ (residual - 0.245 – 0.23). A slight trend towards underestimation of hydrophilic compounds ($\log D'_{oct}$ < 0.5) and overestimation of lipophilic compounds ($\log D'_{oct}$ < 1.5) was observable (see Discussion). No such general trend in residuals is evident with respect to different charge classes.

5. Discussion

To overcome difficulties of the traditional shake flask method arising from time - consuming and possibly incomplete phase separation, we have developed and validated a novel approach (CAMDIS) to measure octanol/water distribution coefficients in a high - throughput manner. The assay is based on the immobilization of octanol on a filter support which is fixed at the bottom of our in - house developed DIFI tubes [27]. A sandwich with the buffer plate can be easily assembled and disassembled, enabling concentration analysis of the distributed solute in one or both phases. The implications of using a filter support for throughput, accuracy and applicability range of CAMDIS are discussed in the following.

5.1. Throughput

The octanol/water distribution coefficient is a thermodynamic measure presuming equilibrium conditions in the solute - solvent system. Leo and Hansch found that in the classical shake flask method approximately 100 inversions in roughly 5 min are sufficient to achieve equilibrium [6]. Equilibration times in the new assay were longer (optimal: 16 - 22 h) because the filter device separates the bulk phases and precludes an intense interexchange of the solvents. The fact, however, that the filter prevents amphiphilic compounds from forming troublesome emulsions is of great advantage, making time - consuming waiting for the phases to separate or an additional centrifugation step [6] unnecessary.

In response to the possible emulsification in shake flask, also slow stir modifications of the classical ‘shake’ method have been advocated which are in closer analogy with CAMDIS in terms of agitation procedure and equilibration time [32]. Even though reaching steady state in CAMDIS may take a certain time, the fact that the assay is fully automated in the 96 - well plate format and the removal of octanol is a matter of seconds reduces not only the net manpower hours, but also the overall assay time. Integration of CAMDIS into the laboratory routine is most efficiently achieved by running two phase volume ratios in parallel and analyzing the distributed solute after overnight incubation (16 - 22 h). This procedure allows measurement of approximately 200 compounds per week.

5.2. Accuracy

Incomplete and laborious phase separation is the Achilles heel of the classical shake flask method which has been challenged by several efforts (see Introduction). A filter support prevents contamination of the aqueous phase with octanol more efficiently than any other yet

published technique (water plug aspiration [14, 15], frozen water phase [12]). Moreover, and distinct from conventional filter plates, the geometry of the DIFI plates (Fig. 1) avoids experimental artifacts arising from capillary effects at the vessel wall. In addition, the small filter volume allows working with very small volumes of octanol, and thus even very lipophilic compounds can be measured.

The drawback of using a filter is enhanced interfacial drug adsorption due to the spreading of octanol (if V_{oct} = 1 µL) across an enlarged boundary layer. The slightly more pronounced adsorption in CAMDIS as compared to the shake flask technique even at similarly - sized boundary layers (if V_{oct} = 15µL) suggests that the filter itself somewhat aggravates the interface effect. The surface potential of PVDF, used as the filter material, has been found to be negative (approximately - 22 mV [33]) giving rise to electrostatic attraction of oppositely charged drugs. This might explain the fact that only bases but neither negatively charged nor non - ionized compounds enriched at the interface. Since mass - balance derived apparent $\log D'_{oct}$ reflects both, adsorption to the filter and distribution into octanol, it will be naturally higher than the 'true' $\log D_{oct}$. However, overestimation due to drug adsorption to te filter was only significant in the rare case that several unfavourable conditions coincided, including i) presence of positive charge, ii) low volume of octanol, iii) drug concentrations below a certain limit, and iv) low lipophilicity. Under these conditions, less drug enters the octanol phase, and, in turn, drug adsorption to the filter cannot anymore be considered insignificant (eq. 2, $\left(C_{aq}^{0} - C_{aq}^{eq}\right) \cdot V_{aq} >> n_{fi}^{eq}$ is not fulfilled). Under these conditions, eq. 2 predicts, and our experimental data showed, an overestimation of the true $\log D_{oct}$. The convergence of $\log D'_{oct}$ and $\log D_{oct}$ with a rise in concentration and volume of octanol points to surface saturation even at the lowest concentration investigated (5 µM, Fig. 5). This is in contrast to the nature of a simple distribution process into octanol where the amount of drug in octanol linearly increases with a rise in the initial drug concentration and the volume of octanol. In order to shift the balance towards drug dissolved in octanol, high drug concentrations (100 µM) and high volumes of octanol (15 µL) are preferable. Taking these precautions into account, an excellent agreement with the true $\log D_{oct}$ was achieved.

Provided that optimized experimental conditions were used, the comparability of CAMDIS $\log D'_{oct}$ with the literature shake flask data was excellent. Although RP - HPLC derived capacity factors are an attractive alternative from a throughput point of view [34], distribution into octanol and retention on reversed silica phases are not equivalent and direct lipophilicity

measures are clearly preferable. Distribution coefficients derived with CAMDIS are more reproducible (SD= 0.04 ± 0.02) than those from potentiometric titrations (typically expected SD = 0.4 ($\log D_{oct}$) [16] and octanol - PAMPA (SD = 0.31 ($\log P$) [26]), despite the fact that each approach relies on solute distribution into bulk phase octanol. The variability introduced by the need for estimating ionization constants (potentiometry, octanol - PAMPA) or by using different column batches in RP - HPLC is not present in CAMDIS. Moreover, the fact that troublesome emulsification is prevented by introduction of a filter is beneficial not only from a throughput point of view but also for improved accuracy. The possibility to apply different volumes of octanol (up to 25 µL) guarantees high sensitivity over a wide $\log D'_{oct}$ range (see below). In contrast, octanol - PAMPA is restricted to the particular volume of octanol (3 µL) that is necessary to impregnate a filter and to form a permeation barrier. Because the variation of permeability with $\log P$ flattens in the $\log P$ range 0 - 2, octanol - PAMPA leads to less accurate results in this case [26]. Finally, the integration of a calibration check in CAMDIS, able to detect possible artifacts arising from precipitation and drug adsorption to the well plate, provides a higher level of certainty.

5.3. Applicability Domain

5.3.1. Charge Class

CAMDIS works with acids, bases, neutral and zwitter – ionic compounds which allows for the assessment of $\log D'_{oct}$ for all classes of compounds with a single screening platform. This is a major benefit compared to RP - HPLC (no acids)[34], potentiometry (no neutrals) or octanol-PAMPA (no zwitter - ionic compounds)[26] where a backup capacity for the respective missing charge class must always be provided. Particularly neutral compounds constitute a major part in the portfolio of potential drug candidates and omitting the lipophilicity characterization of those is not a viable option.

5.3.2. Lipophilicity Range

If no adsorption at the filter - supported interface takes place (acids, neutral compounds), the accessible lipophilicity range is mainly determined by the selected phase volume as well as the precision and sensitivity of the analytical method. Use of HPLC - MS then allows the measurement of $\log D_{oct}$ in the range - 0.5 - 4.2 (with V_{oct} = 15 µL and 1 µL octanol, V_{aq} = 150 µL).

However, for the evaluation of the accessible lipophilicity range in case of interfacial drug adsorption (bases), the associated experimental error needs to be considered and can be simulated as described in Fig. 10.

Fig. 10

The parabolic shape of the error curve (experimental error as a function of $\log D_{oct}$) can be understood as follows: At the extremely low and the extremely high end of the $\log D_{oct}$ range, very low drug concentrations will be found in one of both solvents. This means that any enrichment at the interface will have a significant effect on the equilibrium aqueous drug concentration translating into the increasing error sensitivity of $\log D_{oct}$ (see also eq.3). It was shown that the overestimation of $\log D_{oct}^{'}$ due to drug enrichment at the octanol/buffer interface is a general pattern which also occurs in shake flask. A quantitative assessment on the accuracy of octanol/water distribution coefficients has, however, not been delineated before. This was possible and necessary in CAMDIS because the area of common interface is increased when minute volumes of octanol (1 µL) are forced to spread throughout the filter. The opposite effect is of course true when larger volumes of octanol are framed by the DIFI tube. Combining the thresholds governed by the phase volume ratio and those dictated by interfacial drug adsorption, a reliable assessment of CAMDIS $\log D_{oct}^{'}$ at the desired accuracy level (max. error 0.1 $\log D_{oct}^{'}$ units) is possible in the $\log D_{oct}^{'}$ range - 0.3 - 2.5 (15 µL octanol) and 0.9 - 3.8 (1 µL octanol). Despite the fact that the applicability range is much smaller than with RP - HPLC [34] and the PAMPA-octanol assay [26] ($\log D_{oct}$ = - 1.5 - 6 and - 2 - 8, respectively), we consider the range as sufficiently wide and optimized for potential drug candidates. Compounds with higher or lower lipophilicity are in general terms also undesirable from a biopharmaceutical point of view [35]. More important than an extended measurement domain is the reliability of experimental data in the relevant $\log D_{oct}$ range.

5.4. Limitations and Future Perspectives

We have shown that CAMDIS is a valuable tool for measurement of $\log D_{oct}$ which is the most frequently used parameter for the prediction of a compound's pharmaceutical, environmental and biological fate [10]. The use as of octanol as a membrane - mimicking system is justified by itsdielectric constant of ε_r = 10 [36] which reflects the dielectric

conditions in the head group region of a membrane. However, octanol lacks the anisotropy and asymmetry of a biological membrane[37]. To overcome this deficit we tested CAMDIS with other solvent systems than octanol, including phospholipid membranes and tissue homogenates from animal and human organs (e.g. brain homogenates). A proof has already been established in our lab (*manuscript 6*).

6. Conclusions

We have demonstrated on a chemically diverse and broad set of compounds (n = 52) that the novel CAMDIS assay (i) produces accurate $\log D'_{oct}$ values in excellent agreement with literature shake flask data, (ii) is applicable for all charge classes, (iii) is easily implemented on a screening platform as a 96 - well plate based high - throughput assay, (iv) reduces the net manpower hours required as compared to the classical shake flask technique by accelerating the phase separation process, (v) is more reproducible than RP - HPLC, potentiometry and octanol - PAMPA based techniques (SD < 0.1), and (iv) allows the assessment of $\log D_{oct}$ values in a range matching the expected scope within a typical drug development process ($\log D_{oct}$ = - 0.5 - 3.8 [maximal 4.2]). We believe that CAMDIS thus bridges the gap between the requirement for high quality AND rapid $\log D_{oct}$ assessment. In this light, CAMDIS can aid the optimization and prioritizing of potential drug candidates in the earliest phase of the drug development process.

Acknowledgements

The authors thank Marta Hidalgo, Daniel Zimmerli and Ann-Kathrin Spaete for excellent technical assistance and Joerg Voelkle for the construction of the well plates.

TABLES

Table 1 CAMDIS $\log D'_{oct}$ (pH 4) values for zolpidem obtained with different octanol volumes and initial drug concentrations. The values correspond to the CAMDIS $\log D'_{oct}$ profile in Fig. 4C, at pH 4. The difference between CAMDIS $\log D'_{oct}$ and the shake flask $\log D'_{oct}$ is given along ($\Delta \log D'_{oct}$).

V_{oct} [µL][a]	$\log D'_{oct}$ at pH 4[b]		$\Delta \log D'_{oct}$ [c]	
	12.5 µM	100 µM	12.5 µM	100 µM
1	0.65±0.02	0.35±0.01	0.46	0.16
15	0.28±0.04	0.20±0.10	0.09	0.00

[a] V_{aq} = 130 µL, [b] fraction ionized 99.7 %, [c] the shake flask value ($\log D'_{oct}$ = 0.20) obtained at 100 µM and 15 µL octanol is used as the reference.

Table 2 Summary of model parameters and estimates of the number of drug layers, N_{layers}, adsorbed at the octanol/buffer interface.

Compound	Method	r^2		$\log D_{oct}$		n_{fi}^{eq} (µmol)		N_{layers}	
	V_{oct}	1µL	15µL	1µL	15µL	1µL	15µL	1µL	15µL
Buspiron	CAMDIS	0.971	-	2.27	-	8 E-05	-	2.28	
Propranolol[a]	CAMDIS	0.972	0.682	1.32	1.32	6 E-05	6 E-05	2.07	2.07
Propranolol	Shake flask	0.727	0.807	1.30	1.33	1 E-05	5 E-05	0.34	1.72

[a] The $\log D_{oct}$ - concentration profile for the 15µL setup was fitted by using the n_{fi}^{eq} - estimate from the 1µL setup (set as fixed parameter) while only allowing the true $\log D_{oct}$ to vary.

Table 3 Key molecular properties of the validation dataset including neutral (n = 20), basic (n = 20), acidic (n = 11) and zwitter - ionic (n = 1) compounds.

Parameter	Range
Molecular weight [g/mol]	147 - 734
Highest basic pK_a - lowest acidic pK_a	10.18 - 4.2
$c\log P$ [a]	0.46 - 5.92
$\log D_{oct}$ at pH 7.4 (shake flask)[b]	-0.43 - 4.18

[a] $c\log P$ v4.71 Daylight, [b] literature values, for references see Table 4.

Table 4 Properties of the 52 compounds used for validation of CAMDIS.

ID	Compound	Charge class[a]	$\log D_{oct}$ (pH 7.4) ± SD		Reference
			CAMDIS	Shake flask (Literature)	
1	Albendazole	N	3.35±0.03	3.29	[38]
2	Alprenolol · HCl	B	1.00±0.15	0.88±0.13	[39-43]
3	Amitriptyline	B	2.99±0.03	2.79±0.34	[39, 44, 45]
4	Antipyrine	N	0.28±0.06	0.24±0.01	[46-48]
5	Buspirone · HCl	B	2.28±0.02	2.14	*b*
6	Caffeine	N	-0.01±0.01	-0.04±0.06	*[39, 49-52]*
7	Carbamazepine	N	1.75±0.01	1.65	[53, 54]
8	Chloramphenicol	N	1.15±0.06	1.12±0.04	[55, 56]
9	Chlorpromazine · HCl*	B	3.35±0.03	3.16±0.11	[39, 45, 57, 58]
10	Chlorthalidone	A	0.93±0.01	0.85	[59][; c]
11	Cimetidine	B	0.26±0.06	0.33	[60, 61]
12	Clomipramine · HCl*	B	3.34±0.02	3.28±0.06	[45, 62]
13	Clozapine	B	3.09±0.02	2.99	[45]
14	Coumarin	N	1.43±0.08	1.42±0.04	[49, 63]
15	Desipramine · HCl	B	1.30±0.13	1.41±0.09	[45, 62, 64]
16	Dexamethason	N	1.97±0.03	1.82±0.11	[6, 65, 66]
17	Diazepam	N	2.93±0.02	2.74±0.10	[39, 67-69]
18	Diclofenac · Na	A	1.20±0.05	1.14±0.05	[70-74]
19	Disopyramide	B	-0.55±0.08	-0.43±0.35	[42, 75]
20	Erythromycin	B	0.99±0.17	0.96±0.42	[76, 77]
21	Fentanyl	B	2.98±0.02	2.86	[78]
22	Fluoxetine · HCl	B	2.02±0.01	1.88±0.08	[39, 79]
23	Flurbiprofen	A	0.95±.07	0.91	[70]
24	Glyburide	A	2.23±0.04	2.19	[38]
25	Griseofulvin	N	2.33±0.02	2.18±0.00	[80]
26	Hydrochlorothiazide	A	-0.11±0.05	-0.12	[81]
27	Hydrocortisone	N	1.54±0.05	1.57±0.06	[6, 82]
28	Ibuprofen	A	1.04±0.07	1.27±0.34	[39, 70, 71]
29	Imipramine · HCl	B	2.49±0.05	2.51±0.02	[45, 62]
30	Indomethacin	A	1.00±0.10	0.76±0.22	[71, 74]

ID	Compound	Charge class[a]	$\log D_{oct}$ (pH 7.4) ± SD		Reference
			CAMDIS	Shake flask (Literature)	
31	Ketoprofen	A	-0.12±0.01	-0.23±0.04	[71, 83]
32	Labetalol · HCl	Z	1.05±0.11	1.09	[84]
33	Lidocaine	B	1.74±0.05	1.61±0.31	[39, 45, 85]
34	Meprobamate	N	0.88±0.02	0.70	[49]
35	Mesoridazine	B	1.79±0.07	1.81	[45]
36	Metoclopramide · HCl	B	0.44±0.01	0.53±0.10	[42, 86]
37	Metoprolol · Tartrate	B	-0.35±0.01	-0.17±0.20	[40, 42, 43, 84, 87, 88]
38	Metronidazole	N	-0.05±0.01	-0.07±0.06	[50, 89]
39	Naproxen	A	0.25±0.07	0.32±0.02	[71, 83]
40	Nimodipine	N	4.00±0.04	4.18	[90]
41	Paracetamol	N	0.30±0.05	0.30	[39]
42	Phenytoin	A	2.44±0.01	2.23±0.38	[47, 87]
43	Prednisolone	N	1.63±0.05	1.45±0.04	[6, 49]
44	Primidone	N	0.85±0.03	0.91	[91]
45	Progesterone	N	3.89±0.02	3.76±0.19	[6, 92, 93]
46	Propranolol · HCl	B	1.21±0.08	1.21±0.16	[40-42, 84, 87, 88, 94-98]
47	Temazepam	N	2.22±0.02	1.98±0.11	[39, 99]
48	Testosterone	N	3.38±0.01	3.23±0.16	[39, 92, 100, 101]
49	Theophylline	N	-0.01±0.01	-0.02	[50]
50	Triflupromazine · HCl*	B	3.63±0.03	3.39	[58]
51	Trimethoprim	B	0.52±0.01	0.64	[102]
52	Warfarin	A	0.94±0.08	1.12±0.11	[103, 104]

[a]N: neutral (less than 3 % ionization at pH 7.4); A: acid pK_a < 8.9; B: base pK_a > 6; Z: zwitterions with acid pK_a < 8.9 and base pK_a > 6 (pK_a calculated with MoKa); [b]in-house measured shake flask value obtained in Tris buffer (pH 7.4), [c]measured with countercurrent chromatography, *evidence for drug adsorption to the well plate

FIGURES

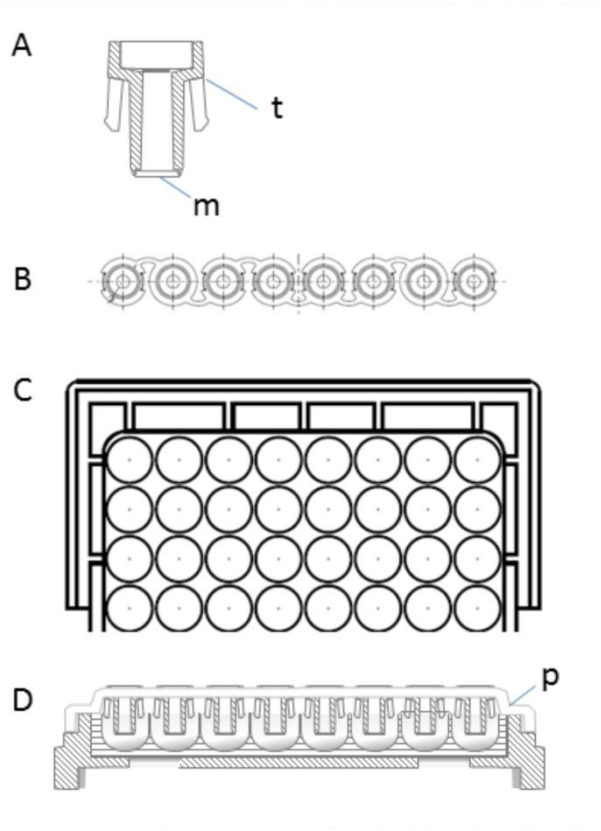

Figure 1 Design of the novel DIFI© tubes used as solid support for octanol (**A**). The lipophilic PVDF membrane (m) fixed on the bottom of the polypropylene tubes (t) is suited to be coated with commonly 1 µL or 15 µL octanol. Eight DIFI tubes are aligned in one stripe (**B**) conforming to the typical 8x12 well plate format. The coated DIFI tubes are dipped into an in - house made Teflon plate (**C**) prefilled with analyte - spiked aqueous phase as shown in (**D**). A 96 - well polypropylene plate (p) is used as a carrier for the DIFI tubes to enable convenient handling. The sandwich is put on a shaker to allow the solute to distribute in the octanol - buffer system. After distribution equilibrium is achieved, the two phases are separated by removal of the DIFI plate.

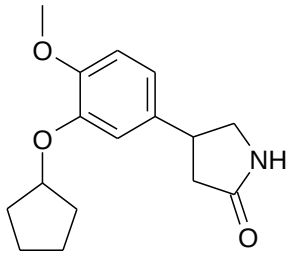

Rolipram

($\log D_{oct}$ 2.1[a], no pK_a)

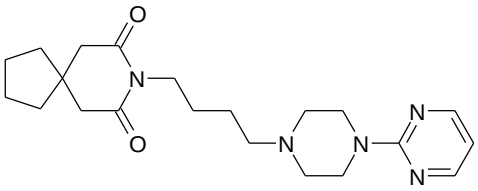

Buspiron

($\log D_{oct}$ 2.14[b], pK_a 7.61)

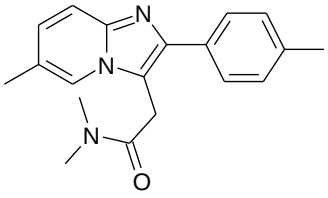

Zolpidem

($\log D_{oct}$ 2.29[b], pK_a 6.47)

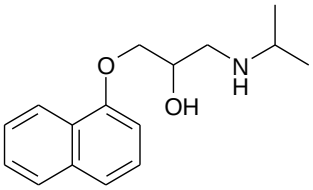

Propranolol

($\log D_{oct}$ 1.21[c], pK_a 9.48)

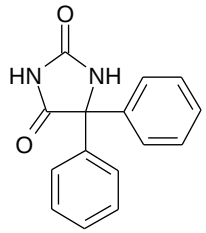

Phenytoin

($\log D_{oct}$ 2.23[c], pK_a 8.18)

Figure 2 Structures, $\log D_{oct}$ (pH 7.4) and pK_a values (in - house) of the test compounds used for assay development. [a]literature value [105], [b] in - house shake flask value at pH 7.4 (Tris/NaCl), [c]mean of literature shake flask data (see Table 4).

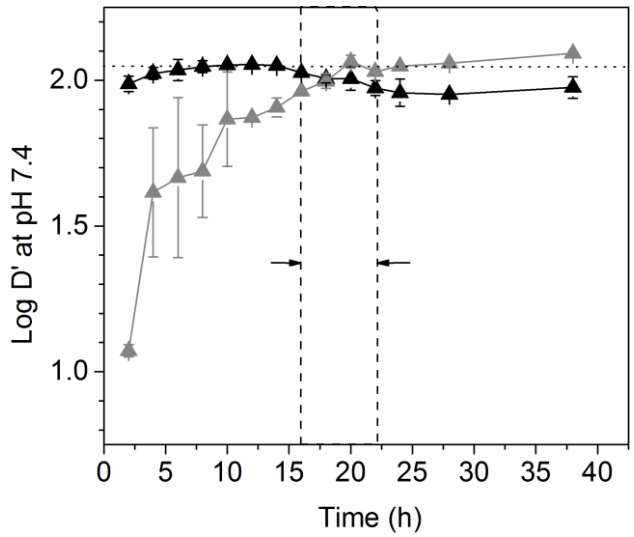

Figure 3 Kinetics of rolipram distribution in the octanol - filter - buffer system. Rolipram (100 µM) was introduced into 150 µL buffer (50 mM Tris, 114 mM NaCl, pH 7.4) and covered with the octanol - precoated DIFI tubes (V_{oct} = 1 µL (▲) and 15 µL (▲)). Distribution coefficients were obtained after shaking the CAMDIS assembly for up to 38 h. Similar $\log D'_{oct}$ values with both phase volume ratios were attained after 16 - 22 h (vertical **--**). This value is identical with the reference shake flask $\log D'_{oct}$ (horizontal ·····).

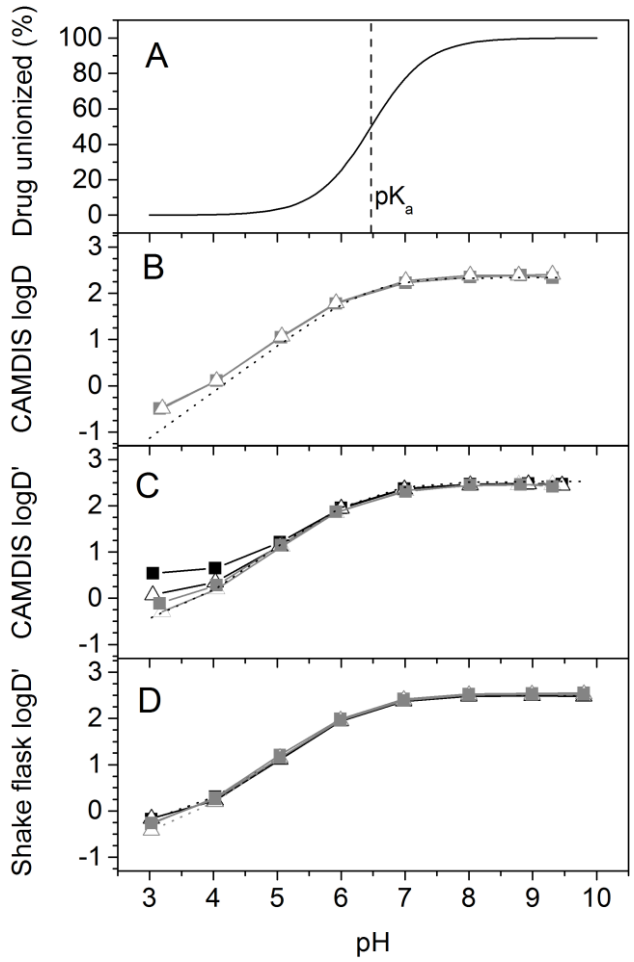

Figure 4A Ionization profile of zolpidem for the pH range 3 - 10. The fraction unionized was calculated from the pH and the measured pK_a (basic pK_a = 6.47) according to the Henderson - Hasselbalch equation. **B-D:** Distribution coefficient - pH profiles for zolpidem obtained with different methods (see below). The volume of octanol was 1 µL (black symbols) and 15 µL (grey symbols), respectively. The volume of the aqueous phase was 130 µL. The initial aqueous drug concentration was 12.5 µM (squares) and 100 µM (triangles), respectively. **B:** CAMDIS $\log D_{oct}$ - pH profile (gold standard) relying on the measurement of both phases (15 µL octanol necessary). The theoretical $\log D_{oct}$ - pH profile (·····) was estimated from the measured $\log D_{oct}$ at pH > 10 via the Henderson - Hasselbalch equation. **C:** CAMDIS $\log D'_{oct}$ - pH profile relying on mass balance (only the aqueous phase was measured). **D:** Shake flask $\log D'_{oct}$ - pH profile relying on mass balance.

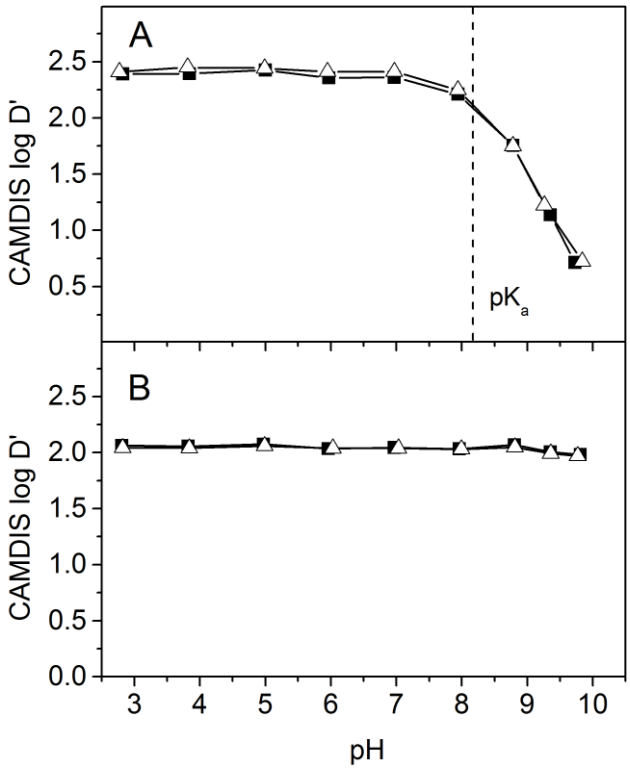

Figure 5 pH - $\log D'_{oct}$ profile of **A:** phenytoin (acid, pK_a = 8.18) and **B:** rolipram (neutral). Conditions and symbols were as in Fig. 4C, however, only 1 µL octanol was used.

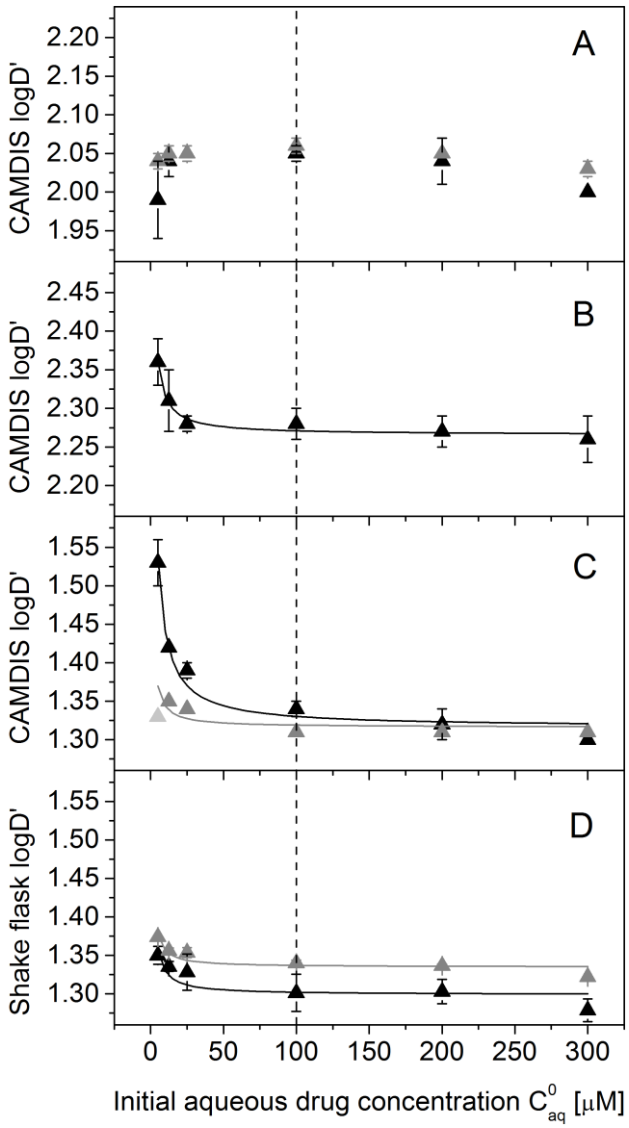

Figure 6 $Log\,D'_{oct}$ - concentration (pH 7.4) profiles at two volumes of octanol (V_{oct} = 1 µL (▲) and 15 µL (▲), respectively) for the non - charged rolipram (**A**), the weak base buspirone (61.9 % ionized, **B**), and the strong base propranolol (99.2 % ionized **C,D**). $Log\,D'_{oct}$ values were measured with the new CAMDIS assay (**A-C**) and with the classical shake flask technique (**D**). Initial and equilibrium drug concentrations in bulk buffer (130 µL, 50 mM Tris, 114 mM NaCl, pH 7.4) were directly measured. The total concentration in octanol and the filter was estimated by difference. Triangles are experimental data; solid lines are fits to experimental data according to eq. 4. **B:** Concentrations of buspiron remaining in solution when using 15 µL octanol were too low for reliable analysis, and therefore only data obtained with V_{oct} = 1 µL is shown.

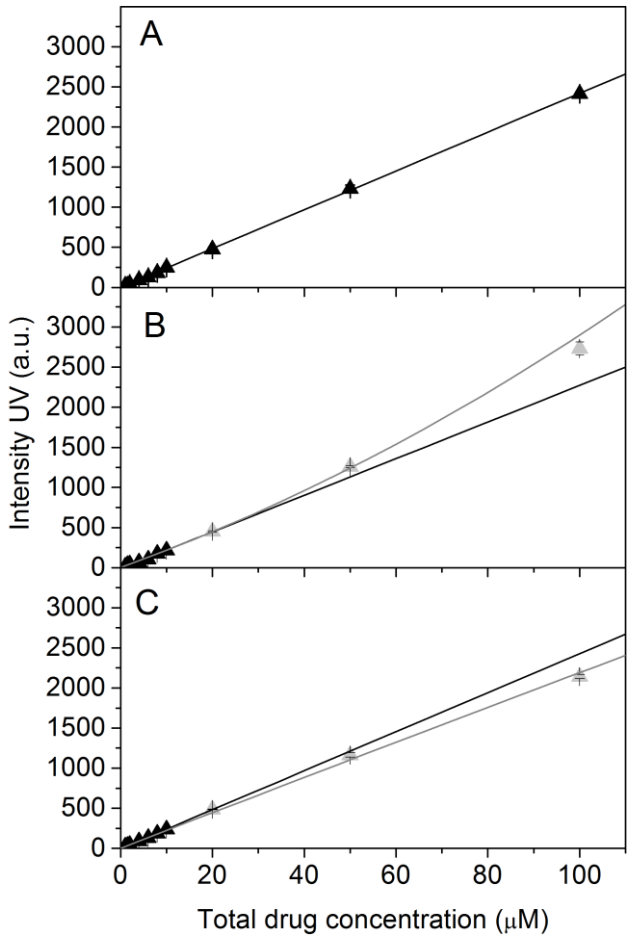

Figure 7 UV response as a function of total concentration for olanzapine (**A**), chlorpromazine (**B**) and RO - 1 (**C**) after storing the drug solutions in a Teflon well plate for 18 h. The UV intensity is a measure of the free aqueous drug concentration remaining in solution. Drugs were dissolved in octanol pre-saturated buffer (50 mM Tris, 114 mM NaCl, pH 7.4). **A:** Non - adsorbing compound. The line is the linear fit to the experimental data (triangles) over the whole concentration range (r^2 = 0.998). **B, C:** The lines are the fits to the experimental data over the whole concentration range (—, polynomial fit) or in the range 0 - 20 µM (**━**, linear fit). The discrepancy between both fits at 100 µM indicates saturable drug adsorption to Teflon (**B)** or drug precipitation (**C**).

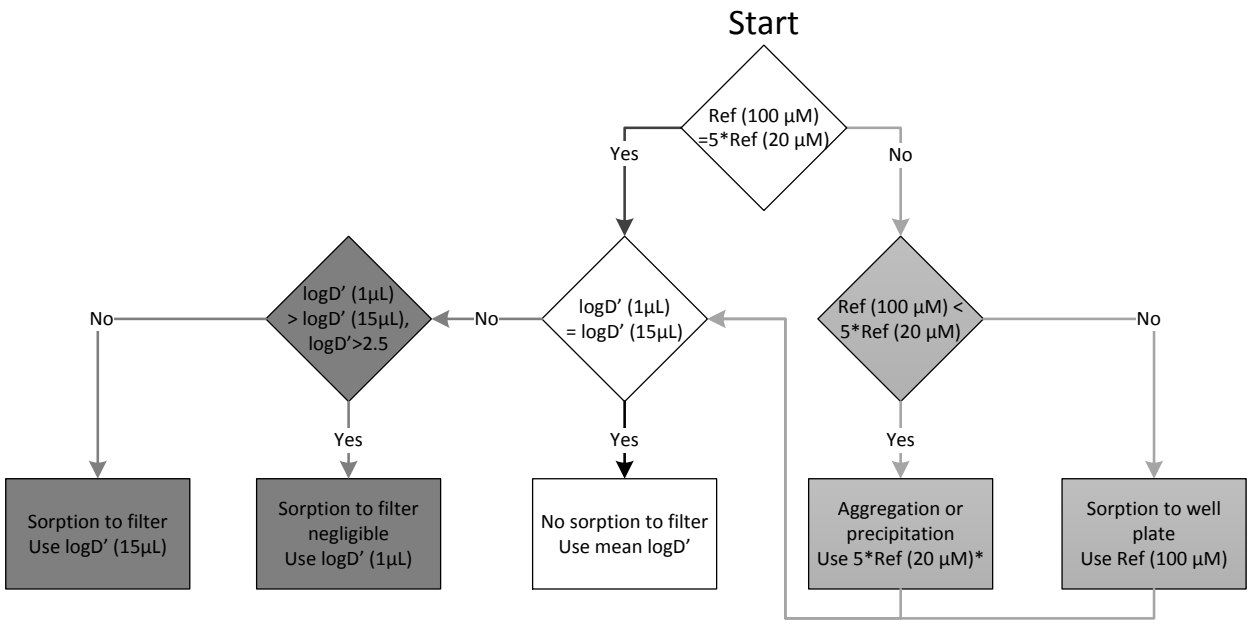

Figure 8 Decision tree for assessing the correct $\log D'_{oct}$ value taking into account i) drug adsorption to the filter (dark grey boxes, left) and ii) precipitation or drug adsorption to the well plate (light grey boxes, right). The most common and simplest case is, however, when no sorption occurs (white boxes, middle). *Valid, provided that neither in the 1:5 diluted reference nor in the actual distribution experiment precipitation occurs. If, however, discrepancies among $\log D'_{oct}$ values with different phase volume ratios are obtained, which are not within the scope of the expected filter - related error (compare Table 2, maximal 0.16 $\log D_{oct}$ units), the assumption is violated and no $\log D'_{oct}$ value can be obtained.

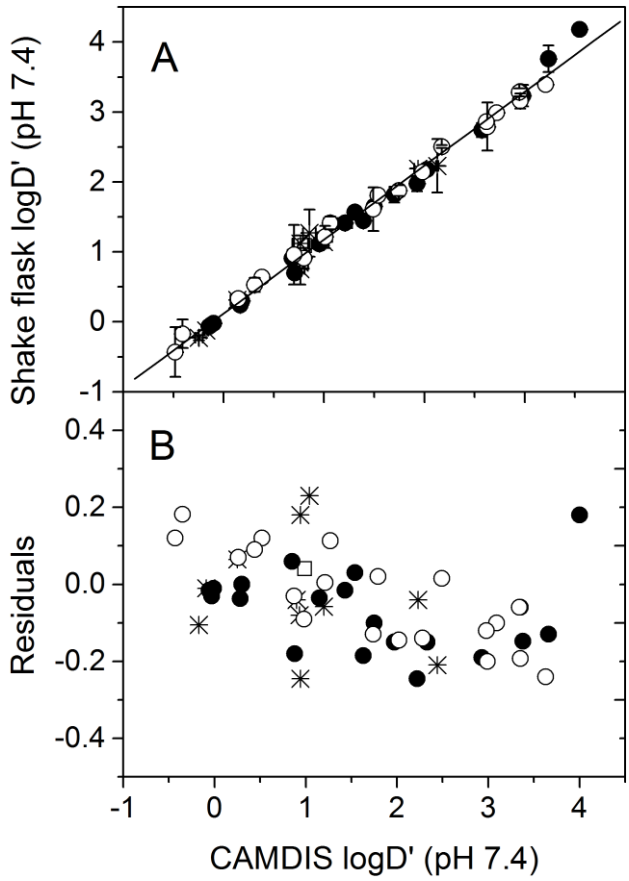

Figure 9A: Correlation between CAMDIS $\log D'_{oct}$ and literature shake flask $\log D'_{oct}$ (or $\log D_{oct}$) values (pH 7.4) for bases (○), neutrals (●), acids (✳) and zwitter - ionic compounds (□). Shake flask $\log D'_{oct}$ = 0.960 * CAMDIS $\log D'_{oct}$ + 0.025 (correlation statistics: r^2 = 0.996, SEE = 0.111, n = 52). Vertical error bars are the standard deviations of the literature data with respect to the different literature reports. Horizontal error bars are not shown and correspond approximately to the symbol size. **B:** Residulas of CAMDIS $\log D'_{oct}$ with respect to the literature values. Residuals = literature $\log D'_{oct}$ - CAMDIS $\log D'_{oct}$.

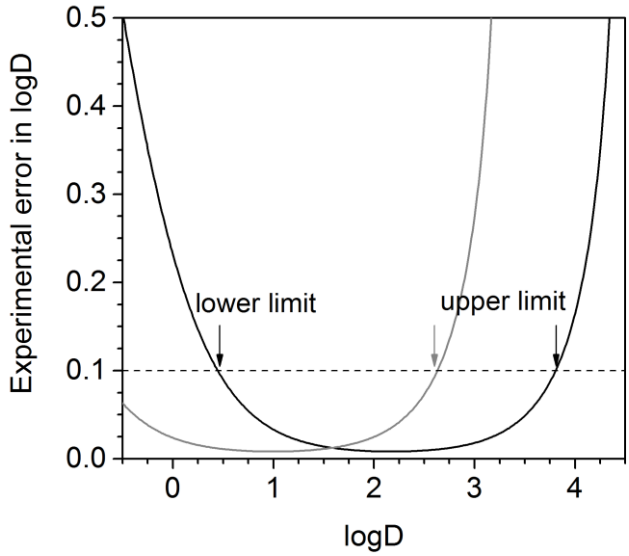

Figure 10 Applicability range of CAMDIS assuming adsorption of one monolayer at each interface (filter/buffer and filter/air) and allowing for an experimental error of 0.1 $\log D_{oct}$ units. The experimental error in $\log D_{oct}$ corresponds to the difference between the true $\log D_{oct}$ and the estimated $\log D'_{oct}$. $Log\, D'_{oct}$ was calculated by entering the n_{fi}^{eq} - estimate for propranolol into eq. 4 along with a given initial aqueous drug concentration (100 µM) and the $\log D_{oct}$ value of interest. Simulations were performed with 1 µL (**—**) and 15 µL (—) octanol. The volume of the aqueous phase was set to 150 µL.

Supporting Information

S1. Estimation of $\log D'_{oct}$ under Consideration of Drug Adsorption to the Filter

Per definition, the octanol/water distribution coefficient is given by:

$$\log D_{oct} = \log\left(C_{oct}^{eq} / C_{aq}^{eq}\right), \tag{S1}$$

where C_{oct}^{eq} and C_{aq}^{eq} denote the equilibrium drug concentrations in octanol and in the aqueous phase, respectively [21]. For practical reasons, C_{oct}^{eq} is commonly determined by difference between initial (C_{aq}^{0}) and equilibrium (C_{aq}^{eq}) aqueous drug concentrations. This approach is valid for a two-phase system comprised of octanol and water, however, the PVDF filter used in CAMDIS to facilitate the phase separation may constitute an additional compartment. In the ideal case, the filter should only act as a support for octanol without affecting the solute's transfer between the phases and without promoting drug adsorption. Since the average pore size of a filter (0.45 µm = 4500 Å) is much larger than the typical cross sectional area of a drug (approximately70 $Å^2$) [31], the filter does not bottleneck the transfer of drug. However, a possible drug adsorption to the filter needs to be considered in the mass balance equation which is given by

$$n_{aq}^{0} = n_{aq}^{eq} + n_{oct}^{eq} + n_{fi}^{eq}\,. \tag{S2}$$

Here, the initial amount of drug in the aqueous phase, n_{aq}^{0} , will be distributed along the buffer - filter - octanol system yielding n_{aq}^{eq} , n_{fi}^{eq} and n_{oct}^{eq} moles of drug in each respective compartment (equilibrium conditions, Fig. S1). We define the filter - adsorbed drug, n_{fi}^{eq}, as a composite of the drug adsorbed to the filter matrix and that enriched at the filter - supported interfaces. Likewise, n_{oct}^{eq} comprises the drug in bulk octanol and that in filter - supported octanol. Expressed in terms of solute concentrations in the aqueous phase and in the octanol phase, eq.S2 corresponds to:

$$C_{aq}^{0} \cdot V_{aq} = C_{aq}^{eq} \cdot V_{aq} + C_{oct}^{eq} \cdot V_{oct} + n_{fi}^{eq}, \tag{S3}$$

where V_{aq} and V_{oct} denote the volumes of the aqueous and the octanol phase, respectively. By rearrangement of equation S3, it can be shown that the difference between the initial and the equilibrium aqueous drug concentrations, corrected for the phase volume ratio ($\left(C_{aq}^{0} - C_{aq}^{eq}\right) \cdot V_{aq} / V_{oct}$), corresponds to a composite parameter, i.e. the sum of the solute concentration in octanol and that at the filter according to:

$$\left(C_{aq}^{0} - C_{aq}^{eq}\right) \cdot V_{aq} / V_{=oct} = C_{oct}^{eq} + n_{fi}^{eq} / V_{oct} \ . \tag{S4}$$

Neglecting a compound's adsorption to the filter and attributing the term $\left(C_{aq}^{0} - C_{aq}^{eq}\right) \cdot V_{aq} / V_{oct}$ exclusively to the octanol phase thus yields erroneously high apparent $\log D_{oct}^{'}$ values according to:

$$\log D_{oct}^{'} = \log\left(\frac{\left(C_{aq}^{0} - C_{aq}^{eq}\right) \cdot V_{aq} + n_{fi}^{eq}}{C_{aq}^{eq} \cdot V_{oct}}\right). \tag{S5}$$

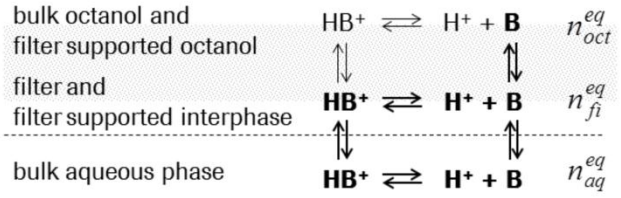

Figure S1 Distribution of a basic compound along the buffer/filter/octanol system. At equilibrium, the initial amount of drug is distributed into the aqueous bulk compartment, into the filter which is composed of the filter supported interfase and the filter matrix, and into the octanol phase, composed of immobilized octanol and bulk octanol.

S2. Quantification of Drug Adsorption to the Filter

Provided the boundary conditions are properly assessed, the apparent octanol/water distribution coefficient, $\log D'_{oct}$, can be used to estimate the molar amount of drug adsorbed at the filter - supported interface. n_{fi}^{eq} can be derived as follows: At a predefined initial concentration, C_{aq}^{0} , the equilibrium drug concentration in the bulk aqueous phase, C_{aq}^{eq} , may be expressed as a function of the true $\log D_{oct}$ according to

$$C_{aq}^{eq} = C_{aq}^{0} / \left(10^{\log D} \cdot V_{oct} / V_{aq} + 1\right). \tag{S6}$$

A combination of eq.S5 and eq. S6 yields

$$\log D'_{oct} = \log \left(\frac{C_{aq}^{0} - \left(C_{aq}^{0} / \left(10^{\log D_{oct}} \cdot V_{oct} / V_{aq} + 1\right)\right) \cdot V_{aq} + n_{fi}^{eq}}{C_{aq}^{0} / (10^{\log D_{oct}} \cdot V_{oct} / V_{aq} + 1) \cdot V_{oct}} \right). \tag{S7}$$

In eq. S7, the composite parameter $\log D'_{oct}$ is separated into a term for the distribution into octanol and into a term for the adsorption to the filter (n_{fi}^{eq}). The unknown parameters in eq. S7, namely the true octanol/water distribution coefficient, $\log D_{oct}$, and the amount of drug at the filter, n_{fi}^{eq} , can be obtained from a fit of eq. S7 to experimental $\log D'_{oct}$ - C_{aq}^{0} profiles. The inherent assumption is that, within the applied concentration range, the filter - supported interface is saturated with solute, and thus n_{fi}^{eq} is constant.

S3. Investigated Lipophilicity Range in the $\log D'_{oct}$ - pH Profiles

When measuring the $\log D_{oct}$ ($\log D'_{oct}$) as a function of pH, the investigated lipophilicity range is approximately determined by the intrinsic lipophilicity of the non - ionized drug, $\log P_{oct}$, reduced by the fraction ionized according to [106]:

$$\text{base: } \log D_{oct} = \log P_{oct} - \log\left(1+10^{pK_a - pH}\right) \tag{S8}$$

$$\text{acid: } \log D_{oct} = \log P_{oct} - \log\left(1+10^{pH - pK_a}\right). \tag{S9}$$

Equation S8 and S9 are simplified since the distribution of ionized species and ion pairs into octanol is ignored [16].

S4. The Number of Drug Layers Sticking to the Filter

From the estimate of the filter - bound drug amount, n_{fi}^{eq} , the total number of molecules at the filter, N_{total} , can be calculated. This number can then be related to the number of molecules, $N_{monoayer}$, required for saturating the filter surface with one monolayer. From the ratio of both, the number of drug layers at the filter, N_{layer} , can be gained according to

$$N_{layer} = \frac{N_{total}}{N_{monolayer}} = \frac{n_{fi}^{eq} \cdot N_A}{A_{fi} / A_D} \tag{S10}$$

where N_A is the Avogadro constant, A_{fi} is the area of common interface between buffer and the filter (based on a filter diameter of 3.26 mm), and A_D is the cross - sectional area of the drug in its most amphiphilic conformation[107], respectively. Eq. S10 assumes that the solute forms a condensed film on the filter. Cross sectional areas were calculated according to [107] yielding 39.5 $Å^2$ and 47.8 $Å^2$ for propranolol and buspiron, respectively.

References

1. Caron, G. and G. Ermondi, *Lipophilicity: chemical nature and biological relevance*, in *Molecular Drug Properties*2008. p. 315-329.
2. Kerns, E.H., *High throughput physicochemical profiling for drug discovery.* J. Pharm. Sci., 2001. **90**(11): p. 1838-1858.
3. Meyer, H., *To the theory of the alcohol arose: First report about which characteristics of the Anaesthetica causes its narcotic effect?* Arch. exp. Pathol. u. Pharmak., 1899. **42**: p. 109-18.
4. Overton, E., *Osmotic properties of cells in their bearing on toxicology and pharmacy.* Zeit. physikal. Chem., 1897. **22**: p. 189-209.
5. Hansch, C., J.P. Bjoerkroth, and A. Leo, *Hydrophobicity and central nervous system agents: on the principle of minimal hydrophobicity in drug design.* J. Pharm. Sci., 1987. **76**(9): p. 663-87.
6. Leo, A., C. Hansch, and D. Elkins, *Partition coefficients and their uses.* Chem. Rev., 1971. **71**(6): p. 525-616.
7. Mannhold, R. and C. Ostermann, *Prediction of log P with substructure-based methods.* Methods Princ. Med. Chem., 2008. **37**(Molecular Drug Properties): p. 357-379.
8. Tetko, I.V. and G.I. Poda, *Prediction of Log P with property-based methods.* Methods Princ. Med. Chem., 2008. **37**(Molecular Drug Properties): p. 381-406.
9. van de Waterbeemd, H., *Physicochemical properties in drug profiling*, in *Molecular Drug Properties*2008. p. 25-52.
10. Poole, S.K. and C.F. Poole, *Separation methods for estimating octanol-water partition coefficients.* Journal of chromatography. B, Analytical technologies in the biomedical and life sciences, 2003. **797**(1-2): p. 3-19.
11. Dearden, J.C. and G.M. Bresnen, *The measurement of partition coefficients.* Quant. Struct.-Act. Relat., 1988. **7**(3): p. 133-44.
12. Yamashita, T., E. Yamamoto, and I. Kushida, *Frozen water phase method for log D measurement using a 96-well plate.* Talanta, 2011. **84**(3): p. 809-813.
13. Yang, M., et al., *Solid-liquid phase equilibria in binary (1-octanol + n-alkane) mixtures under high pressure Part 1. (1-Octanol +n-tetradecane or n-hexadecane) systems.* Fluid Phase Equilib., 2002. **194-197**: p. 1119-1129.
14. Dohta, Y., et al., *A System for LogD Screening of 96-Well Plates Using a Water-Plug Aspiration/Injection Method Combined with High-Performance Liquid Chromatography-Mass Spectrometry.* Anal. Chem. (Washington, DC, U. S.), 2007. **79**(21): p. 8312-8315.
15. Nishimura, I., et al., *Improvement of the high-speed log D assay using an injection marker for the water plug aspiration/injection method.* J. Chromatogr., A, 2009. **1216**(15): p. 2984-2988.
16. Lombardo, F., et al., *The good, the bad and the ugly of distribution coefficients: current status, views and outlook*, in *Molecular Drug Properties*2008. p. 407-437.
17. Hersey, A., et al., *Principles of method selection in partition studies.* Quant. Struct.-Act. Relat., 1989. **8**(4): p. 288-96.
18. Andersson, J.T. and W. Schraeder, *A Method for Measuring 1-Octanol-Water Partition Coefficients.* Anal. Chem. , 1999. **71**(16): p. 3610-3614.
19. Edelbach, D.J. and K.B. Lodge, *Insights into the measurement of the octanol-water partition coefficient from experiments with acrylate esters.* Phys. Chem. Chem. Phys., 2000. **2**(8): p. 1763-1771.

20. Avdeef, A., *pH-metric log P. Part 1. Difference plots for determining ion-pair octanol-water partition coefficients of multiprotic substances.* Quant. Struct.-Act. Relat. , 1992. **11**(4): p. 510-17.
21. Sangster, J., *Octanol-Water Partition Coefficients: Fundamentals and Physical Chemistry*, ed. P. Fogg. Vol. 2. 1996: Wiley.
22. Van De Waterbeemd, H., et al., *Part 5: Lipophilicity measurement by reversed-phase high-performance liquid chromatography (RP-HPLC)*, in *Lipophilicity in Drug Action and Toxicology*1996. p. 73-87.
23. Cantwell, F.F. and H.Y. Mohammed, *Photometric acid-base titrations in the presence of an immiscible solvent.* Anal. Chem., 1979. **51**(2): p. 218-23.
24. Tomlinson, E., *Filter-probe extractor: a tool for the rapid determination of oil-water partition coefficients.* J. Pharm. Sci., 1982. **71**(5): p. 602-4.
25. Camenish, G., *Drug transport Across Membranes: Structure-property correlations in the prediction of passive membrane permeation*, 1996, ETH Zürich: Zürich.
26. Faller, B., et al., *High-Throughput Lipophilicity Measurement with Immobilized Artificial Membranes.* J. Med. Chem., 2005. **48**(7): p. 2571-2576.
27. Fischer, H., M. Kansy, and B. Wagner, *Determination of high lipophilicity values*, 2006, (Hoffmann-La Roche Inc., USA). Application: US. p. 16 pp.
28. Kansy, M., et al., *Linear cuvette array, a two-dimensional cuvette array built therewith anda system comprising such two-dimensional cuvette arrays*, 2002, (F. Hoffmann-La Roche Ag, Switz.; Weidmann Plastics Technology Ag). Application: EP.
29. Manners, C.N., D.W. Payling, and D.A. Smith, *Lipophilicity of Zwitterionic Sulfate Conjugates of Tiaramide, Propranolol and 4'-Hydroxypropranolol.* Xenobiotica, 1989. **19**(12): p. 1387-1397.
30. Dalpozzo, A., et al., *Invitro Model for the Evaluation of Drug Distribution and Plasma Protein-Binding Relationships.* International Journal of Pharmaceutics, 1989. **50**(2): p. 97-101.
31. Fischer, H., R. Gottschlich, and A. Seelig, *Blood-brain barrier permeation: molecular parameters governing passive diffusion.* The Journal of membrane biology, 1998. **165**(3): p. 201-11.
32. Brooke, D.N., A.J. Dobbs, and N. Williams, *Octanol:water partition coefficients (P): measurement, estimation, and interpretation, particularly for chemicals with P greater than 10(5).* Ecotoxicology and environmental safety, 1986. **11**(3): p. 251-60.
33. Feng, L., et al., *Surface interactions and fouling properties of Micrococcus luteus with microfiltration membranes.* Applied biochemistry and biotechnology, 2011. **165**(5-6): p. 1235-44.
34. Lombardo, F., et al., *ElogD(oct): a tool for lipophilicity determination in drug discovery. 2. Basic and neutral compounds.* Journal of medicinal chemistry, 2001. **44**(15): p. 2490-7.
35. Lipinski, C.A., *Lead- and drug-like compounds: the rule-of-five revolution.* Drug Discovery Today: Technologies, 2004. **1**(4): p. 337-341.
36. Schmidt, A.B. and R.M. Fine, *Applicability of a continuum solvation model to the octanol water transfer: CFF91 based model for amino acids.* Biopolymers, 1995. **36**(5): p. 599-605.
37. Seelig, A., *The role of size and charge for blood-brain barrier permeation of drugs and fatty acids.* Journal of molecular neuroscience : MN, 2007. **33**(1): p. 32-41.
38. Austin, R.P., et al., *The influence of nonspecific microsomal binding on apparent intrinsic clearance, and its prediction from physicochemical properties.* Drug Metab. Dispos. , 2002. **30**(12): p. 1497-1503.

39. Hitzel, L., A.P. Watt, and K.L. Locker, *An increased throughput method for the determination of partition coefficients.* Pharm. Res., 2000. **17**(11): p. 1389-1395.
40. Sada, H. and T. Ban, *Time-independent effects on cardiac action potential upstroke velocity (resting block) and lipid solubility of beta adrenergic blockers.* Experientia, 1981. **37**(2): p. 171-2.
41. Facino, R.M. and R. Lanzani, *Interaction of a series of beta-adrenergic blocking drugs with rat hepatic microsomal monooxygenase.* Pharmacol Res Commun, 1979. **11**(5): p. 433-45.
42. Mannhold, R., K.P. Dross, and R.F. Rekker, *Drug lipophilicity in QSAR practice: I. A comparison of experimental with calculative approaches.* Quant. Struct.-Act. Relat., 1990. **9**(1): p. 21-8.
43. Hinderling, P.H., O. Schmidlin, and J.K. Seydel, *Quantitative relationships between structure and pharmacokinetics of β-adrenoceptor blocking agents in man.* J. Pharmacokinet. Biopharm., 1984. **12**(3): p. 263-87.
44. Elonen, E., *Correlation of the cardiotoxicity of tricyclic antidepressants to their membrane effects.* Med. Biol., 1974. **52**(6): p. 415-23.
45. Unger, S.H. and G.H. Chiang, *Octanol-physiological buffer distribution coefficients of lipophilic amines by reversed-phase high-performance liquid chromatography and their correlation with biological activity.* J. Med. Chem., 1981. **24**(3): p. 262-70.
46. Hansch, C. and S.M. Anderson, *The effect of intramolecular hydrophobic bonding on partition coefficients.* J. Org. Chem., 1967. **32**(8): p. 2583-6.
47. Dickinson, R.G., D.W. Fowler, and R.M. Kluck, *Maternofetal transfer of phenytoin, p-hydroxyphenytoin and p-hydroxyphenytoin glucuronide in the perfursed human placenta.* Clin. Exp. Pharmacol. Physiol., 1989. **16**(10): p. 789-97.
48. Frey, K.A., et al., *Development of a tomographic myelin scan.* Ann. Neurol., 1981. **10**(3): p. 214-21.
49. Anderson, S. and C. Hansch, Pomona College, Unpublished Results.
50. Sanvordeker, D.R., S. Pophristov, and A. Christensen, *Relationship between in vitro intestinal absorbability and partition coefficients of xanthene derivatives.* Drug. Dev. Ind. Pharm., 1977. **3**(2): p. 149-61.
51. Nahum, A. and C. Horvath, *Evaluation of octanol-water partition coefficients by using high-performance liquid chromatography.* J. Chromatogr., 1980. **192**(2): p. 315-22.
52. Nakatsu, K. and J. Diamond, *Role of cGMP in relaxation of vascular and other smooth muscle.* Can. J. Physiol. Pharmacol., 1989. **67**(4): p. 251-62.
53. Henczi, M., J. Nagy, and D.F. Weaver, *Determination of octanol-water partition coefficients by an HPLC method for anticonvulsant structure-activity studies.* J. Pharm. Pharmacol., 1995. **47**(4): p. 345-7.
54. Sugawara, M., et al., *A General Approach for the Prediction of the Intestinal Absorption of Drugs: Regression Analysis Using the Physicochemical Properties and Drug-Membrane Electrostatic Interaction.* J. Pharm. Sci., 1998. **87**(8): p. 960-966.
55. Helmer, F.H., C., Pomona College, Unpublished Analysis.
56. Nikaido, H., *Outer membrane of Salmonella typhimurium. VIII. Transmembrane diffusion of some hydrophobic substances.* Biochim. Biophys. Acta, Biomembr., 1976. **433**(1): p. 118-32.
57. Elferink, J.G.R., *The asymmetric distribution of chlorpromazine and its quaternary analog over the erythrocyte membrane.* Biochem. Pharmacol., 1977. **26**(24): p. 2411-16.
58. Krieglstein, J., W. Meiler, and J. Staab, *Hydrophobic and ionic interactions of phenothiazine derivatives with bovine serum albumin.* Biochem. Pharmacol., 1972. **21**(7): p. 985-97.

59. Berthod, A., S. Carda-Broch, and M.C. Garcia-Alvarez-Coque, *Hydrophobicity of ionizable compounds. A theoretical study and measurements of diuretic octanol-water partition coefficients by countercurrent chromatography.* Anal. Chem., 1999. **71**(4): p. 879-888.
60. Buur, A. and H. Bundgaard, *Prodrugs of cimetidine with increased lipophilicity: N-acyloxymethyl and N-alkoxycarbonyl derivatives.* Acta Pharm. Nord. , 1991. **3**(1): p. 51-6.
61. Nisato, D.B., S.; Lavezzo, A.; Manzoni, L.; Bianchetti, A.; Aureggi, A., *Structure-activity relationships in a series of potetnial anti-H2 NO amides*, in *Quantitative Approaches to Drug Design* J. Dearden, C., Editor 1983, Elsevier. p. 273.
62. Glasser, H. and J. Krieglstein, *Protein binding of some psychoactive drugs with a tricyclic ring system in relation to their chemical constitution.* Naunyn-Schmiedebergs Arch. Pharmakol., 1970. **265**(4): p. 321-34.
63. Toulmin, A., J.M. Wood, and W. Kenny Peter, *Toward prediction of alkane/water partition coefficients.* J Med Chem, 2008. **51**(13): p. 3720-30.
64. Maxwell, R.A., et al., *Phenyl rings of tricyclic antidepressants and related compounds as determinants of the potency of inhibition of the amine pumps in adrenergic neurons of the rabbit aorta and in rat cortical synaptosomes.* J. Pharmacol. Exp. Ther., 1974. **191**(3): p. 418-30.
65. Lullmann, H., P.B. Timmermans, and A. Ziegler, *Accumulation of drugs by resting or beating cardiac tissue.* Eur J Pharmacol, 1979. **60**(4): p. 277-85.
66. Tomida, H., T. Yotsuyanagi, and K. Ikeda, *Solubilization of steroid hormones by polyoxyethylene lauryl ether.* Chem. Pharm. Bull., 1978. **26**(9): p. 2832-7.
67. Seiler, P. and I. Zimmermann, *5-Phenyl-1,3-dihydro-1,4-benzodiazepin-2-ones. Experimental verification of substituent constants.* Arzneim.-Forsch., 1983. **33**(11): p. 1519-22.
68. Maruyama, T., et al., *Comparative study of interaction mode of diazepines with human serum albumin and α1-acid glycoprotein.* J. Pharm. Sci., 1992. **81**(1): p. 16-20.
69. Muller, W. and U. Wollert, *Interactions of benzodiazepines with human serum albumin. Circular dichroism studies.* Naunyn Schmiedebergs Arch Pharmacol, 1973. **278**(3): p. 301-12.
70. Chiarini, A., A. Tartarini, and A. Fini, *pH-solubility relationship and partition coefficients for some anti-inflammatory arylaliphatic acids.* Arch. Pharm. (Weinheim, Ger.), 1984. **317**(3): p. 268-73.
71. La Rotonda, M.I., et al., *Relationships between octanol-water partition data, chromatographic indexes and their dependence on pH in a set of nonsteroidal anti-inflammatory drugs.* Quant. Struct.-Act. Relat. Pharmacol., Chem. Biol., 1983. **2**(4): p. 168-73.
72. Moser, P., A. Sallmann, and I. Wiesenberg, *Synthesis and quantitative structure-activity relationships of diclofenac analogs.* J. Med. Chem., 1990. **33**(9): p. 2358-68.
73. Tammara, V.K., et al., *Morpholinoalkyl Ester Prodrugs of Diclofenac: Synthesis, In vitro and In vivo Evaluation.* J. Pharm. Sci., 1994. **83**(5): p. 644-8.
74. Rainer, G., U. Krueger, and K. Klemm, *Synthesis and physicochemical properties of lonazolac-calcium, a new antiinflammatory antirheumatic agent.* Arzneim.-Forsch., 1981. **31**(4): p. 649-55.
75. Chien, Y.W., H.J. Lambert, and A. Karim, *Comparative binding of disopyramide phosphate and quinidine sulfate to human plasma proteins.* J. Pharm. Sci. , 1974. **63**(12): p. 1877-9.
76. Wildfeuer, A. and J.D. Lemme, *Pharmacokinetics of josamycin.* Arzneim.-Forsch., 1985. **35**(3): p. 639-43.
77. Debnath, G.H., C., Pomona College, Unpublished Results.

78. Jow, P.H., C., Pomona College, Unpublished Analysis.
79. Gould, G.H., C., Pomona College, Unpublished Results.
80. Lien, E.H., C., Pomona College, Unpublished Analysis.
81. Zhu, C., et al., *A comparative study of artificial membrane permeability assay for high throughput profiling of drug absorption potential.* Eur. J. Med. Chem., 2002. **37**(5): p. 399-407.
82. Moser, P., Ciba-Geigy Co., Private Communication.
83. Rautio, J., et al., *Synthesis and in vitro evaluation of novel morpholinyl- and methylpiperazinylacyloxyalkyl prodrugs of 2-(6-methoxy-2-naphthyl)propionic acid (Naproxen) for topical drug delivery.* J Med Chem, 2000. **43**(8): p. 1489-94.
84. Barbato, F., et al., *Relationships between log D and Rm values in a set of beta adrenoceptor blocking agents.* Pharmacochem. Libr. , 1991. **16**(QSAR: Ration. Approaches Des. Bioact. Compd.): p. 95-8.
85. Chorvat, R.J., et al., *Mono- and bis(aminomethyl)phenylacetic acid esters as short-acting antiarrhythmic agents. 2.* J Med Chem, 1993. **36**(17): p. 2494-8.
86. Fleminger, S., et al., *Potent lipophilic substituted benzamide drugs are not selective D-1 dopamine receptor antagonists in the rat.* J. Pharm. Pharmacol., 1983. **35**(6): p. 363-8.
87. Ungell, A.L., et al., *Membrane Transport of Drugs in Different Regions of the Intestinal Tract of the Rat.* J. Pharm. Sci., 1998. **87**(3): p. 360-366.
88. Ros, F.E., H.C. Innemee, and P.A. Van Zwieten, *Ocular penetration of β-adrenergic blocking agents. An experimental study with atenolol, metoprolol, timolol and propranolol.* Doc. Ophthalmol., 1980. **48**(2): p. 291-301.
89. Anderson, R.F. and K.B. Patel, *Effect of lipophilicity of nitroimidazoles on radiosensitization of hypoxic bacterial cells in vitro.* Br. J. Cancer, 1979. **39**(6): p. 705-10.
90. Barbato, F., M.I. La Rotonda, and F. Quaglia, *Chromatographic indexes determined on an immobilized artificial membrane (IAM) column as descriptors of lipophilic and polar interactions of 4-phenyldihydropyridine calcium-channel blockers with biomembranes.* Eur. J. Med. Chem. , 1996. **31**(4): p. 311-318.
91. Bjorkroth, J.P.H., C., Pomona College, Unpublished Results.
92. Kutter, E., Unpublished Analysis.
93. Mazak, K., et al., *Lipophilicity of vinpocetine and related compounds characterized by reversed-phase thin-layer chromatography.* J. Chromatogr., A, 2003. **996**(1-2): p. 195-203.
94. Zamora, J.M., H.L. Pearce, and W.T. Beck, *Physical-chemical properties shared by compounds that modulate multidrug resistance in human leukemic cells.* Mol. Pharmacol., 1988. **33**(4): p. 454-62.
95. Zaagsma, J. and W.T. Nauta, *β-Adrenoceptor studies. 1. In vitro β-adrenergic blocking, antiarrhythmic, and local anesthetic activities of a new series of aromatic bis(2-hydroxy-3-isopropylaminopropyl) ethers.* J. Med. Chem., 1974. **17**(5): p. 507-13.
96. Kaiser, C., et al., *6,7-Dichloro-1-(3,4,5-trimethoxybenzyl)-1,2,3,4-tetrahydroisoquinoline. A structurally novel β-adrenergic receptor blocking agent.* J. Med. Chem., 1986. **29**(11): p. 2381-4.
97. Oatis, J.E., Jr., et al., *Ring-hydroxylated propranolol: synthesis and β-receptor antagonist and vasodilating activities of the seven isomers.* J. Med. Chem., 1981. **24**(3): p. 309-14.
98. Russell, M.P., et al., *Cardiovascular effects of a 4'-methylthio analog of propranolol.* J. Pharmacol. Exp. Ther., 1981. **219**(3): p. 685-90.

99. Hulshoff, A. and J.H. Perrin, *A comparison of the determination of partition coefficients of 1,4-benzodiazepines by high-performance liquid chromatography and thin-layer chromatography.* J. Chromatogr., 1976. **129**: p. 263-76.
100. Soderberg, D.H., C., Pomona College, Unpublished Anlaysis.
101. Plesiat, P. and H. Nikaido, *Outer membranes of Gram-negative bacteria are permeable to steroid probes.* Mol. Microbiol., 1992. **6**(10): p. 1323-33.
102. Seiler, P., O. Bischoff, and R. Wagner, *Partition coefficients of 5-(substituted benzyl)-2,4-diaminopyrimidines.* Arzneim.-Forsch., 1982. **32**(7): p. 711-14.
103. Otagiri, M., et al., *The interaction of some coumarin anticoagulants with β-cyclodextrin in phosphate buffers.* Pharm. Acta Helv., 1978. **53**(8): p. 241-7.
104. Baars, L.G.M., et al., *Enantioselective structure-pharmacokinetic relationships of ring substituted warfarin analogs in the rat.* J. Pharm. Pharmacol., 1990. **42**(12): p. 861-6.
105. Rosso, L., A.D. Gee, and I.R. Gould, *Ab initio computational study of positron emission tomography ligands interacting with lipid molecule for the prediction of nonspecific binding.* Journal of Computational Chemistry, 2008. **29**(14): p. 2397-2405.
106. Waterbeemd, H.v.d., *Physicochemical Properties in Drug Profiling*, in *Molecular Drug Properties*2006, WILEY-VCH. p. 25-52.
107. Gerebtzoff, G. and A. Seelig, *In silico prediction of blood - Brain barrier permeation using the calculated molecular cross-sectional area as main parameter.* Journal of Chemical Information and Modeling, 2006. **46**(6): p. 2638-2650.

4.2 The Impact of Drug Adsorption to Microtiter Plates on the Accuracy of $LogD_{oct}$

Frauke Assmus, Bjoern Wagner, Holger Fischer,Anna Seelig

Author's Contributions:

Frauke Assmus	• Idea and design of the study • Performing experiments including data analysis and development of a theoretical model • Writing the manuscript
Björn Wagner	• Idea of testing organic solvents as desorbing agents • Valuable discussions
Holger Fischer	• Supervision of the work • Valuable discussions • Reviewing the manuscript
Anna Seelig	• Supervision of the work • Valuable discussions • Help in writing the manuscript

ABSTRACT

The octanol/water distribution coefficient, $\log D_{oct}$, is a key physicochemical parameter for the prediction of a drug's ADMET (Absorption, Distribution, Metabolism, Elimination, Toxicity) properties. In response to the industrial demand for fast and low - cost methodologies, shake flask $\log D_{oct}$ values are commonly measured with miniaturized high - throughput assays, implemented on (semi)automated screening platforms. The optimization in terms of throughput may, however, lead to experimental artifacts arising from increased non-specific binding to the assay construct and undetected compound precipitation/aggregation. At the example of 24 structurally different drugs, we i) characterized the processes leading to drug loss from aqueous solution to a miniaturized Teflon well plate, and we ii) investigated which experimental conditions warrant (and vice versa prevent) the accurate determination of $\log D_{oct}$, in case that non-specific binding to the well plate or precipitation occurs. Our data show that, even though large and lipophilic compounds tend to extensively adsorb to Teflon, accurate $\log D_{oct}$ values are obtained, provided that only one drug layer adsorbs to the Teflon surface. Then, the distribution equilibrium is shifted towards drug dissolved in the octanol phase and drug adsorption to the well plate can be neglected. In contrast, drug precipitation in the well plate or the formation of stacked multilayers (typical for compounds with coplanar ring systems) lead to an underestimation of $\log D_{oct}$, which is the more pronounced the lower the lipophilicity of a compound. Experimental artifacts can be counteracted by increasing the drug concentration (limited by solubility) and/or the volume of octanol, or by recovering adsorbed drug with 2 - propanol. This work may contribute to avoid misinterpretations of measured $\log D_{oct}$ values in order to guide the ADMETox optimization of drug candidates in a reasonable way.

KEYWORDS

Non-specific binding, Drug adsorption to Teflon, Drug recovery, Octanol/water distribution coefficient, Artifacts

1. Introduction

Early ADMET profiling is of major importance in rational drug development in order to predict a drug candidate's likely development success and to avoid high attrition rates in the later, most expensive clinical phases [1]. The octanol/water distribution coefficient, $\log D_{oct}$, is at the core of many ADMET properties [2] and related to such elementary parameters like permeability, solubility, biodistribution and metabolism.

Determining $\log D_{oct}$ values with the traditional shake flask method is still considered the gold standard approach, and miniaturized versions thereof have found entry in many screening laboratories. Miniaturization, high-throughput (HT) technology and automation have generally become the industrial strategies to accelerate the nomination of drug candidates and to meet the industrial demand for speed, efficiency, and low costs [2]. Recently, however, it has been recognized that physicochemical artifacts like aggregation or non-specific binding to microtiter plates may falsify the measures of interest in HT screens, as shown for membrane permeability [2] and target affinity [3].

Various plastic materials are being used for the construction of microtiter plates including polystyrol, polypropylene and Teflon. Previous studies of non-specific binding to polypropylene and polystyrol demonstrated that particularly lipophilic non-ionic as well as lipophilic cationic compounds (polystyrol) show a high tendency for adsorption, indicating that hydrophobic and electrostatic interactions are involved in drug-plastic interactions [4]. On the contrary, Teflon is often considered as inert to adsorption [5] and therefore widely used as an alternative microtiter plate material. It is interesting to note that the sorptive loss of p-hydroxybenzoate [6], detergents [7, 8], organic environmental pollutants [9], inorganic acids/bases [10] and organic solvents [11] to Teflon has demonstrated that the common a priori assumption of negligible drug loss is invalid. However, previous studies of non-specific binding to Teflon have focused on single and/or non-drug-like compounds, whilst a comprehensive study on a large and structurally diverse dataset of drugs is lacking. Generalizations as to the rate and extent of drug loss to Teflon are thus not possible, and it is not clear which drug properties make a compound a prime candidate for sorptive loss. Moreover, the influence of drug loss on the measurement accuracy in miniaturized ADMET assays has barely been quantified so far, neither due to non-specific binding to plastics nor du to aggregation or degradation. This is all the more surprising in view of the extensive use of plastic material (microtiter plates, filter membranes, pipetting devices) in ADMET screens

and the high awareness of drug-plastic interactions in other research areas like clinical pharmacy [12] and environmental toxicology [13]. The attention drawn to poor recovery in Caco-2 assays and equilibrium dialysis, caused by non-specific binding to microtiter plates, is rather the exception than the rule [14, 15].

The aim of this study was to provide a quantitative basis for the estimation of artifacts related to drug loss in miniaturized HT $\log D_{oct}$ assays. Specifically, we aimed to assess the experimental boundary conditions at which drug precipitation and non-specific binding to microtiter plates does not significantly compromise the accuracy of $\log D_{oct}$. To this purpose, we developed a mathematical model for the error estimation of $\log D_{oct}$ which takes into account both a compound's distribution between octanol and water, and its adsorption onto a microtiter plate. The latter process was investigated independently on a structurally diverse 24 compound dataset which also allowed us to explore the physicochemical and structural properties making compounds prone to adsorption. Teflon was chosen as the well plate material of interest because it is widely used and preliminary studies in our lab were not in line with the often supposed inertness to adsorption. Results from the sorption studies were used to parameterize the proposed model, which was finally validated by comparison of octanol/water distribution coefficients measured with a miniaturized and a large scale shake flask experiment. A method for correcting erroneous $\log D_{oct}$ values is moreover proposed which may be applied to compounds for which low recovery would manifest as an underestimation in $\log D_{oct}$.

2. Theory

2.1. Three-Compartment-Model for Drug Adsorption to Teflon and Drug Distribution between Octanol and Water

When a volume of aqueous solution, V_{aq}, containing n_{total} drug is in contact with a miniaturized well plate, certain compounds will tend to stick to the assay plate yielding n_p^0 drug binding to the well plate and n_{aq}^0 drug remaining free in solution:

initial conditions (reference): $n_p^0 \leftrightharpoons n_{aq}^0$; $n_{total} = n_{aq}^0 + n_p^0$ (1a)

If an aliquot of octanol, V_{oct}, is added to the system, the drug will distribute once more until equilibrium between plastic-bound drug, n_p^{eq}, free drug in the aqueous phase, n_{aq}^{eq}, and drug in the octanol phase, n_{oct}^{eq}, is attained. Due to the solubilizing properties of octanol, it is reasonable to assume that only drug from the aqueous solution, but not from the octanol phase, is lost to the well plate. The distribution system can then be summarized by a three-compartmental model, as follows:

distribution experiment: $n_p^{eq} \leftrightharpoons n_{aq}^{eq} \leftrightharpoons n_{oct}^{eq}$; $n_{total} = n_{aq}^{eq} + n_{oct}^{eq} + n_p^{eq}$, (1b)

A combination of eq. 1a and 1b yields the overall mass balance equation which is given by:

$$n_{total} = C_{aq}^0 \cdot V_{aq} + n_p^0 = C_{aq}^{eq} \cdot V_{aq} + C_{oct}^{eq} \cdot V_{oct} + n_p^{eq}, \quad (1c)$$

where C_{aq}^0 and C_{aq}^{eq} denote the free initial and the free equilibrium aqueous drug concentration, respectively, and C_{oct}^{eq} denotes the equilibrium concentration of drug in octanol. The octanol/water distribution coefficient is defined by the ratio of C_{oct}^{eq} and C_{aq}^{eq}, or expressed in logarithmic form as:

$$\log D_{oct} = \log\left(C_{oct}^{eq} / C_{aq}^{eq}\right). \quad (2)$$

When determining $\log D_{oct}$, and particularly if adsorption is suspected, it is clearly preferable to assay both phases, octanol and water, for the distributed solute [16]. However, in miniaturized well plates, very low volumes of octanol are required for measuring compounds with intermediate to high lipophilicity, which hampers the retrieval and direct analysis of the octanol phase. In such a situation, the drug distributed into octanol may be obtained by difference between initial and equilibrium aqueous drug concentrations, but then a potential adsorption to the well plate needs to be considered in the mass balance equation, such that (rearrangement of eq. 1c):

$$\log D_{oct} = \log\left(\frac{\left(C_{aq}^{0} - C_{aq}^{eq}\right)\cdot V_{aq} + \Delta n_p}{C_{aq}^{eq}\cdot V_{oct}}\right). \qquad (3a)$$

The term $\Delta n_p = n_p^0 - n_p^{eq}$ accounts for the fact that the amount of drug bound to the microtiter plate may differ between the reference (eq.1a) and the distribution experiment (eq.1b). While C_{aq}^{0} and C_{aq}^{eq} can be measured, Δn_p is not accessible unless recovery experiments are performed.

2.2. The Assessment of $\log D_{oct}$ with a Simplified Mass Balance Equation

In large - scale experiments, adsorption to the laboratory equipment may be neglected ($n_p^0 \approx n_p^{eq} \approx 0$) and eq. 3a simplifies to

$$\log D_{oct}^{'} \approx \log D_{oct} = \log\left(\frac{\left(C_{aq}^{0} - C_{aq}^{eq}\right)\cdot V_{aq}}{C_{aq}^{eq}\cdot V_{oct}}\right), \qquad (3b)$$

which is the most frequently used equation for the assessment of mass-balanced derived octanol/water distribution coefficients , indicated as $\log D_{oct}^{'}$ (all parameters are known or can easily be measured).

In contrast, plastic surface to phase volume ratios are elevated in miniaturized assays and a significant quantity of drug might be lost to the Teflon plate ($n_p^0 > 0$, $n_p^{eq} > 0$). If the amount of drug sticking to the well plate is different in the reference and in the distribution experiment

($n_p^{eq} \neq n_p^0, \Delta n_p \neq 0$), then drug loss may lead to erroneous $\log D_{oct}^{'}$ values. Yet, if Δn_p becomes insignificant in relation to the amount of drug in octanol ($\Delta n_p << \left(C_{aq}^0 - C_{aq}^{eq}\right) \cdot V_{aq}$), $\log D_{oct}$ is still approximated by eq.3b.

During the course of this study, we i) characterized the process of drug loss to Teflon in order to ii) assess the experimental conditions which warrant (and vice versa prevent) the accurate determination of $\log D_{oct}$ with eq. 3b, in case that non-specific binding to Teflon or drug precipitation occur.

3. Materials and Methods

3.1. Drugs and Chemicals

All drugs, buffers and solvents were either obtained from commercial sources (Sigma, Acros Organics, Bepharm Ltd., Chem Pacific, HRITIK Chemicals Cooperation, Molekula) or were available through our in-house Compound Depository Group as proprietary compounds. All chromatographic solvents were of HPLC grade.

3.2. Selection of the Dataset

A dataset was compiled containing drugs for which sorption to any kind of plastic material has been reported before, i.e. paclitaxel, doxorubicin, saquinavir, vinblastine, chlorpromazine, midazolam and diazepam [4, 17, 18]. Moreover, compounds were included which have not been studied yet in terms of drug-plastic interactions (colchicine, amprenavir), but for which we suspected that adsorption-related artifacts could potentially explain their behavior as outliers in a novel *in vitro* Lipid Membrane Binding Assay (LIMBA, *accompanying manuscript 6*). In order to increase the investigated physicochemical property space, additional compounds were selected which differed in at least one key property ($\log D_{oct}$, $c\log P$, ionization state, molecular weight). Further selection criteria were (i) baseline separation from the internal standard caffeine in HPLC, (ii) a sensitive UV chromophore and (iii) compound stability during assay time (at least 16 h).

3.3. Measurement of Drug Loss to a Teflon Microtiter Plate

3.3.1. Time Dependence

Assay buffer (227 µL, 50 mM Tris/114 mM NaCl/ pH 7.4) was first spiked with DMSO stock solutions (1.5 µL) of the test compounds and the internal standard caffeine (each 10 mM) and was then filtered into an in-house made Teflon block. The filtrate thus contained 50 µM caffeine, 50 µM of the test compound (= maximal nominal concentration, for exact concentrations see Table 1) and 1 %, v/v DMSO. Caffeine was inert to adsorption (data not shown) and was added to correct for potential changes in drug concentration due to evaporation. An aliquot of the filtrate (100 µL) was transferred into a 96 well Teflon plate and was immediately injected and analyzed on a HPLC-UV system. The well was sealed and all other sample solutions were consecutively transferred, injected and analyzed again after t = 1½ h, 3 h, 6 h, 16 h, 72 h and 2 weeks. All measurements were performed at room

temperature (RT). Drug loss in percent was estimated from the decrease of the test compound's UV response according to:

$$Drug\ loss\,(\%) = 100 - \left(100 \cdot \frac{A_D^0 / A_{IS}^0}{A_D^t / A_{IS}^t}\right), \quad (4)$$

where A_D^0, A_{IS}^0, A_D^t and A_{IS}^t denote the peak areas of drug and the internal standard at t = 0 h and at a given time t. In order to exclude degradation as the source of drug loss, UV chromatograms were investigated with regard to additional peaks, along with ESI-MS spectra recorded after t = 72 h.

3.3.2. Concentration Dependence

Experiments were performed as described for the time dependent measurements; however, sample solutions covered a wide concentration range (0.5 - 500 μM) of diverse test compounds, i.e. doxorubicin, chlorpromazine, ritonavir, diazepam and indomethacin. The filtration step was omitted and drug loss in terms of percent was determined after t = 16 h as described above.

The degree of binding was expressed as the molar amount of drug bound to Teflon, $X_b = n_{Teflon}^t$, per surface area of a Teflon well (A =70*10-6 m^2). The sorption isotherms (X_b vs. C_{aq}^{eq}) were fitted according to the Brunauer - Emmet - Teller (B.E.T.) - type of adsorption described by:

$$n_{aq}^{eq} = \frac{k \cdot n_{mono} \cdot C_{aq}^{eq}}{\left(C_{sat} - C_{aq}^{eq}\right) \cdot \left(1 + (k-1) \cdot \frac{C_{aq}^{eq}}{C_{sat}}\right)}, \quad (5)$$

where C_{aq}^{eq} is the free aqueous drug concentration after t = 16 h, n_{aq}^{eq} is the amount of drug adsorbed at a given free aqueous drug concentration, k is the sorption coefficient, n_{mono} is the amount of drug required to form a single layer and C_{sat} is the saturation concentration of the adsorbate. Note that even though equilibrium was not reached, the term C_{aq}^{eq} was used to be in line with the nomenclature used for the assessment of $\log D_{oct}$ ($\log D_{oct}^{'}$).

Alternatively, the Langmuir-type of adsorption was used to fit the data according to:

$$n_{aq}^{eq} = \frac{k \cdot n_{\max} \cdot C_{aq}^{eq}}{1 + k \cdot C_{aq}^{eq}}, \quad (6)$$

where $n_{\max}$ is the amount of drug required to saturate the surface (monolayer adsorption). From the $n_{\max}$-estimate, the total number of molecules adsorbed to Teflon, N_{total}, was calculated. This number can then be related to the number of molecules, $N_{monolayer}$, required for saturating the Teflon surface with one monolayer. From the ratio of both, the number of layers on the Teflon surface, N_{layer}, can be gained according to

$$N_{layer} = \frac{N_{total}}{N_{monolayer}} = \frac{n_{\max} \cdot N_A}{A_{Teflon} / A_D}, \quad (7)$$

where N_A is the Avogadro constant, A_{Teflon} is the area of common interface between buffer and a well of the Teflon microtiter plate (A_{Teflon}=70 mm^2), and A_D is the cross - sectional area of the drug in its most amphiphilic conformation [19]. Eq. 7 presumes that the solute forms a condensed film on the Teflon surface. Cross sectional areas were calculated according to [19], yielding 71.4 Å^2 for doxorubicin, 55.3 Å^2 for fluvoxamine, 120.6 Å^2 for ritonavir, 144.7 Å^2 for saquinavir, 155.25 Å^2 for paclitaxel and 47.8 Å^2 for chlorpromazine.

3.3.3. Calibration

A calibration curve in HPLC/UV for the compounds investigated was obtained as follows: A defined amount of drug was dissolved in DMSO to obtain a stock solution (10 mM). Five consecutive dilutions in DMSO (1+1) were prepared and an aliquot of each secondary stock solution (3 µL) was further diluted with DMSO (297 µL). The dilutions were injected onto the HPLC-UV system. A plot of the UV response vs. the concentration yielded a straight line. Concentrations of drug compounds dissolved in aqueous buffer could be directly calculated from the correlation line obtained in DMSO since DMSO did not co-elute with the test compounds and therefore showed no influence on the UV spectra.

3.4. HPLC Instrumentation and Chromatographic Conditions

Drug concentrations in aqueous solutions were quantified using an Agilent 1290 Infinity HPLC-UV system. An aliquot (5 µL) of each sample was injected onto a Kinetex 2.6 µm,

2.1 x 50 mm analytical column. The flow rate was 2 mL/min and the integrated column heater was set to 60 °C. The mobile phase consisted of A (water) and B (acetonitrile), each containing formic acid (0.1 %, v/v). The gradient elution was performed as follows: initially 2 % B, 0 - 0.35 min linear gradient from 2 % B to 95 % B, 0.35 min - 0.5 min 95 % B, post time: 0.3 min. The gradient program for doxorubicin, vinblastine, buspirone and colchicine was slightly different: initially 2 % B, 0 - 0.5 min linear gradient from 2 % B to 95 % B, 0.5 min - 0.65 min 95 % B. Peak areas were recorded at an appropriate wavelength.

3.5. Calculation of Molecular Descriptors and Development of a Prediction Model for Drug Adsorption to Teflon

Partition coefficients were calculated using $c\log P$ v4.71 (Daylight Chemical Information Systems, Irvine, CA). Calculations of three-dimensional descriptors were based on single conformations *in vacuo* generated with Corina v3.46 (Molecular Networks GmbH, Erlangen, Germany). Surface, volume, size and shape (d0, d1, d2) descriptors as well as the number of hydrogen bond donors were calculated with an in-house developed modeling package Moloc (Gerber Molecular Design, Amden, Switzerland). The number of hydrogen-bond acceptors was retrieved from the Pubchem database. Ionized fractions at pH 7.4 were calculated from measured pK_a values (in-house, potentiometrically) for each dissociable group, and the net charge for the whole molecule was derived. A summary of all calculated descriptors (n = 20) is provided in the Supporting Information.

Data derived from the studies of drug loss to Teflon was pre-processed by applying the following steps: The percentage of drug loss, observed after 16 h from 5 µM drug solutions, was log transformed. Drugs which showed no adsorption to Teflon were arbitrarily set to $\log Drug\ loss$ = -1, so that they could still be used for model generation. Partial least square (PLS) regression using centered and scaled descriptors was performed with Simca-P+ v12.0.1 (Umetrics, Umea, Sweden). Due to the limited number of observations, a PLS analysis was performed on the complete dataset without assignment of an external test set. Cross-validation was performed internally by the leave-1/7th-out approach. The number of principal components was determined considering the explained variation r^2 (goodness of fit) and the predicted variation q^2 obtained from prediction of the omitted group (goodness of prediction [20]). During model refinement, less important variables were permanently eliminated as judged by q^2 and by the variable influence on projection. Redundant variables, identified as groups in the loading plot of the first two principal components, were left out if their

influence on q^2 was evaluated as negligible or reluctant. In order to provide an estimation of the statistical significance of q^2, 200 parallel models on randomly re-ordered $\log Drug\ loss$ data were developed. A comparison of q^2 based on permuted and on real data was used to preclude a chance or overfitted model. Finally, the regression coefficients of the derived model were unscaled so that the contribution of each variable could enter an ordinary regression equation.

3.6. Measurement of Octanol/Water Distribution Coefficients (Miniaturized Format)

Octanol-water distribution coefficients were measured with a novel filter-based 96 well plate technique (CAMDIS) as described in our *accompanying manuscript 1* [21]. Briefly, a hydrophobic PVDF membrane (pore size 0.45 µm) fixed on the bottom of the in-house developed DIFI tubes (EP 1232792) was impregnated with buffer-saturated octanol (V_{oct} = 0.9 µL). The tubes were dipped into a Teflon plate prefilled with filtrated drug solutions (V_{aq} = 140 µL, C_{aq}^{0} = max. 22.2 µM drug, 50mM Tris/114 mM NaCl/pH 7.4, DMSO content 0.22 %, v/v). The assay kit was sealed and allowed to shake at room temperature for 24 h. After removal of the tubes, buffer (46.7 µL) was added to the Teflon plate. The free equilibrium drug concentration in the buffer-diluted aqueous phase, C_{aq}^{eq}, was determined by HPLC-UV. The drug concentration in the octanol phase relied on mass balance and was obtained in two ways:

i) A reference experiment was performed under the same conditions as described above but without octanol. The aqueous concentration of free drug in the reference well, C_{aq}^{0}, was measured and the drug concentration in octanol was estimated by difference between C_{aq}^{0} and C_{aq}^{eq}. Eq.3b was used to calculate $\log D_{oct}^{'}$ (uncorrected mass balance derived $\log D_{oct}^{'}$)

ii) An independent experiment was performed but instead of diluting the aqueous phase with assay buffer, 2 - propanol (46.7 µL) was used to discharge drug from the Teflon surface of the well plate after removal of the DIFI tubes (2 - propanol was added in both the reference experiment and the distribution experiment).

The drug concentration in octanol was estimated by difference between the total concentration of drug in the reference experiment, $C_{aq,total}^{0}$, and the total equilibrium aqueous drug concentration, $C_{aq,total}^{eq}$, in the distribution experiment. Eq.9 was used to calculate $\log D_{oct}^{'}$ (corrected, mass balanced derived $\log D_{oct}^{'}$).

The recovery of drug adsorbed to the microtiter plate by means of 2-propanol enabled the estimation of the percentage of drug adsorbed to Teflon, both in the reference and in the distribution experiment. Experiments were performed in triplicate and mean values were reported.

3.7. Measurement of Octanol/Water Distribution Coefficients (Large Format)

Stock solutions of the test compound (10 mM, except saquinavir/ritonavir:5 mM and paclitaxel: 2.5 mM) were prepared in DMSO and diluted with buffer (Tris/114 mM NaCl/pH7.4, saturated with octanol) to yield the final sample solutions (10 µM, except for saquinavir/ritonavir: 5 µM and paclitaxel: 2.5 µM,[3]). The aqueous drug solution was transferred into a 1L shake flask (V_{aq} = 1 L, except for doxorubicin: 500 mL) and octanol pre-saturated with buffer was added (V_{aq} = 1 mL, except for doxorubicin: 500 mL). After 100 phase inversions, the shake flasks were left undisturbed for at least 24 h, until the two phases were free from emulsions (visual inspection). Both phases were sampled with a 1 mL glass pipette, then they were transferred into a glass HPLC vial (aqueous phase) and into a 96 well PCR plate (octanol phase), respectively, and analyzed with HPLC-UV. Gold standard $\log D_{oct}$ values and mass balanced derived $\log D_{oct}^{'}$ values were estimated by using eq. 2 and eq. 3b, respectively. Distribution experiments were performed in duplicate and mean values are reported.

[3] Compounds for which precipitation was suspected were measured at two concentrations (paclitaxel:5 µM and 2.5µM; saquinavir: 10 µM and 5 µM) and the difference of the $\log D_{oct}$ values was within a standard deviation of 0.1 $\log D_{oct}$ units

4. Results and Discussion

4.1. Characterization of Drug Loss to Teflon

4.1.1. Rate and Extent of Drug Loss

The rate and extent of drug loss from aqueous bulk solution to a 96 well Teflon plate was measured at the example of 24 structurally diverse compounds including acids (3), bases (8), neutral (10) and zwitter - ionic (3) drugs covering a wide physicochemical property space ($\log D_{oct}$ = -1.15 - 3.68, $c\log P$ = 0 - 5.3, Molecular weight, MW = 194 - 854 g/mol). The preparation of aqueous test solutions followed a common practice in HT screening assays and involved i) dilution of DMSO stock solutions of test compounds (10 mM) with buffer, proceeded by ii) filtration and iii) transfer of the filtrate to the microtiter plate of interest. Even though drug concentrations in the filtrate ($C_{filtrate} = C_{total}$, Table 1) thus varied according to the compound's solubility limit, we applied this protocol for the sake of higher informative content with respect to potential artifacts in HT assays. In addition, studies of drug loss to Teflon were conducted at a standardized drug concentration, C_{total} = 5 µM, which was > 50% below the lowest drug concentration measured in any of the filtrates. A summary of the extent of drug loss from both the filtrate and the 5 µM test solutions after t =16 h storage in a Teflon plate is provided in Table 1, along with key physicochemical properties of the compounds investigated.

Table 1

Fig. 1 gives a more detailed picture of drug loss from the filtrate over a period of two weeks. While drug loss of neutral (Fig. 1A) and basic (Fig. 1B) compounds ranged between 0 and 99% after 2 weeks, drug loss of acidic (Fig. 1C) and zwitter-ionic (Fig. 1D) compounds was generally low and never exceeded 10%. More precisely, digoxin and rolipram (neutral), buspiron, sumatriptan and alfentanil (basic) as well as cetirizine and tigabine (zwitterionic) showed < 2% drug loss, irrespective of the charge class of the compounds. Moreover, drug loss of colchicine (neutral), diclofenac (acidic), dexamethasone, diazepam (both neutral) and ketorolac (acidic) was only evident after 2 weeks (compounds are given in order of decreasing drug loss with a maximum value of 10%). Compound degradation is a likely explanation for the delayed drug loss which cannot be excluded despite the absence of

additional peaks in HPLC-UV/MS. Drug loss of the remaining compounds was fastest within the first 1 ½ h and was highest for paclitaxel, followed by doxorubicin > chlorpromazine > saquinavir > ritonavir > raclopride > fluvoxamin > indomethacin > vinblastine > midazolam. Compound degradation was observed for chlorpromazine and indomethacin after t =72 h and t =2 weeks, respectively, and therefore the ranking of the compounds refers to drug loss after t =16 h.

Fig. 1

When comparing the time dependent drug loss profiles from filtrated and 5 µM test solutions, two characteristic profiles can be distinguished with an example of each given in Fig. 2A and Fig. 2B.

Fig. 2

Pertaining to the filtrate, drug loss was biphasic with a rapid initial phase which then either continued with reduced, yet pronounced extent (Fig. 2B, paclitaxel, and also doxorubicin) or approximated a plateauing minimum (Fig. 2A, ritonavir and all other drugs). Equilibrium was only approximated but not reached within the investigated time frame.

Biexponential drug loss profiles as observed in Fig. 2 may result from various processes, including i) simple diffusion into the plastic matrix [22] and ii) a combination of fast drug adsorption to the plastic surface followed by either slower dissolution [23] or diffusion into the Teflon matrix [24]. Moreover iii) multilayer adsorption or iv) adsorption followed by kinetically hindered precipitation/aggregation are reasonable. Diffusion as the sole mechanisms could be excluded since experiments conducted at lower drug concentrations (C_{total} = 5µM) yielded a higher percentage drug loss for e.g. ritonavir as compared to the filtrate (C_{total} = 13.2 µM), indicating saturation of available binding sites on the Teflon surface (Fig. 2A). A similar behavior was also observed for saquinavir, vinblastine and doxorubicin. In contrast, drug loss of paclitaxel was higher from the filtrate (C_{total} = 13.2 µM) than from the 5 µM test solution (exact C_{total} = 3.1 µM) after t =16 h, pointing to supersaturation and delayed precipitation in the filtrate (same trend for raclopride and indomethacin, Table 1). Precipitation of paclitaxel in the filtered, but not the 5 µM test solution, was confirmed by an increase in UV absorbance (650 nm) over time (data not shown). The poor solubility of paclitaxel is well known, however, large variability in reported solubility data (solubility:

0.5 µM - 35 µM [25-27]) hampers a direct comparison with our results. Moreover, the slight recovery of paclitaxel after initially rapid drug loss at C_{total} = 5µM requires further investigation, in particular measurements at longer time points (the experiment was terminated after 3 d).

4.1.2. Concentration Dependency of Drug Loss

To further explore the nature of the processes underlying drug loss to Teflon, drug loss was studied over a wider concentration range (0.5-500 µM) using the example of diazepam and indomethacin (negatively charged) as well as chlorpromazine, doxorubicin (cationic) and ritonavir (non-ionic). Drug loss was recorded after t =16 h to avoid drug degradation and to take into account that a many ADMET assays involve overnight incubation, e.g. assays for the assessment of $\log D_{oct}$ (CAMDIS, *accompanying manuscript 1*), solubility (in-house assay, unpublished) and permeability (PAMPA) [28].

Diazepam and indomethacin barely adsorbed over the whole investigated concentration range (0.5 - 250 µM, Fig. 3A) whereas decreasing concentrations of the other compounds were associated with an exponential rise in percentage drug loss (Fig. 3A, logarithmic concentration axis).

Fig. 3

The respective sorption isotherms for chlorpromazine and doxorubicin are shown in Fig. 4B - D, and estimates for k, $n_{\max}$ and C_{sat} from fits of the B.E.T (Fig. 3B) and the Langmuir-type model (Fig.3C,D) to the experimental data are given in Table 2.[4]

Table 2

Regarding chlorpromazine, the sorption isotherm up to C_{total} = 500 µM (Fig. 3B) indicated multilayer adsorption or diffusion (B.E.T. model), whereas the Langmuir-type model for monolayer adsorption was only appropriate up to C_{total} =25 µM (Fig. 3C). The surface coverage at C_{total} =25 µM, estimated as N_{layer} ~1, was in agreement with the Langmuir model. With respect to doxorubicin, precipitation hindered recording the adsorption profile at

[4] Adsorption isotherm for ritonavir not shown due to insufficient sensitivity in UV at the drug concentrations used.

C_{total} > 500 µM (Fig. 3C). A fit of the Langmuir model to the data (up to C_{total} =100µM) indicated multilayer adsorption or diffusion into the Teflon matrix (N_{layer} ~3).

It is important to note that a differentiation between adsorption of multiple drug layers to the Teflon surface and diffusion into the Teflon block is not possible with the experimental setup used. Other authors assumed (but could not show evidence) that some extent of drug loss might occur due to incorporation of compound (p-hydroxybezoate) into the Teflon matrix while a significant amount of solute should remain on the surface [23]. In this respect it is worth noting that, apart from paclitaxel, chlorpromazine and doxorubicin, the maximum observed drug loss in this study corresponded to not more than approximately one drug layer covering the Teflon surface which points to the dominance of an adsorption process.

This is in contrast to the main processes involved in drug loss to polyvinylchloride (PVC) which is prevailed by drug diffusion and dissolution into the PVC matrix [23, 28]. In contrast to Teflon, PVC contains plasticizers [29] which are the main offenders of drug - plastic interactions [28]. Plasticizers prevent the formation of a rigid network by weakening the polymer-polymer interactions thereby increasing the free volume for diffusion [30]. Although hard plastics, in general, and Teflon, in particular are therefore clearly advantageous compared to soft plastics [12], the reduced significance of diffusion should not mislead over the fact that drug loss by adsorption could become relevant in miniaturized formats. As our study shows, the widespread opinion that Teflon is inert to adsorption [5] is not true.

4.1.3. Prediction of Drug Adsorption to Teflon

In order to investigate the relationship between the physicochemical properties of a compound and its likelihood to show adsorption to Teflon, only drug loss data obtained at C_{total} = 5 µM and after t =16 h was considered. Data from experiments with filtrated drug solutions was not used for the development of a prediction model since non-uniform drug concentrations would complicate the distinction between concentration dependent and structure related effects.

An attempt to relate measured or calculated molecular descriptors to log transformed adsorption data (expressed as $\log Drug\ loss$) in a two-dimensional manner resulted in rather weak correlation statistics, e.g. r^2 = 0.61 (MW), r^2 = 0.43 ($\log D_{oct}$ (pH 7.4), r^2 = 0.26 ($c\log P$), r^2 = 0.43 (PSA). The poor correlation between $\log Drug\ loss$ and $c\log P$ can be attributed to i) the relevance of drug ionization for the adsorption process, which is not captured by $c\log P$, and ii) the high uncertainty in the $c\log P$ estimate for doxorubicin ($c\log P$ (Daylight) = 0.33,

$c\log P$ (XLogP, Pubchem database) = 1.3). Omitting doxorubicin from the dataset improved the correlation with $c\log P$ (r^2 = 0.43), and excluding all other charged drugs further improved the statistics (r^2 = 0.61). It is worth noting that also the correlation of $\log Drug\ loss$ with $\log D_{oct}$ (pH 7.4) was much weaker than that observed in literature studies which were based on smaller datasets or structurally related, nondrug-like compounds [9, 29, 30]. Apart from the limited physicochemical property space studied, previous prediction approaches relied on data describing diffusion into PVC rather than adsorption onto a Teflon surface [31]; the related driving forces are considerably different. While small, lipophilic compounds such as diazepam are in favor for diffusion [17], the adsorption of diazepam to Teflon was insignificant. Only midazolam, a compound with the same chemical scaffold but a higher $\log D_{oct}$ was somewhat adsorbed (1.8%, see Table 1) pointing to the contribution of hydrophobic binding forces.

Since the prediction accuracy based on univariate analysis was relatively poor, we investigated whether a PLS model based on 20 shape, lipophilicity, size and charge descriptors yields superior model performance. The 20-dimensional space was reduced to one principal component (r^2 = 0.755, RMSEE = 0.53, q^2 = 0.749) constructed by the following descriptors given in order of decreasing importance: MW > number of hydrogen-bond donors (HBD) > measured $\log D_{oct}$ (pH 7.4), such that:

$$\text{Predicted } \log Drug\ loss = -1.87 + 0.0023 \cdot MW + 0.18 \cdot HBD + 0.25 \cdot \log D_{oct}. \quad (8)$$

Despite the fact that also the PLS model did not account for the full variability of the data, superior model performance as compared to univariate prediction approaches was achieved. Moreover, the PLS model was useful for illustrating the likelihood of drug adsorption to Teflon in a property-based classification map. The correlation between $\log D_{oct}$ (pH 7.4) and molecular weight in Fig. 4 shows three regions which differ with respect to the extent of drug adsorption to Teflon (the darker the symbol the higher $\log Drug\ loss$). The number of HBD is reflected by the size of the symbols.

Fig. 4

Region I contains large, hydrophobic drugs which readily adsorb to Teflon (ritonavir (9), saquinavir (19), paclitaxel (8) and vinblastine (21)). Extensive drug loss of paclitaxel from other plastic materials (polystyrol, polyprolylene) and from glass containers has been recognized before [4, 32]. Moreover, pronounced non-specific binding reported for structurally related compounds (nelfniavir, saquinavir, vinblastine) to ultrafiltration and dialysis membranes is in line with our results [33, 34].

Projections of small compounds ($MW < 450$) with low to intermediate lipophilicity ($\log D_{oct} < 3$) are embedded in region III where the probability for drug-Teflon interactions is very low. The only exception in Region III is fluvoxamine (18) which notably is the only fluorinated compound in region III. Increased drug adsorption of fluorinated compounds like midazolam and fluvoxamine would be in agreement with enhanced Teflon-interactions reported for fluorocarbons (e.g. fluorinated PEG - tags, [35]) and contrariwise the weak interaction of Teflon with hydrocarbons. A possible explanation on the molecular level could be a hydrophobic mismatch found between a CH_2 and a CF_2 group [36].

The central region II contains either large, but relatively hydrophilic compounds (e.g. digoxin (6), doxorubicin (17)), or vice versa small compounds with high lipophilicity (e.g. chlorpromazine (16), midazolam (7)). The number of HBD and the shape of the compound seem to determine whether compounds in Region II show extensive or only moderate adsorption to Teflon. For example, at similar molecular weights, doxorubicin (17) is more hydrophilic than amprenavir (1). The nonetheless higher drug loss of doxorubicin may be explained by the better ability to build hydrogen bonds (7 vs. 4 HBD) with negatively polarized fluorides from Teflon acting as H-bond acceptors [37]. Drug loss of doxorubicin to PTFE (Teflon) membranes has already been reported [38], yet the possible contribution of hydrogen bonding for the prediction of drug adsorption to Teflon has not been recognized before. Notably, the engagement of coplanar ring systems in stacking interactions is also plausible and in line with the formation of highly ordered structures of overlapping rings reported for doxorubicin [39] and other compounds [40]. Similarly, a comparison of chlorpromazine and midazolam (similar MW, $\log D_{oct}$ and HBD) shows that the compound with an almost planar ring structure, i.e. chlorpromazine, showed a higher extent of adsorption. The classification map in Fig. 4 does not take into account the shape of a molecule, however, stacking of coplanar ring systems should be considered as a potential driving force of adsorption.

The generally low drug loss found for acidic and zwitterionic drugs may be explained by the low tendency of negatively charged entities to interact with the hydrophobic but negatively polarized CF_2 groups on the Teflon surface [37]. Negligible drug loss of acidic compounds has been reported before for other plastic materials (polypropylene and polystyrol) [4] and likewise electrostatic repulsion from negatively charged surfaces may be involved.

4.2. Drug Loss to Teflon within $\log D_{oct}$ Assays

4.2.1. The Impact of Drug Adsorption to the Well Plate on the Accuracy of $\log D_{oct}$

The drug loss - concentration profiles in Fig. 3 have demonstrated that non-specific binding to Teflon is an adsorption process and therefore concentration dependent, as long as the Teflon surface is not saturated. In an assay for the measurement of $\log D_{oct}$ ($\log D'_{oct}$) octanol attracts drug from the aqueous phase, leading to difference between the free initial and free equilibrium aqueous drug concentrations ($C_{aq}^{eq} < C_{aq}^{0}$) which will be mirrored in a difference in the amount of drug enriched at the Teflon surface such that $\Delta n_p \neq 0$ with $n_p^{eq} < n_p^0$. It follows that estimating $\log D'_{oct}$ with the simplified mass balance eq. 3b leads to an underestimation of the true $\log D_{oct}$, which is associated with the amount of drug released from Teflon in presence of octanol (Δn_p). A numerical example of the impact of drug adsorption to Teflon on the accuracy of $\log D'_{oct}$ is given in Fig. 5.

Fig. 5

4.2.2. Distribution Coefficients from Traditional and Miniaturized Shake Flask Methods

In order to experimentally verify the predicted adsorption-related underestimation of $\log D_{oct}$, we compared octanol/water distribution coefficients (pH 7.4) derived with i) 1 L shake flasks (glass, V_{aq}=1 L, V_{oct}=1 mL, except for doxycycline: $V_{aq} = V_{oct}$=500 mL) and with ii) a miniaturized assay in 96-well format (Teflon, V_{aq}=140 µL, V_{oct}=1 µL, except for doxorubicin: V_{oct}=15 µL). Five test compounds (doxorubicin, fluvoxamine, ritonavir, saquinavir, paclitaxel) were investigated which showed pronounced drug loss from filtrated

test solutions (>3 % of drug loss after t = 16 h[5]), and which covered a wide lipophilicity range ($\log D_{oct}$ = 0.36 - 3.65).

The large format experiments with 1 L glass flasks provided the possibility to recover octanol at sufficient quantity and to assay both solvents for the distributed drug. This, in turn, allowed the estimation of $\log D_{oct}$ with eq. 2 making assumptions about mass balance unnecessary. $LogD_{oct}$ values measured in this way are considered the gold standard and are shown in Fig. 6A (white columns) for each investigated compound. For comparison, mass balance derived distribution coefficients ($\log D'_{oct}$) as estimated by eq. 3b are shown for both the large format experiments (Fig. 6A, grey columns) and for the miniaturized setup (Fig. 6A, black columns). The dashed columns in Fig. 6A relate to corrected $\log D'_{oct}$ values and will be discussed later (desorption with 2 - propanol was performed).

Fig. 6

No major discrepancy between $\log D_{oct}$ (gold standard, eq.2) and $\log D'_{oct}$ (eq.3b) was evident, provided that experiments were performed with 1L glass flasks. The only exception was doxorubicine, whose $\log D'_{oct}$ was slightly too low by 0.19 $\log D_{oct}$ units. Since the use of 1L glass flaks and large phase volumes ensures low surface to phase volume ratios, a possible adsorption to the glass surface can be neglected, at least at the drug concentrations tested (for discussion see below).

Interestingly, the $\log D'_{oct}$ values obtained from the miniaturized assay (Fig. 6A, black columns) were also in agreement with the gold standard $\log D_{oct}$ (Fig. 6A, white columns), except for paclitaxel (underestimation by 0.8 $\log D_{oct}$ units). The extent of drug loss (%) in the distribution experiment (Fig. 6B, grey columns) and in the reference experiment (Fig. 6B, black columns) seemed to be somehow associated with the error in $\log D_{oct}$ (paclitaxel), yet, it cannot explain the accuracy of $\log D'_{oct}$ obtained for ritonavir and saquinavir (Fig. 6A, black columns). Despite the fact that a significant fraction of both drugs was lost from aqueous bulk solution (Fig. 6B), the $\log D'_{oct}$ values agreed well with the gold standard $\log D_{oct}$, just like in

[5] Chlorpromazine was also measured but $\log D_{oct}$ values were overestimated with the filter-based assay due to enrichment at the filter supported interface. For details see accompanying manuscript 1.

case of fluvoxamine (maximal error 0.03 $\log D'_{oct}$ units). Adsorption to the well plate was however much less pronounced for fluvoxamine (Fig. 6B).

A better predictor for the experimental error in $\log D'_{oct}$ can be obtained when relating the amount of drug released from the well plate due to distribution into octanol, Δn_p, to the drug entering the octanol phase n_{oct}^{eq} (Fig. 6C). When Δn_p becomes negligible with respect to n_{oct}^{eq}, the preconditions for the validity of eq. 3b are fulfilled and the octanol/water distribution coefficients can be obtained from C_{aq}^{eq} and C_{aq}^{0}. However, the larger the $\Delta n_p / n_{oct}^{eq}$ ratio, the higher the error in $\log D'_{oct}$ (Fig. 6C).

The $\Delta n_p / n_{oct}^{eq}$ ratio was unfavorably high for paclitaxel, explaining the gross underestimation of $\log D_{oct}$. In this context it is important to note that the initial aqueous drug solutions in the miniaturized assay were prepared according to the standard industrial protocol which involves diluting 10 mM DMSO stock solutions with buffer and using the filtrated fraction for the measurement (maximal C_{total} = 22.2 µM). We could demonstrate that precipitation of paclitaxel continues with time (see also [37]), leading to drug loss greater than that expected from monolayer adsorption. Precipitation, similar to adsorption, causes an underestimation in $\log D'_{oct}$, but Δn_p is not restricted to the capacitance of the Teflon surface, with consequences for the accuracy of $\log D'_{oct}$. In case of paclitaxel, Δn_p can thus not be neglected despite the high lipophilicity (high n_{oct}^{eq}) of the drug. Moreover, the total concentration of paclitaxel was lower compared to all other compounds due to poor solubility, both effects explaining the pronounced underestimation in $\log D_{oct}$. For clarity, the large scale experiments were performed at aqueous drug concentrations well below the solubility limit (C_{total} = 10 µM; except for saquinavir/ritonavir: C_{total} = 5 µM, paclitaxel: C_{total} = 2.5 µM) to avoid post-filtration precipitation of sparingly soluble drugs.

4.2.3. Comparison of $\log D_{oct}$ *Data (this Study) with Literature Shake Flask Data*

The literature was searched for measured shake flask $\log D_{oct}$ values for the abovementioned compounds for the purpose of comparison with the gold standard $\log D_{oct}$ values measured in this study (Table 3).

Table 3

We explicitly abstained from considering the literature results as gold standards because large variations were encountered in reported shake flask data, particularly for paclitaxel. Unfortunately, experimental conditions in literature were not sufficiently specified to track back the source of variation in case of paclitaxel.

Likewise, reliable $\log D_{oct}$ values for doxorubicin, measured at pH 7.4 and at RT, were not available. A $\log D_{oct}$ slightly higher than the $\log D_{oct}$ value from this study was published ($\log D_{oct}$ = 0.8 [35]), but at pH 7.3 (RT). Other reports better agreed with our data ($\log D_{oct}$ = 0.52 and 0.44), albeit, the pH of the buffer or even the method for determination, respectively, have not been described. The literature $\log D_{oct}$ value for fluvoxamine was in line with our result, and it was also the only compound for which the experimental conditions were comparable with this study (shake flask, both phases analyzed, pH7.4). With respect to ritonavir and saquinavir we found only internal, not further specified data or calculated values, respectively, disallowing a comparative evaluation with our own data. Since distribution coefficients are sensitive to e.g. pH, buffer, drug concentration and temperature we cannot isolate discrepancies arising from the sorption to the assay construct and those related to the other experimental conditions.

4.2.4. Minimization of the Error in $\log D'_{oct}$

As shown in Fig. 5, there is a risk of underestimating octanol/water distribution coefficients when calculating the drug concentration in octanol by difference between free initial and free equilibrium aqueous drug concentrations. However, the underestimation will not manifest as experimental artifact as long as Δn_p can be neglected compared to the amount of drug entering the octanol phase, n_{oct}^{eq}. We therefore propose the following possibilities to minimize the $\Delta n_p / n_{oct}^{eq}$ ratio and, in turn, the experimental error in $\log D'_{oct}$: i) increase the analyte concentration such that $n_{oct}^{eq} \uparrow$ and $\Delta n_p \downarrow$ - the drop in Δn_p is related to the increasing saturation level of the Teflon surface, leading to a smaller difference between n_p^0 and n_p^{eq} ; and ii) increase the volume of octanol such that $n_{oct}^{eq} \uparrow\uparrow$ - since the distribution of drug into octanol is not saturable, the increase in n_{oct}^{eq} will outweigh the increase in Δn_p.

It is important to note that the $\Delta n_p / n_{oct}^{eq}$ ratio not only depends on the experimental conditions, but also on the drug's intrinsic lipophilicity which, to a large part, determines n_{oct}^{eq}. Hence, the

magnitude of error in $\log D'_{oct}$ associated with Δn_p can be described as a function of $\log D_{oct}$. Fig. 7 shows the estimated error in $\log D'_{oct}$ as a function of the true $\log D_{oct}$ for various sets of experimental conditions.

Fig. 7

The simulated error in $\log D'_{oct}$ was derived from the difference between $\log D_{oct}$ and $\log D'_{oct}$ as described in the Supporting Information. Parameter estimates from the Langmuir adsorption isotherm of chlorpromazine were used (Table 2). We are aware of the fact, that chlorpromazine is only an example and the error would be higher when using e.g. the $n_{\max}$-estimate and k-estimate from doxorubicin (Table 2), which showed multilayer adsorption. However, we describe the behavior of chlorpromazine because saturation was reached already at 25 µM corresponding to the drug concentration we used in our $\log D'_{oct}$ measurements ($n_p^0 = n_{\max}$ was a precondition for applying the model, see Supporting Information). As expected, the experimental error in $\log D'_{oct}$ increases exponentially with a drop in lipophilicity ($n_{oct}^{eq} \downarrow$), and is the higher, the lower the total drug concentration and the lower the volume of octanol. For the theoretical case of two compounds with the same affinity to the well plate but different lipophilicity, the less lipophilic drug will then have the higher experimental error in $\log D'_{oct}$. Accordingly, compounds with low lipophilicity but high affinity for Teflon (e.g. doxorubicin [37]) are the most critical compounds. It is a favorable coincidence that hydrophilic compounds also demand the use of elevated volumes of octanol (for increased sensitivity) counteracting the influence of drug adsorption to Teflon. The model used for simulating the error in $\log D'_{oct}$ was based on adsorption theory, and therefore the error estimate will be higher if precipitation occurs.

4.2.5. Correction of Erroneous $\log D'_{oct}$ *Values by Recovery with 2-Propanol*

None of the methods suitable for counteracting adsorption of hydrophilic compounds is applicable for compounds with high lipophilicity. An increase of V_{oct} is precluded by the limit of detection in the aqueous phase; and an increase of drug concentration cannot go beyond the solubility limit which is often very low for lipophilic compounds. Even though sorption to

the well plate should not affect the accuracy of $\log D_{oct}^{'}$ for lipophilic compounds (Fig. 7), precipitation potentially causes higher errors, and therefore needs to be considered.

Here, we propose a method to correct erroneous $\log D_{oct}^{'}$ values by recovery of adsorbent and/or precipitated drug with an organic solvent. If added to the aqueous phase in both the reference and the distribution experiment, the *total* initial, $C_{aq,total}^{0}$, and *total* equilibrium aqueous, $C_{aq,total}^{eq}$, drug concentration can be assessed. The difference between them corresponds to C_{oct}^{eq} (after normalization of phase volumes). Drug recovery from the well plate is possible with e.g. 2-propanol which among various investigated excipients proved to be favorable in terms of efficiency, practicability and compatibility with mass spectrometric analysis (*accompanying manuscript 3*). To avoid disturbing the phase equilibrium, 2 - propanolol has to be added to the micotiter plate only after distribution equilibrium has been achieved and, importantly, after the octanol phase has been removed from the aqueous phase. Phase separation might be facilitated by immobilizing octanol on a filter support, as described elsewhere (*accompanying manuscript 1*, [21]).

Note that the assessment of $\log D_{oct}^{'}$ still requires the measurement of the free equilibrium aqueous drug concentration, C_{aq}^{eq}, which can be obtained from an independent measurement conducted without 2-propanol. The corrected $\log D_{oct}^{'}$ value is then given by

$$\log D_{oct}^{'} = \log D_{oct} = \log\left(\frac{\left(C_{aq,total}^{0} - C_{aq,total}^{eq},\right)\cdot V_{aq}}{C_{aq}^{eq}\cdot V_{oct}}\right), \qquad (9)$$

and should agree with the gold standard $\log D_{oct}$, even if $n_p^{eq} < n_p^0$. A numerical example is given in Fig. 5.

To prove the validity of the correction procedure, we compared the accuracies of the uncorrected and the corrected $\log D_{oct}^{'}$ values (measured with the miniaturized assay), using the example of doxorubicin, fluvoxamine, ritonavir, saquinavir and paclitaxel. Inspection of Fig. 6A shows that the corrected $\log D_{oct}^{'}$ value for paclitaxel (dashed column) was in better agreement with the gold standard $\log D_{oct}$ (white column) than uncorrected $\log D_{oct}^{'}$ values (black columns). The other compounds were not affected. The reason why the $\log D_{oct}^{'}$ value of paclitaxel was still slightly too low may be that paclitaxel could not be recovered to 100 %, or that aggregation changed the overall distribution behavior. Even if further research is

necessary to understand the slight discrepancy, we consider the recovery method by using 2 - propanol as useful for approximating the true $\log D_{oct}$ if adsorption or precipitation occurs.

4.3. Recommendations for Managing Drug Loss in other *in vitro* Assays

Non-specific binding to microtiter plates is a general problem likely to arise if several unfavorable conditions coincide, namely miniaturized assay constructs, submicromolar to micromolar concentrations, and test compounds with high affinity for plastic well plates. It is rather the rule than the exception that all of these criteria are met in a typical industrial screening assay; a $\log D_{oct}$ assay is just one of many examples.

To avoid experimental artifacts in other screenings assays which likewise rely on mass balance (e.g. PAMPA, CaCo-2) or on absolute concentrations (e.g. IC 50, solubility), we recommend considering the following: i) The main error in $\log D'_{oct}$ was due to post-filtration precipitation (paclitaxel). Therefore we recommend to prepare sample solutions from DMSO stock solutions, and to wait at least ~2 h before filtration. The filtrate should be diluted with assay buffer afterwards to avoid drug concentrations close to or above the solubility limit, ii) each assay should be evaluated individually considering concentration ranges, phase volumes, etc. and iii) the assay plate should be selected carefully. As distinct from Teflon, surface treated polystyrol contains negative charges catalyzing the adsorption of cationic compounds [4]. Sorptive loss from a polypropylene plate was only slightly higher than from Teflon, but we observed that plastic components were leaching out from the plastic matrix after addition of 2-propanol.

The use of glass containers might be a viable alternative to Teflon since no multilayer adsorption was observed and, e.g., only 5.5 % of filtrated doxorubicin remained unrecovered as compared to 19.9% drug loss when using a Teflon plate (Supplementary Information). However, the fragility of glass complicates the handling of well plates and, moreover, extensive non-specific binding of other compounds has been reported (e.g. anandamide [41]). Preliminary studies in our lab using metallic well plates indicated that drug adsorption is lower as compared to Teflon but further research is required to confirm the observed trend on a larger dataset.

5 Conclusions

In summary we have shown that non-specific binding to a Teflon well plate is a very fast, saturable adsorption phenomenon which therefore likely occurs even in the highest-throughput $\log D_{oct}$ assay. Large, coplanar and lipophilic compounds with many H-bond donors showed the highest propensity to adsorption corresponding to hydrophobic, H-bonding and stacking interactions. Drug loss to Teflon leads to an underestimation in $\log D_{oct}$ for i) hydrophilic compounds with high affinity for Teflon and ii) compounds likely to precipitate during the time course of the distribution experiment. Even though lipophilic compounds likely adsorb to Teflon, the error in $\log D'_{oct}$ is negligible as long as only monolayer adsorption takes place. Then, the distribution equilibrium is shifted towards drug dissolved in the octanol phase and drug adsorption to the well plate can be neglected. Experimental artifacts related to drug loss can be counteracted by recovering drug from the Teflon surface with 2-Propanol (applicable for lipophilic compounds) or by increasing the volume of octanol (applicable for hydrophilic compounds). We consider our investigation as a guideline to eventually survey and improve also other miniaturized *in vitro* screens. More certainty in the desired outcome measure will avoid potentially costly misinterpretations and aid the drug discovery process in what it aims to be: efficient.

Acknowledgement

The authors thank Marta Hidalgo for excellent technical assistance.

Table 1 Key properties for the dataset investigated along with percentages drug loss from filtrated and 5µM test solutions after 16 h storage in a Teflon plate.

No	Compound	Charge class[a]	pK_a (acid)[b]	pK_a (base)[b]	*MW* [g/mol]	*HBD*	$c\log P$	$LogD_{oct}$ (pH7.4)[c]	Drug loss (5µM)[d][%]	Drug loss (filtrate)[e][%]	$C_{filtrate}$ [µM]
1	Amprenavir	N			505.6	4	3.29	2.46	1.9±0.6	1.7 ±1.6±0.6	43.7
2	Caffeine	N		<2	194.2	0	-0.04	-0.1	-	-	45.6
3	Colchicine	N			399.4	1	1.20	0.95	-	-	59.5
4	Dexamethasone	N			392.5	3	1.79	1.79	-	-	44.6
5	Diazepam	N		3.38	284.7	0	2.96	2.84	-	-	43.2
6	Digoxin	N			780.9	6	1.42	1.34	4.4±1.3	2.1 ±0.5	39.9
7	Midazolam	N			325.8	0	4.73	3.32	1.8±1.4	2.7 ±0.1	42.2
8	Paclitaxel	N			853.9	4	4.94	3.09[c1]	54.2±1.0	57.3±14	13.2
9	Ritonavir	N			720.9	4	1.72	3.68	36.6±3.3	8.3 ±1.3	18.9
10	Rolipram	N		5.71	275.3	1	3.42	1.91	-	-	46.5
11	Diclofenac · Na	A	4.02		296.2	2	4.73	1.15	-	-	46.0
12	Indometacin	A	4.43		357.8	1	4.18	0.79	-	3.0 ±1.7	44.1
13	Ketorolac · Tromethamin	A	3.44		255.3	1	1.62	-0.58[b2]	-	-	56.9
14	Alfentanil · HCL	B		6.46	416.5	0	2.13	2.2	-	-	12.1
15	Buspirone · HCL	B		7.61	385.5	0	2.19	2.13	-	-	50.0
16	Chlorpromazine · HCL	B		9.38[b1]	318.9	0	5.30	3.36	9.7±0.0	10.6±2.1	26.0
17	Doxorubicin	B	9.45	8.16	543.5	7	0.32	0.36[c2]	24.4±0.2	19.9±2.8	54.9
18	Fluvoxamine·Maleate	B		9.11/5.82	318.3	2	3.03	1.81	3.1±2.5	3.2 ±0.5	44.4
19	Saquinavir	B		7/3	670.9	6	4.73	3.78	59.4±1.0	12.9±1.3	22.8
20	Sumatriptan	B		9.49	295.4	2	0.74	-1.15[c1]	-	-	50.0
21	Vinblastine · Sulfate	B		7.4/5.4[b2]	811.0	3	5.23	3.11	20.1±1.6	2.8 ±0.8	35.2
22	Cetirizine	Z	2.86	8.00	388.9	1	2.08	1.28	-	-	50.0
23	Raclopride · Tartrate	Z	5.95	9.46	347.2	2	4.06	1.13	0.5 ±0.0	4.0 ±0.0	50.3
24	Tiagabine · HCL	Z	3.1	9.02	375.5	1	2.78	1.23	-	-	63.0

[a]N: neutral (less than 3 % ionization at pH 7.4); A: acid with $ApK_a < 8.9$; B: base $BpK_a > 6$; Z: zwitterions with $ApK_a < 8.9$ and $BpK_a > 6$.
[b]Measured by potentiometry (in-house), [b1] Value taken from [42]. [b2] Value taken from Therapeutic Drugs [43].
[c]Measured in-house as described in this study. $LogD_{oct}$ values for compounds with high affinity for Teflon were corrected by using 2-propanol (see Theory).
[c1]Measured in-house with a miniaturized shake flask logD assay, no filter-device used (50mM Tapso, pH 7.4, 5%DMSO) [c2]Large scale shake flask value obtained from measurement in both phases.
[d]Drug loss from 5µM aqueous drug solutions. The exact concentration was in some cases slightly lower due to rapid drug adsorption to the preparation plate and drug loss to pipetting devices during transfer to the Teflon measurement plate (e.g. C_{total} (Paclitaxel) = 3.1 µM)
[e]Drug loss from filtered aqueous drug solutions (C_{total}= maximal 50 µM). Only drug loss > 2% listed.

Table 2 Summary of model parameters for the adsorption isotherms shown in Fig. 3B - C along with the n_{layer} estimate at the Teflon surface for chlorpromazine and doxorubicin.

Compound	Langmuir				B.E.T.			
	r^2	k [μM^{-1}]	n_{max} [a] [$\mu M/m^2$]	n_{layer}	r^2	k [μM^{-1}]	n_{max} [a] [$\mu M/m^2$]	C_{sat} [μM]
Chlorpromazine	0.949	0.2895	1.433	1.2	0.997	9.19	6.98	645
Doxorubicin	0.990	0.0282	7.239	2.9	-	-	-	-

[a] Estimated contact area of aqueous solution with the Teflon well: 70mm^2.

Table 3 Comparison of gold standard $\log D_{oct}$ (pH 7.4) values obtained in this study (1L glass flasks, both phases analyzed) and $\log D_{oct}$ values obtained from literature.

Compound	This study (gold standard)		Literature studies			
	$\log D_{oct}$ (pH 7.4)	SD	$\log D_{oct}$	Experimental conditions	V_{aq}, V_{oct}	Phase analyzed
Doxorubicin	0.36	0.00	0.44[31]	not specified	?	?
			0.52[17]	shake flask, pH ?	1mL both	aqueous phase
			0.8[35]	shake flask, pH 7.3	750µL both	both phases
Fluvoxamin	1.72	0.00	1.8[36]	shake flask, pH 7.4	5mL, both	octanol phase
Ritonavir	3.65	0.00	3.1[32]	not specified	?	?
Saquinavir	3.58	0.00	4.1[4]	calculated ?	-	-
Paclitaxel	3.17	0.01	>2[17]	shake flask, pH ?	1mL, both	aqueous phase
			2.49[33]	shake flask, not further specified	?	?
			3.5[34]	not specified	?	?

FIGURES

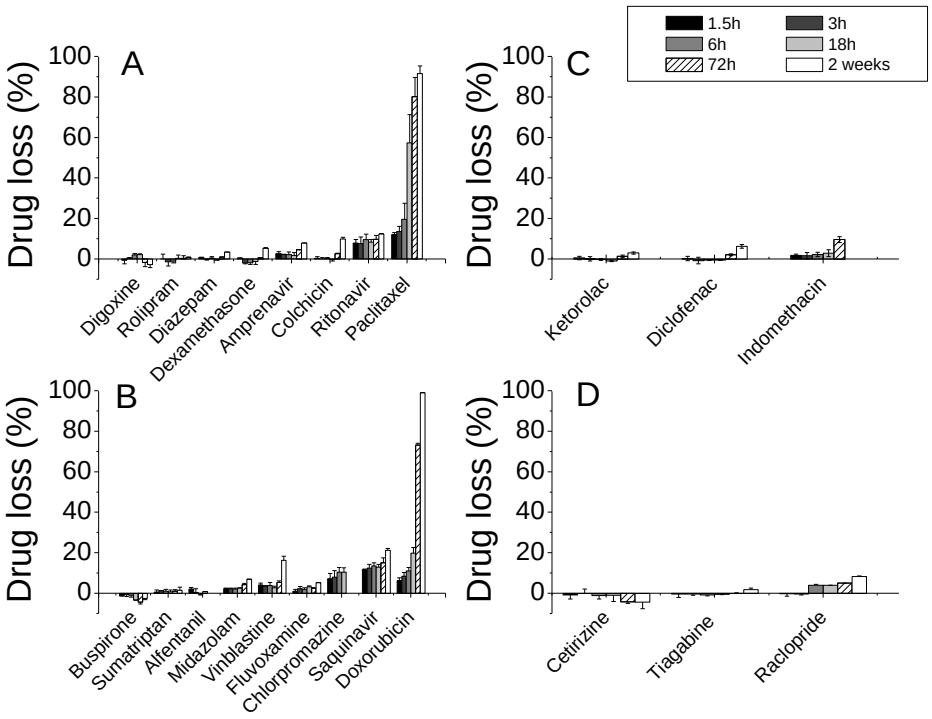

Figure 1 Drug loss from filtered aqueous test solutions to a 96 well Teflon plate for (**A**) neutral, (**B**) basic, (**C**) acidic and (**D**) zwitter-ionic compounds. Drug loss was measured over a period of maximal 2 weeks. Total concentrations of drug in the filtrate are given in Table 1.

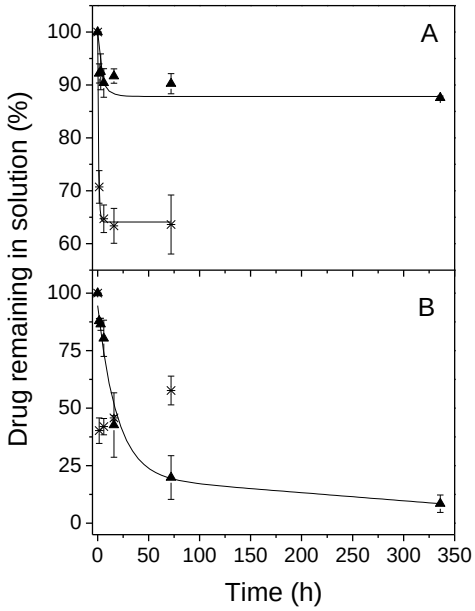

Figure 2 Time dependent loss for ritonavir (**A**) and paclitaxel (**B**) from aqueous bulk solution stored in a 96 well Teflon plate. Experiments were performed at standardized drug concentrations (C_{total} =5 µM, ✳) or at drug concentrations obtained after filtration of 50 µM test solutions, yielding C_{total} = 18.9 µM ritonavir and 13.2 µM paclitaxel (▲). Lines are biexponential decay curves fitted to the experimental data.

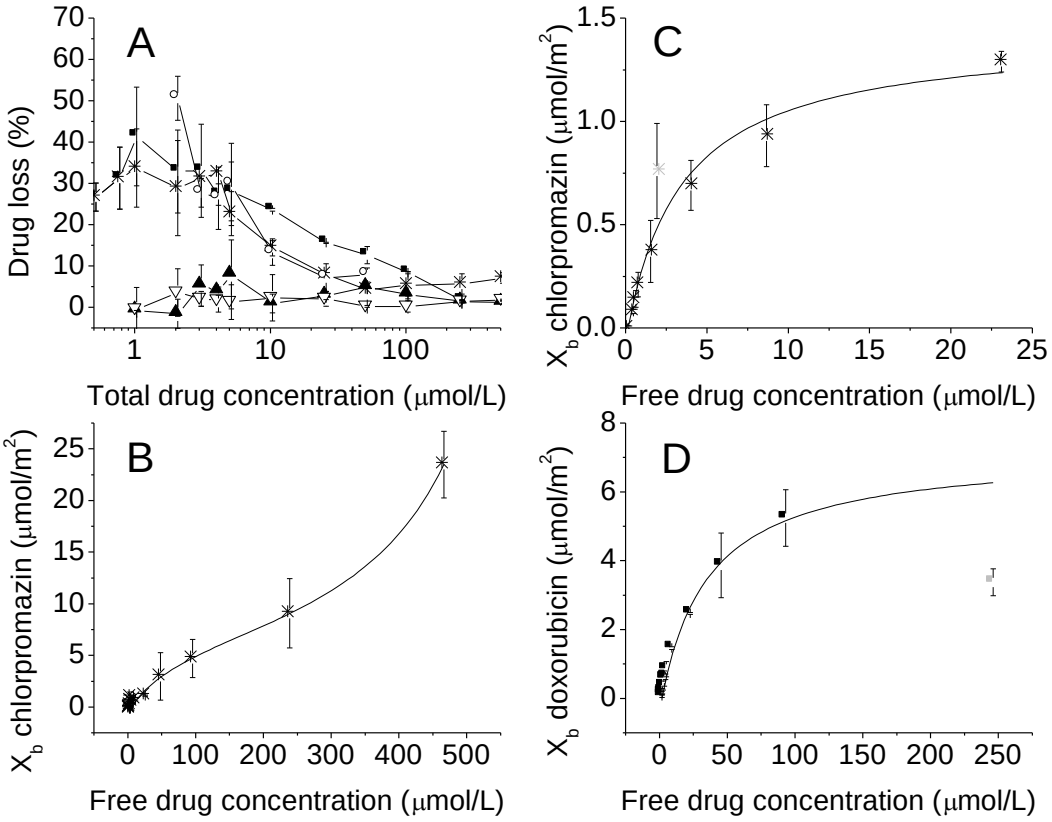

Figure 3 Concentration - dependency of drug loss from aqueous bulk solutions (0.5 - 500 μM drug in 50 mM Tris/114 mM NaCl/pH 7.4) after 16 h - storage in a Teflon plate. **A:** Percentage drug loss as a function of total aqueous concentrations of the bases doxorubicin (■) and chlorpromazine (✳), the neural drugs ritonavir (○) and diazepam (▽) and the acid indomethacin (▲). **B - D**: Adsorption isotherms of chlorpromazine (**B, C**) and doxorubicin (**D**). Lines are fits to the experimental data using either the BET (**B**) or the Langmuir type (**C, D**) adsorption isotherm at maximal 500 μM (B), 25 μM (**C**) and 100 μM (**D**) total concentration. Greyed out data points were not used for the fit and considered as real experimental artifacts (**C**) or were outliers because the compound precipitated (**D**).

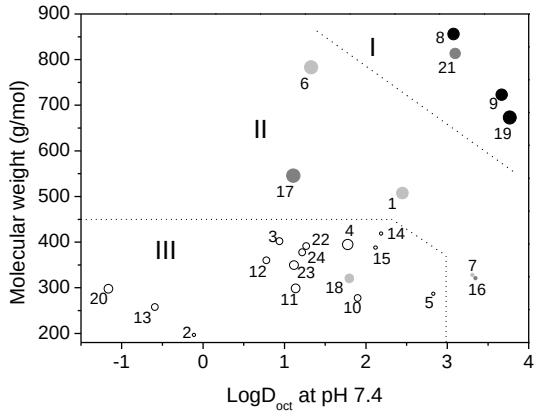

Figure 4 Classification map for drug adsorption to Teflon based on $\log D_{oct}$, *MW* and number of H-bond donors (increasing size of the symbols with increasing numbers of HBD (range = 0 - 7)). Colors of the symbols reflect the extent of drug loss from 5 µM aqueous solutions after t = 16h: 0 – 1 % (○), 1 – 5 %(●), 5 – 25 % (●), > 25 % (●) drug loss.

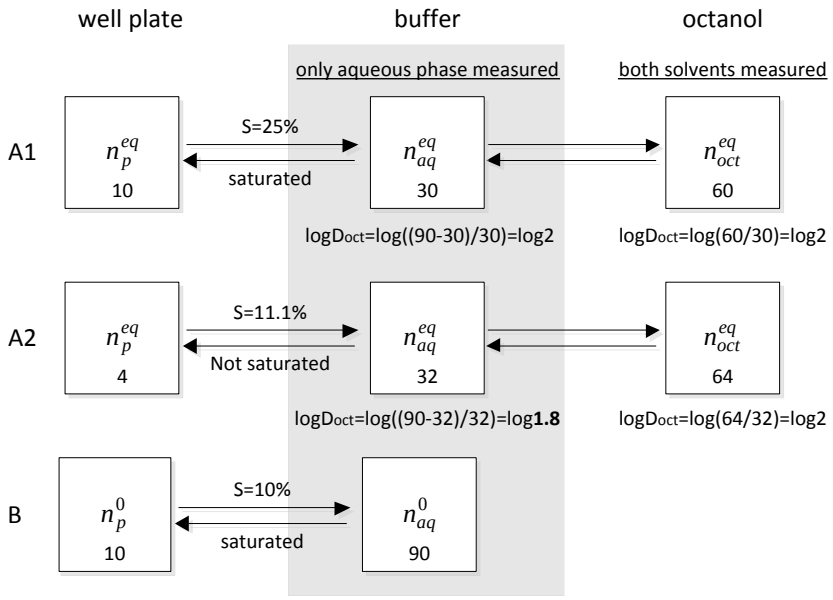

Figure 5 Numerical example showing the impact of drug adsorption to a well plate on the accuracy of $\log D_{oct}$ (for simplicity: $V_{aq} = V_{oct}$ allowing to substitute concentrations, C, by amounts, n). **A1,2**: Three-compartment model describing the distribution of a solute (n_{total}=100 µmol) throughout the well plate-buffer-octanol system yielding n_p^{eq}, n_{aq}^{eq} and n_{oct}^{eq} drug in each compartment (equilibrium conditions). The solute is distributed according to its affinity for the well plate (plastic sorption, S) and its $\log D_{oct}$ value ($\log D_{oct} = \log\left(n_{oct}^{eq} / n_{aq}^{eq}\right) = \log 2$). While n_{aq}^{eq} can be directly measured, n_{oct}^{eq} is usually assessed by difference between the free initial and the free equilibrium aqueous drug concentration (n_{aq}^0, n_{aq}^{eq}) such that $\log D' = \log\left(\left(n_{aq}^0 - n_{aq}^{eq}\right) / n_{aq}^{eq}\right)$. A reference experiment without octanol (**B**) is performed to retrieve n_{aq}^0. Provided that all available adsorption sides on the Teflon surface are saturated in the reference (**B**) and in the distribution experiment (**A1**), then $n_p^{eq} = n_p^0$, and application of the mass balance equation yields the correct $\log D_{oct}$ (=2). However, when the distribution of drug into octanol leads to a removal of drug from the well plate such that $n_p^{eq} < n_p^0$, assumptions of mass balance are violated resulting in underestimation of $\log D_{oct}^{'}$ ($\log D_{oct}^{'}$=1.8) (**A2**). Recovery experiments with 2-propranol, involving the measurement of the total and the free aqueous drug concentration, will yield correct $\log D_{oct}$ values (here: $\log D_{oct}^{'} = \log((100-40)/30) = \log 2$).

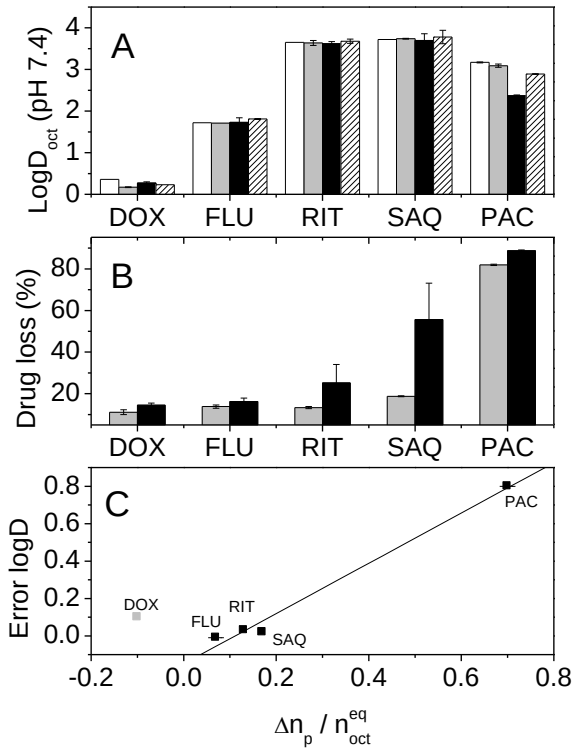

Figure 6A: Shake flask $\log D_{oct}$ (pH 7.4) values measured in 1L glass flasks (white and grey columns) and in 96-well Teflon plates (black and dashed columns), respectively. $LogD_{oct}$ values were obtained from concentration analysis in both phases (white columns) or by assaying only the aqueous phase and applying distinct mass balance equations: Disregard of precipitation or adsorption to glass or Teflon (eq.3b, grey and black columns) vs. correction with 2-propanol (eq. 9, dashed columns). Recovery from precipitated or adsorbed drug with 2-propanol enabled quantification of the percentage drug loss shown in **B:** Drug loss from initial (grey columns) and from equilibrium (black columns) aqueous drug solutions corresponding to the reference experiment without octanol and to the actual distribution experiment with octanol. **C:** Experimental error in $\log D_{oct}$ as a function of the change in drug loss with respect to the reference and the distribution experiment, related to the amount of drug in octanol. The line is the linear fit to the experimental data (symbols). Doxorubicin was not included in the fit because phase volume ratios were different (V_{aq}=140 µL, V_{oct}=1 µL, except doxorubicin: V_{oct}=15 µL).

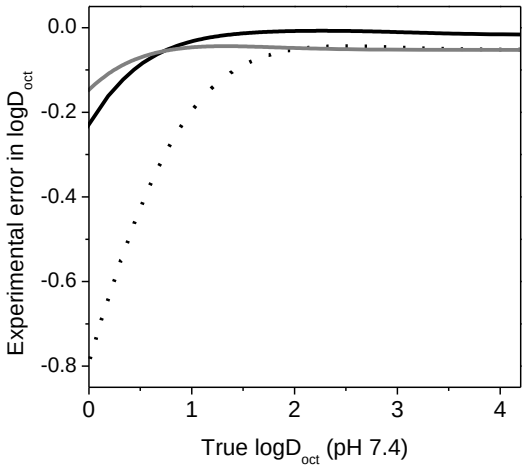

Figure 7 Expected experimental error in $\log D'_{oct}$ as a function of the true $\log D_{oct}$ for the theoretical situation that compounds with different lipophilicity exhibit the same affinity for the microtiter plate. The experimental error corresponds to the difference between $\log D_{oct}$ (simulated with eq. S4a) and $\log D'_{oct}$ (simulated with eq. S4b) calculated for different experimental conditions: C_{total}=25 µM, V_{oct}=1 µL (—); C_{total}=9 µM, V_{oct}=1 µL (·····); C_{total}=9 µM, V_{oct}=15 µL (—). V_{aq}=const.=140 µL (corresponding contact area with Teflon~90 mm^2). Parameter estimates for k and n_{max} were gained from the Langmuir-type adsorption isotherm of chlorpromazine (Fig. 3C), but corrected for the different contact area with Teflon.

Supporting Information

The Magnitude of Error due to Drug Loss to Teflon as a Function of $\log D_{oct}$

When determining a solute's octanol/water distribution coefficient, defined as

$$\log D_{oct} = \log \left(C_{oct}^{eq} / C_{aq}^{eq} \right), \quad \text{(S1)}$$

direct concentration analysis of both phases for the distributed solute is clearly preferable rather than possibly violate mass balance by analyzing only one. If compounds show adsorption to the well plate, a third compartment needs to be considered in the mass balance equation which is given by (for details see Section 2 in the main manuscript):

$$n_{total} = C_{aq}^{0} \cdot V_{aq} + n_{p}^{0} = C_{aq}^{eq} \cdot V_{aq} + C_{oct}^{eq} \cdot V_{oct} + n_{p}^{eq} . \quad \text{(S2)}$$

Neglecting potential drug adsorption, and estimating octanol/water distribution coefficients with a simplified mass balance equation (eq. 3b) leads to an underestimation of $\log D_{oct}$, which is associated with $\Delta n_p = n_p^0 - n_p^{eq}$, or more precisely the ratio between Δn_p and n_{oct}^{eq} (see Section 4.2.2. in the main manuscript). Accordingly, the magnitude of error in mass balance derived $\log D_{oct}^{'}$ values depends on the compound's lipophilicity, and can be described as a function of the true $\log D_{oct}$.

In this study, we related the error estimation to the simplest case, i.e. when drug adsorption cannot go beyond the point where one layer of adsorbate ($n_{\max}$) is formed, and the amount of adsorbed drug (n_p^{eq}) at a certain aqueous concentration is approximated by the Langmuir type of isotherm (eq. 6, main manuscript). We further assumed that the applied concentration in the reference experiment (without octanol) is high enough to saturate the surface, such that $n_p^0 = n_{\max}$ and $\Delta n_p = n_{\max} - n_p^{eq}$, leading to:

$$\Delta n_p = n_{\max} - \frac{k \cdot n_{\max} \cdot C_{aq}^{eq}}{1 + k \cdot C_{aq}^{eq}} . \qquad \text{(S3)}$$

Substitution of eq. S2 and eq. S3 into eq.S1 yields (after rearrangement):

$$\log D_{oct} = \log\left[\frac{1}{C_{aq}^{eq}} \cdot \frac{C_{aq}^{0} \cdot V_{aq}}{V_{oct}} - \frac{n_{\max}}{V_{oct} \cdot C_{aq}^{eq}} + \frac{k \cdot n_{\max}}{1 + k \cdot C_{aq}^{eq}} \cdot \frac{1}{V_{oct}} - \frac{V_{aq}}{V_{oct}} \right], \qquad \text{(S4a)}$$

where V_{aq} and V_{oct} are the given phase volumes, $n_{\max}$ and k can be obtained from an independent measurement of the adsorption isotherm and C_{aq}^{0} is given by $C_{aq}^{0} = C_{total} - n_{\max} / V_{aq}$. When now allowing C_{aq}^{eq} to vary, for each C_{aq}^{eq} a corresponding $\log D_{oct}$ may be calculated.

It is then possible to simulate the situation when adsorption is neglected and experimentally derived $\log D_{oct}^{'}$ values are obtained with eq. 3b, namely by simply discarding the adsorption-related terms in eq.S4a such that

$$\log D_{oct}^{'} = \log\left[\frac{1}{C_{aq}^{eq}} \cdot \frac{C_{aq}^{0} \cdot V_{aq}}{V_{oct}} - \frac{V_{aq}}{V_{oct}} \right]. \qquad \text{(S4b)}$$

The difference between $\log D_{oct}$ (eq.S4a) and $\log D_{oct}^{'}$ (eq.S4b) corresponds to the experimental error in $\log D_{oct}^{'}$ encountered when applying eq.3b despite the fact that adsorption to the well plate occurs.

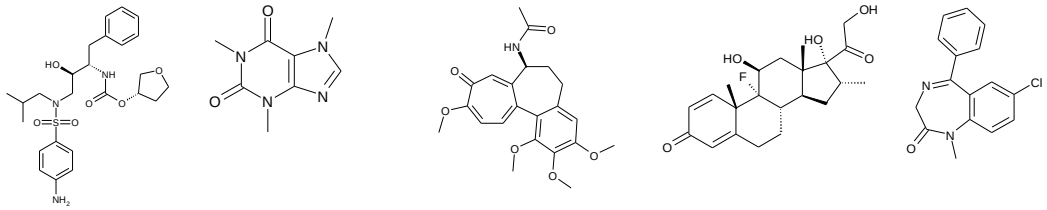

Amprenavir Caffeine Colchicine Dexamethasone Diazepam

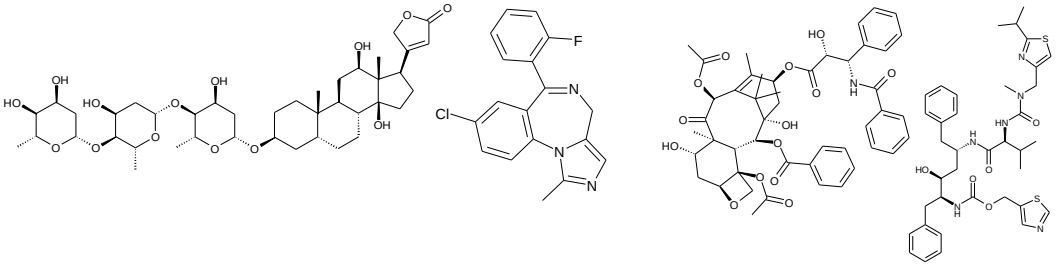

Digoxin Midazolam Paclitaxel Ritonavir

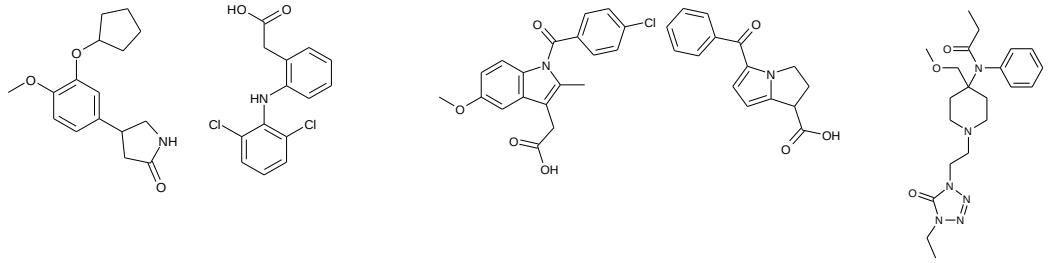

Rolipram Diclofenac Indometacin Ketorolac Alfentanil

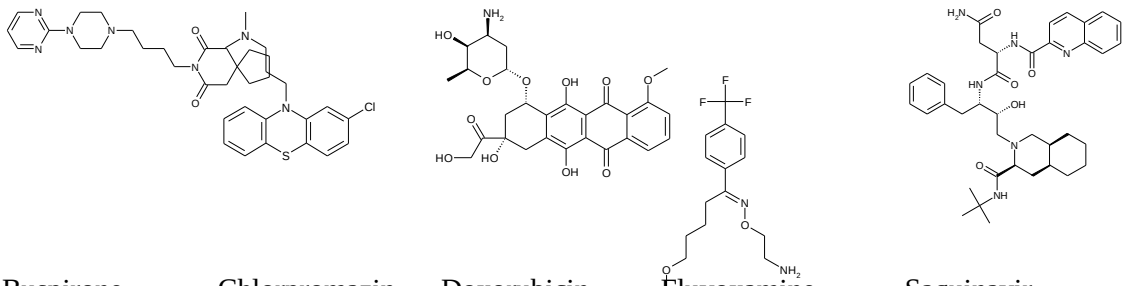

Buspirone Chlorpromazine Doxorubicin Fluvoxamine Saquinavir

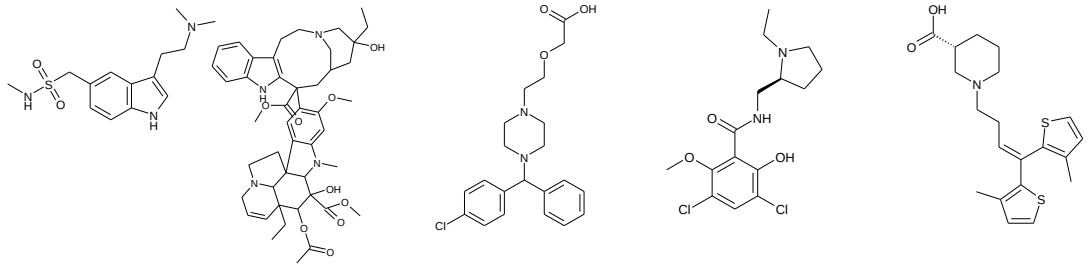

Sumatriptan Vinblastine Cetirizine Raclopride Tiagabine

Figure S1 Structures of the compounds investigated.

Table S1 Physicochemical and structural descriptors used for the development of the prediction model.

Descriptor	Comment
clogP	Calculated octanol-water partition coefficient
$LogD_{oct}$	Measured octanol-buffer distribution coefficient at pH 7.4
MW	Molecular weight of the desalted drug
Hydrophobic surface	
Hydrophobic volume	
PSA	Polar surface area
Hydrophilic volume	
Total surface	
Total volume	
A_D	Calculated cross-sectional area of the drug in the membrane bound-conformation
No. of rings	
No. of aromatic rings	
No. of H-bond acceptors	Value taken from Pubchem database
No. of H-bond donors	calculated with our in-house developed modeling package Moloc
No of sp3 carbons	
d0	Root mean square deviation of the atom positions from the plane defined by the maximum and medium principal axes (2*d0 = "thickness" of the structure); Parameter representing the thickness of a molecule
d1	Same as d0 but for the maximum and minimum axes (2*d1 = "width" of structure); Parameter representing the width of a molecule
d2	Same as d0 but for the medium and minimum axes (2*d2 = "length" of structure); Parameter representing the length of a molecule
d0/d2	d0 divided by d2; "Globularity" measure of a molecule. High values are indicative for "spherical" shaped molecules, molecules with low values are more prolate and elongated
Fraction ionized	Net charge at pH 7.4 as calculated from measured pK_a according to Henderson-Hasselbalch-equation.

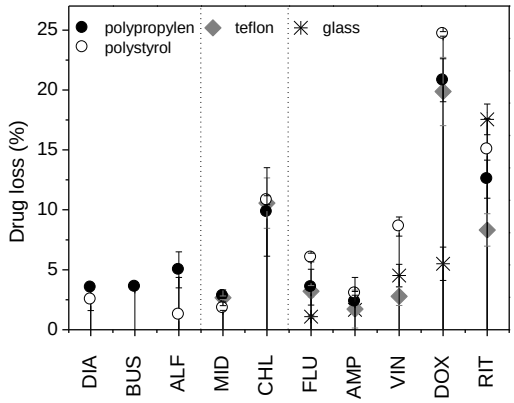

Figure S2 Drug loss from filtrated aqueous bulk solutions (100 µL, 50 mM Tris/114 mM NaCl/pH 7.4) to microtiter plates (polystyrol, polypropylene, Teflon) and to glass vials. Only compounds are shown for which drug loss was > 2.5% to at least one vessel. Drug sorption was arbitrarily set to 0 if less than 1% remained unrecovered. Paclitaxel, indomethacin, raclopride and saquinavir were excluded because precipitation occurred in at least one experiment. Vinblastine was excluded because co-elution of leaching plastic components from polypropylene disturbed the analysis.

References

1. van de Waterbeemd, H., B. Testa, and Editors, *Drug Bioavailability; Estimation of Solubility, Permeability, Absorption and Bioavailability; Second, Completely Revised Edition. [In: Methods Princ. Med. Chem., 2009; 40]*2009. 623 pp.
2. DeWitte, R.S., *Avoiding physicochemical artefacts in early ADME-Tox experiments.* Drug Discovery Today, 2006. **11**(17 & 18): p. 855-859.
3. McGovern, S.L., et al., *A Common Mechanism Underlying Promiscuous Inhibitors from Virtual and High-Throughput Screening.* J. Med. Chem., 2002. **45**(8): p. 1712-1722.
4. Fukazawa, T., Y. Yamazaki, and Y. Miyamoto, *Reduction of non-specific adsorption of drugs to plastic containers used in bioassays or analyses.* J. Pharmacol. Toxicol. Methods 2010. **61**(3): p. 329-333.
5. Banker, M.J., T.H. Clark, and J.A. Williams, *Development and validation of a 96-well equilibrium dialysis apparatus for measuring plasma protein binding.* J. Pharm. Sci. , 2003. **92**(5): p. 967-974.
6. Loh, W. and P.L.O. Volpe, *Adsorption of alkyl p-hydroxybenzoates from aqueous solution onto Teflon.* J. Colloid Interface Sci., 1996. **179**(1): p. 322-3.
7. Ogita, M., et al., *Application of the adsorption effect of optical fibres for the determination of critical micelle concentration.* Sens. Actuators, B 2000. **B64**(1-3): p. 147-151.
8. Ogita, M., et al., *The detection of critical micelle concentration based on the adsorption effect using optical fibers.* Jpn. J. Appl. Phys., Part 2, 1998. **37**(1A/B): p. L85-L87.
9. Parker, L.V. and T.A. Ranney, *Effect of concentration on sorption of dissolved organics by PVC, PTFE, and stainless steel well casings.* Ground Water Monit. Rem., 1994. **14**(3): p. 139-49.
10. Jardim, I.C.S.F., et al., *Preparation of pure hexavalent chromium-51 and 51Cr(H2O)63+: problems with acid contaminated polytetrafluoroethylene beakers.* Appl. Radiat. Isot., 1989. **40**(7): p. 643.
11. Galembeck, F., *Sorption of iron pentacarbonyl in Teflon.* J. Polym. Sci., Polym. Chem. Ed., 1978. **16**(11): p. 3015-17.
12. D'Arcy, P.F., *Drug interactions with medicinal plastics.* Adverse Drug React. Toxicol. Rev., 1996. **15**(4): p. 207-219.
13. Parker, L.V. and T.A. Ranney, *Effect of concentration of sorption of dissolved organics by well casings*, 1993, Cold Regions Res. Eng. Lab., Hanover, NH, USA. p. 22 pp.
14. Palmgren, J.J., et al., *Drug adsorption to plastic containers and retention of drugs in cultured cells under in vitro conditions.* Eur. J. Pharm. Biopharm., 2006. **64**(3): p. 369-378.
15. Di, L., et al., *Impact of recovery on fraction unbound using equilibrium dialysis.* J Pharm Sci, 2012. **101**(3): p. 1327-35.
16. Dearden, J.C. and G.M. Bresnen, *The measurement of partition coefficients.* Quant. Struct.-Act. Relat. , 1988. **7**(3): p. 133-44.
17. Yahya, A.M., J.C. McElnay, and P.F. D'Arcy, *Drug sorption to glass and plastics.* Drug Metab. Drug Interact., 1988. **6**(1): p. 1-45.

18. Fayet, A., et al., *Determination of unbound antiretroviral drug concentrations by a modified ultrafiltration method reveals high variability in the free fraction. [Erratum to document cited in CA150:047250]*. Ther. Drug Monit., 2010. **32**(1): p. 117.
19. Gerebtzoff, G. and A. Seelig, *In silico prediction of blood - Brain barrier permeation using the calculated molecular cross-sectional area as main parameter.* Journal of Chemical Information and Modeling, 2006. **46**(6): p. 2638-2650.
20. Eriksson, L., et al., *Multi- and Megavariate Data Analysis*2006: Umetrics.
21. Wagner, B., et al., *Carrier Mediated Distribution System (CAMDIS): A new approach for the measurement of octanol/water distribution coefficients.* Eur J Pharm Sci, 2014. **68C**: p. 68-77.
22. Illum, L. and H. Bundgaard, *Sorption of drugs by plastic infusion bags.* Int. J. Pharm., 1982. **10**(4): p. 339-51.
23. Malick, A.W., et al., *Loss of nitroglycerin from solutions to intravenous plastic containers: a theoretical treatment.* J. Pharm. Sci., 1981. **70**(7): p. 798-800.
24. Roberts, M.S., *Modeling solute sorption into plastic tubing during organ perfusion and intravenous infusions.* J. Pharm. Sci. , 1996. **85**(6): p. 655-665.
25. Swindell, C.S., et al., *Biologically active taxol analogues with deleted A-ring side chain substituents and variable C-2' configurations.* J Med Chem, 1991. **34**(3): p. 1176-84.
26. Zhang, J.A., et al., *Development and characterization of a novel Cremophor EL free liposome-based paclitaxel (LEP-ETU) formulation.* Eur. J. Pharm. Biopharm. , 2005. **59**(1): p. 177-187.
27. Liggins, R.T., W.L. Hunter, and H.M. Burt, *Solid-State Characterization of Paclitaxel.* J. Pharm. Sci., 1997. **86**(12): p. 1458-1463.
28. Kansy, M., F. Senner, and K. Gubernator, *Physicochemical high throughput screening: parallel artificial membrane permeation assay in the description of passive absorption processes.* J Med Chem, 1998. **41**(7): p. 1007-10.
29. Kadar Eugene, P., et al., *Evaluation of the relationship between a pharmaceutical compound's distribution coefficient, log D and adsorption loss to polypropylene in urine and CSF.* Bioanalysis, 2010. **2**(4): p. 755-67.
30. Parker, L.V., A.D. Hewitt, and T.F. Jenkins, *Influence of casing materials on trace-level chemicals in well water.* Ground Water Monit. Rev. , 1990. **10**(2): p. 146-56.
31. Illum, L., H. Bundgaard, and S.S. Davis, *A constant partition model for examining the sorption of drugs by plastic infusion bags.* Int. J. Pharm., 1983. **17**(2-3): p. 183-92.
32. Song, D., L.-F. Hsu, and J.L.S. Au, *Binding of Taxol to Plastic and Glass Containers and Protein under in Vitro Conditions.* J. Pharm. Sci., 1996. **85**(1): p. 29-31.
33. Lee, K.-J., et al., *Modulation of nonspecific binding in ultrafiltration protein binding studies.* Pharm. Res., 2003. **20**(7): p. 1015-1021.
34. Herforth, C., et al., *Determination of nelfinavir free drug concentrations in plasma by equilibrium dialysis and liquid chromatography/tandem mass spectrometry: important factors for method optimization.* Eur. J. Pharm. Sci., 2002. **15**(2): p. 185-195.
35. Tojino, M., et al., *Immobilization of fluorous oligosaccharide recognized by influenza virus on polytetrafluoroethylene filter.* Bioorg. Med. Chem. Lett. , 2012. **22**(2): p. 1251-1254.

36. Fowkes, F.M., *Attractive forces at interfaces.* J. Ind. Eng. Chem. (Washington, D. C.) 1964. **56**(12): p. 40-52.
37. Biswal, N.R. and S. Paria, *Effect of Electrolyte Solutions on the Adsorption of Surfactants at PTFE-Water Interface.* Ind. Eng. Chem. Res. , 2010. **49**(15): p. 7060-7067.
38. Michael Allwood, A.S., Patricia Wright, *The cytotoxics handbook*2002: Racliffe Medical Press Ltd. .
39. Bogardus, J.B. and R.K. Blackwood, Jr., *Solubility of doxycycline in aqueous solution.* J Pharm Sci 1979. **68**(2): p. 188-94.
40. Skowronek, M., et al., *Self-assembly of Congo Red. A theoretical and experimental approach to identify its supramolecular organization in water and salt solutions.* Biopolymers, 1998. **46**(5): p. 267-281.
41. Oddi, S., et al., *Pitfalls and solutions in assaying anandamide transport in cells.* J Lipid Res, 2010. **51**(8): p. 2435-44.
42. Fischer, H., *Passive Diffusion and Active Transport through Biological Membranes - Binding of Drugs to Transmembrane Receptors* 1998.
43. Dollery, C., *Therapeutic drugs* 2ed1998: Churchill Livingstone.

4.3 Drug Adsorption to Teflon and Excipient-Aided Drug Recovery

Frauke Assmus, Marta Hidalgo, Holger Fischer,Anna Seelig

Author's Contributions:

Frauke Assmus	• Idea and design of the study • Performing the experiments • Writing the manuscript
Marta Hidalgo	• Help in performing ion suppression studies in HPLC-MS •
Holger Fischer	• Supervision of the work • Valuable discussions • Proofreading the manuscript
Anna Seelig	• Supervision of the work • Valuable discussions • Reviewing the manuscript

ABSTRACT

Drug adsorption to microtiter plates has been recognized as a potential source of experimental artifacts in high-throughput screening assays used in pre-clinical drug development, however, little efforts have been made to correct for adsorption. In this study, we investigated different excipients in terms of their ability to recover drug adsorbed to a Teflon well plate. Recovery experiments were performed at the example of 24 structurally diverse drugs and by using various classes of excipients including i) detergents of different charge state (taurocholic acid, CHAPS, CTAB, SDS, Brij 35, ii) cyclodextrines (2,6-di-O-methyl-β-cyclodextrin), and iii) organic solvents (2-propanol, DMSO, acetonitrile). Drug adsorption before and after addition of excipients was measured in terms of percentage drug loss from aqueous bulk solution as determined by means of HPLC-UV. Drug loss before addition of excipients was generally negligible for anionic and zwitter-ionic drugs whereas some cationic (fluvoxamine, chlorpromazine, saquinavir, doxorubicin) and neutral drugs (ritonavir, paclitaxel) showed pronounced adsorption to Teflon. Complete recovery of neutral drugs was achieved by all of the investigated detergents, provided that experiments were performed above critical micellar concentrations such that solubilization into the micelle dominated over adsorption to the Teflon surface. Recovery of cationic drugs was detergent- and drug - specific and improved in the order of taurocholic acid ≈ CHAPS < Brij35 ≈ CTAB < SDS. The superior detergency of SDS may be explained by electrostatic repulsion between SDS residing at the Teflon surface and mixed SDS-drug micelles free in solution. Submicellar concentrations of detergent should be avoided since drug recovery was either incomplete or adsorption of charged drugs reinforced by oppositely charged detergents. Regarding 2-propanol, acetonitrile and 2,6-di-O-methyl-β-cyclodextrin, recovery of all drugs except for doxorubicin was achieved. Since 2-propanol was the only excipient which caused no ion suppression in mass spectrometry, we recommend using 2-propanol for drug recovery when relying concentration analysis on HPLC-MS, and SDS when relying on HPLC-UV. The proposed guideline for excipient-aided drug recovery may be applied for the correction of potentially erroneous results in high-throughput assays to avoid misinterpretations and achieve higher certainty in the data of interest.

KEYWORDS

Drug adsorption to Teflon, Drug recovery, Non-specific binding to plastics, Excipients, Ion suppression

1. Introduction

Miniaturization, high throughput (HT) technology and automation have become routine standards in preclinical drug development to accelerate the nomination of drug candidates and to meet the demand for efficiency, speed and low costs. Assay miniaturization has evolved by the extensive use of plastic materials and the availability of microliter plates with as much as 1536 wells per plate. Recently, however, it has been recognized that non-specific binding to the lab ware as well as drug precipitation/aggregation may become significant in miniaturized assays and potentially lead to experimental artifacts [1]. Many examples for falsified experimental results due to non-specific binding have been reported including overestimation of IC_{50} values [2], underestimation of plasma, urine and cerebrospinal fluid (CSF) concentrations [3], misinterpretation of adsorption as protein binding [4], misjudged exposure to environmental pollutants [5] and unreliable drug permeability estimates [6].

Drug sorption to a multitude of laboratory equipment (e.g. infusion bags, syringes, filtration units, tubings, microtiter plates, cover slips, pipettes, hollow fibres, microdialysis tubings [7-21]), has been studied and it is now well known that plasticizers, mainly present in polyvinylchloride (PVC), are a major source of pronounced drug loss to plastic material [22]. However, the absence of plasticizers in other commonly used laboratory materials such as polypropylene, polystyrol, glass and silicone does not necessarily guarantee inertness to drug adsorption. Notably, also sorptive loss to Teflon has been observed at the example of environmental pollutants [18], amphiphilic benzoates [23] and detergents [24] which disproves the widespread, but erroneous a priori assumption that Teflon is inert to adsorption. The affinity of proteins to Teflon membranes has even successfully been applied for the adsorption of proteins in Western blotting [25].

Predominantly lipophilic compounds show a high likelihood of non-specific binding to plastic materials which points to the relevance of hydrophobic binding forces in drug-plastic interactions [23]. In addition, electrostatic interactions contribute to the process of drug loss if functionalized plastic materials containing charged surface residues are concerned. In our *accompanying manuscript 2* we moreover show that hydrogen bonding and engagement of coplanar ring systems in stacking interactions can be associated with drug loss to Teflon, yet drug lipophilicity was a dominant

factor determining drug adsorption. Consequently, the trend towards favoring rather lipophilic drug candidates in the lead optimization and selection process increases the relevance of drug loss to the labware and poses new challenges for the development of HT screening assays.

In view of potential experimental errors associated with drug loss to plastics, methods to inhibit or reverse drug adsorption are of major interest. Some insights can be gained from antigen diagnostics with the ELISA assay in which bovine serum albumin and detergents are applied to block the surface of the assay plate (polystyrol) and to prevent adsorption of excess antibody [26-28]. With respect to small molecules, much less attention has been paid to the inhibition or recovery of non-specific binding. The existing knowledge is mainly based on case studies focusing on the minimization of drug loss to filtration units [29] and polypropylene containers for urine and CSF sampling [3, 30-34]. Desorption from other plastic lab ware has barley been investigated with the exception of polystyrol and polypropylene microtiter plates [35]. The typical strategy for minimizing drug loss involves the use of buffer additives such as organic solvents (acetonitrile, methanol, ethanol, DMSO, PEG 400, propylene glycol [35-39]), cyclodextrins [40], detergents [41, 42] and bovine serum albumin [43-45], which work by either or both increasing drug solubility and competing with adsorbed drug for available binding sites on the plastic surface. It is interesting to note that organic solvents, cyclodextrines and detergents have also extensively been explored in terms of their ability to remediate contaminated soil from hydrophobic organic pollutants [46-48].

To the best of our knowledge, information about the inhibition of drug adsorption to Teflon, or the recovery of adsorbed drug is missing, reflecting the rather uncritical use of Teflon as ‘inert’ material. Moreover, it is unclear whether the knowledge gained from case studies of excipient-aided drug recovery is applicable to the minimization of drug loss to Teflon, in particular with respect to larger datasets.

The aim of this study was to investigate various excipients in terms of their ability to reverse drug adsorption to Teflon. More specifically, we were also interested in the mechanisms of excipient-aided drug recovery in order to derive a general guideline for applying excipients for compounds of all types of charge classes and propensity to adsorption. To these purposes, we first studied the sorption of 24 structurally diverse drugs from aqueous bulk solution to a Teflon microtiter plate, followed by the study

of recovery of adsorbed drug after addition of excipients. Various classes of excipients were tested, including i) aliphatic and steroidal detergents of different ionization state, namely sodium dodecyl sulfate (SDS, anionic), cetyltrimethylammonium bromide (CTAB, cationic), Brij 35 (neutral), Na • 3-[(3-Cholamidopropyl) dimethylammonio]-1-propanesulfonate (CHAPS, zwitterionic, steroidal) and taurocholic acid (anionic, steroidal). In addition, the desorbing ability of ii) organic solvents (DMSO, 2-propanol, acetonitrile) and iii) cyclodextrins was evaluated. The selection of the excipients was to a great extent inspired by case studies in which the minimization of drug loss to other plastic materials has been explored. From the multitude of commercially available cyclodextrins, we studied 2,6-di-O-methyl-β-cyclodextrin because it showed the highest solubilizing power for paclitaxel [49]. The drug is well known for its pronounced likelihood for drug adsorption to various surfaces [35] and was therefore included in the dataset.

A requirement for the application of excipients for minimizing drug loss to Teflon may not only be efficiency in recovering adsorbent drug, but also compatibility with mass spectrometric analysis. SDS, for example, is known to suppress the ionization efficiency of co-eluting analytes in electrospray ionization - mass spectrometry (ESI-MS) [50]. In order to identify the most suitable excipient in terms of efficiency of drug recovery and MS compatibility, we finally explored matrix effects in ESI-MS in presence of the selected excipients at concentrations used in the desorption studies. A guideline for the best practice of excipient-aided drug discovery is derived and may be applied for correcting potentially erroneous results in HT screening assays.

2. Materials and Methods

2.1. Drugs and Chemicals

Caffeine, DMSO and cetyltrimethylammonium bromide (CTAB) were purchased from Acros (Geel, Belgium). 2-propanol was obtained from Burdick & Johnson (Seelze, Germany). Indomethacin, Tris, sodium chloride, sodium dodecylsulfate (SDS) and polyoxyethylene (23) lauryl ether (Brij 35, 10% solution) were purchased from Fluka (Buchs, Switzerland). Ritonavir was received from Molekula (Vaterstetten, Germany). Chlorpromazine • HCl, diclofenac • Na, taurocholic acid, Na• 3-[(3-Cholamidopropyl) dimethylammonio]-1-propanesulfonate (CHAPS) and 2,6-di-O-methyl-β-cyclodextrin were supplied from Sigma (Steinheim, Germany). All other drugs were available through our in-house Compound Depository Group as proprietary compounds. Water and Acetonitril were supplied from Merck (Darmstadt, Germany) and were of HPLC-grade.

2.2. Measurement of Drug Loss to a Teflon Microtiter Plate

Assay buffer (227 µL, 50 mM Tris/114 mM NaCl/ pH 7.4) was first spiked with DMSO stock solutions (1.5 µL) of the test compounds and the internal standard caffeine (each 10 mM) and was then filtered into an in-house made Teflon block. The filtrate thus contained 50 µM caffeine, 50 µM of the test compound (= maximal nominal concentration, for exact concentrations see Table 1) and 1 % (v/v) DMSO. Caffeine was inert to adsorption (data not shown) and could therefore be used as an internal standard to compensate for evaporation and dilution (see Section 2.3). An aliquot of the filtrate ($V_{filtrate}$= 50 µL) was transferred into a 96 well Teflon plate and was immediately injected and analyzed on a HPLC-UV system. The well was sealed and all other sample solutions were consecutively transferred, injected and analyzed again after t = 16 h. All measurements were performed in duplicate at room temperature (RT). Drug loss was calculated according to:

$$Drug\ loss\,(\%) = 100 - \left(100 \cdot \frac{A_D^0 / A_{IS}^0}{A_D^t / A_{IS}^t}\right), \qquad (1)$$

where A_D^0, A_{IS}^0, A_D^t and A_{IS}^t denote the peak areas of drug and the internal standard at t = 0 h and after t = 16 h storage, respectively.

2.3. Measurement of Drug Recovery by Excipients

Stock solutions of excipients were prepared in assay buffer at a concentration of C = 50 mM (taurocholic acid, CHAPS, CTAB, SDS, Brij35, 2,6-di-O-methyl-β-cyclodextrin) and C = 0.5 mM (only detergents). An aliquot of the stock solution (V_{stock} = 10 µL) was added to the aged aqueous drug solution stored for t = 16 h in the Teflon plate. Since the analysis of drug loss at t = 0 h and after t = 16 h required 5 µL injection volume for each analysis, only $V_{filtrate}$ = 40 µL was left in the Teflon plate and the dilution with stock solutions of excipients yielded a final excipient concentration of C = 10 mM and C = 0.1 mM. Regarding recovery experiments with 2-propanol, DMSO and acetonitrile, the respective organic solvent ($V_{solvent}$=13.33 µL) was added to the aged aqueous drug solution instead of adding stock solutions of excipients. The final concentration of organic solvent in the drug solution was 25% (v/v). Excipient-spiked test solutions were put on a shaker for 3 h before drug concentrations were analyzed again by means of HPLC-UV. Drug loss after addition of excipients was calculated in the same way as described above (eq.1). Experiments were performed in duplicate for each of the individual experimental conditions tested (n = 26).

2.4. HPLC Instrumentation and Chromatographic Conditions

Drug concentrations in aqueous solutions were quantified using an Agilent 1290 Infinity HPLC-UV system. An aliquot (5 µL) of each sample was injected onto a Kinetex 2.6 µm, 2.1 x 50 mm analytical column. The flow rate was 2 mL/min and the integrated column heater was set to 60 °C. The mobile phase consisted of A (water) and B (acetonitrile), each containing formic acid (0.1 % (v/v)). The gradient elution was performed as follows: initially 2 % B, 0 - 0.35 min linear gradient from 2 % B to 95 % B, 0.35 min - 0.5 min 95 % B, post time: 0.3 min. The gradient program for doxorubicin, vinblastine, buspirone and colchicine was slightly different: initially 2 % B, 0 - 0.5 min linear gradient from 2 % B to 95 % B, 0.5 min - 0.65 min 95 % B. Peak areas were recorded at an appropriate wavelength.

2.5. Determination of the Critical Micellar Concentration of the Detergents

Surface activity experiments were carried out on a multichannel microtensiometer (Delta-8, Kibron, Helsinki) utilizing a modified Du Nouy method as described elsewhere [51]. Prior to the measurements, the system was cleaned by heating the microbalances and calibrated with distilled water to 72.8 mN/m. Stock solutions of SDS (12.5 mM), CTAB (1.5625 mM), Brij 35 (1.5625 mM), CHAPS (12.5 mM) and taurocholic acid (3.125 mM) were prepared in 10 mL glass flasks using the same assay buffer as described above (50 mM Tris, 114 mM NaCl, pH 7.4). Eleven consecutive 1:1 dilutions were made by diluting the detergent stock solution (1 mL) with assay buffer (1 mL) in a glass flask. An aliquot of each dilution (50 µL) was transferred to the 96-well measurement plate (aluminium) and the surface pressure, $\pi = \gamma_0 - \gamma$, where γ_0 is the surface tension of the pure buffer and γ the surface tension of the drug solution, was monitored in the order of increasing detergent concentration. The critical micellar concentration (CMC) was determined from π - concentration profiles in the usual manner. All experiments were performed at room temperature in triplicate and mean values are reported.

2.6. Evaluation of Excipient-Related Matrix Effects in ESI/MS

DMSO stock solutions of test analytes (rolipram or ketorolac) were dissolved in either blank buffer (50 mM Tris/114 mM NaCl/ pH 7.4) or excipient-spiked buffer yielding a final test solution containing C = 25 µM analyte (DMSO content: 0.1 % (v/v)). Final excipients concentrations corresponded to the concentrations used in the drug recovery studies. The test solutions were injected onto a HPLC system (Agilent 1290 Infinity) equipped with an API single quadrupole mass spectrometer (Agilent 6140) which was working at the following source settings: capillary voltage +3.5 kV/-3.5 kV, drying gas flow (N_2) 13 L/min, nebulizer pressure 60 psi, drying gas temperature 350 °C. The flow from the HPLC system was set to 1 mL/min (instead of 2 mL/min in the sorption studies) and was introduced into the ESI interface with a delay time of 0.25 min to prevent contamination of the ionization source with buffer salts. Each 0.1 s the intensity of the pseudo - molecular ion, $[M+H]^+$ (positive mode) and $[M-H]^-$ (negative mode), respectively, was acquired in single reaction monitoring mode (SRM). Analyte recovery from excipient-spiked buffer was calculated from the ratio of the average mass responses of the analyte in presence and in absence of the

excipient (each time n = 5 consecutive injections). Experiments were conducted separately in both positive and negative ionization mode, using rolipram (neutral compound) and ketorolac (acidic compound, pK_a 3.44 (potentiometric measurement, in-house)) as test analytes, respectively. Retention times in HPLC were similar for both compounds (R_t = 0.54 min for rolipram and R_t = 0.546 min for ketorolac).

3. Results

3.1. Characterization of the Dataset

Drug adsorption from aqueous bulk solution to a 96 well Teflon plate and excipient-aided drug recovery was studied at the example of 24 drugs including acids (3), bases (8), neutral (10) and zwitter-ionic (3) compounds. Compounds with known propensity to adsorption to any kind of plastic material were included in the dataset, i.e. paclitaxel, doxorubicin, saquinavir, vinblastine, chlorpromazine, midazolam and diazepam [8, 35, 52]. Moreover, compounds were investigated which have not been studied yet in terms of drug-plastic interactions (colchicine, amprenavir), but for which we suspected that adsorption-related artifacts could potentially explain their behavior as outliers in a novel *in vitro* Lipid Membrane Binding Assay (LIMBA, *accompanying manuscript 6*). The dataset was extended for anionic, zwitter-ionic and generally rather hydrophilic compounds resulting in a structurally diverse dataset covering a wide physicochemical property space ($\log D_{oct}$ = -1.15 - 3.68, $c\log P$ = 0 - 5.3, molecular weight, MW = 194 - 854 g/mol, Table 1). Structures of the investigated drugs are provided in the Supporting Information.

Table 1

3.2. Studies of Drug Loss from Blank Buffer to Teflon

3.2.1. The Extent of Drug Loss to Teflon

Percentages drug loss from filtrated aqueous bulk solution before addition of excipients were obtained from 26 independent measurements (n=2 for each independent measurement) and average values are provided in Table 1. The dataset was diverse in terms of likelihood of drug sorption to Teflon as indicated by the wide range of drug loss observed ($Drug\,loss$ <2 % (16 compounds) - 41.4 % (paclitaxel)).

The following classes of compounds showed a moderate to high extent of drug loss: i) large and lipophilic compounds ($\log D_{oct}$ (pH 7.4) > 3, here: MW > 670) such as paclitaxel ($Drug\,loss$ = 41.4 %), ritonavir (8.2 %), saquinavir (12.0 %) and vinblastine (4.3 %); ii) Compounds which are either moderately large and moderately lipophilic

and carry many hydrogen-bond donors (doxorubicin, 21.6% drug loss), or which are iii) small, lipophilic and fluorinated (fluvoxamine and midazolam). In addition, the presence of a planar ring system seems to be associated with increased drug loss (e.g. doxorubicin, chlorpromazine (12.1 %)). Drug loss from blank buffer was negligible (< 2 %) for 16 of the 24 compounds investigated. More precisely, all anionic and zwitter-ionic compounds showed no or negligible adsorption to Teflon in addition to small compounds with low to intermediate lipophilicity ($\log D_{oct}$ (pH 7.4) < 3) lacking the abovementioned patterns. For details about the relationship between the physicochemical properties of a drug and the extent of drug adsorption to Teflon (measured at a standardized concentration ($C_{filtrate}$ = 5 µM), the reader is referred to our *accompanying manuscript 2*.

3.2.2. Reproducibility of Drug Loss Data

Drug loss data from blank buffer was available from 26 independent measurements since drug recovery studies in presence of excipients required the study of drug adsorption in advance. Each of the 26 independent experiments was performed in duplicate on the same day, using the same stock solution and the same microtiter plates.

The variability of drug loss with respect to all 26 independent experiments was exceptionally high for paclitaxel (standard deviation, SD = 24.2%) and doxorubicin (SD = 9.9%), whereas data obtained within one independent experimental run (n = 2) showed much better reproducibility (average SD = 2.36% and 1.73% for paclitaxel and doxorubicin, respectively). A possible explanation for the high variability may be the protocol applied for the preparation of aqueous test solutions which involved i) dilution of DMSO stock solutions of test compounds (10 mM) with buffer, proceeded by ii) filtration and iii) transfer of the filtrate to the Teflon plate. In order to remain as close as possible to the common practice in HT screening assays, we followed this protocol, however, drug concentrations in the filtrate (maximal nominal $C_{filtrate}$ = 50 µM, Table 1) thus varied according to the compound's solubility limit. Moreover, fast sorption to the preparation plate and the filtration unit as well as post-filtration precipitation (paclitaxel) introduced some of degree of variability in the initial aqueous drug concentrations (e.g. $C_{filtrate}$ for paclitaxel and doxorubicin ranged from 3.1 - 14.3 µM and from 34.8 - 56.2 µM, respectively). In this respect it is

important to note that drug loss to Teflon is saturable and therefore concentration dependent (*accompanying manuscript 2*). However, we consider the variability of the drug loss data as secondary since our primary interest in this study was to identify an excipient allowing for the complete recovery of adsorbed drug, irrespective of the extent of adsorption.

3.3. Drug Recovery Studies

Despite the fact that drug loss from blank buffer was negligible for 16 of the 24 compounds investigated, drug recovery studies with excipients were performed on the whole dataset in order to verify that the addition of excipients does not adversely affect compounds with a low propensity to adsorption. In the following, only data for compounds will be presented for which either drug loss from blank buffer was > 4% (ritonavir, paclitaxel, fluvoxamine, chlorpromazine, saquinavir, doxorubicin; vinblastine was excluded due to interference with most excipients in HPLC) or for which adsorption became evident after addition of excipients (diclofenac, indomethacin in combination with detergents).

3.3.1. Recovery Studies with Detergents

3.3.1.1. Characterization of the Detergents

Aliphatic and steroidal detergents of different ionization state were investigated in terms of their desorbing efficiency using the example of CHAPS and taurocholic acid (both steroidal) as well as SDS, CTAB and Brij 35 (aliphatic). Structures and charge classes of the detergents are shown in Table 2, along with *CMC* values in buffer and in water as derived from surface pressure - concentration profiles (Supporting Information) and literature reports, respectively.

Table 2

The buffer used for the *CMC* assessment in this study was the same as in the sorption-desorption experiments and contained physiological concentrations of salt (50 mM Tris, 114 mM NaCl at pH 7.4). It is worth noting that the *CMC* of ionic surfactants in buffer was much lower than reported *CMC* values in water due to NaCl-mediated charge screening. The buffer-related reduction of repulsion between charged head

groups enables closer packing of the detergents and explains the reduced *CMC* of ionic detergents in buffer. However, due to absence of electrostatic repulsion, the *CMC* in buffer was lowest for non-ionic surfactant Brij 35 and increased in the following rank order: Brij 35 < CTAB < SDS < taurocholic acid < CHAPS. As expected, the ranking points to a generally higher *CMC* of detergents with a bulky residue, i.e. of steroidal detergents (taurocholic acid, CHAPS) as compared to those with an aliphatic tail group (Brij 35, CTAB, SDS).

3.3.1.2. Recovery Studies with Aliphatic Surfactants

Each detergent was investigated at concentrations well above the *CMC* ($C_{detergent}$=10 mM) in order to enable the solubilization of drug in the micellar pseudophase. However, during the course of this study it became evident that such high detergent concentrations cause matrix effects in ESI/MS (see below), and hence recovery studies were also performed at $C_{detergent}$ = 0.1 mM.

CTAB (cationic): Drug loss to Teflon before and after addition of CTAB at submicellar (0.1 mM) and at micellar (10 mM) concentrations is shown in Fig.1a and Fig. 1A, respectively.

Fig. 1

Regarding the addition of 0.1 mM CTAB (cationic), adsorption of negatively charged drugs was reinforced while drug loss for neutral and cationic compounds remained unaffected. Complete desorption of positively charged drugs was only achieved for the strong bases fluvoxamine and chlorpromazine (pK_a> 9 and hence >98% ionized at pH 7.4), whereas the pronounced drug loss observed for saquinavir and doxorubicin was not minimized. Regarding micellar concentrations of CTAB (Fig. 1A), the detergent-mediated adsorption of negatively charged drugs was no longer evident. All neutral and most basic compounds were completely recovered with the exception of doxorubicin (no effect) and chlorpromazine (~6% unrecovered).

SDS (anionic): Drug loss before and after addition of submicellar (0.1 mM) and micellar (10mM) concentrations of SDS is shown in Fig.1b and Fig.1B, respectively.

In contrast to CTAB, the addition of 0.1 mM SDS reinforced the adsorption of cationic compounds whereas anionic drugs remained unaffected and showed no adsorption, irrespective of the concentration of SDS applied. With respect to neutral drugs, the effects of SDS and CTAB were comparable, i.e. micellar detergent concentrations were required for an effective desorption, whilst submicellar concentrations were inefficient. The addition of 10 mM SDS allowed moreover almost complete recovery of cationic compounds (5% of doxorubicin and < 3.5% of all other drugs were unrecovered) which demonstrates the superior detergency of SDS as compared to CTAB.

Brij 35 (non-charged): Drug loss before and after addition of Brij 35 is shown in Fig.1c (0.1 mM) and Fig.1C (10 mM). An inspection of drug loss data at $C_{\mathrm{det}ergent}$ = 0.1 mM (Fig. 1c) reveals that Brij 35 neither influenced the sorption of acidic nor of that of basic compounds significantly. Regarding nonionic drugs, the recovering potency was weak, but better as compared to ionic detergents (5% of adsorbed ritonavir and 16 % of adsorbed paclitaxel were recovered, Fig. 1c). A possible explanation is the presence of micelles at 0.1 mM Brij 35, whereas the *CMC* for CTAB and SDS was not yet reached. At concentrations in large excess of the *CMC*, complete recovery of neutral drugs was achieved after addition of Brij 35. However, similar to CTAB, the adsorption of doxorubicin was not minimized, and the recovery of chlorpromazine was incomplete.

3.3.1.3. Recovery Studies with Steroidal Surfactants

Fig. 2A and Fig.2B shows drug loss to Teflon before and after addition of the steroidal detergents, CHAPS (zwitter-ionic) and taurocholic acid (anionic), respectively, at concentrations well above the *CMC* (10 mM). Neutral drugs (ritonavir and paclitaxel) were almost completely recovered from adsorption to Teflon regardless of the charge state of the detergents. However, neither CHAPS nor taurocholic acid enabled the complete recovery of adsorbed cationic drugs.

Fig. 2

3.3.2. Recovery Studies with Cyclodextrins

Fig. 3 shows the drug loss before and after addition of 2,6-di-O-methyl-β-cyclodextrin applied at pH 7.4 and at pH 3 (for clarity only drug loss before addition of the pH 7.4 solution is shown). Recovery of all drugs, except for doxorubicin, was achieved when working at pH 7.4 (drug loss of doxorubicin > 15%). An increase of the fraction of doxorubicin in its ionized form by acidification to pH 3 lowered, but not completely reversed the adsorption of doxorubicin (11 % unrecovered). It is interesting to note that acidification to pH 3 resulted in degradation of midazolam (data not shown) in buffer and also in buffer - organic solvent mixtures (2 - propanol and DMSO, see below), whereas 2,6-di-O-methyl-β-cyclodextrin prevented degradation.

Fig. 3

3.3.3. Recovery Studies with Organic Solvents

Recovery from drug loss to Teflon after addition of DMSO, acetonitrile and 2 - propanol (25 %, v/v) is shown in Fig. 4A, 4B and 4C, respectively. All organic solvents showed only a negligible effect on the pronounced adsorption of doxorubicin, however, almost complete recovery of all other drugs was achieved (max. 4 % unrecovered in presence of 2-propanol and acetonitril). DMSO was slightly less effective than 2-propanol and acetonitrile with respect to the recovery of saquinavir and fluvoxamine (7 % and 5 % unrecovered, respectively). A rise in the DMSO content up to 40 % completely reversed the adsorption of the latter two compounds, whereas even 60 % of DMSO was insufficient to accomplish a complete recovery of doxorubicin (11 % and 6 % unrecovered at 40 % and at 60 % DMSO, respectively, data not shown). Pre-acidification of 2 - propanol resulting in pH 3 of the solvent-buffer solution recovered most doxorubicin from the Teflon plate (3.2 % unrecovered), but lower concentrations of 2-propanol (12.5 %, pH 3) were not effective (32.7 % doxorubicin unrecovered, data not shown).

Fig. 4

3.4 Study of Excipient-Related Matrix Effects in ESI-MS

3.4.1 Compatibility of Detergents with ESI/MS

In order to detect potential changes in the ionization efficiency in ESI/MS in presence of excipients ('matrix effect'), the mass responses of two test analytes, dissolved in either blank buffer or excipient-spiked buffer, were compared. Matrix effects observed as a decrease (ionization suppression) or increase (ionization enhancement) in analyte response in presence of different detergent concentrations ($C_{\mathrm{det}ergent}$ = 0.1 mM, 1 mM and 10 mM) are illustrated in Fig. 5. More precisely, Fig 5A and Fig. 5B show matrix effects in presence of Brij 35, CTAB and SDS in positive and negative ionization mode, respectively.

Fig. 5

With respect to Brij 35, matrix effects were independent of the ionization mode applied: no interference with the test analyte was observed at 0.1 mM Brij 35, whereas at $C_{\mathrm{det}ergent}$ > 0.1 mM ionization suppression was evident and increased with increasing detergent concentrations (13-18% and ~ 50 % drop in mass response at $C_{\mathrm{det}ergent}$ = 1 mM and 10 mM, respectively).

In contrast to Brij 35, ion suppression in presence of ionic detergents was dependent on the ionization mode, and was most pronounced if analyte and detergent carried the same charge. Accordingly, inspection of CTAB (positively charged) in positive ionization mode (Fig. 5A), and SDS (negatively charged) in negative ionization mode (Fig. 5B), revealed ionization suppression even at the lowest investigated detergent concentration (12 % and 5% drop in mass response at $C_{\mathrm{det}ergent}$ = 0.1 mM CTAB and SDS, respectively). A rise in the detergent concentration caused a further depression in the ionization efficiency with only 23% and 25% of the analyte recovered at $C_{\mathrm{det}ergent}$ = 10 mM SDS and CTAB, respectively.

Matrix effects were much less pronounced when the test analyte (more precisely its gas phase ion) and the detergent were oppositely charged, i.e. when the effect of CTAB (positive charge) on the ionization efficiency of ketorolac (negative ion) was observed in negative ionization mode (Fig. 5B) and the effect of SDS (negative

charge) on the ionization efficiency of rolipram (positive ion) was observed in positive ionization mode (Fig. 5A). Under these conditions, matrix effects were only evident at $C_{\mathrm{det}ergent} > 0.1$ mM with maximal 22 % signal decrease at $C_{\mathrm{det}ergent} = 10$ mM CTAB. However, the first injection of excipient-spiked buffer caused a signal increase in presence of SDS (data not shown), and only subsequent injections (n = 4) were consistent and are shown in Fig. 5B. The reason for the initial ionization enhancement is unknown.

3.4.2 Compatibility of Cyclodextrins and Organic Solvents with ESI/MS

Matrix effects in HPLC - MS in presence of DMSO, 2,6-di-O-methyl-β-cyclodextrin and 2-propanol are illustrated in Fig.6 for both ionization modes. 2,6-di-O-methyl-β-cyclodextrin showed the most pronounced matrix effects with > 90 % decrease in the analyte response, irrespective of the ionization mode applied. Regarding the organic solvents, DMSO caused a decrease in the recovery of the test analyte by 62% (positive ionization mode) and 90% (negative ionization mode), whereas 2-propanol did not interfere with MS.

Fig. 6

It is well known that ion suppression only occurs if analyte and matrix components co-elute. In order to verify that 2-propanol does not disturb the analysis of compounds with a retention time different from that of rolipram and ketorolac, 15 additional drugs covering a broad lipophilicity range and eluting at various retention times were tested. For the calculation of analyte recovery in MS, the UV response was used as an internal reference to compensate for variations in injection volume and to account for the release of ‘sticky’ compounds from the well plate after addition of 2-propanol. The UV-normalized recovery of mass response is given in Table 3 along with the fold increase of the mass response after adding 2-propanol. Only compounds which were released from the Teflon plate after adding 2-propanol (fold increase >1) showed a reduced recovery in MS. Therefore, it is plausible that the relative drop in analye signal was due to higher analyte concentrations rather than due to 2-propanol - related matrix effects.

Table 3

4. Discussion

Non-specific binding to miniaturized microtiter plates and other labware has recently been recognized as a potential source of experimental artifacts in high-throughput screening assays [1]. In order to correct for non-specific binding, we have evaluated the ability of i) surfactants of different charge class, ii) cyclodextrins and iii) organic solvents to recover drug adsorbed to a Teflon well plate, using the example of 24 structurally diverse drugs. To the best of our knowledge this is the largest set of drugs and excipients investigated so far in terms excipient-aided drug recovery. The desorption efficiency of the excipients was depending on the drug properties as well as on the type and concentration of the excipient applied. Our data showed that sorption of anionic and zwitter-ionic compounds from blank buffer was generally negligible, and desorption of neutral drugs was achieved by each of the investigated excipients, provided that micellar detergent concentrations were used. The superior efficiency of the anionic surfactant SDS ($C_{detergent}$ = 10 mM) for the recovery of cationic drugs may be explained by different mechanisms involved in the desorption process, which will be discussed in the following. In addition, the compatibility of excipients with ESI/MS was evaluated and will be considered in a guideline proposed for the selection of excipients with potential application in miniaturized screening assays.

4.1 Mechanisms of Excipient - Aided Drug Recovery

4.1.1. The Effect of Charge and Concentration in Detergent-Aided Desorption

Improved drug recovery at micellar concentrations ($C_{detergent}$ = 10 mM) of CTAB and SDS as opposed to submicellar concentrations (CTAB, SDS, 0.1 mM) was observed which indicates that solubilization of drug in the micellar phase is one major process involved in the desorption process. Although no comparison between micellar and submicellar concentrations of Brij35 was performed, improved drug recovery at 10 mM Brij 35 as compared to 0.1 mM (both $C_{detergent} > CMC$) points to the importance of also the number of micelles available for solubilization.

Indirect evidence for the interaction of paclitaxel [53, 54], saquinavir [55], ritonavir [55] and fluvoxamine [56] with SDS can be derived from micellar capillary electrophoresis studies and, moreover, solubilization of e.g. paclitaxel into non-ionic

mixed micelles (Pluronic P123/F127) is well documented [57] and in support of our results. Notably, binding constants of e.g. doxorubicin and chlorpromazine to cationic (CTAB; CTAC), anionic (SDS; HPS) and non-ionic (Tween 20; Brij35) micelles have been reported (excipients given in order of increasing affinity), but neither the trend for micellar affinities (nonionic > anionic > cationic) nor the abundance of micelles ($CMC_{Brji35} < CMC_{CTAB} < CMC_{SDS}$, Table 2) mirrors the efficiency of detergents in terms of drug recovery [58-60]: Since complete recovery of doxorubicin and chlorpromazine was only achieved with SDS, other mechanisms apart from solubilization are likely to be involved in the desorption process.

Our data indicate that electrostatic repulsion between SDS enriched at the Teflon surface and SDS incorporated in drug-loaded micelles (net negatively charged) is of importance for the desorption process and provides a possible explanation for the superior desorption efficiency of SDS. The formation of mixed micelles of SDS and doxorubicin (chlorpromazine) [59, 60] is well documented and in support of the proposed mechanism. Moreover, increased adsorption observed for cationic and anionic drugs after addition of submicellar concentrations of SDS (anionic) and CTAB (cationic), respectively, indicates adsorption of detergents at the Teflon surface and electrostatic attraction of oppositely charged drugs. However, at micellar concentrations of SDS, cationic drugs can be considered as desorbed from adsorbed detergents and solubilized in free SDS micelles, as also described elsewhere in more general terms [61]. The presence of SDS residing at the Teflon surface then likely leads to the repulsion of drug-loaded SDS micelles with a net charge dominated by excess SDS. Our study showed that cationic, but not anionic drugs are prone to adsorption to Teflon. Electrostatic attraction between cationic drugs and negatively charged detergents may result in higher drug affinity to SDS as opposed to negatively charged CTAB, which likely contributes to the superior desorbing ability of SDS. Nonionic detergents such as Brij 35 lack the contribution of charge repulsion which could explain the weaker desorbing potency.

The addition of ionic detergents at submicellar concentrations should be avoided since drug loss of oppositely charged drugs was reinforced, however, only for compounds carrying a hydrophobic residue (e.g. diclofenac and indomethacin, but not ketorolac, in presence of 0.1 mM CTAB). This points to the importance of not only electrostatic, but also hydrophobic interactions and suggests the incorporation of hydrophobic drug

into a layer of detergents residing at the Teflon surface. The phenomenon has been described as adsobilization [61] and has notably found application for e.g. the adsorption of negatively charged antibiotics to vascular PTFE (Teflon) catheters by means of cationic surfactants (CTAB, benzalkonium chloride).

On the molecular level, an orientation of detergents on the Teflon surface, such that the hydrophobic tail interacts with the hydrophobic polymer and the head group points towards the aqueous phase, is reasonable and has been proposed by several authors [62, 63]. This would be in line with both, the coadsorption of drugs with hydrophobic residues of detergents at $C < CMC$ (drug and detergent oppositely charged), and the repulsion of drug loaded micelles at $C > CMC$.

From a theoretical point of view, another possible desorption mechanisms involves electrostatic repulsion and competition of equally charged drug and detergent for available adsorption sites on the Teflon surface. However, only compounds with almost 100 % positive charge (fluvoxamine, chlorpromazine) could be recovered by use of submicellar concentrations of cationic CTAB. However, CTAB was inefficient for saquinavir and doxorubicin carrying 28% and 84% positive charge, respectively, which suggests that neither electrostatic repulsion nor displacement of adsorbent drugs with submicellar detergent concentrations are sufficient to overcome the hydrophobic attraction between Teflon and partially charged drugs. This, in turn, points to rather weak surfactant - Teflon interactions which is in line with the reported weak affinity of SDS, CTAB and Brij 35 for Teflon [63]. Therefore, another conceivable desorption mechanism, involving the hydrophilization of the Teflon surface by detergent adsorption (van der Waals attraction decreases [48]), seems to play only a minor role and is insufficient without the contribution of micellar solubilization.

The inferior desorbing potency found for steroidal detergents as compared to CTAB, SDS and Brij 35 can be explained by the lower tendency of bulky amphiphiles to assemble into micelles (high CMC values, Table 2) [48]. Detergents with bulky residues are also less likely to adsorb to surfaces which is a possible explanation for the weaker effectiveness of taurocholic acid as compared to SDS (both negatively charged).

4.1.2. Mechanisms of Desorption with Solvents and Cyclodextrins

Similar to detergents, cyclodextrins and organic solvents are well known to increase the solubility of hydrophobic compounds which, in turn, contributes to the shift from adsorbed towards solubilized drug [47, 64].

The complete recovery of paclitaxel after addition of 2,6-di-O-methyl-β-cyclodextrin is in line with the well documented increase in drug solubility [65] associated with the formation of paclitaxel-cyclodextrin inclusion complexes. Complete desorption with 2,6-di-O-methyl-β-cyclodextrin was also achieved for saquinavir, ritonavir and chlorpromazine, even though structurally slightly different cyclodextrines are typically applied for their solubilization [66-68]. However, both 2,6-di-O-methyl-β-cyclodextrin (7 sugar units) and γ-cyclodextrin (8 sugar units, data not shown), for which a higher affinity for doxorubicin has been reported [69], were unsuccessful in desorbing doxorubicin, which confirms that solubilization alone may be insufficient for the recovery of certain drugs.

Like cyclodextrines, organic solvents lack the effect of electrostatic repulsion, explaining the weaker desorbing potency as compared to anionic SDS. Similar to SDS, enrichment of 2-propanol at Tefon surfaces has interestingly been reported [70], however, the associated hydrophilization of the Teflon surface was apparently not sufficient for the release of adsorbed doxorubicin. Acidification to pH 3, leading to an increase in the fraction of drug in its ionized form, enhanced the drug recovery which is in line with literature reports demonstrating pH dependent adsorption of doxorubicin to intravenous filters [71].

4.2 Comparison with Excipient-Aided Desorption from other Plastic Materials

Information about drug adsorption to Teflon and excipient-aided drug recovery is very scarce and therefore a discussion of our results only possible in comparison with other hydrophobic surfaces.

With respect to steroidal detergents, taurocholic acid (anionic) and particularly CHAPS (zwitterionic) have been used for minimization of drug loss in urine and CSF samples (polypropylene) [30], however, our results confirmed that the success of their application is compounds specific [33] and drug recovery may only be achieved for some, but not all drugs.

Regarding SDS, Chen et al. [41] and Silvester et al. [72] reported that the detergent was less efficient for the reversal of drug adsorption to polypropylene containers as compared to sodium dodecylbenzene sulfonate (SDBS), which is more hydrophobic. Interestingly, SDS has successfully been applied in soil remediation [46] which points to the difficulty of translating experience gained from one specific compound and detergent to other drugs and experimental conditions. We abstained from using SDBS because of the presence of a chromophore likely to interfer with UV analytics. For the same reason we investigated Brij 35 rather than Tween 20 (80) or Triton-X 100 as an example of non-ionic polyoxyethylene detergents. The inferior efficiency of Brij 35 to recover chlorpromazine and doxorubicin as compared to SDS was surprising because of the frequent use of Tween and Triton - X 100 for blocking protein adsorption in ELISA (non-ionic detergents are mandatory to maintain the protein conformation) [26, 28], and for minimization of drug loss in urine sampling [72]. However, it has also been reported that non-ionic detergents are generally not as effective as anionic agents for the removal of particulate soil [48]. Rosen pointed out that this was due to the fact that adsorption of non-ionic surfactants to the substrate does not significantly increase the electrical potential at the Stern layer [48], which is in line with our explanation for the superior detergency of SDS as compared to Brij 35.

Pertaining to the desorbing ability of cyclodextrins, more efficient minimization of drug loss has been reported when cyclodextrins were applied before the addition of drugs (pre-treatmant as opposed to post-treatment), and even then complete recovery was not achieved for all compounds [33], which is in line with our results.

Regarding the organic solvents, the concentration we found efficient for the recovery of most compounds (25%, but not 12.5%), was of the same order of magnitude used by many other authors [33, 35]. The preference for the addition of 20-30% organic solvent may be due to the constituted change in the solubilization mechanisms at 10-20% organic cosovent which is accompanied with a change from a linear to an exponential increase in solubility [73].

4.3 Compatibility of the Excipients with Mass Spectrometric Analysis

There is a consensus that competition for charge and/or space on the surface of electrosprayed droplets in ESI/MS is involved in the phenomenon of ion suppression since only what resides on the droplet surface can enter the gas phase [74, 75]. Other

factors that disturb the droplet formation and/or the droplet evolution in ESI/MS have also been stressed, among them the presence of additives which are surface active [74], increase the viscosity [76] or form non-volatile ion pairs with the analyte [77]. In a very abstract way, the mechanisms leading to the reversal of drug loss to Teflon, i.e. competition for adsorption sites on the Teflon surface, micellar solubilization of drugs as well as reduction of interfacial tension, are very similar to the mechanisms provoking ion suppression in ESI/MS. Therefore it is conclusive that strongly amphiphilic detergents (Brij35, SDS and CTAB) suppressed the ionization of less amphiphilic test analytes, unfortunately at detergent concentration necessary to be efficient for desorption.

Matrix effects caused by SDS are well documented [50], whereas matrix effects caused by Brij 35 and CTAB have not been recognized before. Yet, reduced analyte response in presence of structurally related nonionic detergents (Tween 80, Triton-X 100) [76], and likewise cationic model amphiphiles, has been observed before which is in support of our results. To the best of our knowledge, this is also the first study showing evidence for ion suppression in presence of 2,6-di-O-methyl-β-cyclodextrin which is consistent with preliminary studies showing ion suppression for other cyclodextrin analogues [40]. With respect to DMSO, matrix effects have been reported before, but received not much attention [38]. We confirmed the DMSO-related matrix effect which likely results from the lower volatility of DMSO as compared to acetonitrile and 2-propanol.

Our initial aim for identifying an excipient which is most suitable in terms of efficiency of drug recovery and MS compatibility turned out to be explicit: the only excipients which are MS compatible at concentrations necessary for desorption are 2-propanol and acetonitrile.

4.4. Guideline for the Selection of a Desorbing Excipient

As a strategy to avoid adsorption-related experimental artifacts in an *in vitro* assay we propose adding excipients to sample solution containing compounds with a high probability for adsorption. The extent of drug loss can roughly be predicted by a linear combination of lipophilicity, molecular weight, number of H-bond donors and molecular shape as described in more detail in our *accompanying manuscript 2*. It is important to note that excipients can have a major impact on the biological or

physicochemical process of interest, examples of which are the excipient-related changes in artificial membrane permeability [78] and solubility [79]. Leaving the drug undisturbed during the experiment and recovering already adsorbed at the end would circumvent the problem of eliminating one artifact by creating just another. Therefore we recommend adding excipients at the end of the process of interest. SDS used at concentrations above the CMC should be the first choice, whereas 2-propanol (25%, v/v) at pH 3 would be an appropriate alternative if compatibility with ESI/MS is required.

A drawback of using 2-propanol is the detrimental effect on the peak shape of compounds eluting close to the solvent front in HPLC (not shown). However, the elution behavior of compounds showing a high propensity to adsorption, i.e. lipophilic drugs with long R_t in HPLC, are not affected by 2-propanol and therefore we consider this issue as secondary. If peak splitting in HPLC occurs, despite having filtered out hydrophilic compounds by means of the prediction model, the experiment could be repeated with acetonitrile. The reason for not choosing acetonitrile as a primary MS compatible excipient is the higher tendency to evaporate which complicates the assay automation. Fig. 7 summarized the proposed guideline in a flow chart.

Fig. 7

4.5. Limitations and Future Perspectives

Despite the relatively large set of drugs tested, monitoring the desorbing ability of excipients (in particular SDS, 2-propanol) on an extended dataset is still desirable for the purpose of a higher statistical certainty of our results.

Furthermore, fluor surfactants may provide a promising alternative to SDS and 2-propanol since i) very low CMC values have been reported indicating high efficiency of solubilization, ii) fluor surfactants show a higher tendency for adsorption to Teflon as compared to hydrocarbons which may lead to more effective competition with drugs for available adsorption sites on the Teflon surface [80]. iii) It was shown that fluor surfactants caused no ion suppression in ESI/MS [41]. Despite these theoretical considerations, the efficiency of fluor surfactants in terms of minimizing drug adsorption to plastic labware still needs to be demonstrated.

Potential areas of application for the recovery of adsorbed drug by means of excipients are, e.g., miniaturized *in vitro* screening assays implemented in drug discovery and development programs. The assessment of the fraction of drug free in solution and bound to the assay plate could be used to correct potentially erroneous assay read-outs, or e.g. to flag compounds according to their likelihood for adsorption to the assay construct.

5 Conclusions

In summary, we have shown at the example of 24 structurally diverse compounds that drug adsorption from aqueous solution to a Teflon microtiter plate can completely be reversed by addition of micellar concentration of SDS. Our data suggests that i) solubilization of drug in the micellar phase and ii) electrostatic repulsion between SDS enriched at the Teflon surface and drug-loaded SDS micelles free in solution are involved in the drug recovery process. SDS and all other investigated excipients, except for 2-propanol, caused matrix effects in ESI/MS and therefore we recommend using SDS for drug recovery experiments only as long as concentration analysis relies on UV. When mass-spectrometric analysis is a necessary criterion for applicability, 2-propanol provides a useful alternative to SDS. The inferior recovery of doxorubicin with 2-propanol as compared to SDS can be resolved by pH adjustment to pH 3, which increases the fraction of drug in its ionized form, and thereby decreases the fraction of drug adsorbed. The proposed guideline for excipient-aided drug recovery may be applied for the correction of potentially erroneous results in a multitude of miniaturized *in vitro* assays implemented in drug development programs. Our results may thus contribute to avoiding misinterpretations and achieving higher reliability of the experimental data in case that drug adsorption to plastic lab ware, in particular Teflon, occurs.

Acknowledgements

We thank Björn Wagner for fruitful discussions and the idea of testing detergents and organic solvents for drug recovery. Moreover, we thank Joerg Voelke for the fabrication of the Teflon plates.

Table 1 Key properties for the dataset investigated along with percentages drug loss from aqueous bulk solution and initial aqueous drug concentrations.

No	Compound	Charge class[a]	pK_a (acid)[b]	pK_a (base)[b]	*MW* [g/mol]	*HBD*	$c\log P$[c]	$LogD_{oct}$ (pH7.4)[d]	Drug loss (filtrate)[e][%]	$C_{filtrate}$[µM][f]
1	Amprenavir	N			505.6	4	3.29	2.46	<2	41.2
2	Caffeine	N		<2	194.2	0	-0.04	-0.1	0[e1]	49.2
3	Colchicine	N			399.4	1	1.20	0.95	<2	57.7
4	Dexamethasone	N			392.5	3	1.79	1.79	<2	44.8
5	Diazepam	N		3.38	284.7	0	2.96	2.84	<2	43.4
6	Digoxin	N			780.9	6	1.42	1.34	<2	41.3
7	Midazolam	N			325.8	0	4.73	3.32	3.1 ± 1.2	41.0
8	Paclitaxel	N			853.9	4	4.94	3.09[d1]	41.4 ± 24.2	6.0
9	Ritonavir	N			720.9	4	1.72	3.68	8.2 ± 2.6	19.1
10	Rolipram	N		5.71	275.3	1	3.42	1.91	<2	45.7
11	Diclofenac · Na	A	4.02		296.2	2	4.73	1.15	<2	47.4
12	Indometacin	A	4.43		357.8	1	4.18	0.79	<2	44.2
13	Ketorolac · Tromethamin	A	3.44		255.3	1	1.62	-0.58[d2]	<2	54.3
14	Alfentanil · HCL	B		6.46	416.5	0	2.13	2.2	<2	14.6
15	Buspirone · HCL	B		7.61	385.5	0	2.19	2.13	<2	50.0
16	Chlorpromazine · HCL	B		9.38[b1]	318.9	0	5.30	3.36	12.1 ± 7.2	35.8
17	Doxorubicin	B	9.45	8.16	543.5	7	0.32	0.36[d2]	21.6 ± 9.9	49.0
18	Fluvoxamine·Maleate	B		9.11/5.82	318.3	2	3.03	1.81	4.3 ± 2.3	46.2
19	Saquinavir	B		7/3	670.9	6	4.73	3.78	12.0 ± 3.8	22.3
20	Sumatriptan	B		9.49	295.4	2	0.74	-1.15[d1]	<2	50.0
21	Vinblastine · Sulfate	B		7.4/5.4[b2]	811.0	3	5.23	3.11	4.3 ± 2.3	32.1
22	Cetirizine	Z	2.86	8.00	388.9	1	2.08	1.28	<2	50.0
23	Raclopride · Tartrate	Z	5.95	9.46	347.2	2	4.06	1.13	<2	49.6
24	Tiagabine · HCL	Z	3.1	9.02	375.5	1	2.78	1.23	<2	60.4

[a] N: neutral (less than 3 % ionization at pH 7.4); A: acid with $ApK_a < 8.9$; B: base $BpK_a > 6$; Z: zwitterions with $ApK_a < 8.9$ and $BpK_a > 6$.
[b] Measured by potentiometry (in-house), [b1] Value taken from [81]. [b2] Value taken from Therapeutic Drugs [82].
[c] clogP v4.71 Daylight.
[d] Measured in-house with CAMDIS (*accompanying manuscript 2*)
[d1] Measured in-house with a miniaturized shake flask logD assay, no filter-device used (50mM Tapso, pH 7.4, 5%DMSO) [d2]Large scale shake flask value obtained from measurement in both phases.
[e]Average drug loss from filtered aqueous drug solutions after 16h storage in a Teflon well plate (n=26). (C_{total} = maximal 50 µM). [e1]Internal standard.
[f]Standard deviation < 4%, except digoxin (5.7%), chlorpromazine (7.5%)and doxorubicin (5.4%).

Table2 Charge class, critical micellar concentrations (*CMC*) and structures of the investigated detergents.

Tenside	Charge class	*CMC* (buffer) (mM)	*CMC* (H_20)[a] (mM)	Investigated concentration (mM)	Structure
CHAPS	zwitter-ionic	3.46±0.12	6	10	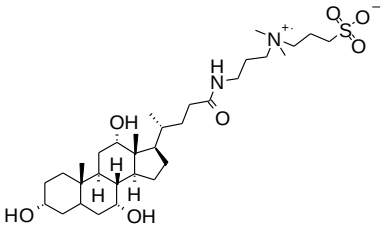
Taurocholic acid	anionic	2.60 ± 0.73	3-11	10	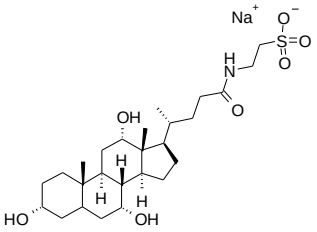
CTAB	cationic	0.14 ± 0.02	1	0.1, 10	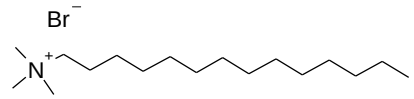
SDS	anionic	1.02 ± 0.06	7-10	0.1, 10	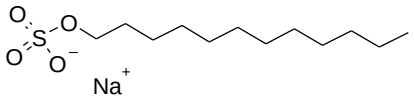
Brij 35	neutral	0.07 ± 0.00	0.09	0.1, 10	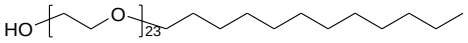

[a] Values taken from [48]

Table 3 Charge class, octanol/water distribution coefficients, retention times in HPLC, recovery of the mass response and the fold increase of the absolute mass signal in presence of 2-propanol for the 16 compounds investigated (given in ascending order of recovery in MS).

Compound	Charge class[a]	$LogD_{oct}$ [b]	Retention time [min]	Recovery in MS, corrected[c] [%]	Increase of mass signal with 2-propanol fold
Trifluperazine	B	4.0	0.544	75.2	1.8
PK 11195	N	3.8	0.736	81.3	1.3
Thioridazine	B	3.6	0.541	84.6	1.5
Cyclobenzaprine	B	3.0	0.506	89.4	1.1
Verapamil	B	2.5	0.513	91.3	1.1
Amitriptyline	B	2.8	0.512	92.3	1.1
Maprotiline	B	1.5	0.509	94.1	1.0
Midazolam	N	3.2	0.490	94.9	1.1
Rolipram	N	1.9	0.580	99.5	1.0
Metoclopramide	B	0.2	0.448	99.9	1.0
Flumazenil	N	1.1	0.525	100.3	1.0
Carbamazepine	N	1.6	0.560	100.8	1.0
Zaleplon	N	1.2	0.560	100.9	1.0
Phenytoin	A	2.3	0.551	107.3	1.1
Theophylline	A	-0.2	0.419		
Rizatriptan	B	-0.7	0.373		

[a]N: neutral (less than 3 % ionization at pH 7.4); A: acid with ApK_a < 8.9; B: base BpK_a >6; pK_a measured potentiometrically, in-house [b]measured with CAMDIS.[c]The peak area in ESI/MS was divided by the peak area in UV of the same run to correct for non-specific binding to the instrument and the well plate. The ratio with and without 2-propanol was related and corresponds to the corrected recovery in MS. Drug concentration: 25µM.

FIGURES

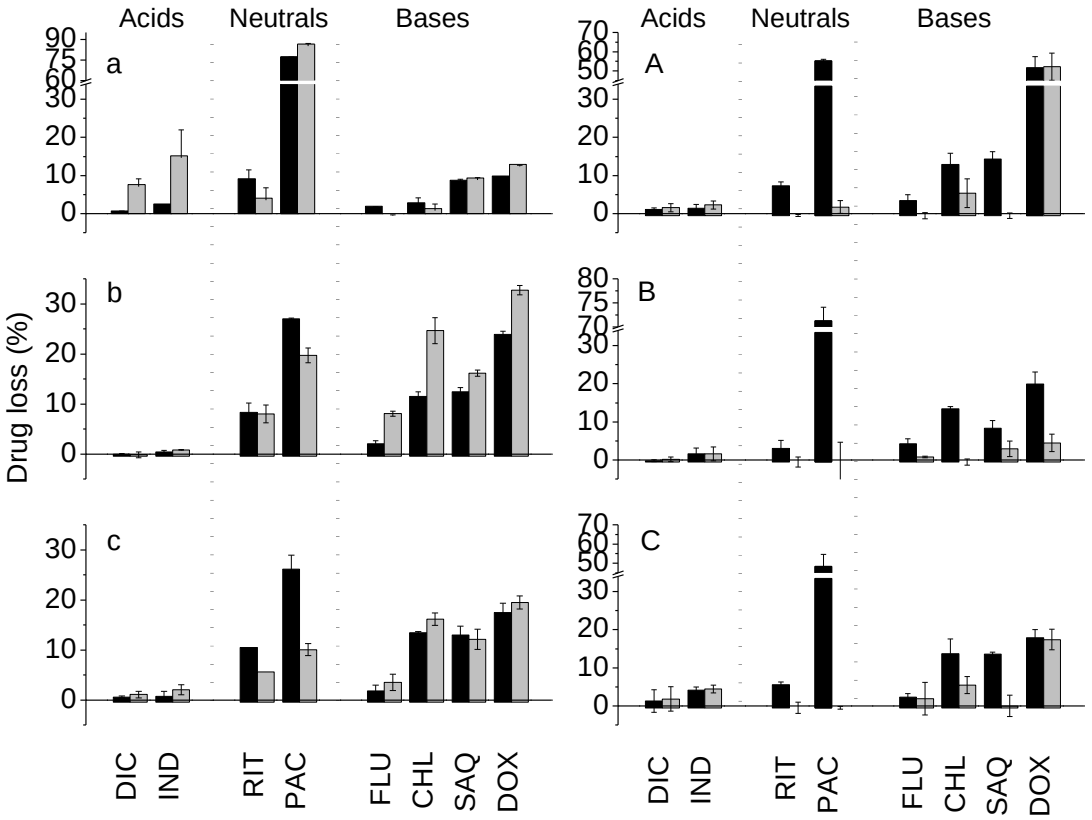

Figure 1 Drug loss from aqueous bulk solution to Teflon before (black columns) and after (grey columns) addition of aliphatic detergents: (**a,A)** positively charged CTAB, (**b,B)** negatively charged SDS, (**c,C**) non-charged Brij 35. Detergents were investigated at $C_{\mathrm{det}ergent}$ = 0.1 mM (**a,b,c**) and $C_{\mathrm{det}ergent}$ = 10 mM (**A,B,C**). The compounds shown are diclofenac and indomethacin (anionic), ritonavir and paclitaxel (neutral) as well as fluvoxamine, chlorpromazine, saquinavir and doxorubicin (bases).

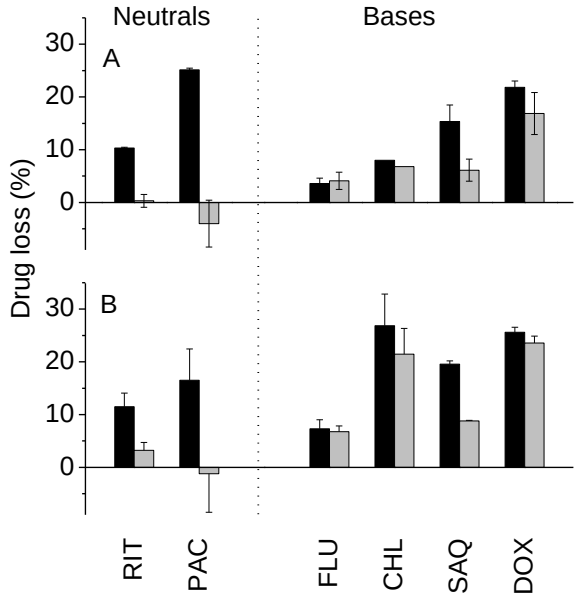

Figure 2 Drug loss from aqueous bulk solution to Teflon before (black columns) and after (grey columns) addition of steroidal detergents: (**A)** anionic taurocholic acid, (**B)** zwitter-ionic CHAPS (both 10 mM). Compounds as indicated in Fig. 1.

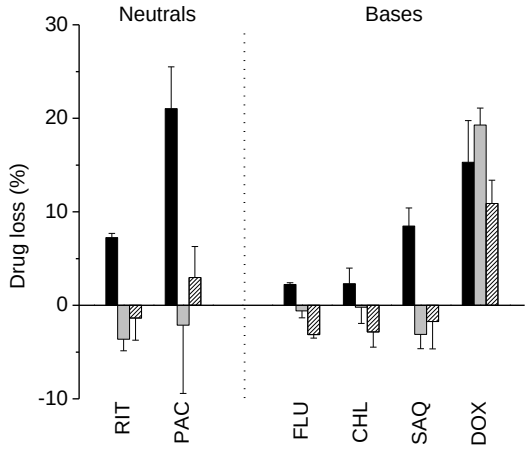

Figure 3 Drug loss from aqueous bulk solution to Teflon (black columns) and recovery from drug loss with 2,6-di-O-methyl-β-cyclodextrin (10 mM) applied at pH 7.4 (grey columns) and at pH 3 (dashed columns). Compounds as indicated in Fig. 1.

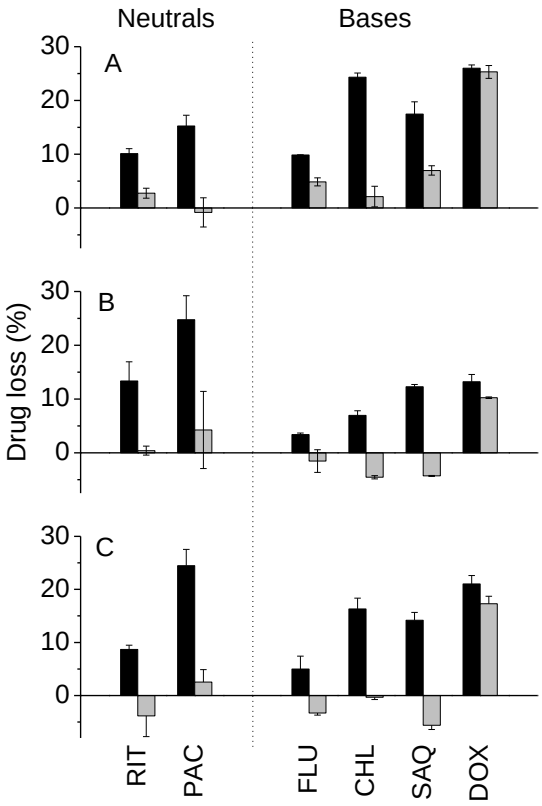

Figure 4 Drug loss from aqueous bulk solution to Teflon before (black columns) and after (grey columns) addition of organic solvents: (**A**) DMSO; (**B**) acetonitrile and (**C**) 2-propanol. The final concentration of solvent was 25 % (v/v). Compounds as indicated in Fig. 1.

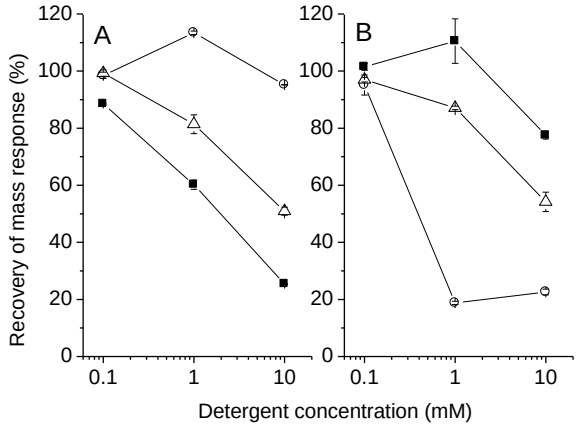

Figure 5 A, B: Concentration dependency of mass analyzed analyte recoveries in presence of Brij 35 (△), CTAB (■) and SDS (○). Recovery studies were conducted separately in positive (**A**) and negative (**B**) ionization mode, using rolipram and ketorolac, respectively, as test analytes (both 25 µM, buffer: 50 mM Tris, 114 mM NaCl, pH 7.4). The ion intensities of the $(M+H]^+$ (rolipram) and the $M-H]^-$ (ketorolac) trace were monitored in SIM mode. All samples were processed with a fast gradient HPLC method before introduction into the ionization source (ESI) of the single quadrupole mass spectrometer.

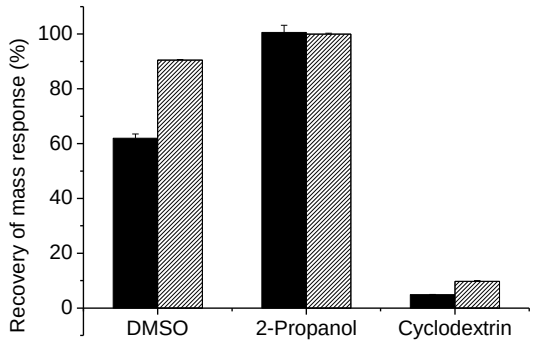

Figure 6 Recovery of mass response after addition of 2-propanol, DMSO (both 25 %, v/v) and 2,6-di-O-methyl-β-cyclodextrin (10 mM) in positive (black column) and negative (hatched columns) ionization mode.

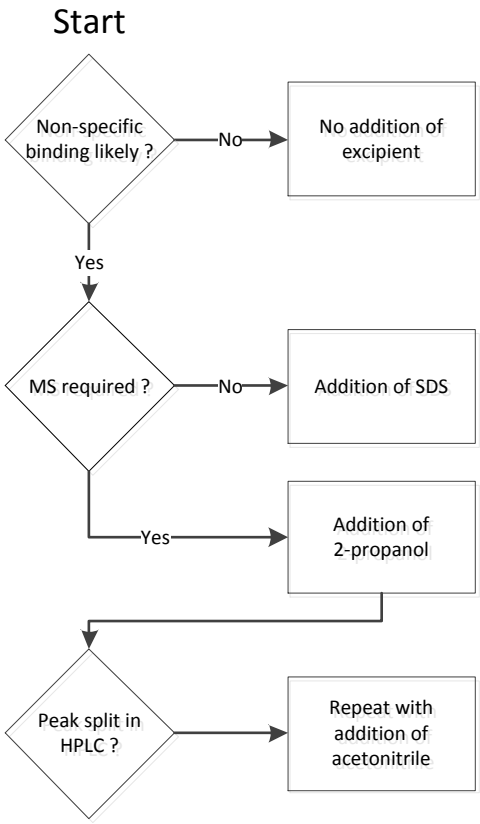

Figure 7 Guideline for the selection of an appropriate detergent for the remediation of drug loss to Teflon. For the prediction of a compound's likelihood for non-specific binding, the reader is referred to our *accompanying manuscript 2*.

Supporting Information

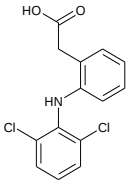

Diclofenac

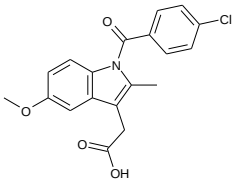

Indomethacin

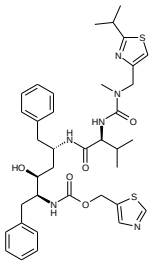

Ritonavir

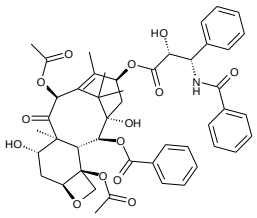

Paclitaxel

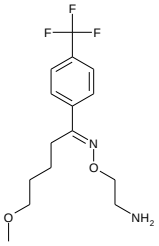

Fluvoxamine

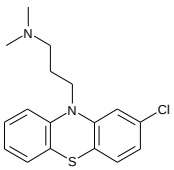

Chlorpromazine

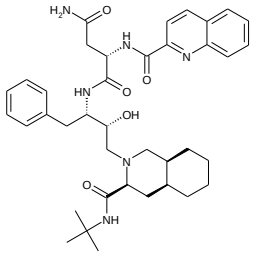

Saquinavir

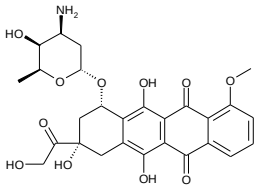

Doxorubicin

Figure S1 Structures of compounds for which adsorption onto Teflon was evident before (ritonavir, paclitaxel, fluvoxamine, chlorpromazine, saquinavir, doxorubicin) or after (diclofenac, indomethacin) addition of excipients.

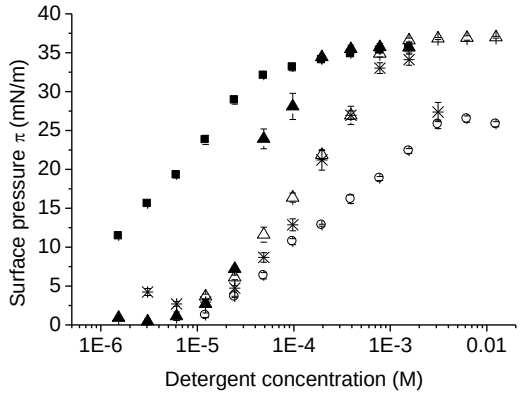

Figure S2 Surface pressure - concentration profiles for Brij 35(■), CTAB (▲), SDS (△), taurocholic acid (✳) and CHAPS (○) dissolved in 50mM Tris/114mM NaCl/pH 7.4 buffer. Experiments were carried out at room temperature, on a multichannel microtensiometer (Delta-8, Kibron, Helsinki) using an aluminium assay plate (capacity: V = 50µL).

References

1. DeWitte, R.S., *Avoiding physicochemical artefacts in early ADME-Tox experiments.* Drug Discovery Today, 2006. **11**(17 & 18): p. 855-859.
2. Aloyo, V.J., et al., *Phosphorylation of the neuronal protein kinase C substrate B-50: in vitro assay conditions alter sensitivity to ACTH.* Neurochem. Res., 1988. **13**(4): p. 343-8.
3. Wagdy, A.M., et al., *Effect of sample collection tubing type used in a clinical study on quantitation of pharmaceutical compounds in CSF by LC-MS/MS.* Bioanalysis, 2011. **3**(2): p. 167-179.
4. Oddi, S., et al., *Pitfalls and solutions in assaying anandamide transport in cells.* J Lipid Res, 2010. **51**(8): p. 2435-44.
5. Pennino, J.D., *There's no such a thing as a representative ground water sample.* Groundwater Monitoring & Remediation, 1988. **8**(3): p. 4-9.
6. Broeders, J.J.W., et al., *Transport of Chlorpromazine in the Caco-2 Cell Permeability Assay: A Kinetic Study.* Chem. Res. Toxicol., 2012. **25**(7): p. 1442-1451.
7. Hyenstrand, P., et al., *Losses of the cyanobacterial toxin microcystin-LR from aqueous solution by adsorption during laboratory manipulations.* Toxicon, 2001. **39**(4): p. 589-594.
8. Yahya, A.M., J.C. McElnay, and P.F. D'Arcy, *Drug sorption to glass and plastics.* Drug Metab. Drug Interact., 1988. **6**(1): p. 1-45.
9. D'Arcy, P.F., *Drug interactions with medicinal plastics.* Adverse Drug React. Toxicol. Rev., 1996. **15**(4): p. 207-219.
10. Kowaluk, E.A., M.S. Roberts, and A.E. Polack, *Interactions between drugs and intravenous delivery systems.* Am J Hosp Pharm, 1982. **39**(3): p. 460-7.
11. Benvenuto, J.A., et al., *Stability and compatibility of antitumor agents in glass and plastic containers.* Am. J. Hosp. Pharm., 1981. **38**(12): p. 1914-18.
12. Beitz, C., et al., *Compatibility of plastics with cytotoxic drug solutions-comparison of polyethylene with other container materials.* Int. J. Pharm., 1999. **185**(1): p. 113-121.
13. Martens, H.J., P.N. De Goede, and A.C. Van Loenen, *Sorption of various drugs in polyvinyl chloride, glass, and polyethylene-lined infusion containers.* Am. J. Hosp. Pharm., 1990. **47**(2): p. 369-73.
14. Song, D., L.-F. Hsu, and J.L.S. Au, *Binding of Taxol to Plastic and Glass Containers and Protein under in Vitro Conditions.* J. Pharm. Sci., 1996. **85**(1): p. 29-31.
15. Bahal, S.M. and J.M. Romansky, *Sorption of benzoic acid, sorbic acid, benzyl alcohol, and benzalkonium chloride by flexible tubing.* Pharm. Dev. Technol., 2002. **7**(1): p. 49-58.
16. Walker, C.W. and J.E. Watson, *Adsorption of estrogens on laboratory materials and filters during sample preparation.* J. Environ. Qual., 2010. **39**(2): p. 744-748.
17. Minder, R., H.J. Weder, and M.H. Bickel, *Experimental errors resulting from uptake of lipophilic drugs by soft plastic materials.* Biochem. Pharmacol., 1970. **19**(6): p. 2179-80.
18. Parker, L.V. and T.A. Ranney, *Sampling trace-level organic solutes with polymeric tubing. Part 2. Dynamic studies.* Ground Water Monit. Rem., 1998. **18**(1): p. 148-155.

19. Ranney, T.A. and L.V. Parker, *Comparison of fiberglass and other polymeric well casings, Part III. Sorption and leaching of trace-level metals.* Ground Water Monit. Rem., 1998. **18**(3): p. 127-133.
20. Marcus, E., H.K. Kim, and J. Autian, *Binding of drugs by plastics. I. Interaction of bacteriostatic agents with plastic syringes.* J. Am. Pharm. Assoc. (1912-1977), 1959. **48**: p. 457-62.
21. Suzuki, T., I. Uchida, and T. Mashimo, *Sorptive Loss of Volatile and Gaseous Anesthetics from In Vitro Drug Application Systems.* Anesth. Analg. (Hagerstown, MD, U. S.), 2005. **100**(2): p. 427-430.
22. Jenke, D.R., *Evaluation of various solvent systems for modeling solute sorption with plasticized polyvinyl chloride materials.* J Pharm Sci, 1993. **82**(6): p. 617-21.
23. Loh, W. and P.L.O. Volpe, *Adsorption of alkyl p-hydroxybenzoates from aqueous solution onto Teflon.* J. Colloid Interface Sci., 1996. **179**(1): p. 322-3.
24. Singh, C.D. and M. Ogita, *Detection of critical micelle concentration (CMC) using uniform and U-shaped optical fiber in sensing region.* Appl. Phys. B: Lasers Opt., 2004. **79**(1): p. 103-105.
25. Tojino, M., et al., *Immobilization of fluorous oligosaccharide recognized by influenza virus on polytetrafluoroethylene filter*. Bioorg. Med. Chem. Lett., 2012. **22**(2): p. 1251-1254.
26. Kenna, J.G., G.N. Major, and R.S. Williams, *Methods for reducing non-specific antibody binding in enzyme-linked immunosorbent assays.* J. Immunol. Methods, 1985. **85**(2): p. 409-19.
27. Peter Esser, *Detergent in polystyrene ELISA.* Technical Bulletin 08, Thermo Scientific, 2010.
28. Hoffman, W.L. and A.A. Jump, *Tween 20 removes antibodies and other proteins from nitrocellulose.* J. Immunol. Methods, 1986. **94**(1-2): p. 191-6.
29. Lee, Y.-h., K.-j. Lee, and K. Holme, *Method for the pretreatment of a surface for the reduction of non-specific binding by chemical entities*, 2003, (USA). Application: US US. p. 10 pp.
30. Kadar, E.P., et al., *Evaluation of the relationship between a pharmaceutical compound's distribution coefficient, log D and adsorption loss to polypropylene in urine and CSF*. Bioanalysis, 2010. **2**(4): p. 755-767.
31. Mulvana, D.E., *Critical topics in ensuring data quality in bioanalytical LC-MS method development.* Bioanalysis, 2010. **2**(6): p. 1051-1072.
32. Aubry, A.-F., *LC-MS/MS bioanalytical challenge: ultra-high sensitivity assays.* Bioanalysis, 2011. **3**(16): p. 1819-1825.
33. Ji, A.J., et al., *Challenges in urine bioanalytical assays: overcoming nonspecific binding.* Bioanalysis, 2010. **2**(9): p. 1573-1586.
34. Dubbelman, A.-C., et al., *Bioanalytical aspects of clinical mass balance studies in oncology.* Bioanalysis, 2011. **3**(23): p. 2637-2655.
35. Fukazawa, T., Y. Yamazaki, and Y. Miyamoto, *Reduction of non-specific adsorption of drugs to plastic containers used in bioassays or analyses.* J. Pharmacol. Toxicol. Methods, 2010. **61**(3): p. 329-333.
36. Pinzauti, S., et al., *Storage study on acidic aqueous hexetidine solutions in polyolefinic and glass containers.* Boll. Chim. Farm., 1980. **119**(9): p. 559-63.
37. Wasiewski, W., et al., *Thrombin adsorption to surfaces and prevention with polyethylene glycol 6,000.* Thromb. Res., 1976. **8**(6): p. 881-6.

38. Xu, R.N., et al., *Simultaneous LC-MS/MS quantitation of a highly hydrophobic pharmaceutical compound and its metabolite in urine using online monolithic phase-based extraction.* J. Sep. Sci., 2007. **30**(17): p. 2943-2949.
39. Wang, P.G., et al., *A high-throughput liquid chromatography/tandem mass spectrometry method for simultaneous quantification of a hydrophobic drug candidate and its hydrophilic metabolite in human urine with a fully automated liquid/liquid extraction.* Rapid Commun. Mass Spectrom., 2006. **20**(22): p. 3456-3464.
40. Sun, L. and J.A. Stenken, *The effect of β-cyclodextrin on liquid chromatography/electrospray-mass spectrometry analysis of hydrophobic drug molecules.* J. Chromatogr., A, 2007. **1161**(1-2): p. 261-268.
41. Chen, C., et al., *Sensitive and cost-effective LC-MS/MS method for quantitation of CVT-6883 in human urine using sodium dodecylbenzenesulfonate additive to eliminate adsorptive losses.* J. Chromatogr., B: Anal. Technol. Biomed. Life Sci., 2009. **877**(10): p. 943-947.
42. Li, W., et al., *Quantitative determination of BAF312, a S1P-R modulator, in human urine by LC-MS/MS: Prevention and recovery of lost analyte due to container surface adsorption.* J. Chromatogr., B: Anal. Technol. Biomed. Life Sci., 2010. **878**(5-6): p. 583-589.
43. Rodila, R., et al., *HPLC-MS/MS determination of a hardly soluble drug in human urine through drug-albumin binding assisted dissolution.* J. Chromatogr., B: Anal. Technol. Biomed. Life Sci., 2008. **872**(1-2): p. 128-132.
44. Schwartz, M., W. Kline, and B. Matuszewski, *Determination of a cyclic hexapeptide (L-743872), a novel pneumocandin antifungal agent in human plasma and urine by high-performance liquid chromatography with fluorescence detection.* Anal. Chim. Acta, 1997. **352**(1-3): p. 299-307.
45. Rose, M.J., et al., *Determination of L-756 423, a novel HIV protease inhibitor, in human plasma and urine using high-performance liquid chromatography with fluorescence detection.* J. Chromatogr., B: Biomed. Sci. Appl., 1999. **732**(2): p. 425-435.
46. West, C.C. and J.H. Harwell, *Surfactants and subsurface remediation.* Environ. Sci. Technol., 1992. **26**(12): p. 2324-30.
47. Guo, H., et al., *Effect of Tween80 and β-cyclodextrin on the distribution of herbicide mefenacet in soil-water system.* J. Hazard. Mater., 2010. **177**(1-3): p. 1039-1045.
48. Rosen, M.J., *Surfactants and Interfacial Phenomena, 3rd Edition*2004. 464 pp.
49. Surapaneni, M.S., S.K. Das, and N.G. Das, *Designing paclitaxel drug delivery systems aimed at improved patient outcomes: current status and challenges.* ISRN Pharmacol., 2012: p. 623139, 15 pp.
50. Rundlett, K.L. and D.W. Armstrong, *Mechanism of Signal Suppression by Anionic Surfactants in Capillary Electrophoresis-Electrospray Ionization Mass Spectrometry.* Anal. Chem., 1996. **68**(19): p. 3493-3497.
51. Suomalainen, P., et al., *Surface activity profiling of drugs applied to the prediction of blood-brain barrier permeability.* J Med Chem, 2004. **47**(7): p. 1783-8.
52. Fayet, A., et al., *Determination of unbound antiretroviral drug concentrations by a modified ultrafiltration method reveals high variability in the free fraction. [Erratum to document cited in CA150:047250].* Ther. Drug Monit., 2010. **32**(1): p. 117.

53. Shao, L.K. and D.C. Locke, *Separation of Paclitaxel and Related Taxanes by Micellar Electrokinetic Capillary Chromatography.* Anal. Chem., 1998. **70**(5): p. 897-906.
54. Hempel, G., et al., *Determination of paclitaxel in biological fluids by micellar electrokinetic chromatography.* J. Chromatogr., A, 1996. **745**(1+2): p. 173-179.
55. Pereira, E.A., G.A. Micke, and M.F.M. Tavares, *Determination of antiretroviral agents in human serum by capillary electrophoresis.* J. Chromatogr., A, 2005. **1091**(1-2): p. 169-176.
56. Hilhorst, M.J., et al., *Towards a general approach for the impurity profiling of drugs by micellar electrokinetic chromatography.* Electrophoresis, 2001. **22**(7): p. 1337-1344.
57. Wei, Z., et al., *Paclitaxel-loaded Pluronic P123/F127 mixed polymeric micelles: Formulation, optimization and in vitro characterization.* Int. J. Pharm., 2009. **376**(1-2): p. 176-185.
58. Caetano, W. and M. Tabak, *Interaction of chlorpromazine and trifluoperazine with ionic micelles: electronic absorption spectroscopy studies.* Spectrochim. Acta, Part A, 1999. **55A**(12): p. 2513-2528.
59. Caetano, W., et al., *Chlorpromazine and sodium dodecyl sulfate mixed micelles investigated by small angle x-ray scattering.* J. Colloid Interface Sci., 2002. **248**(1): p. 149-157.
60. Erdinc, N., S. Goektuerk, and M. Tuncay, *Interaction of Epirubicin HCl with surfactants: Effect of NaCl and glucose.* J. Pharm. Sci., 2004. **93**(6): p. 1566-1576.
61. Treiner, C., *Adsolubilization and related phenomena.* Surfactant Sci. Ser. , 2003. **112**(Structure-Performance Relationships in Surfactants (2nd Edition)): p. 627-672.
62. Desai, T.R. and S.G. Dixit, *Coadsorption of cationic-nonionic surfactant mixtures on polytetra fluoroethylene (PTFE) surface.* J. Colloid Interface Sci., 1996. **179**(2): p. 544-551.
63. Lunkenheimer, K., A. Lind, and M. Jost, *Surface Tension of Surfactant Solutions.* J. Phys. Chem. B, 2003. **107**(31): p. 7527-7531.
64. Paria, S., *Surfactant-enhanced remediation of organic contaminated soil and water*. Adv. Colloid Interface Sci., 2008. **138**(1): p. 24-58.
65. Hamada, H., et al., *Enhancement of water-solubility and bioactivity of paclitaxel using modified cyclodextrins.* J. Biosci. Bioeng., 2006. **102**(4): p. 369-371.
66. Pathak, S.M., et al., *Enhanced oral absorption of saquinavir with methyl-beta-cyclodextrin-preparation and in vitro and in vivo evaluation.* Eur. J. Pharm. Sci., 2010. **41**(3-4): p. 440-451.
67. Venkata Ramana, D. and K.P.R. Chowdary, *Enhancement of solubility and dissolution rate of ritonavir employing β-cyclodextrin, Solutol HS15 and PVP K30: a factorial study.* Int. J. Pharm. Sci. Rev. Res., 2012. **14**(2): p. 38-41.
68. McIntosh, M.P., et al., *Impact of chlorpromazine self-association on its apparent binding constants with cyclodextrins: Effect of SBE7-β-CD on the disposition of chlorpromazine in the rat.* J. Pharm. Sci., 2010. **99**(7): p. 2999-3008.
69. Anand, R., et al., *A close-up on doxorubicin binding to γ-cyclodextrin: an elucidating spectroscopic, photophysical and conformational study.* RSC Adv. , 2012. **2**(6): p. 2346-2357.
70. Zdziennicka, A. and B. Janczuk, *The adsorption of cetyltrimethylammonium bromide and propanol mixtures with regard to wettability of polytetrafluoroethylene. II.*

Adsorption at polytetrafluoroethylene-aqueous solution interface and wettability. J. Colloid Interface Sci., 2008. **318**(1): p. 15-22.

71. Francomb, M.M., J.L. Ford, and M.G. Lee, *Adsorption of vincristine, vinblastine, doxorubicin and mitozantrone to in-line intravenous filters.* Int. J. Pharm., 1994. **103**(1): p. 87-92.
72. Silvester, S. and F. Zang, *Overcoming non-specific adsorption issues for AZD9164 in human urine samples: Consideration of bioanalytical and metabolite identification procedures.* J. Chromatogr., B: Anal. Technol. Biomed. Life Sci., 2012. **893-894**: p. 134-143.
73. Banerjee, S. and S.H. Yalkowsky, *Cosolvent-induced solubilization of hydrophobic compounds into water.* Anal. Chem., 1988. **60**(19): p. 2153-5.
74. Enke, C., *A predictive model for matrix and analyte effects in electrospray ionization of singly-charged ionic analytes.* Anal. Chem., 1997. **69**(23): p. 4885-4893.
75. Tang, L. and P. Kebarle, *Dependence of ion intensity in electrospray mass spectrometry on the concentration of the analytes in the electrosprayed solution.* Anal. Chem., 1993. **65**(24): p. 3654-68.
76. Tong, X.S., et al., *Effect of Signal Interference from Dosing Excipients on Pharmacokinetic Screening of Drug Candidates by Liquid Chromatography/Mass Spectrometry.* Anal. Chem., 2002. **74**(24): p. 6305-6313.
77. King, R., et al., *Mechanistic investigation of ionization suppression in electrospray ionization.* J. Am. Soc. Mass Spectrom., 2000. **11**(11): p. 942-950.
78. Bendels, S., et al., *PAMPA-Excipient Classification Gradient Map.* Pharm. Res., 2006. **23**(11): p. 2525-2535.
79. Kostewicz, E.S., et al., *Forecasting the oral absorption behavior of poorly soluble weak bases using solubility and dissolution studies in biorelevant media.* Pharm. Res., 2002. **19**(3): p. 345-349.
80. Fowkes, F.M., *Attractive forces at interfaces.* J. Ind. Eng. Chem. (Washington, D. C.), 1964. **56**(12): p. 40-52.
81. Fischer, H., *Passive Diffusion and Active Transport through Biological Membranes - Binding of Drugs to Transmembrane Receptors* 1998.
82. Dollery, C., *Therapeutic drugs* 2ed1998: Churchill Livingstone.

4.4 Evaluation and Management of Excipient-Related Matrix Effects in HPLC-ESI/MS Analysis of PAMPA-Permeability

Frauke Assmus, Holger Fischer, Anna Seelig

Author's Contributions:

Frauke Assmus	• Idea and design of the study • Performing experiments including data analysis • Writing the manuscript
Holger Fischer	• Valuable discussions • Reviewing the manuscript •
Anna Seelig	• Supervision of the work • Valuable discussions • Support in writing the manuscript

ABSTRACT

The Parallel Artificial Membrane Permeability Assay (PAMPA) has emerged as a widely used primary *in vitro* screen for passive permeability of potential drug candidates. Excipients such as solubilizers and formulation agents are frequently applied in PAMPA, however, they may suppress the ionization efficiency of the analyte of interest (matrix effect). To ensure the accuracy of mass-analyzed passive permeability, it was crucial to investigate matrix effects related to excipients commonly used in PAMPA, namely glycocholic acid (0.5 %, m/v), hydroxypropyl-β-cyclodextrin, propylene glycol, N-methyl-2-pyrrolidone (each 0.24 %, m/v) and, in addition, the FaSSIF/FeSSIF media. Recovery and post-column infusion studies of the test analyte rolipram were conducted in presence and in absence of excipients. Concentration analysis was achieved with a fast generic gradient method on a HPLC system coupled to an electro-spray single-quadrupole mass spectrometer (HPLC-ESI/MS) working in single reaction monitoring mode. The excipients were characterized by means of surface activity measurements. Matrix effects were pronounced for excipients favoring the air-water interface (glycocholic acid, the FaSSIF/FeSSIF media), forming multiply-charged ions (hydroxypropyl-β-cyclodextrin) and/or carrying a proton acceptor in the form of a nitrogen (1-methyl-2-pyrrolidone). Propylene glycol showed the weakest matrix effect. The non-uniform presence of ion-suppressing excipients only in the PAMPA donor compartment resulted in overestimation of membrane permeability, as was demonstrated with glycocholic acid. We recommend i) to provide the same concentration of excipients in each PAMPA compartment prior to injecting the analyte solution onto the HPLC-MS system and ii) to replace the frequently used solubilizer glycocholic acid with propylene glycol. However, when using HPLC-MS for concentration analysis in PAMPA it should be critically tested whether or not a solubilizer improves the net sensitivity in HPLC-MS. In addition, we suggest surface tension measurements for investigating a potential ion-suppressing effect of buffer matrix components.

KEYWORDS

Excipients, PAMPA, Ion suppression, Matrix effects, ESI-MS

1. Introduction

Membrane permeability plays a key role in drug absorption and drug distribution; its assessment has therefore become an integral part of the early ADME (Absorption, Distribution, Metabolism, Elimination) profiling process[1]. PAMPA (Parallel Artificial Membrane Permeability Assay) has emerged as a widely used primary *in vitro* screen for passive membrane permeability [2, 3] and provides a fast and low - cost alternative to cell-based permeability assays.While the 96 - well plate format allows for the processing of several hundred compounds per week in parallel, concentration analysis remains the bottleneck of PAMPA [4]. Rapid quantification with a UV plate reader is often hampered by the presence of impurities, the lack of a UV chromophore, and the low solubility of many research compounds. Efforts to improve the assay sensitivity and/or selectivity involved for instance the use of solubilizers, the transfer from UV to HPLC-MS analysis, or a combination of both [5]. Particularly MS systems equipped with an electrospray ionization source (ESI-MS) have found entry in many laboratories owing to the gentle ionization of the analytes.

However, reduced ionization efficiency of an analyte in presence of coeluting substances (the 'matrix') is a major concern in ESI-MS and has been referred to as ion suppression or matrix effect [6]. Ion suppression not only impairs the sensitivity but may even lead to erroneous results if variations in the matrix composition among different samples are neglected. The fact that MS is able to monitor a single molecule in complex matrixes can turn out to be a pitfall because coelution of an analyte with other substances is easily overlooked. Use of fast generic gradient methods to accomplish the demand for higher throughput goes at the expense of separation efficiency and further increases the probability of matrix effects [7].

The underlying mechanisms of matrix effects are not yet fully understood and can involve both solution and gas phase processes, the former of which has been considered the more relevant [8]. For example, the formation of charged droplets at the capillary needle entering the ionization source is susceptible to changes in surface tension, conductivity and viscosity, and is thus likely perturbed by coeluting matrix compounds [9-11]. Additionally, competition for the limited charge and/or space on the surface of the electrosprayed droplet has been proposed as a major factor involved in ion suppression [12, 13]: According to the ion evaporation model [14], only molecules which reside on the surface of the electrosprayed droplets can be considered as precursors of the gas phase ions that finally enter the mass spectrometer [15]. Therefore, surface active ions enriching on the droplet surface have been found to prevent less amphiphilic compounds from ion evaporation [11, 16, 17]. The

observation that precursors of the gas phase ions (i.e. the offspring droplets) are formed from the liquid close to the surface of the parent droplet further enhances the importance of surface activity [18]. Other processes involved in ion suppression are the formation of solid residues from highly concentrated analyte and/or matrix solutions [8] in addition to proton transfer reactions in the gas phase [19].

Much of the knowledge about the underlying mechanisms of ion suppression must be credited to Kebarle and coworkers [20] and Enke [16], who primarily focused on the concentration dependent mass responses of simple amines. In the last decade, excipients used as dosing vehicles in DMPK (Drug Metabolism and Pharmacokinetics) studies have also been recognized to cause ion suppression and, in turn, erroneous estimates of pharmacokinetic parameters [10, 21-26]. Notably, an EMEA guideline [27] provides recommendations for the evaluation of matrix effects in bioanalytical studies. In view of the above it is all the more surprising that excipient-related matrix effects have barely been considered in classical physicochemical screening assays such as PAMPA. Excipients are frequently used in PAMPA, either as solubilizers [28] , model formulation agents [29] or sink compounds [30], at concentrations several orders of magnitude higher than the analyte itself.

The aim of this study was to test whether the excipients used in PAMPA cause ion suppression in ESI-MS, and whether the presence of ion suppression affects the accuracy of the permeability measures. We investigated (i) the amphiphilic solubilizer glycocholic acid (GCA), (ii) the model formulation agents propylene glycol (PG), 2-hydroxypropyl-β-cyclodextrin (HP-β-CD) and N-methyl-2-pyrrolidone (NMP), and (iii) the simulated gastrointestinal fluid in the fasted (FaSSIF) and the fed (FeSSIF) state (taurocholic acid-phospholipid-salt mixture)[31]. Although pure taurocholic acid has been studied as a model formulation agent in PAMPA [29], we studied the FaSSIF/FeSSIF media instead, to account for the greater relevance for predicting food-induced changes in permeability [32].

There is a certain overlap between the dosing vehicles which have already been evaluated in the framework of DMPK studies (PG, HP - β - CD) and the excipients tested in this study. However, the literature lacks information on possible matrix effects in the presence of the FaSSIF/FeSSIF media, GCA and NMP. In addition, the published studies on excipient-related matrix effects focus on concentrations matching the expected excipient concentrations in plasma. Here, we were interested in the effect of higher concentrations required for efficient solubilization in PAMPA. Moreover, the implications from literature studies on the impact of PG and HP - β - CD on the accuracy of MS were based on recovery studies of a

specific analyte without giving insight into the elution behavior of the excipient [10]. For a more complete picture of excipient-related matrix effects, we performed recovery and post-column infusion studies with the test analyte rolipram, and diagnosed coelution with the excipients by means of full scan MS experiments. In addition the effect of non-uniform presence of excipients in the PAMPA sandwich on the accuracy of mass-analyzed permeability values was evaluated using GCA as an example.

2. Materials and Methods

2.1. Drugs and Chemicals

Rolipram, amitriptyline, midazolam, PK 11195, thioridazine · HCl, trifluperazine · HCl, verapamil · HCl and zaleplone were available through our in-house Compound Depository Group as proprietary compound. Theophylline was obtained from Acros (New Jersey, MA, USA). Rizatriptane was available from Bepharm (Shanghai, China). Carbamazepine, cyclobenzaprine · HCl, flumazenil, maprotiline · HCl, metoclopramide · HCl, phenytoin, GCA, HP-β-CD and PG were purchased from Sigma (Steinheim, Switzerland). Tris, sodium chloride, sodium dihydrogen phosphate and acetic acid were obtained from Fluka (Buchs, Germany). DMSO was obtained from Acros (Geel, Belgium). N - methyl-2-pyrrolidone (NMP) was purchased from Merck (Hohenbrunn, Germany). SIF Powder for the preparation of the FaSSIF / FeSSIF media was obtained from Phares (Muttenz, Switzerland). Formic acid, water and acetonitril were supplied from Merck (Darmstadt, Germany) and were of HPLC-grade.

2.2. HPLC Instrumentation and Chromatographic Conditions

All experiments were performed on an Agilent 1290 Infinity HPLC system equipped with degasser, auto - sampler, column oven, pump, DAD detector and mass spectrometer. If not mentioned otherwise, the sample solution (5 µL) was injected onto a Kinetex C_{18} analytical column (2.6 µm particle size, 2.1 x 50 mm, Phenomenex, Torrence, CA) operated at 60 °C. The mobile phase was delivered at 1 mL/min and consisted of A (water) and B (acetonitril), each containing 0.1 % (v/v) formic acid. In the gradient program, B was held at 5 % for 0.1 min and then was linearly increased to 40 % in 0.1 min and further to 95 % in 0.4 min. After 2.5 min, the gradient was set back from 95 % B to the initial conditions.

2.3. Mass Spectrometry

The API single quadrupole mass spectrometer (Agilent 6140) was equipped with an electrospray ionization source operated in positive mode. Each 0.1 s the intensity of the pseudo - molecular ion, $[M+H]^+$, was acquired in single reaction monitoring mode (SRM). Recovery studies were also conducted in full scan mode (MRM dwell time 50 ms) at m/z in the range 50 – 1350 (NMP, HP-β-CD, PG) or 100 - 1000 (all other excipients). The source settings were as follows: capillary voltage + 3.5 kV, drying gas flow (N_2) 13 L/min, nebulizer pressure 60 psi, drying gas temperature 350 °C. In the recovery studies and permeability

measurements, the flow from the HPLC system was introduced into the ESI interface only after 0.25 min to prevent contamination with buffer salts and DMSO. In contrast, the whole time window without any delay was used to monitor matrix effects in the post-column infusion studies.

2.4. Evaluation of Matrix Effects

2.4.1. Selection of the Test Analyte

The selection of the test analyte rolipram was based on the following criteria: (i) presence of a UV chromophore enabling direct comparison of analyte response in MS and UV (the UV analysis was not disturbed by the presence of excipients, see Figure 11A in Results and Discussion), (ii) negligible adsorption to plastic plates and pipetting devices (data not shown), which could otherwise bias the recovery studies, and (iii) moderate lipophilicity (measured $logD_{oct}$ 1.91 at pH 7.4 [33]), which meets the intention to study a drug with intermediate retention in HPLC.

2.4.2. Concentration of Excipient Solutions and their Preparation

Excipient solutions spiked with GCA and the formulation agents (HP-β-CD, PG and NMP) were prepared in blank buffer (50 mM Tris, 114 mM NaCl, pH 7.4). The final working concentrations corresponded to those routinely used in the Roche PAMPA setup (GCA, 0.5 %, m/v) or applied in PAMPA excipient profiling to resemble the quantities expected in gastrointestinal fluids under clinically relevant conditions (formulation agents, each 0.24 %, m/v)[29]. FaSSIF and FeSSIF medium, respectively, was prepared from blank FaSSIF buffer (0.029 M phosphate, 0.106 M NaCl, pH 6.5) and blank FeSSIF buffer (0.144 M acetate, 0.203 M NaCl, pH 5.0). Instant SIF Powder (2.24 g/L and 11.2 g/L) was reconstituted in the corresponding blank buffers resulting in 3 mM and 15 mM sodium taurocholate and 0.75 mM and 3.75 mM lecithin of the final FaSSIF and the FeSSIF medium, respectively. For the post-column infusion studies, all excipient solutions were prepared in an eluent mixture (50:50 water-acetonitril, 0.1% formic acid) instead of using buffer.

2.4.3. Recovery Studies

Analyte solutions containing the test drug (25µM rolipram, DMSO content: 0.25%, v/v) were prepared either in excipient-spiked buffer (50 mM Tris, 114 mM NaCl, pH 7.4, excipient concentrations see above) or in blank buffer (reference). The reference was injected onto the HPLC-MS system (n=5), followed by five consecutive injections of the excipient-spiked test

solutions. Recovery of the test drug was determined from the ratio of the average peak area in presence and in absence of excipient.

2.4.4. Post-Column Infusion Studies

Analyte solution (25 µM rolipram in eluent, DMSO content: 0.25 %, v/v) was infused into the HPLC-MS system using an external pump (Dionex P680 HPLC Pump) set at 50 µL/min. During the infusion, eluent spiked with excipient was injected on - column via the installed autosampler (n=5). Between the injection of excipients, blank eluent was injected five times to confirm complete recovery and to provide an initial reference. The flow from the HPLC column (1 mL/min) was combined with the constant flow of the analyte solution from the external pump via a T-piece, implemented directly before the ionization source.

2.5. Measurement of Surface Activity

Surface activity experiments were carried out on a multichannel microtensiometer (Delta-8, Kibron, Helsinki) utilizing a modified Du Nouy method as described elsewhere [34]. Prior to the measurements, the system was cleaned by heating the microbalances and calibrated with distilled water to 72.8 mN/m. Stock solutions of GCA (12.5mM), NMP (5M), PG (5M) and HP-β-CD (100 mM) were prepared in 50mM Tris/ 114mM NaCl/ pH 7.4 buffer. Eleven consecutive 1:1 dilutions of the excipient stock solutions and the FaSSIF medium (buffer: 0.029 M phosphate, 0.106 M NaCl, pH 6.5) were perpared and an aliquot of each dilution (50 µL) was transferred to the 96-well measurement plate (aluminium). The surface pressure, $\pi=\gamma_0-\gamma$, where γ_0 is the surface tension of the pure buffer and γ the surface tension of the drug solution, was monitored in the order of increasing excipient concentration (n=3). The air-water partition coefficient, K_{aw}, was gained from extrapolation of the linear part of the $\pi/\log C$ plot to zero surface pressure as described elsewhere [34, 35].

2.6. Prediction of Matrix Effects by Means of $logD_{oct}$ (pH3.3)

The recoveries from GCA-spiked buffer as well as the retention times in HPLC/MS were recorded for an extended 16 compound dataset covering a wide physicochemical property space. Key properties, i.e. molecular weight (MW), pK_a, and calculated octanol/water partition coefficients, $c\log P$, for the test compounds are enclosed in Supporting Information. Experimental conditions (25µM analyte, 0.5%, m/v GCA, MS in SIM) were the same as described in Section 2.4.3. However, the UV response was used as an internal standard to

correct for the loss of lipophilic compounds to labware devices. The $C\log P$ values for the test compounds were calculated using $c\log P$ v4.71 (Daylight Chemical Information Systems, Irvine, CA), and the Henderson-Hasselbalch equation was used to calculate $\log D_{oct}$ (pH 3.3) from the $C\log P$ values and from the in-house measured pK_a. The retention times for the test compounds in HPLC-MS were linearly correlated with the calculated $\log D_{oct}$ (pH 3.3) values.

2.7. PAMPA Measurements

In PAMPA, a sandwich is formed consisting of an aqueous donor solution spiked with analyte, an artifiical membrane and an aqueous acceptor solution. The permeation of the test analyte rolipram across the membrane was measured according to the following protocol and as summarized in Figure 1.

Fig. 1

An aliquot (320 µL) of buffer solution (50 mM Tris/114 mM NaCl/ pH 7.4, DMSO content: 0.25 %, v/v) containing the analyte (100 µM rolipram) and a solubilizer (0.5 % (m/v) GCA) was transferred into an in-house made Teflon plate constituting the PAMPA donor compartment. The remaining solution was kept as a reference. A hydrophobic filter (PVDF, 125 µm, pore size 0.45 µm) fixed at the bottom of an acceptor plate (Millipore, Billerica, MA), MAIPN 4550) was coated with 4 µL lipid mixture (10 % (m/v) egg lecithin, 0.5 % (m/v) cholesterol, dissolved in dodecane) forming the barrier between the donor and the acceptor compartment. The pre-coated acceptor plate was filled with 280 µL of blank buffer devoid of glycocholic acid (50 mM Tris/ 114 mM NaCl/ pH 7.4) and was placed on top of the donor plate. The so formed sandwich was left undisturbed for 19 hours (room temperature) while the permeation of rolipram occurred. Then, the sandwich was disassembled and the reference, the donor and the acceptor compartment were assayed for the distributed drug. Sample injection onto the HPLC-UV-ESI/MS system followed three strategies (n=3), a) the reference, donor and acceptor solutions were directly injected, b) the reference, donor and acceptor solutions were diluted 1:100 with blank buffer and c) the concentration of excipient in each compartment was adjusted to the same level (0.25% GCA). For this purpose, the reference and the donor solution (each 50 µL) were diluted 1:1 with blank buffer, while the acceptor solution (50 µL) was diluted 1:1 with buffer containing 0.5 % GCA.

For determining the test analyte's concentration in each compartment, a calibration curve using external standards was created (a calibration with different injection volumes is not viable, see Figure 11B in Results and Discussion). Therefore, sixteen consecutive dilutions of a stock solution (200 µM rolipram, in 50 mM Tris/114 mM NaCl/pH 7.4, 0.25 % (m/v) GCA, DMSO content 0.25 %, v/v) were prepared to cover the whole concentration range of rolipram (1.25 µM – 200 µM) while keeping the GCA concentration constant. Since the calibration function yielded a straight line (r^2 in UV and MS > 0.998, through origin), the concentration of rolipram in the donor and acceptor compartment was expressed as percentage of the analyte's response in the reference solution. Mass balance was used to determine the amount of rolipram remaining in the PAMPA barrier. The effective permeability, P_e, was calculated according to [28] and as described below:

$$P_e = \frac{2.303 V_D}{A(t - t_s)} \cdot \left(\frac{1}{1 + V_D / V_A} \right) \log_{10} \left[1 - \left(\frac{1 + V_A / V_D}{1 - R} \right) \left(\frac{C_{A,t}}{C_{D,t=0}} \right) \right], \quad (1)$$

where A is the area of the filter, t the time, t_s the time at steady state, V_A and V_D the acceptor and the donor volumes, respectively and $C_{A,t}$ and $C_{D,t}$ are the measured acceptor and donor concentrations at time t. The retention factor R is defined as:

$$R = 1 - \frac{\left(C_{D,t} + \left(C_{A,t} V_A / V_D \right) \right)}{C_{D,t=0}}. \quad (2)$$

2.8. Matrix Effects at Various Sample Loads

Analyte solutions (100 µM rolipram) containing increasing amounts of GCA (0.005, 0.05, 0.1, 0.5%, m/v) were prepared in buffer (50 mM Tris/114 mM NaCl/pH 7.4, DMSO content: 1%, v/v). Aliquots of these solutions (1-10 µL, incremented by 1µL) were then injected onto the HPLC-ESI/MS system. The peak areas of rolipram in UV and MS (m/z 276.2) were plotted as a function of the concentration of rolipram.

3. Results and Discussion

3.1. Recovery Studies

Matrix effects were evaluated by comparing the HPLC-ESI/MS - analyzed signal intensity of the test analyte rolipram (Figure 2) in presence and in absence of excipients. The structures and concentrations of the investigated excipients, namely GCA (0.5 %, m/v), NMP, HP-β-CD, PG (each 0.24 %, m/v) as well as of taurocholic acid (the main component in the FaSSIF/FeSSIF media) are shown in Figure 3. We used different excipient concentrations in order to match the quantities applied in PAMPA, either for solubilization of drugs (GCA) [9] or for the simulation of formulation (NMP, HP - β - CD, PG [4]) and food effects (FaSSIF/FeSSIF) on drug permeability.

Fig. 2, Fig. 3

Figure 4A shows an example of overlaid mass chromatograms of rolipram (m/z 276.2) in absence and in presence of GCA, obtained with a generic fast gradient HPLC-ESI/MS method. Setting the mass response of rolipram in blank buffer to 100 %, the intensity in excipient - spiked buffer was depressed by 89.3 ± 0.03% corresponding to 10.6 ± 0.03% recovery. In Figure 4B, the recovery from each investigated excipient solution is shown. Solutions spiked with HP-β-CD or PG did not disturb the MS analysis, whereas recovery was severely diminished in presence of the other excipients given in order of increasing analyte recovery: GCA (recovery 10.6 ± 0.03%) < NMP (64.0 ± 1.62%) < FaSSIF (76.0 ± 0.6%) ~ FeSSIF (76.7 ±0.7%).

Fig. 4

3.2. Proof of Coelution

For the sake of improved sensitivity, monitoring only the $[M+H]^+$ trace of rolipram was favored in the recovery studies. However, information about coelution with the excipients was gained from full scan experiments. The full scan mass chromatograms of GCA, the FeSSIF medium (also representative for FaSSIF) and NMP shown in Figure 5 in conjunction with the retention time of rolipram (R_t=0.575 min) confirm coelution in each case.

Fig. 5

The broad elution window of the excipients, particularly for the FeSSIF medium and NMP, can be explained as follows: First, the FeSSIF medium consists of several components including taurocholic acid (sharp peak at R_t = 0.626 min) and a mixture of various phospholipids [36]. Second, the investigated excipient concentrations were extremely high (millimolar range) giving rise to overload of the column and 'breakthrough' with the dead volume. The mass chromatograms of PG and HP -β-CD (not shown) were less informative and only slightly different from blank buffer, probably due to weaker ionization tendency (PG) and the limitations of the used mass spectrometer at the boundaries of the specified mass range (mass range ESI-MS: 50-1350; *MW* (PG) = 74; *MW* (HP-β-CD) ~1350 [37]).

3.3. The Influence of Excipients on the Mass Spectra

In order to provide further evidence for ion suppression, changes in the mass spectra of rolipram in presence of excipients were investigated. Fig. 6 A-C shows a snapshot of the mass spectra of rolipram (Fig. 6A), GCA (Fig. 6B) and the mixture of both (Fig. 6C), depicted at the retention time of rolipram.

Fig. 6

The mass spectrum of pure rolipram (Fig. 6A) was dominated by the sodium adduct of its dimer and the mono - protonated pseudo - molecular ion. In contrast, the characteristic spectrum of rolipram in the mixture of GCA and rolipram (Fig. 6C) was almost completely superimposed by that of GCA (Fig. 6B). Mass spectra of rolipram in presence of the other excipients are enclosed in Supporting Information. The abundance of the $[M+H]^+$ trace of rolipram was higher in presence of the other excipients as compared to GCA, which is in line with the results from the recovery studies (Fig. 4B).

3.4. Post-Column Infusion Studies

The effect of excipients on the mass response over the whole time window of the gradient method was investigated by means of post-column infusion (setup see Fig. 7) [6].

Fig. 7

Matrix effects were evaluated by comparing the infusion chromatograms of rolipram after on-column injection of either blank eluent (buffer) or excipient-spiked eluent (buffer). Figure 8A' shows the overlaid mass chromatograms of rolipram obtained from the injection of buffer in presence and in absence of GCA. Both chromatograms showed a negative peak close to the solvent front (R_t = 0.15 min) which was absent in the experiments with eluent (Figure 8A) instead of buffer (Fig. 8A'). The first negative peak could thus be attributed to the buffer salts used, either NaCl or Tris, which of the two was not further investigated. The negative peak at the higher retention time (R_t ~0.6 - 0.7 min) was only observed in presence of GCA, independent of whether buffer or eluent was used as solvent (Fig. 8A' und Fig. 8A). The suppression zone mirrored the elution window of GCA from the full scan experiments (Fig. 5A) and thus gave further evidence for ion suppression as the reason for the incomplete recovery of rolipram.

Fig. 8

Post-column infusion studies of all other excipients are shown only in eluent (Fig. 8 B - E). The FeSSIF medium, NMP and HP-β-CD caused severe ion suppression, observed as broad negative peaks (NMP, Fig. 8C), and in case of the FeSSIF medium (Fig. 8B) and HP - β - CD (Fig. 8D) even several suppression zones were evident. Similar to the FeSSIF medium (see above), HP - β - CD is not a single molecule, but a mixture of β-cyclodextrins labeled on average with 0.6 – 0.8 hydroxypropyl units per glucose molecule (information provided by the supplier Sigma). The broad suppression zones are probably a reflection of the various retention times of the different derivatives. The primary negative peak caused by HP - β - CD is most likely the consequence of column overload. Also the FeSSIF medium (Fig. 8B) showed a suppression region close to the solvent front which – in contrast to NMP- was not seen in the full scan spectra shown in Fig. 5. Rather hydrophilic and probably low molecular weight components, not observed in the full scan chromatograms in sufficient intensity, might be responsible for the additional ion suppression zone. Even though PG also showed a reduction in the signal intensity close to the solvent front (Fig. 8E), it was lower than for any other investigated excipient. While for both, PG and HP - β - CD, no ion suppression was observed in the preliminary recovery studies (Fig. 4B), the post-column infusion

chromatograms indicate that pronounced ion suppression in presence of HP - β - CD is likely for analytes eluting earlier than rolipram.

3.5. Trend Analysis of the Excipients-Related Matrix Effects

The extent of ion suppression observed in the recovery and post-column infusion studies varied considerably between the excipients. However, strictly speaking a comparison is only possible in a qualitative manner because different excipient concentrations, C_e, were used (Fig. 3).

An inspection of the surface pressure, π, vs. C_e profiles (Fig. 9) revealed that each excipient tested has the tendency to enrich at the air-water interface (Gibbs adsorption isotherm), thereby lowering the surface tension of pure buffer and, vice versa, increasing the surface pressure, π. By extrapolation of the linear part of the π-$\log C$ plot to zero π, the air-water partition coefficients of the excipients, K_{aw}, can be approximated (Table 1) together with the maximal surface pressures, π_{max} [38]. The excipients, which showed the most pronounced ion suppression zones in the post-column infusion studies, i.e. GCA (Fig. 8B), HP - β - CD (Fig. 8D) and the FaSSIF/FeSSIF (Fig. 8B) media, showed also a higher surface activity than the other formulation agents, NMP (Fig. 8C) and PG (Fig. 8E). This was indicated by the higher tendency of GCA, HP - β - CD and the FaSSIF/FeSSIF media to adsorb at the air-water interface and the concomitant stronger increase of π at the applied excipient concentration (π > 10 mN/m).

Fig. 9, Table 1

The trend towards pronounced matrix effects with increasing surface activity is in line with the observation of Tang and coworkers [11] on simple amines: The authors recognized that in a two - component mixture of electrolytes the electrolyte with the higher surface activity yielded the higher relative ion intensity in MS. They attributed the effect to the elevated surface population of amphiphilic electrolytes on the ESI droplet. The ions finally observed in the mass spectra are most likely those that constitute the excess surface charge (see Introduction).

Applied to excipients, our data suggests that a stronger partitioning of e.g. GCA to the air-water interface as compared to NMP (K_{aw} (GCA) >> K_{aw}(NMP)) resulted in a stronger competition with rolipram for the limited charge and/or space on the surface of the ESI

droplet, even though GCA was applied at lower molar concentrations than NMP (10.2 mM GCA, 24.3 mM NMP). Considering the nitrogen in NMP and GCA as the most probable protonation site, the ranking of ionization suppression goes along with the larger N-residue of GCA which renders GCA more surface active.

Regarding the FaSSIF/FeSSIF media, the surface activity of the main component, taurocholic acid, was similar to that of the structurally related GCA (π-$\log C$ plot of taurocholic acid not shown). However, taurocholic acid did not coelute with rolipram (Fig. 5B), and the matrix effect observed in the recovery studies (Fig. 4B) had to be attributed to the presence of phospholipids. The decline in recovery was moderate, not only because the concentration of lipids was much lower compared to that of the other excipients (Fig. 3) but also because only a fractional amount of lipids coeluted with rolipram (Fig. 5B). The substantial matrix effect observed in the post-column infusion study (Fig. 8B) renders a more complete picture which is in line with literature reports on matrix effects caused by endogenous phospholipids in tissue and plasma samples [10] [39].

It is important to note that surface activity alone was not the only property relevant for the extent of matrix effects as the following example shows: Whereas the π-$\log C$ profiles of NMP and PG were comparable (Fig. 9), matrix effects were stronger in presence of NMP despite lower concentrations (24.2 mM NMP vs. 31.5 mM PG, respectively, Fig. C,E). This could be explained by the stronger basicity of the amide-nitrogen in NMP as compared to the hydroxyl-groups present in PG. Chech and Enke[19, 39] notably stressed that basicity is one determining factor for the relative gas phase ion intensities. Tong et al. [10] related the stronger matrix effect observed for HP - β - CD (multiply-charged ion) as compared to PG (singly-charged ion) to the different charge densities and inferred that gas-phase reactions might play a major role in ion suppression. Our results confirm the inverse relationship between number of charges and extent of matrix effects. However, rather than by gas phase proton transfer reactions, the stronger matrix effect of HP - β - CD may also be explained by more effective displacement of rolipram from the surface of the ESI droplet, which is supported by the higher preference of HP-β-CD for the air-water interface (K_{aw}(HP-β-CD) >> K_{aw} (PG)). Irrespective of which mechanism applies, our results confirm that PG caused the least matrix effect, which we suggest was due to a combination of i) the low surface activity, ii) the lack of basic nitrogen, and iii) the presence of only two OH-groups available for protonation.

In contrast to our results, Shou et al. did not observe matrix effects in presence of HP-CD, but they used other test compounds and experimental conditions [21]. This clearly illustrates the need for careful and compound-specific evaluation of matrix effects. Generalization from recovery studies should be treated with caution, particularly if information on the elution behavior of both analyte and excipient is lacking.

3.6. Prediction of Matrix Effects

Coelution is a precondition for ion suppression [21], and therefore the prediction of matrix effects is theoretically possible from estimates of an analyte's retention time in HPLC-MS and knowledge about the elution behavior of the excipient. Retention times on reversed phase columns have been frequently used as surrogates for $\log D_{oct}$ (pH 7.4) [40]. Vice versa, we evaluated whether the $\log D_{oct}$ value at pH 3.3 (corresponding to the eluent pH at 95% acetonitrile) is predictive for an analyte's retention time in HPLC/MS and, moreover, whether this information allows the prediction of matrix effects at sufficient accuracy. Prediction packages for the calculation of $c\log P$ are commonly available; and from knowledge of an analyte's pK_a (which can be predicted) and the eluent's pH (pH 3.3), the $\log D_{oct}$ values at pH 3.3 can easily be estimated.

For validation purposes, we prepared analyte solutions of 16 physicochemically different drugs in excipient-spiked buffer (0.5%, m/v GCA) and determined their recoveries and retention times in HPLC-MS, in addition to their $\log D_{oct}$ (pH 3.3) values. Figure 10A, showing the recovery of each test compounds as a function of retention time, confirms that only analytes coeluting with GCA (rolipram, no.15) severely suffered from ion suppression (> 90 % suppression).

Fig. 10

Compounds close to the elution window of GCA (no. 10-14 [R_t = 0.545-0.556 min]; no. 16 [R_t = 0.733 min]) were moderately suppressed (recovery 78.1-87.4 %, carbamazepine (no. 14) 94.9 %), pointing to trace amounts of GCA present in the ESI source. It is interesting to note that despite equal retention times of carbamazepine (no. 14) and zaleplone (no. 13) (R_t = 0.556 min), differences in the recovery rates (94.9 % vs. 78.1 %) were observed. The higher recovery of the more lipophilic compound (carbamazepine, $c\log P$ 2.4 vs. zaleplone, $c\log P$ 1.4) is in line with literature describing hydrophilic compounds as more vulnerable to

matrix effects [7]. Like for excipients, drug compounds with a hydrophobic moiety attached to the protonation side are favored for the place on the electrosprayed droplet surface due to their higher amphiphilicity. Rolipram is relatively hydrophilic and less amphiphilic as compared to GCA which explains the low analyte recovery.

In the next step, we transformed the critical range of retention times (R_t = 0.545-0.556 min) into the more useful, critical range of $\log D_{oct}$(pH 3.3) values. Therefore, we plotted $\log D_{oct}$(pH 3.3) of the analytes as a function of their retention times (Figure 10 B) yielding a straight line with r^2 = 0.62 (standard error of estimate, see = 1.54, Figure 10B). A weaker correlation was observed with $c\log P$ (r^2 = 0.16, SEE = 1.71) and $\log D_{oct}$ at pH 7.4 (r^2 = 0.53, see = 1.08). The latter two parameters do not account for the different ionization state of the drugs at the eluent pH. According to the above correlation, we could identify a critical $\log D_{oct}$(pH 3.3) range in which severe ionization suppression due to coelution of GCA would be expected (i.e. $c\log D_{oct}$ (pH 3.3) range 1-4). Hence, under the given experimental conditions, the prediction model is able to exclude matrix effects for compounds with $c\log D_{oct}$<1 and $c\log D_{oct}$ >4. For compounds in the intermediate $c\log D_{oct}$ range 1-4, the surface activity of the compound in relation to that of the excipient and other parameters (e.g. concentration ratio, proton base affinity) will determine the extent of ion suppression. Although surface active, lipophilic compounds are less susceptible to ion suppression, an ultimate proof of the presence or absence of matrix effects requires recovery or post-column infusion studies.

3.7. The Effect of Excipients on the PAMPA Read-Out

The results obtained so far have shown that the excipients used in PAMPA cause matrix effects; the extent of which relates to the properties of both the excipient and the analyte. In the next step we pursued our overall goal, namely to investigate whether the presence of excipients in PAMPA eventually affects the accuracy of permeability measures, and if so, how to correct the assay read-out. The concern of matrix effects arises because excipients are commonly applied non-uniformly in the PAMPA compartments, i.e. either in the donor or in the acceptor compartment of the PAMPA sandwich. GCA, for example, is frequently used as a solubilizer in the donor and in the reference solution (Figure 1, Roche setup[28]) while blank buffer is applied in the acceptor. On the other hand, the post-experimental addition of matrix to the acceptor compartment, to obtain the same matrix effect, reduces significantly the analytical sensitivity.

For the evaluation of matrix effects in PAMPA, we followed the above protocol using GCA (0.5%, m/v) as a solubilizer and rolipram (100μM) as a model analyte. The permeation of rolipram from the donor across an artificial membrane into the acceptor compartment was measured by determining the concentration of rolipram in each compartment (after 19h incubation), using HPLC-UV and HPLC-MS for concentration analysis. The presence of GCA did not affect the UV data (see below, Figure 11A) which therefore provided a gold standard to prove the accuracy of the mass-analyzed results. Regarding the mass spectrometric analysis, differences in the matrix composition of the various compartments were (a) disregarded, (b) reduced (by 1:100 dilution of each compartment) or (c) adjusted (by providing in each compartment the same concentration of excipient before injection onto the HPLC-MS system). A summary of the assay read-outs (compartmental distribution of rolipram, proof of mass balance, permeability) obtained from each analytical strategy is given in Table 2.

Table 2

The UV analysis yielded 65.9 ± 2.3 % of rolipram left in the donor and 34.9 ± 0.7 % permeated into the acceptor indicating approximetely 100% recovery. When using the MS data, disregard of ion suppression in the reference and in the donor solution resulted in 12.6 fold overestimation of the percentage rolipram present in the acceptor (437.8 ± 23%), which was obviously not in agreement with mass balance (the sum of drug in the donor and acceptor compartment was 505.3% of the initial drug amount in the reference). While the 1:100 dilution of each solution still yielded 1.6 fold overestimation of the acceptor concentration due to residuals of GCA, the results obtained after adjustment of each compartment to the same GCA content (0.25 %, m/v) were consistent with the UV data. The erroneous compartmental concentration of rolipram from untreated (a) or diluted (b) solutions are mirrored in the effective permeability values showing 31.5 fold and 2.9 fold overestimation, respectively (details for the calculation of P_e see Table 2).

3.8. Minimization of Matrix Effects

While several possibilities to eliminate or handle matrix effects have been proposed, most of them are not feasible in the earliest phase of the drug discovery process when PAMPA measurements are conducted. For example, a deuterated internal standard compensating for matrix effects [41] is usually not available. Although optimization of chromatographic

separation may be a possibility for a limited amount of compounds [23], the broad range of physicochemical properties covered by research compounds and screened in PAMPA complicates the situation. Solid and liquid phase extraction generally bare the risk of incomplete recovery of the test analyte itself [42]which again cannot be compensated by an internal standard. Another option is the dilute-and-shoot-approach which involves diluting the analyte solutions prior to injecting them onto the HPLC-MS. From a practical point of view this would be feasible, however, even a 1:100 dilution of the PAMPA donor and reference solution (GCA concentration 0.5 %, m/v) yielded reduced ion intensities as compared to the acceptor solution (Table 2, injection volume: 5 µL).

A reduction in sample load injected onto the HPLC-MS system may further minimize the matrix effects and the associated error in effective permeability. To evaluate this strategy, we studied the mass and UV response of rolipram (100 µM) as a function of injection volume (1 - 10 µL) for a broad range of GCA concentrations (0 - 0.5 %, m/v). Inspection of Fig. 11A reveals that the UV response was not disturbed by the presence of GCA as observed by the linear calibration function, which was independent of the excipient concentration. In contrast, a non-linear behavior was evident when using MS (Fig. 11B).

Fig. 11

The mass responses of the analyte in excipient-spiked buffer was lower than that in excipient - free buffer, except for the two smallest injection volumes (1 µL and 2 µL) of the 0.005 % GCA sample. Hence, matrix effects in PAMPA can be minimized in this specific case by a 1:100 dilution of the GCA concentration (0.5 % to 0.005 %, m/v) in combination with a reduction in injection volume (5 µL to 1 µL). Similar to the adjustment of excipient concentrations in each compartment (Table 2), accurate results would be provided, however, at the expense of sensitivity.

Regarding the application of GCA as a solubilizer, its replacement with PG is a viable alternative. At a concentration of 0.24 % (m/v), PG showed only minor matrix effects in the post-column studies (Fig. 8E). However, Fig. 12 shows that with increasing concentrations of PG an exponential decrease in analyte response was observed that was the higher the closer the retention time was to the solvent front.

Fig. 12

Nevertheless, even at 20 % PG, the matrix effect was still moderate as compared to GCA (e.g. rizatriptan, Rt = 0.372 min, recovery in PG: 54 %). Our results provide a more complete picture of PG effects in ESI-MS than can be drawn from published dosing vehicle studies [10]. In literature a focus has only been put on max.1 % excipient solution corresponding to the expected plasma concentration. As Figure 12 shows, ion suppression caused by PG is compound specific and concentration dependent, and therefore generalizations cannot be made from negligible or moderate (15 % recovery) [4] matrix effects reported for other datasets. Our results show that PG is the most suitable solubilizer with respect to MS compatibility. But contrary to an uncritical use of PG, sample pretreatment is still required regarding compounds eluting close to the solvent front. For the sake of completeness, we would like to mention that the solubilizing power of PG needs to be evaluated and distinct effects on passive permeability of the different excipients should be considered [29].

4. Conclusions

In summary, we have investigated matrix effects related to excipients commonly used in PAMPA. All of the tested excipients reduced the gas phase ion intensities of the test analyte rolipram to some extent, but PG was the excipient best compatible with MS. The strongest matrix effects were observed for excipients that enriched at the air-water interface (GCA, the FaSSIF/FeSSIF media) and/or that carried multiple charges (HP - β - CD). Appropriate management of excipient-related matrix effects is essential to avoid overestimation (excipient in donor compartment) or underestimation (excipient in acceptor compartment) of permeability values retrieved via HPLC-MS analysis. Excipients distributed non-uniformly in the different PAMPA compartments during the actual permeation process, for instance to study formulation effects, to increase compound solubility, or to simulate sink conditions, should be adjusted to the same excipient level before injecting aliquots of each compartment onto the HPLC-MS system. This also applies to the external calibration standards. The sample pretreatment can only be avoided if ion suppression caused by coeluting matrix components can be excluded in advance, either based on recovery studies or on $\log D_{oct}$ (pH 3.3) based prediction of the elution behavior. If the use of excipients aims to increase compound solubility, rather than to inspect a specific effect of one particular excipient, replacement of the frequently used GCA by PG is suggested. However, when using HPLC-MS for concentration analysis, the gain in sensitivity due to higher analyte concentration in presence of a solubilizer should be viewed in context with the possible loss in sensitivity due to ion suppression. It should therefore be critically tested whether or not a solubilzer is required for higher sensitivity.

Acknowledgements

We gratefully thank Andreas Stämpfli for helpful discussions and for critically reading the manuscript, Daniel Zimmerli for installing the post-column infusion pump and Björn Wagner for excellent help with the HPLC-MS system.

TABLES

Table 1 The air-water partition coefficients, K_{aw}, of the excipients tested and the maximum surface pressures, π_{max}, reached in their presence. Due to the fact that the FaSSIF medium is a taurocholic - phospholipid - mixture, no K_{aw} is given.

Excipient	K_{aw}	π_{max}[mN/m]
Glycocholic acid	3.42E+04	25.9
FaSSIF		>37.8
N-methyl-2-pyrrolidone	1.57E+01	>21.0
2-hydroxypropyl-β-cyclodextrin	4.67E+04	>18.0

Table 2 Comparison of the assay read-outs of a typical PAMPA measurement (Roche setup) using HPLC-UV and HPLC-MS, and different approaches for sample pretreatment. Rolipram (25µM) was used as the test analyte and glycocholic acid (0.5 %, m/v) as a model solubilizer in the donor but not in the acceptor compartment.

Detection Mode	Sample pretreatment	Drug amount in compartment[a]		Mass balance[a]	P_e[b]
		[%], Donor	[%], Acceptor	[%], Donor + Acceptor	[10^{-6}cms^{-1}]
UV	None	65.9±2.3	34.9±0.7	100.7±1.8	10.5±0.6
MS	None	67.5±2.0	437.8±23.1	505.3±25.1	(330.5±0)
MS	1:100 dilution	62.5±3.5	56.2±2.1	118.7±5.6	30.1±10.1
MS	Matrix adjustment	66.0±1.0	36.4±1.0	102.5±2.0	11.4±0.2

[a]A part of the donor solution was not used for the permeability measurement but was used as the reference. The amounts in the donor and acceptor compartment (after incubation) were calculated as the percentage of the analyte response in the reference. If the concentration in the acceptor measured in HPLC-MS was higher than in the reference (due to ion suppression), the sum of analyte in the donor and the acceptor was considered as a new reference in order to still enable the calculation of effective permeability values (Pe).

FIGURES

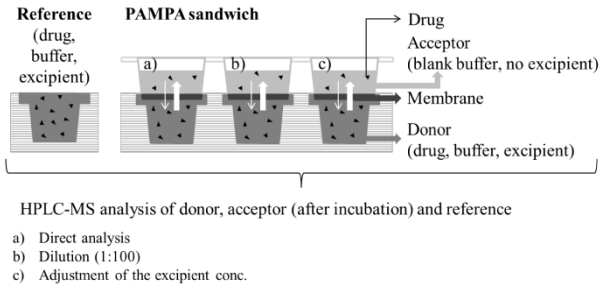

Figure 1 Setup of PAMPA.

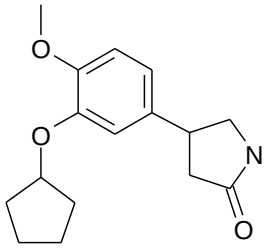

Figure 2 Structure of the test analyte rolipram
(MW 275.35, $\log D_{oct}$ (pH 7.4) 1.91, no pK_a)

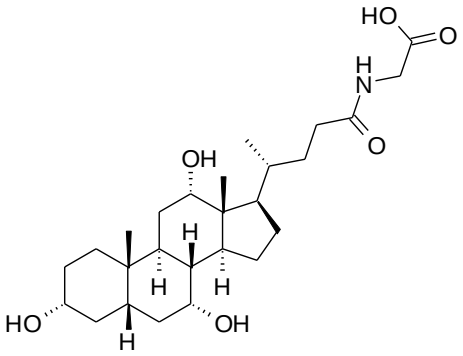

Glycocholic acid (GCA)
0.5% (m/v) = 10.7 mM
MW = 465.309 g/mol

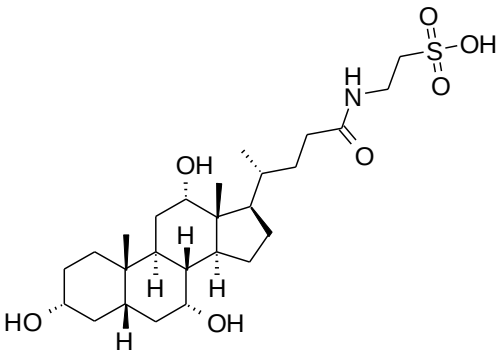

Taurocholic acid, (TC)
10 mM in FeSSIF, 3 mM in FaSSIF
MW = 515.292 g/mol

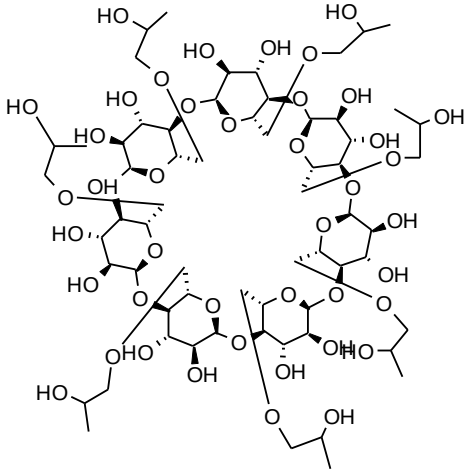

2-hydroxypropyl-β-cyclodextrin (HP-β-CD) 0.24% (m/v) = 1.78 mM
MW = 1300-1541 g/mol

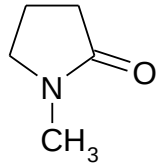

N-methyl-2-pyrrolidone (NMP),
0.24% (m/v) = 24.2 mM
MW 99.13 g/mol

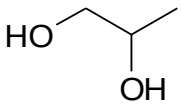

Propylenglycol (PG)
0.24% (m/v) = 31.5 mM
MW = 76.09 g/mol

Figure 3 Structures, concentrations and molecular weights of the investigated excipients

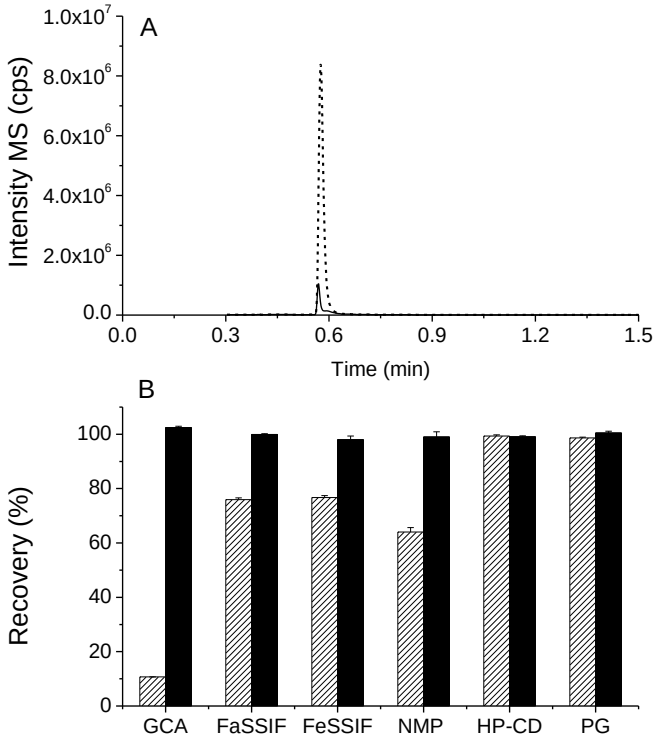

Figure 4 A, B: The effect of excipients on the signal intensity of rolipram (25 µM) in HPLC - ESI/MS (SIM mode). A: Example of overlaid mass chromatograms of rolipram (m/z 276.2, [M+H]+ trace) in absence (⋯⋯) and in presence (—) of glycocholic acid (0.5 %, m/v). B: Percentage recovery of rolipram in presence of excipients (dashed bars): GCA (0.5 %, m/v), the FaSSIF and FeSSIF media, NMP (0.24 %, m/v), HP-CD (0.24 %, m/v) and PG (0.24 %, m/v). The black columns show the percentage recovery of rolipram in blank buffer after preliminary injection of the excipient-spiked buffer.

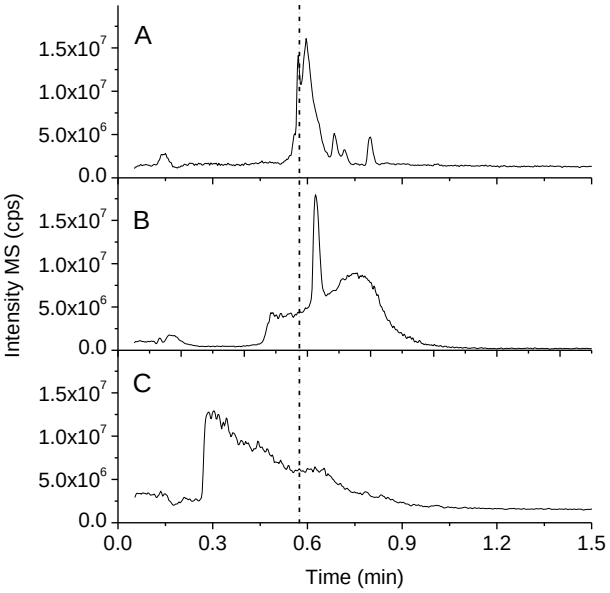

Figure 5 Full scan mass chromatograms obtained from fast gradient elution of GCA (0.5 %, m/v) (**A**), the FeSSIF medium (**B**) and NMP (0.24 %, m/v) (**C**). The retention time of rolipram is indicated by the vertical dashed line.

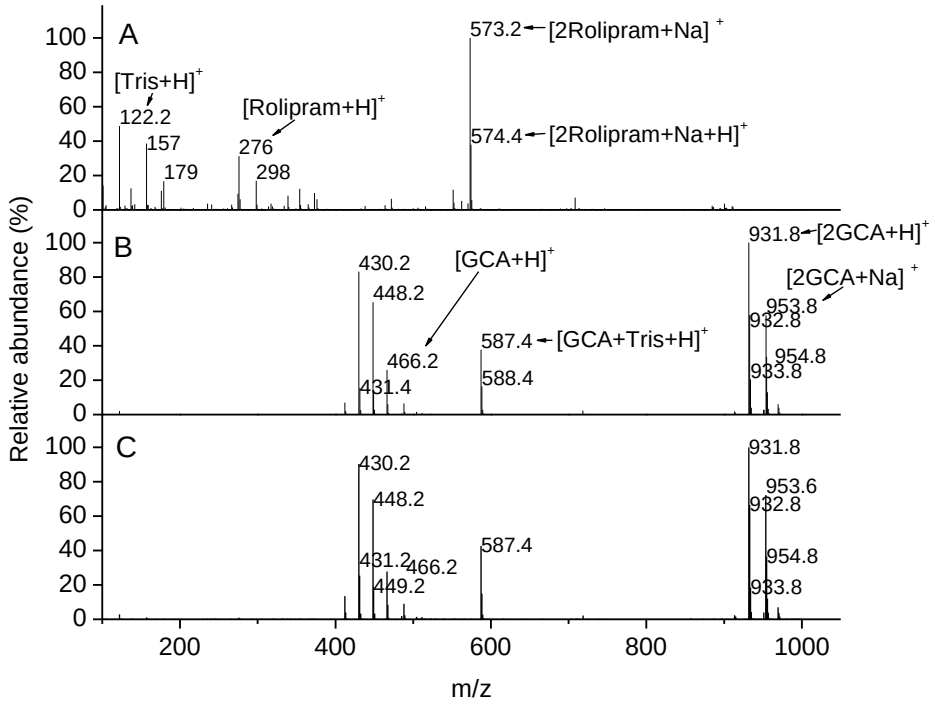

Figure 6 Comparison of the mass spectra of **A:** buffer spiked with rolipram, **B:** buffer spiked with glycocholic acid and **C:** buffer spiked with both, rolipram and glycocholic acid. The concentration of rolipram and glycocholic acid was 25 µM and 0.5 % (m/v), respectively. The spectra were obtained at 0.575 min corresponding to the retention time of rolipram.

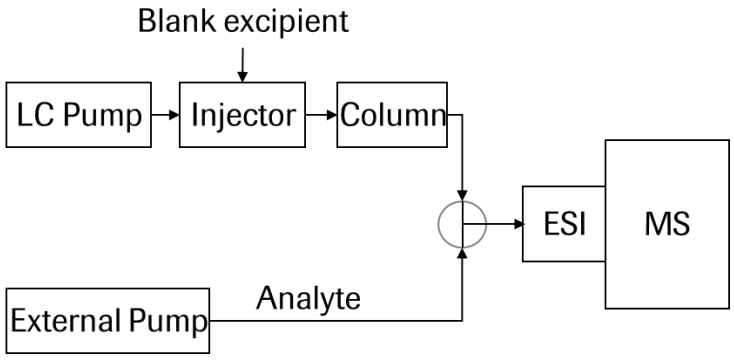

Figure 7 Setup for assessment of matrix effects with the post-column infusion technique. The analyte (rolipram, 25 µM), dissolved in eluent (50:50 mixture of water : acetonitril), was continuously infused at 50 µL/min by means of an external pump. Blank matrix (excipient dissolved in eluent), or eluent (reference), was injected into the LC column and eluted with 1 mL/min using a fast gradient method. Both flows were combined with a T - piece before entering the ESI-interface of the mass spectrometer.

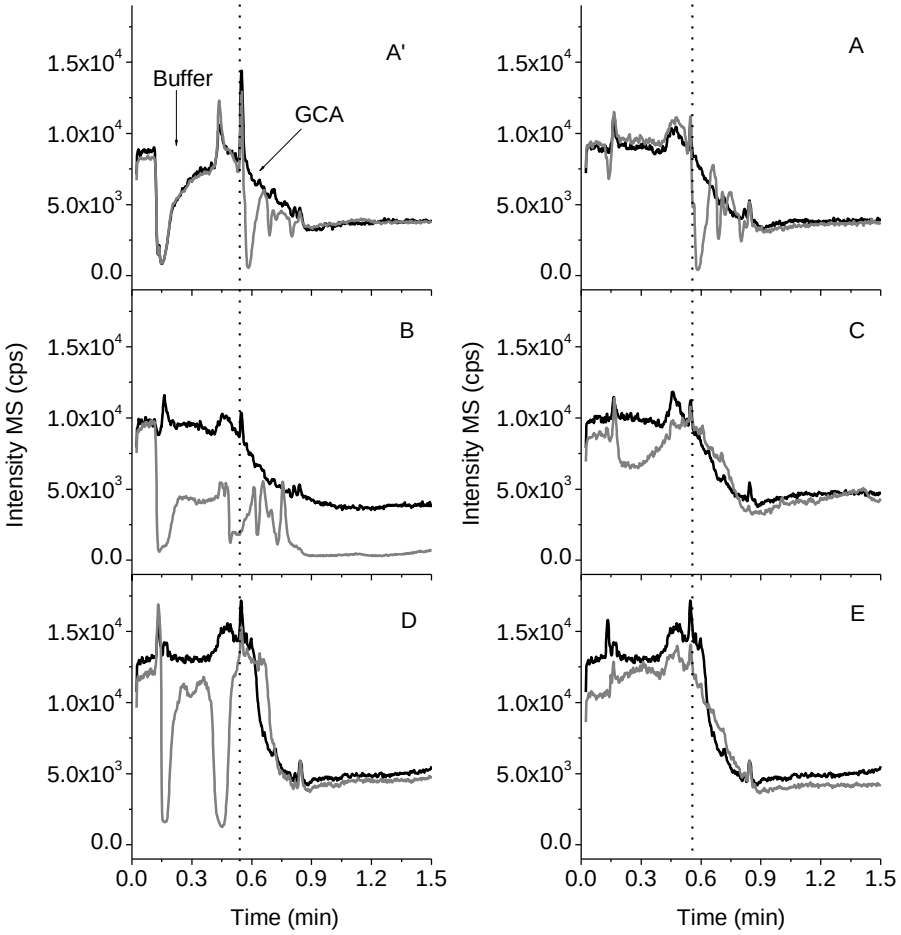

Figure 8 Overlaid post-column infusion chromatograms of rolipram ([M+H]+ trace) in absence (**—**) and in presence (—) of excipients. The mass chromatograms with and without glycocholic acid were obtained using either buffer (**A'**) or eluent (**A**) as solvent. The mass chromatograms of all other excipients, i.e. the FeSSIF medium (**B**), NMP (**C**), HP-β-CD (**D**) and PG (**E**), are only shown in eluent. The excipient concentrations were matching those used in the recovery studies described in Fig. 3. The retention time of rolipram is indicated by the vertical dashed line.

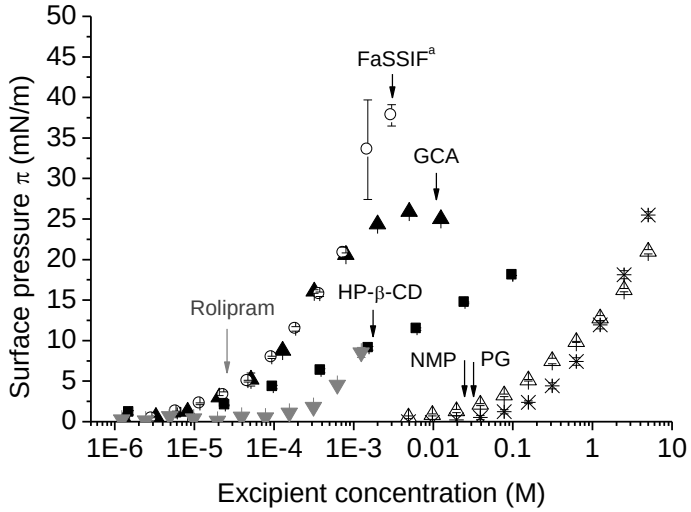

Figure 9 Surface pressure - concentration profiles for the FaSSIF media (○) and the excipients GCA (▲), HP-β-CD (■), NMP (△) and PG (✳) dissolved in 50mM Tris/114mM NaCl/pH 7.4 buffer. For comparison, the surface pressure-concentration profile of the test analyte rolipram (▼) is shown (50mM Tris/114mM NaCl/pH 7.4/1%DMSO). The arrows indicate the concentrations of the excipients and rolipram used in the ion suppression studies. Although the FaSSIF medium is a taurocholic - phospholipid - mixture, the concentration used for the plot relates to the concentration of taurocholic acid (maximal 3 mM). The π -logC - profiles were measured at room temperature with a multichannel microtensiometer (Delta-8, Kibron, Helsinki).

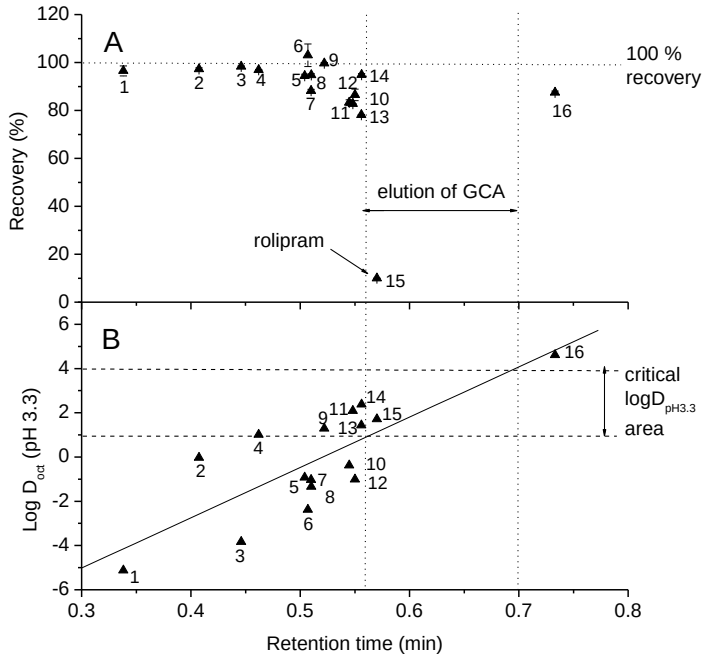

Figure 10 A: Percentage recovery for 16 compounds (each 25 µM) in presence of GCA (0.5%, m/v) and B: $\log D_{oct}$ (pH 3.3=eluent pH) as a function of retention time. Analytes were measured independently with a fast gradient LC/ESI-MS method. The Henderson-Hasselbalch equation was used to calculate $\log D_{oct}$ (pH 3.3) from $c\log P$ and in-house measured pK_a values. Rizatiptan (1), theophylline (2), metoclopramide (3), midazolam (4), cyclobenzaprine (5), maprotiline (6), verapamil (7), amitriptyline (8), flumazenil (9), thioridazine (10), phenytoin (11), trifluperazine (12), zaleplon (13), carbamazepine (14), rolipram (15), PK 11195 (16). **B:** The y-intercept confined by the interception point of the correlation line and the elution window of GCA describes the $\log D_{oct}$ (pH 3.3) range in which severe ionization suppression due to coelution of GCA is expected ($\log D_{oct}$ (pH 3.3) range 1 - 4).

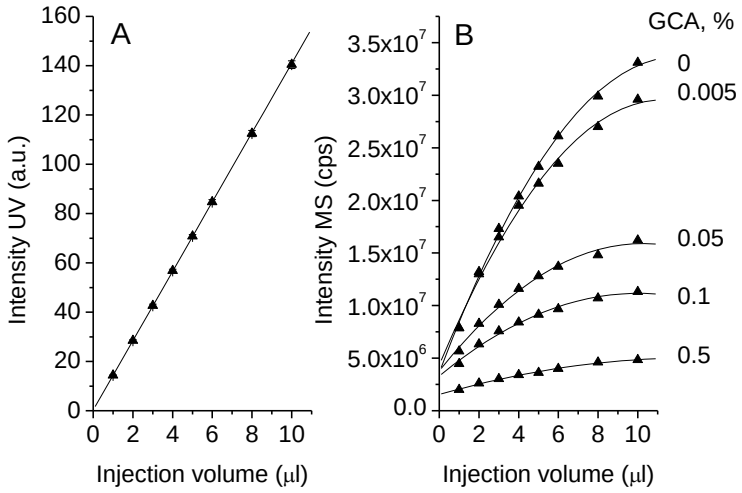

Figure 11 Intensity of analyte response (100 µM rolipram, 50mM Tris/114mM NaCl, pH 7.4) in **A:** UV and **B:** MS (SIM) as a function of the volume injected into an HPLC-ESI-MS system. The test solutions contained different concentrations of glycocholic acid (0-0.5 %, m/v). The UV responses of rolipram at a particular injection volume were averaged taking into account all different concentrations of GCA (n=5, the standard deviation was smaller than the size of the symbol).

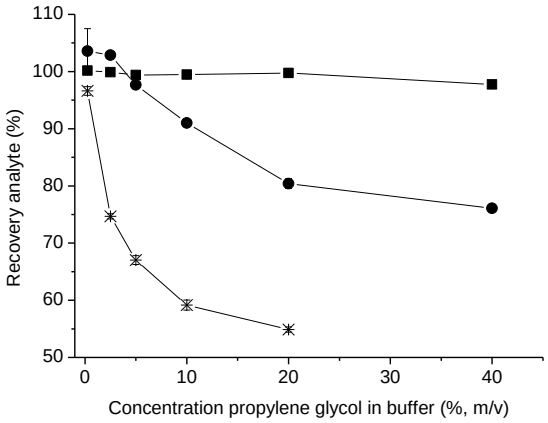

Figure 12 Recovery obtained in HPLC-ESI/MS of rolipram (■, Rt = 0.579 min), theophyllin (●, Rt = 0.420 min) and rizatriptan (✳, Rt = 0.372 min) from buffer spiked with increasing concentrations of propylene glycol. Analysis of rizatriptan at 40 % propylenglycol was obviated due to the detrimental effect of propylene glycol on the peak shape at concentrations above 20 %.

Supporting Information

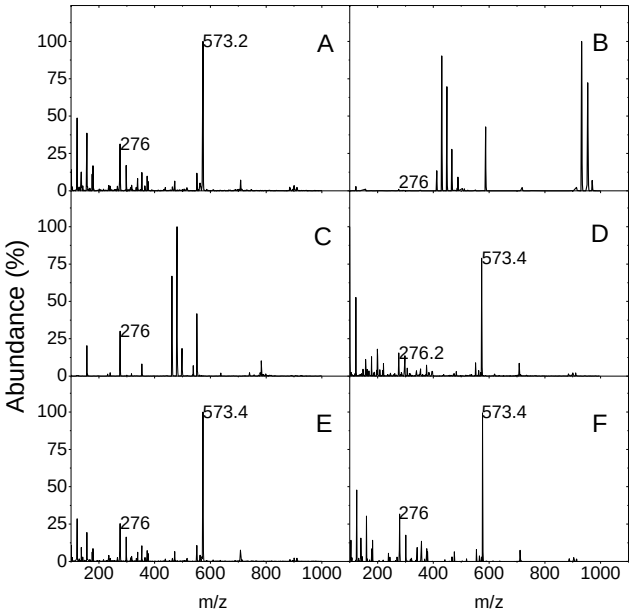

Figure S1 Mass spectra of buffer spiked with rolipram (**A**) and buffer spiked with rolipram and excipient (**B-F**): glycocholic acid, 0.5%, m/V (**B**), the FeSSIF media (**C**), NMP, 0.24%, m/v (**D**), HP-β-CD, 0.24%, m/v (**E**) and propylene glycol, 0.24%, m/v (**F**). The concentration of rolipram was 25 µM. The spectra were obtained at 0.575 min corresponding to the retention time of rolipram. The assigned m/z ratios correspond to the sodium adduct of the dimer of rolipram and the mono-protonated pseudo-molecular ion. For experimental conditions see Materials and Methods.

Table S1 Properties for the 16 compounds used for recovery studies with glycocholic acid (0.5%, m/v. The drugs are sorted in ascending order of retention time n HPLC.

No.	Compound	*MW* [c] [g/mol]	pK_a (acid)[a]	pK_a (base)[a]	clogP[b]
1	Rizatriptan	269.4		9.59	1.2
2	Theophylline	180.2	8.51		0.0
3	Metoclopramide	299.8		9.36	2.2
4	Midazolam	325.8		5.71	3.4
5	Cyclobenzaprine[d]	275.4		9.32	5.1
6	Maprotiline	277.4		10.2	4.5
7	Verapamil	491.1		8.8	4.5
8	Amitriptyline	277.4		9.49	4.9
9	Flumazenil	303.3			1.3
10	Thioridazine	370.6		9.68	6.0
11	Phenytoin	252.2	8.18		2.1
12	Trifluperazine	407.5		8.43/3.74	4.7
13	Zaleplon	305.3			1.4
14	Carbamazepine	236.3			2.4
15	Rolipram	275.2[e]			1.7
16	PK 11195	352.9			4.6

[a]measured photometrically (SGA), [b]clog P v4.71 Daylight [c][Molecular weight + H]$^+$ ion monitored in ESI/MS,[d]measured with capillary electrophorsis [e]monoisotopic

References

1. van de Waterbeemd, H., *Physicochemical approaches to drug absorption.* Methods Princ. Med. Chem. , 2009. **40**(Drug Bioavailability): p. 71-99.
2. Avdeef, A., *The rise of PAMPA.* Expert Opin. Drug Metab. Toxicol. , 2005. **1**(2): p. 325-342.
3. Kansy, M., F. Senner, and K. Gubernator, *Physicochemical High Throughput Screening: Parallel Artificial Membrane Permeation Assay in the Description of Passive Absorption Processes.* J. Med. Chem. , 1998. **41**(7): p. 1007-1010.
4. Mensch, J., et al., *Novel generic UPLC/MS/MS method for high throughput analysis applied to permeability assessment in early Drug Discovery.* J. Chromatogr., B: Anal. Technol. Biomed. Life Sci. , 2007. **847**(2): p. 182-187.
5. Liu, H., et al., *In Vitro Permeability of Poorly Aqueous Soluble Compounds Using Different Solubilizers in the PAMPA Assay with Liquid Chromatography/Mass Spectrometry Detection.* Pharm. Res., 2003. **20**(11): p. 1820-1826.
6. Taylor, P.J., *Matrix effects: the Achilles heel of quantitative high-performance liquid chromatography-electrospray-tandem mass spectrometry.* Clin. Biochem. , 2005. **38**(4): p. 328-334.
7. Tiller, P.R., L.A. Romanyshyn, and U.D. Neue, *Fast LC/MS in the analysis of small molecules.* Anal. Bioanal. Chem. , 2003. **377**(5): p. 788-802.
8. King, R., et al., *Mechanistic investigation of ionization suppression in electrospray ionization.* J. Am. Soc. Mass Spectrom. , 2000. **11**(11): p. 942-950.
9. Rundlett, K.L. and D.W. Armstrong, *Mechanism of Signal Suppression by Anionic Surfactants in Capillary Electrophoresis-Electrospray Ionization Mass Spectrometry.* Anal. Chem., 1996. **68**(19): p. 3493-3497.
10. Tong, X.S., et al., *Effect of Signal Interference from Dosing Excipients on Pharmacokinetic Screening of Drug Candidates by Liquid Chromatography/Mass Spectrometry.* Anal. Chem. , 2002. **74**(24): p. 6305-6313.
11. Tang, L. and P. Kebarle, *Dependence of ion intensity in electrospray mass spectrometry on the concentration of the analytes in the electrosprayed solution.* Anal. Chem. , 1993. **65**(24): p. 3654-68.
12. Cech, N.B. and C.G. Enke, *Effect of Affinity for Droplet Surfaces on the Fraction of Analyte Molecules Charged during Electrospray Droplet Fission.* Anal. Chem., 2001. **73**(19): p. 4632-4639.
13. Kebarle, P. and U.H. Verkerk, *Electrospray: from ions in solution to ions in the gas phase, what we know now.* Mass Spectrom. Rev. , 2009. **28**(6): p. 898-917.
14. Iribarne, J.V. and B.A. Thomson, *On the evaporation of small ions from charged droplets.* J. Chem. Phys. , 1976. **64**(6): p. 2287-94.
15. Blades, A.T., M.G. Ikonomou, and P. Kebarle, *Mechanism of electrospray mass spectrometry. Electrospray as an electrolysis cell.* Anal. Chem. , 1991. **63**(19): p. 2109-14.
16. Enke, C., *A predictive model for matrix and analyte effects in electrospray ionization of singly-charged ionic analytes.* Anal. Chem., 1997. **69**(23): p. 4885-4893.
17. Iribarne, J.V., P.J. Dziedzic, and B.A. Thomson, *Atmospheric pressure ion evaporation-mass spectrometry.* Int. J. Mass Spectrom. Ion Phys., 1983. **50**(3): p. 331-47.
18. Gomez, A. and K. Tang, *Charge and fission of droplets in electrostatic sprays.* Phys. Fluids 1994. **6**(1): p. 404-14.
19. Amad, M.a.H., et al., *Importance of gas-phase proton affinities in determining the electrospray ionization response for analytes and solvents.* J. Mass Spectrom. , 2000. **35**(7): p. 784-789.

20. Kebarle, P., *A brief overview of the present status of the mechanisms involved in electrospray mass spectrometry.* J. Mass Spectrom., 2000. **35**(7): p. 804-817.
21. Shou, W.Z. and N. Weng, *Post-column infusion study of the "dosing vehicle effect" in the liquid chromatography/tandem mass spectrometric analysis of discovery pharmacokinetic samples.* Rapid Commun. Mass Spectrom. , 2003. **17**(6): p. 589-597.
22. Temesi, D., B. Law, and N. Howe, *Synthesis and evaluation of PEG414, a novel formulating agent that avoids analytical problems associated with polydisperse vehicles such as PEG400.* J. Pharm. Sci. , 2003. **92**(12): p. 2512-2518.
23. Weaver, R. and R.J. Riley, *Identification and reduction of ion suppression effects on pharmacokinetic parameters by polyethylene glycol 400.* Rapid Commun. Mass Spectrom. , 2006. **20**(17): p. 2559-2564.
24. Morgan, D.G. and T.V. Olah, *Ion suppression and cannulation locking solutions.* Bioanalysis, 2009. **1**(3): p. 523-528.
25. Larger, P.J., et al., *Ion-suppression effects in liquid chromatography-tandem mass spectrometry due to a formulation agent, a case study in drug discovery bioanalysis.* J. Pharm. Biomed. Anal. , 2005. **39**(1-2): p. 206-216.
26. Xu, X., et al., *A study of common discovery dosing formulation components and their potential for causing time-dependent matrix effects in high-performance liquid chromatography tandem mass spectrometry assays.* Rapid Commun. Mass Spectrom., 2005. **19**(18): p. 2643-2650.
27. European Mecicines Agency, D.R.E.C.E., *Guideline on validation of bioanalytical methods,* 2009. p. 1-17.
28. Fischer, H., et al., *Permeation of permanently positive charged molecules through artificial membranes-Influence of physico-chemical properties.* Eur. J. Pharm. Sci., 2007. **31**(1): p. 32-42.
29. Bendels, S., et al., *PAMPA-Excipient Classification Gradient Map.* Pharm. Res. , 2006. **23**(11): p. 2525-2535.
30. Avdeef, A. and O. Tsinman, *PAMPA - A drug absorption in vitro model. 13. Chemical selectivity due to membrane hydrogen bonding: in combo comparisons of HDM-, DOPC-, and DS-PAMPA models.* Eur. J. Pharm. Sci., 2006. **28**(1-2): p. 43-50.
31. Marques, M., *Dissolution Media Simulating Fasted and Fed States.* Dissolution Technologies, 2004. **11**(2): p. 16.
32. Kostewicz, E.S., et al., *Forecasting the oral absorption behavior of poorly soluble weak bases using solubility and dissolution studies in biorelevant media.* Pharm. Res. , 2002. **19**(3): p. 345-349.
33. Rosso, L., A.D. Gee, and I.R. Gould, *Ab initio computational study of positron emission tomography ligands interacting with lipid molecule for the prediction of nonspecific binding.* J Comput Chem, 2008. **29**(14): p. 2397-405.
34. Suomalainen, P., et al., *Surface activity profiling of drugs applied to the prediction of blood-brain barrier permeability.* Journal of medicinal chemistry, 2004. **47**(7): p. 1783-8.
35. Fischer, H., R. Gottschlich, and A. Seelig, *Blood-brain barrier permeation: molecular parameters governing passive diffusion.* The Journal of membrane biology, 1998. **165**(3): p. 201-11.
36. Marques, M., *Dissolution Media Simulating Fasted and Fed States.* Dissolution Technologies, 2004.
37. *Agilent Technologies LC/MSD der Series 1100 Verfahren und Software-Bedienung.* Software Version B.01.xx.

38. Fischer, H., *Passive diffusion and active transport through bilogical membranes - binding of drugs to transmembrane receptors* 1998, University of Basel.
39. Mulvana, D.E., *Critical topics in ensuring data quality in bioanalytical LC-MS method development.* Bioanalysis, 2010. **2**(6): p. 1051-1072.
40. Martel, S., et al., *Chromatographic approaches for measuring Log P.* Methods Princ. Med. Chem. , 2008. **37**(Molecular Drug Properties): p. 331-355.
41. Matuszewski, B.K., M.L. Constanzer, and C.M. Chavez-Eng, *Matrix Effect in Quantitative LC/MS/MS Analyses of Biological Fluids: A Method for Determination of Finasteride in Human Plasma at Picogram Per Milliliter Concentrations.* Anal. Chem. , 1998. **70**(5): p. 882-889.
42. Selman, M.H.J., et al., *Cotton HILIC SPE Microtips for Microscale Purification and Enrichment of Glycans and Glycopeptides.* Anal. Chem. (Washington, DC, U. S.) 2011. **83**(7): p. 2492-2499.

4.5 ^{31}P and ^{1}H-NMR Studies on the Molecular Organization of Lipids in the PAMPA Permeation Barrier

Frauke Assmus, Holger Fischer, Alfred Ross, Joachim Seelig, Anna Seelig

Author's Contributions:

Frauke Assmus	• Idea of measuring PAMPA lipid/water distribution coefficients • Performing experiments including data analysis • Writing the manuscript
Holger Fischer	• Supervision of the work • Valuable discussions • Reviewing the manuscript
Alfred Ross	• Idea of performing ^{1}H-NMR experiments • Help in performing and analyzing ^{1}H-NMR experiments
Joachim Seelig	• Help in analyzing ^{31}P-NMR spectra
Anna Seelig	• Idea of performing ^{31}P-NMR studies • Supervision of the work • Valuable discussions • Support in writing the manuscript

ABSTRACT

The parallel artificial membrane permeability assay (PAMPA) has emerged as a widely used primary *in vitro* screen for passive permeability of potential drug candidates. However, the structure of the permeation barrier (filter supported alkane - lipid mixture) had never been characterized on a molecular level. Therefore we investigated the organization of lipids in the PAMPA barrier by means of different nuclear magnetic resonance (NMR) techniques: i) the phase behavior of the egg lecithin - dodecane system in presence and in absence of water, cholesterol and a PVDF filter support was investigated by ^{31}P-NMR; ii) the diffusion coefficients of the individual lipid components in the egg lecithin - cholesterol - dodecane system were determined using the pulsed magnetic field gradient NMR technique (^{1}H-NMR). In addition, the distribution of several test drugs between the PAMPA-lipid solution and buffer was measured ($\log D'_{PAMPA}$(pH7.4)). Addition of n-dodecane to the system egg lecithin - water (lamellar phase, L_α) induced the formation of inverted hexagonal (H_{ii}) and isotropic phases. At n - dodecane concentrations matching those used in PAMPA (9 %, m/v) only an 'isotropic' phase was observed, irrespective of whether or not a filter-support was used. The 'isotropic' phase corresponded to lipid aggregates of a diameter assessed as d = 4 - 7 nm. The data can be explained by the existence of inverted micelles. A size cutoff for $\log D'_{PAMPA}$, typically observed for the binding of drugs to biological membranes (bilayers), was not found. The data suggests that the binding to and, in turn, the diffusion across the PAMPA barrier is facilitated by the presence of reversed egg lecithin micelles. They act as a carrier rather than as a barrier particularly for amphiphilic solutes.

KEYWORDS

PAMPA, Lipid organization, NMR, Bilayer, Phase transition

1. Introduction

The importance of an appropriate absorption, distribution, metabolism, excretion and toxicity (ADME/Tox) profile for the likely success of a drug candidate has widely been recognized in today's drug development programs [1]. Membrane permeability is at the core of many ADME/Tox parameters and determines for example the extent of gastrointestinal absorption and blood-brain-barrier (BBB) permeation of a drug [2]. Early assessment of permeability is therefore crucial in order to identify molecules with inadequate properties and to guide structural optimization of promising lead series [3].

Various systems of different complexity have been used to mimic the barrier properties of biological membranes *in vivo*, among them cell-based *in vitro* models (e.g. CaCo-2 assay [4]), artificial membranes (e.g. liposomes [5], black lipid membranes [6]) as well as membrane-mimicking systems [7] (e.g. octanol-water [8], immobilized artificial membranes, IAM [9]). Although cell-based models are favored for studying active transport pathways, the lower throughput and higher cost as compared to the artificial systems has limited their application [10]. The popularity of membrane mimicking systems originates from the fact that most compounds (exception: peptides and peptidomimetics) cross biological membranes by passive diffusion; the extent of which depends on both, the properties of the membrane and the diffusing drug [11].

Biological membranes are highly ordered, anisotropic systems, made up of lipid bilayers into which proteins are embedded [12]. The bilayer ordering and packing is determined by the lipid composition which, in turn, governs the barrier properties of the membrane. In the first step of passive diffusion, the drug binds to the membrane by hydrophobic, hydrogen - bond and ionic interactions with the phospholipid head group and then penetrates into the lipophilic core. Charged and uncharged molecules can insert into the lipid - water - interface, but only the fraction of uncharged drugs can permeate a lipid membrane. The energy (ΔW) required to form a cavity in the bilayer large enough to accommodate the solute is proportional to the lateral packing density of the lipid layer (π_M) and the cross sectional area (A_D) of the penetrating compound ($\Delta W = \pi_M \cdot A_D$) [13, 14]. This explains the greater resistance to permeation with increasing lipid chain ordering and permeant size [2, 15].

Unlike binding to anisotropic membranes, the partitioning into bulk organic phases, such as n - octanol and n - hexadecane, increases with molecular volume as a result of the less structured nature of organic solvents [14]. Despite the great popularity of particularly n - octanol as surrogate for membrane binding and permeation, bulk solvents in general fail to

mimic the anisotropy of the bilayer as well as the charge of the phospholipid head group. The linear relationship between bulk octanol/water distribution coefficients ($\log K^*_{ow} = \log D_{oct}$) and lipid bilayer/water distribution coefficients ($\log K^*_{lw}$) therefore likely breaks down for compounds which are large (usually also high $\log D_{oct}$) [14, 16], ionized [17] or structurally unrelated (different hydrogen-bonding, etc.).

The example of $\log D_{oct}$ illustrates that knowledge of the molecular organization and properties of a membrane-mimicking system is crucial for understanding the limitations of a particular model system. Surprisingly, the molecular organization of the standard industrial membrane model for passive permeability [18, 19], present in the Parallel Artificial Membrane Permeability Assay (PAMPA), is still unresolved [20]. The PAMPA barrier consists of synthetic or natural phospholipids (e.g. egg yolk lecithin, exception Novartis: 100 % hexadecane) dissolved in excess organic solvent (e.g. n - dodecance), coated on a filter support (e.g. polyvinylidene difluoride (PVDF)) which is in contact with an aqueous buffer solution [19]. The widespread assumption that bilayers are formed in the PAMPA filter can be traced back to the early work of Thompson et al. on several microfiltration units used as stabilizing support for black (= bilayer) lipid membranes (BLM) [21]. Based upon electrochemical similarities between macro-BLMs and the filter-lipid system, and largely relying on the effect of amphothericin, the author hypothesized that each pore in the filter was spanned by a single lipid bilayer [21]. Notably, the combination of solvent (n - decane), filter material (polytetrafluorethylene (PTFE), cellulose ester, polycarbonate) and lipid (egg phosphatidylcholine, cholesterol) studied by Thompson et al. has never been used for PAMPA and the transferability of the results to other experimental conditions is uncertain. Phung et al. recently evaluated the suitability of a greater variety of filter materials with respect to the ability to support membranes for biosensors [22]. Unfortunately the solvent (n - octane) used was again different from that applied in PAMPA and therefore the observation that micro-BLM were formed in a PTFE but not in a PVDF filter (PAMPA filter = PVDF) is still insufficient to allow conclusions to be drawn on the PAMPA barrier. Nevertheless it demonstrates the importance to rely on the particular combination of filter, lipid, and organic solvent used when discussing the molecular organization of lipids in the system of interest.

It is worth to note that considerable effort has been put into optimization of PAMPA, and specifically its barrier property, towards improved predictability of e.g. gastrointestinal drug absorption and BBB permeation. Every individual barrier component has been varied

including the organic solvent (e.g. hexadecane [23], 1,7 octadiene [24]), the lipid (1-palmitoyl-2-oleoyl-phosphatidylcholine (POPC), soy lecithin [25], brain polar lipids, biomimetic lipid mixtures [26]) and the filter unit (PVDF [18], polycarbonate [23]). However, none of the optimization procedures was guided by an inspection of the filter-supported barrier at a molecular level. Relationships found between lipid composition and bilayer membrane fluidity, on the one hand, and PAMPA permeability, on the other hand, relied on fluorescence anisotropy measurements of liposomes whereas anisotropy measurements of the PAMPA barrier itself failed [27]. However, disregarding the presence of both, organic solvent and filter support, in the interpretation of the PAMPA barrier structure and function is only of limited value.

The purpose of this study was to investigate the lipid structure in the PAMPA barrier by means of ^{31}P-NMR and ^{1}H-NMR self-diffusion experiments, specifically we addressed the question whether the terms bilayer membrane and PAMPA membrane can be used synonymously. We centered our investigation around the PAMPA-lipid solution used at F. Hoffmann-La Roche which is a mixture of egg yolk lecithin (9 %, m/v), cholesterol (0.45 %, m/v) and excess n - dodecane[6], supported on a lipophilic PVDF filter [28].

The ^{31}P-NMR technique is a powerful tool to study the long range order of phospholipids and to allow a distinction between coarse dispersions of lipid bilayers, hexagonal phases and lipid phases in which 'isotropic' motion occurs [29]. The pulsed field gradient NMR (PFGNMR) technique was used to estimate the individual diffusion coefficients in the PAMPA - lipid solution which in turn were related to the size of the diffusing associates [30]. Background information on the principles of ^{31}P-NMR and PFGNMR is provided in the Appendix. In addition, we measured the permeability across, and the distribution into, the PAMPA barrier for drugs of different charge state, lipophilicity, size, and concentration, and moreover, as a function of the egg lecithin content of the PAMPA barrier. The results were interpreted in terms of barrier properties and function of the PAMPA-lipid solution.

[6] In literature 10 %, m/v egg lecithin and 0.5 %, m/v cholesterol is reported, however, this is not exact, because adding egg lecithin to dodecane increases the volume of the resultant solution which has not been considered so far.

2. Materials and Methods

2.1. Materials

Egg yolk lecithin (60 % TLC), n - dodecane, deuterated n - dodecane - d26 and diazepam were purchased from Sigma (Steinheim, Germany). 1-palmitoyl-2-oleoyl-phosphatidylcholine (POPC) and phosphatidylethanolamine (PE) were obtained from Avanti Polar Lipids (Alabaster, Alabama). Propanolol was available through our in - house Compound Depository Group as proprietary compound. Tris and sodium chloride were obtained from Fluka (Buchs, Germany). DMSO was obtained from Acros (Geel, Belgium). Formic acid, water and acetonitril were supplied from Merck (Darmstadt, Germany) and were of HPLC-grade.

2.2. ^{31}P-NMR and ^{1}H-NMR Studies

2.2.1. Sample Preparation

Samples for the ^{31}P-NMR studies were prepared as follows: Lipid as a powder (egg yolk lecithin, pure POPC, or egg yolk lecithin - cholesterol at a ratio (m/m) 5 : 1) was dissolved in dichlormethane (52 %, m/v) and the solvent was removed by rotary evaporation and subsequent high vacuum evaporation for > 6h. The dry lipid film was dispersed in buffer (50 mM Tris/114 mM NaCl, pH 7.4) at a molar POPC : water ratio of 1 : 45 (51 wt % water). Regarding the egg lecithin samples, the molar ratio referred to the amount of POPC, which was present at ~ 60 wt % in the egg lecithin batch used. The lipid dispersion was covered with an Argon layer, vortexed vigorously and freeze - thawed in at least five cycles until no more sediments were visible by eye. Each freeze - thaw cycle consisted of three steps: freezing the sample in dry ice, warming to room temperature and vortexing. Dodecane was added to the homogenous lipid suspension (0.25; 0.5; 1; 2; 3; 4; 5; 33.5 mol dodecane per mol POPC) up to the POPC : dodecane ratio typically used in PAMPA (1 : 33.5). The samples were vortexed, freeze - thawed, vortexed again and appropriate amounts were then instantly transferred into in - house made glass tubes which were flame sealed. The samples were thermally equilibrated for at least 1 h before the measurements.

A second series of samples was prepared containing only egg lecithin and dodecane at the same POPC : dodecane ratio as described above. Dodecane was added directly to the lipid and the samples were vortexed, freeze - thawed and transferred into the NMR tubes.

A third series of experiments involved the PAMPA - lipid solution as prepared for the high throughput permeability screens: a mixture of egg yolk lecithin (2.5 g), cholesterol (125 mg) and dodecane (25 mL) was stirred for >1h, filtrated (paper filter) and i) transferred into the NMR tube without further treatment, ii) added to a PVDF filter (diameter 3 mm, punched - out from a Millipore filter plate, Cat. MAIPN 4550, 4.5 µL per filter) with 40 of them stacked into the NMR tube or iii) added to the PVDF filter and stacked as in ii) but with a hydrophilic filter (punched - out from a Millipore filter plate, Cat. MSGVN 22; impregnated with 5 µL H_20) separating each PVDF layer.

The samples for the diffusion experiments (^{1}H-NMR) were prepared by adding 5 mL perdeuterated dodecane to 0.5 g egg yolk lecithin and 25 mg cholesterol in a 10 mL glass flask. The mixture was vortexed thoroughly, filtrated and filled in disposable 5 mm NMR tubes.

2.2.2. ^{31}P-NMR

Solid-state ^{31}P-NMR measurements were recorded at 298 K on a Bruker Avance 400 spectrometer (Bruker AXS, Karlsruhe, Germany) operating at a phosphorous - 31 frequency of 161 MHz and using a pulse - acquire sequence with broadband proton decoupling (400 MHz). The recycling delay and the excitation pulse length were 6 s and 3 µs, respectively. A typical spectrum was obtained from 500 - 12.000 scans depending on the lipid content of the sample.

2.2.3. ^{1}H-NMR Self-Diffusion Measurements

Translational diffusion coefficients of phosphatidylcholine, phosphatidylethanolamine and cholesterol in the egg lecithin - cholesterol - d26 - dodecane system (PAMPA - lipid solution) were determined using the pulsed field gradient technique (PFGNMR [31]). Measurements were carried out on a Bruker 600-MHz Avance II spectrometer equipped with a cryogenic TCI probe head and a Bruker pulsed magnetic field gradient unit. Experiments were performed at 303 K with an internal lock on d26 - dodecane. Spectrometer operation and data processing were performed using Topspin 2.1 (Bruker, Fällanden, Switzerland). A pulsed gradient stimulated echo pulse sequence incorporating bipolar gradient pulses [32] was used to generate the magnetic field gradient. The proton signals (i.e. the spin echo amplitudes) of phosphatidylcholine (chemical shift, δ = 3.42 ppm), phosphatidylethanolamine (δ = 1.62 ppm), cholesterol (δ = 0.77 ppm) and dodecane (δ = 0.87 ppm) were analyzed after Fourier transformation in the frequency domain.

In presence of a gradient, molecular diffusion attenuates the ^{1}H signal amplitude, I, according to

$$I = I_0 \exp\left[- D\gamma^2 g^2 \delta^2 (\Delta - \delta/3 - \tau/2)\right], \quad (1)$$

where I_0 is the ^{1}H signal intensity in absence of a gradient, D is the diffusion coefficient of the nuclei, γ is the gyromagnetic ratio, g is the gradient strength (0 - 45 Gcm^{-1}), δ is the duration of the pulse (δ = 1 ms), Δ is the interval between the gradient pulses (Δ = 300 ms) and τ is the time spacing between the *individual* bipolar gradient pulses (τ = 1 ms). Other parameters were as follows: 32k data points, 18 ppm spectroscopical line width, 1.5 s interscan delay, no H_20 suppression, exponential filtering (LB = 1 Hz), smoothed square gradient shape (SMSQ10.100), manual baseline correction of the ^{1}H integral regions.

A plot of the signal attenuation, $\ln I/I_0$, versus g^2, yielded a straight line (in most cases) with a negative slope ($Slope_{lipid}$, $Slope_{dodecane}$) relating to the individual diffusion coefficients (D_{lipid}, $D_{dodecane}$). The diffusion constant of dodecane at 303 K ($D_{dodecane}$ = 9.15 10^{-10}m^{2}s^{-1}) was used to calibrate the magnitude of the field gradient pulses such that

$$D_{lipid} = Slope_{ipid} \cdot D_{dodecane} / Slope_{doedcane}. \quad (2)$$

The D-estimate for dodecane at 303 K was estimated by performing a linear regression on the known temperature - dependent self - diffusion constants of dodecane [33].

The apparent hydrodynamic radius (r_0) of the diffusing aggregates was obtained using the Stokes-Einstein equation:

$$D = \frac{kT}{6\pi\eta r_0}, \quad (3)$$

where k is the Boltzmann constant (1.38×10^{-23}J K^{-1}), T is the temperature (303 K) and η is the solvent viscosity at 303 K (1.24 mPas, estimated from a biexponential decay fit of the known temperature dependent viscosities of dodecane [34]).

2.3. Studies on the Function of the PAMPA Barrier

2.3.1. Measurement of PAMPA - Lipid Solution/Buffer Distribution Coefficients

For the measurement of the PAMPA-lipid/buffer distribution coefficients as a function of the egg lecithin concentration, stock solutions of propranolol and diazepam were prepared in DMSO (10 mM and 2.5 mM). The stock solutions were diluted 1 : 100 to obtain the final sample solutions (100 µM and 25 µM test compound, DMSO content 1 %, v/v). Similarly, stock solutions of propranolol (0.5, 1.25, 2.5, 10, 20 and 30 mM) were used to prepare the sample solutions (5, 12.5, 25, 100, 200 and 300 µM propranolol, 1 % DMSO, v/v) for the measurement of $\log D'_{PAMPA}$ - drug concentration profiles. The sample solutions (V_{aq} = 200 µL) were transferred into an in-house made 96 - well Teflon plate which was covered with a 96 - well filter plate (PVDF, pore size 0.45 um, Cat. 4550, Millipore, Billerica, MA) pre - coated with PAMPA-lipid solution (V_{lipid} = 2.25 µL). To investigate the influence of the egg lecithin concentration, PAMPA - lipid solutions containing 0 - 50 wt % egg yolk lecithin (Sigma) dissolved in dodecane were used (0; 1; 2; 3; 4; 5, 6; 7; 8; 9; 10; 12.5; 15; 17.5; 20; 22.5; 25; 30; 35; 40; 45; 50 wt %). For the $\log D'_{PAMPA}$ - drug concentration profiles only one concentration of egg lecithin was investigated, namely that used in the Roche PAMPA setup (11.9 wt % egg lecithin, corresponding to 9 %, m/v). It is important to note that the assay construct was designed such that the PAMPA lipid solution was not in contact with the border of the Teflon well (Supplementary Information). The assembly was sealed and left undisturbed (room temperature) for at least 8 h during which the solute was allowed to distribute into the PAMPA-lipid solution. It was assured that equilibrium was reached within the 8 h of incubation (Supplementary Information). After removal of the filter plate, the drug concentration left in the aqueous phase, C_{aq}^{eq}, was determined by means of HPLC - UV. The PAMPA - lipid solution/buffer distribution coefficient was calculated by mass balance according to:

$$\log D'_{PAMPA} = \log\left(\frac{\left(C_{aq}^{0} - C_{aq}^{eq}\right)\cdot V_{aq}}{C_{aq}^{eq}\cdot V_{lipid}}\right), \qquad (4)$$

where C_{aq}^{0} is the initial aqueous drug concentration, which was obtained from a reference experiment, carried out under the same conditions but without coating the filter with lipid

solution. The apostrophe indicates that the distribution coefficient was determined by mass balance rather than by measuring both phases directly. Therefore $\log D'_{PAMPA}$ is a composite parameter reflecting the drug distribution into the PAMPA-lipid solution and the adsorption of drug at the filter-supported interface.

The results from the concentration dependent $\log D'_{PAMPA}$ measurements were converted into binding data such that the degree of binding, X_b, was determined as the molar ratio of bound drug, n_D, per total lipid, n_L, according to $X_b = n_D / n_L$, where $n_L = \left\lfloor \rho_{dodecane} \cdot V_{lipid} \cdot \%lipid \right\rfloor \cdot M_{POPC}$ (in a simplified manner the density of dodecane (ρ =0.75 gcm^{-3}) and the molecular weight of POPC (MW_{POPC} = 760.1 g/mol) was used.

2.3.2. Measurement of PAMPA - Lipid Solution/Buffer Distribution Coefficients in Combination with Permeability for a Large Dataset

Stock solutions of the test compounds (10 mM) in DMSO were diluted with buffer (50 mM Tris/114 mM NaCl/pH 7.4) to obtain an aqueous drug solution (150 µM). The solution was filtrated and the filtrate (V_D = 320 µL) was transferred into a Teflon donor plate which was covered with a 96 - well filter plate (PVDF, pore size 0.45 µm, Cat. 4550, Millipore, Billerica, MA) pre-coated with the PAMPA-lipid solution (V_{lipid} = 4.5µL). In contrast to the measurements described above, blank assay buffer (V_A = 280 µL, 50 mM Tris/114 mM NaCl/pH 7.4) was added on top of the filter pate. After 19.5 h incubation, the sandwich was separated and the amount of drug in the acceptor and the donor solution was determined by comparison with the UV spectra from the initial filtrate using a 96 - well UV plate reader (Molecular Devices, model Spectra Max 190, Sunnyvale, CA and pION PSR4 p software). All measurements were performed in triplicate with an automated liquid handling system. Effective permeability values (P_e) were calculated as described by [35]. Briefly, P_e values can be calculated according to the following equation which also takes into account the membrane retention of the compound:

$$P_e = \frac{2.303 V_D}{A(t - t_s)} \cdot \left(\frac{1}{1 + V_D / V_A} \right) \log_{10} \left[1 - \left(\frac{1 + V_A / V_D}{1 - R} \right) \right] \left(\frac{C_{A,t}}{C_{D,t=0}} \right) \quad (5)$$

where A is the area of the filter (corrected for the apparent filter porosity, as described by [36]), t the time, t_s the time at steady-state, V_D and V_A are the acceptor and the donor

volumes, respectively, and $C_{A,t}$ and $C_{D,t}$ are the measured acceptor and donor concentrations, respectively, at time t. The PAMPA barrier retention factor R can be obtained by mass balance according to:

$$R = 1 - \left(\frac{C_{D,t} + \left(C_{A,t} V_A / V_D \right)}{C_{D,t=0}} \right). \quad (6)$$

Distribution coefficients, $\log D'_{PAMPA}$, were calculated as described above but with $V_{aq} = V_D + V_A$.

2.3.3. Measurement of Octanol/Buffer Distribution Coefficients

Octanol / buffer (50 mM Tris/114 mM NaCl/pH 7.4) distribution coefficients, $\log D'_{oct}$ (pH 7.4), were measured by a miniaturized filter - based shake flask assay, referred to as CAMDS and described in full detail in our *accompanying manuscript 1*. As described for $\log D'_{PAMPA}$, the apostrophe indicates that the distribution coefficients were determined by mass balance rather than by measuring both phases directly.

2.4. HPLC Instrumentation and Chromatographic Conditions

Drug concentrations in aqueous solutions were quantified using an Agilent 1290 Infinity HPLC-UV system. A 5 µL aliquot of each sample was injected onto a Kinetex 2.6 µm, 2.1 x 50 mm analytical column. The flow rate was 2 mL/min and the integrated column heater was set to 60 °C. The mobile phase consisted of A (water) and B (acetonitril), each containing 0.1 % (v/v) formic acid. The gradient elution was performed as follows: initial 2 % B, 0 - 0.35 min linear gradient from 2 % B to 95 % B, 0.35 min - 0.5 min 95 % B, posttime 0.3 min. The gradient program for doxorubicin, vinblastine, buspirone and colchicine was slightly different: initial 2 % B, 0 - 0.5 min linear gradient from 2 % B to 95 % B, 0.5 min - 0.65 min 95 % B. Peak areas were recorded at an appropriate wavelength.

3. Results

3.1. Characterization and Specification of Egg Lecithin

The egg lecithin used in our studies was a yellow to orange-colored, sticky and not odorless material, isolated from egg yolk and used as received from the supplier (Sigma). It is important to note that lecithin in this sense is not synonymous with the well - defined, pure lecithin POPC. Rather it is a crude mixture of phospholipids, other lipids as well as a variety of other components such as triglycerides, sterols (e.g. cholesterol), fatty acids, glycolipids and carbohydrates. The exact composition of egg lecithin depends on the stage of the purification process (extraction solvent, deoiling, bleaching, hydrolysis, etc. [37]) and also varies batch - wise within one supplier chain (personal communication, Sigma). The composition of the egg lecithin used in our studies is given in Table 1 and relies on thin layer chromatography analysis provided by the selected supplier (Sigma).

Table 1

3.2. Characterization of the Filter

Fig. 1 shows a scanning electron micrograph of the PVDF filter used by ourselves and by most PAMPA experimenters. The filter was punched out from the Millipore filter plate constituting the support for the PAMPA - lipid solution and shown herein in the form of the non - coated filter. The structure of the filter is highly porous, irregular in shape and without any preferred orientation of the fibers. The pore size of the filter ranges from approximately 0.4 - 2.5 μM, showing that the nominal aperture (0.45 μM) is only a rough average. It should be mentioned that SEM images of PVDF have been published before [38], but we preferred to characterize the particular filter that was used throughout our studies. Thereby we took into account that the structure of the filter, in particular the pore size, vary among different suppliers and, in addition, that surface treatment and stretching of the filter during the manufacturing process might change the morphology of the filter.

Fig. 1

3.3. NMR Studies on the Structure of the PAMPA Barrier

3.3.1. Phase Equilibria in the System Egg lecithin - Dodecane - H_20 (- Cholesterol)

The first question we addressed in a series of ^{31}P-NMR experiments was whether egg yolk lecithin, used as received without further purification, is able to form lipid bilayers under optimal experimental conditions, i.e. in presence of water. Furthermore, we investigated the effect of increasing amounts of dodecane on the phase behavior of the egg lecithin - H_20 system at 298 K. Therefore, egg lecithin was dispersed in excess water (water : phospholipid ratio was 45 : 1 corresponding to 51 wt % water) and dodecane was added, up to the dodecane : phospholipid ratio typically used in PAMPA (33.5 mol dodecane : 1 mol phospholipid corresponding to 11.8 wt % egg lecithin). The mol percentages were referred not to egg lecithin as a whole, but to the POPC content present therein. In addition we tested the effect of cholesterol taking into consideration that small quantities (0.45 %, m/v) are used as a stabilizer in the Roche PAMPA - lipid solution (personal communication). The cholesterol quantity was selected to match the concentration used in PAMPA (6 mol phospholipid : 1 mol cholesterol) while the selection of the water concentration was somewhat arbitrary (but small enough to create multilamellar vesicles).

The ^{31}P-NMR spectra of the egg lecithin - H_20 and the egg lecithin - cholesterol - H_20 system in presence of increasing amounts of dodecane are shown in Fig. 2. Generally, the spectra of both systems (with and without cholesterol) were almost superimposable indicating that the applied quantities of cholesterol were too small to alter significantly the long-range order of the lipids.

Fig. 2

In the absence of dodecane (Fig. 2A) the line width, shape (low field shoulder and high field peak) and the residual chemical shielding anisotropy (approximately - 50 ppm) of the spectra were characteristic for coarse dispersions of lipid bilayers. Upon addition of 0.25 mol (Fig. 2B) and 0.5 mol (Fig. 2C) dodecane per mol phospholipid the bilayer structure was essentially preserved, although, a small isotropic line was superimposed on the bilayer spectra. At 1 mol dodecane per mol phospholipid (Fig. 2D), the ^{31}P-NMR spectra corresponded to a pure hexagonal phase. Further addition of dodecane caused the homogenous phase to separate which was macroscopically observed as islands of pure dodecane alongside the lipid dispersion. The ^{31}P-NMR spectrum at 2 mol dodecane per mol

phospholipid (Fig. 2E) was a superimposition of all three types of spectra, namely those corresponding to coarse lipid bilayers, hexagonal and isotropic phases. With increasing amounts of dodecane up to 5 mol dodecane per mol phospholipid, the portion of the 'isotropic' phase increased at the expense of the lamellar and the hexagonal phase (Fig. 2F - H). At 33.5 mol dodecane per mol phospholipid (Fig. 2I), which meets the dodecane - lecithin ratio in the Roche PAMPA setup, the intrinsic chemical shielding anisotropy was almost completely averaged out and a single isotropic peak at 0 ppm predominated.

In the above described experiments, dodecane was subsequently added to the coarse bilayer dispersions. The ^{31}P-NMR spectra of samples prepared in an inverse order (addition of water to the egg lecithin-dodecane mixture) were essentially identical (spectra not shown). However, when pure POPC instead of egg lecithin was used as the lipid and dodecane was added to the POPC-buffer dispersions, the bilayer structure was preserved except for a very small isotropic peak at >0.5 mol dodecane : mol POPC (Fig. 3A-I).

Fig. 3

3.3.2. Phase Equilibria in the System Egg lecithin - Dodecane

In the next series of experiments, the PAMPA - lipid solution was not spiked with water to take into account that also the bulk phase of the PAMPA barrier only contains moisture water. Since homogeneity of an egg lecithin - cholesterol mixture would not be easily achieved at low dodecane concentrations, we abstained also from the addition of cholesterol. Facilitated mixing in dichlormethane following evaporation of the solvent was not undertaken to avoid falsifying the residual water content. Fig. 4A - F show the ^{31}P - NMR spectra of egg lecithin in presence of increasing amounts of dodecane up to the dodecane : lipid ratio used in PAMPA (Fig. 4F).

Fig. 4

It is interesting to note that two batches of egg lecithin, namely an "old" one (stored for > 3 month at 2 - 8°C) and a new one just ordered, yielded different spectra at low dodecane : phospholipid ratios (up to 1 mol dodecane : mol phospholipid). The overlayed spectra of the two batches are shown in Fig. 4A at the most striking example of "pure" egg

lecithin (no dodecane added). Phospholipids are extremely hygroscopic and the bilayer pattern observed in the aged batch as compared to the powder pattern in the new batch indicates that water had been readily adsorbed. Although it is not uncommon to use aged egg lecithin in PAMPA (a bottle from Sigma contains 100 g egg lecithin), all experiments (including the studies above in presence of 45 mol water per mol phospholipid) were performed with the new batch. An inspection of Fig. 4A - I reveals that with increasing amounts of dodecane the line width narrows and the powder type of spectra collapsed into a classical isotropic peak which characterizes the egg lecithin - dodecane mixture used in PAMPA (33.5 mol dodecane per mol phospholipid, Fig. 4F).

3.3.3. Phase Equilibria in the System Egg Lecithin - Dodecane - Cholesterol (- Filter)

The first two series of experiments have demonstrated that a large excess of dodecane with respect to egg lecithin (such as in PAMPA) induces the lamellar-to-isotropic phase transition, irrespective of the presence of extra water. However, if painted across a smooth Teflon aperture immersed in water, lipid-organic solvent solutions containing as low as 2% (m/v) phospholipid are known to form bilayer (black) lipid membranes [39] . Therefore we tested whether in analogy to BLMs the phase equilibrium changes when coating the PAMPA-lipid solution across multiple apertures (i.e. the PVDF filter), specifically we were interested if an isotropic-to-lamellar phase transition occurs. Fig. 5A and Fig. 5B show the ^{31}P-NMR spectra of the PAMPA-lipid solution either free in solution or coated on a PVDF filter. The spectra were essentially identical and correspond to an isotropic movement of the phospholipids. Separating the phospholipid - coated PVDF filters by means of hydrophilic filters soaked with water (alternate stacking) did not change the pattern of the spectra (Fig. 5C).

Fig. 5

3.3.4. Diffusion in the Isotropic Phase of the System Egg lecithin - Dodecane - Cholesterol

The presence of an isotropic phase as observed in the ^{31}P - NMR spectra of the PAMPA - lipid solution (Fig. 5A - C) does not exclude lipid association with a definite microstructure [29]. Since the viscosity of the PAMPA-lipid solution is low, it is safe to say that the isotropic peak does not correspond to a cubic phase.

To further characterize the isotropic phase we measured the translational diffusion coefficients of phosphatidylcholine (PC), phosphatidylethanolamie (PE), cholesterol and

dodecane in the egg lecithin - dodecane - cholesterol system, by means of ^{1}H - NMR diffusion experiments. First, it was necessary to assign the signals in the ^{1}H-NMR spectrum (Fig. 6A,B) of the PAMPA lipid-solution (egg lecithin-dodecane-cholesterol).

Fig. 6

As indicated above, the composition of egg lecithin is complex and therefore not all signals could be identified, moreover, a number of peaks displayed a superposition of various components. For diffusion experiments, we paid attention to follow the spin echo decay of only pure peaks or of peak shoulders with a single diffusion pattern. In order to investigate the influence of the egg lecithin concentration in dodecane we tested the PAMPA - lipid itself and also a 1:4, 1:16 and 1:64 dilution thereof in dodecane.

Experimental spin echo decays of PC, PE, cholesterol, and d26 - dodecane at the four concentrations are shown in Fig. 7 A, B, C and D, respectively, as a function of the squared gradient strength (Stejskal - Tanner plot). The interpretation of the plots is straightforward: the faster the signal decay (i.e. the steeper the slope), the faster the translational diffusion of the particle. The diffusion constants were derived from the slopes and are listed in Table 2 along with the corresponding apparent hydrodynamic diameters of the diffusing objects. The latter were obtained via the Stokes - Einstein equation and were based upon the assumption that the particles were spherical. The diffusion constant of dodecance was independent on the egg lecithin concentration and therefore the average value was used for calibration.

Fig. 7, Table 2

The rate of diffusion increased in the following order: PC < PE << cholesterol << dodecane, which corresponds to the reverse order of particle size. There was a clear trend towards decreased diffusion at higher egg lecithin concentration which was most pronounced for cholesterol. In the undiluted PAMPA - lipid solution, the diffusion of cholesterol was approximately twice as fast as PC whereas in the most diluted solution it was about seven fold faster. The sensitivity of the diffusion coefficient of cholesterol to concentration was mirrored in the varying apparent hydrodynamic diameters ranging from 0.8 - 3.5 nm. The growth in aggregate size with an increase in the egg lecithin concentration was also observed for PE and PC. The apparent hydrodynamic radius of PE (4.1 - 4.6 nm) was at each concentration slightly lower than that of PC (5.9 - 6.9 nm).

It is important to note that the echo decays of PE (Fig. 7B) deviated from a simple Gaussian diffusion behavior for which a straight line in the Stejskal - Tanner plot would be predicted. Non-spherical geometry of the diffusing particles and overlap of the selected PE signal with another component (either chemically different or another aggregate form of associates) could contribute to the deviation. Measurements with a lipid - coated filter failed due to the severe line - broadening which most disturbed the homogeneity of the magnetic field.

3.4. Studies on the Function of the PAMPA Barrier

3.4.1. The Binding of Propranolol and Diazepam to the PAMPA - Lipid Solution

The NMR studies gave insight into the organization of lipids in the lipid - dodecane - filter system. In order to understand also the role of the lipids for the permeation process, we first studied the binding of drugs to the PAMPA - lipid phase as a function of the egg lecithin content in dodecane. For this purposes, we investigated compounds of different charge state and lipophilicity, namely diazepam (neutral, lipophilic) and propranolol (cationic, intermediate lipophilicity), at two drug concentrations (100 μM and 25 μM) to gain additional information about the role of electrostatics (charged species) for the binding step. The structures, $\log D_{oct}$(pH7.4) and pK_a values of the two test compounds are given in Table 3 along with the number of hydrogen bond donors and acceptors (the latter were reported to play an important role for the permeation of solutes [25]).

Table 3

The distribution coefficients between the PAMPA - lipid solution (coated on the PVDF filter) and buffer were determined by mass balance, i.e. the drug that has left the aqueous phase was considered as distributed into the PAMPA - lipid solution. A direct concentration analysis in both phases was not possible due to the inaccessibility of the PAMPA - lipid solution which resided in the pores of the PVDF filter. The distribution coefficients for each drug concentration and egg lecithin content are shown in Fig. 8A for propranolol and Fig. 8B for diazepam.

Fig. 8

Generally, the more egg lecithin was present in the PAMPA - lipid solution, the higher was the distribution coefficient. However, there were marked differences between the distribution patterns of the two drugs: i) in contrast to diazepam where distribution was concentration independent, lipid binding of propranolol was higher for the lower drug concentration (details see below), ii) the 'booster' effect of egg lecithin was more pronounced for propranolol giving rise to even higher $\log D'_{PAMPA}$ (pH 7.4) values (if % egg lecithin > ~20%) for propranolol than for diazepam despite the lower $\log D_{oct}$ (pH 7.4). The component responsible for the distribution of propranolol was therefore essentially egg lecithin and not dodecance (see discussion). iii) Only for propranolol was an exceptionally strong effect of egg lecithin observed when comparing the distribution coefficients into pure dodecane with those into a 1 % egg lecithin - dodecane mixture (see discussion).

The observed discrepancy between $\log D'_{PAMPA}$ (pH 7.4) obtained with 25 µM and 100 µM propranolol was further investigated. For this purpose we measured the binding of drug to a 9 % egg lecithin - dodecane mixture (= egg lecithin content like in Roche PAMPA) for a larger range of propranolol concentrations (C^0_{aq} = 5 - 300 µM). For comparison we also coated the filter support with octanol and measured the distribution coefficients in the same manner as with the PAMPA - lipid solution. Fig. 9A shows the $\log D'_{PAMPA}$ (pH 7.4), and $\log D'_{oct}$ (pH 7.4) values as a function of C^0_{aq} confirming the trend towards lower distribution coefficients at higher drug concentrations. The discrepancy between the lowest and the highest $\log D'_{oct}$ was much higher for the PAMPA - lipid solution ($\Delta \log D'_{PAMPA}$ = 0.96) whereas almost constant distribution coefficients were obtained with octanol ($\Delta \log D'_{oct}$ = 0.22).

Fig. 9

A transformation of the data shown in Fig. 9A for the PAMPA - lipid solution into a conventional adsorption isotherm (Fig. 9B) shows a typical saturation curve. When the same data is redrawn into a Scatchard plot (Fig. 9A), a biphasic pattern becomes evident which can formerly be interpreted in terms of two binding sites. However, it is well known from binding studies to lipid bilayers that the same type of pattern may be a consequence of membrane surface charge [40]: The insertion of cationic drugs such as propranolol into the electrically neutral PAMPA - lipid phase should create a positive surface potential, Ψ_0, which leads to

the repulsion of molecules with the same charge. Therefore surface distribution becomes increasingly difficult at higher drug concentrations and the apparent $\log D'$ (interfacial and bulk phase distribution) decreases. Apart from saturation- and electrostatic effects at the PAMPA - lipid solution/water interface, the same principles may apply for the interface created by the reverse phopspholipid micelles present in bulk dodecane.

3.4.2. Binding to and Permeation across the PAMPA Barrier for a Large Set of Drugs

Hitherto we have concentrated our study on the structure of the PAMPA barrier and the binding of drugs to it. However, membrane binding is only the first step in the process of passive diffusion and we were also interested in how membrane binding relates to permeability, with a particular focus on the role of size and charge.

It is well known that the linear correlation between effective membrane permeability (P_e) in PAMPA and distribution into octanol levels off [41] at approximately $\log D_{oct}$ > 3 (Roche data), i.e. when compounds become increasingly large. We specifically raised the question whether the bilinear relationship is due to a size restriction of the PAMPA barrier, not reflected by the distribution of drug into bulk octanol. Therefore, we investigated the relationship between $\log D'_{PAMPA}$ and $\log D'_{oct}$ and tested whether their correlation pattern reflects the typical bilinear relationship between P_e and $\log D'_{oct}$. The dataset tested (Table 4) included 104 structurally diverse acidic, basic and non-charged compounds spanning a wide range of lipophilicity ($\log D'_{oct}$ = - 1.15 - 4.41) and molecular size (cross sectional area, A_D = 25 - 155 Å^2). The P_e values were obtained from a classical PAMPA experiment and from the fraction of drug retained in the membrane we deduced $\log D'_{PAMPA}$, which is shown in Fig. 10A as a function of $\log D'_{oct}$.

Table 4, Fig. 10

$LogD'_{PAMPA}$ linearly increases with an increase in $\log D'_{oct}$ although the data considerably scatter around the linear regression line (r^2 = 0.782, standard deviation, SD = 0.571). There is a clear trend towards higher $\log D'_{PAMPA}$ values for cationic drugs and lower $\log D'_{PAMPA}$ values for anionic drugs as compared to the non - charged compounds. Moreover, it becomes evident that basic compounds with low $\log D'_{oct}$ values (approximately $\log D'_{oct} < 1.5$) tend to prefer the PAMPA-lipid solution as compared to octanol ($\log D'_{PAMPA} > \log D'_{oct}$), and vice versa

compounds with high $\log D'_{oct}$ values tend to have a lower $\log D'_{PAMPA}$. Non-charged and anionic drugs have higher $\log D'_{oct}$ values as compared to $\log D'_{PAMPA}$ with the exception of ketorolac, indomethacin and theobromin (the exceptions are however close to the 1:1 line).

Strictly speaking, an evaluation of whether or not the PAMPA membrane impedes the insertion of large compounds must be confined to an inspection of non - charged drugs. This circumvents the problem of concentration effects due to charge repulsion (see above) and takes into account that the initial drug concentrations differed according to solubility.

An inspection of the $\log D'_{PAMPA}$ - $\log D'_{oct}$ profiles for the non-charged drugs (grey symbols) reveals that large molecules are equally good accommodated in octanol and in the PAMPA barrier. For example, paclitaxel (60), the compound with the largest A_D, did not deviate from the regression line, and just a slight discrepancy was observed for ritonavir (77) and indinavir (39).

Therefore, it can be excluded that the bilinear relationship between P_e and $\log D'_{oct}$ (Fig. 10B) is due to a size restriction of the PAMPA barrier and a loss of linear correlation between $\log D'_{PAMPA}$ and $\log D'_{oct}$ for increasingly large compounds. It can be inferred that the presence of the unstirred water layer [42], which limits the diffusion of lipophilic compounds, is the main reason for the observed bilinearity.

4. Discussion

Predicting a drug candidate's permeation *in vivo* by means of an *in vitro* membrane mimicking system requires an understanding of the structure and barrier properties of the particular model system in order to assess its scope and limitations. In response to the hitherto unexplored structure of the PAMPA barrier, we have performed NMR studies which gave insight into the organization of PAMPA lipids on the molecular level. Moreover, we have investigated the role of concentration, charge and size for the binding of drugs to the PAMPA barrier. In the following, the results will be interpreted in terms of structure and function of the lipids. Finally, a hypothetical model for the permeation mechanisms across the PAMPA barrier will be proposed.

4.1. The Structure of the PAMPA Barrier

4.1.1. The Instability of a Bilayer in Presence of Excess Dodecane

One major difference between the composition of biological membranes and the PAMPA barrier is the presence of excess dodecane in PAMPA [18]. This was the main reason for studying the phase behavior of the egg lecithin - water system upon addition of dodecane. We could show that dodecane promotes the formation of an inverted hexagonal (H_{II}) phase, at a relatively low dodecane concentration (1 mol %), and an isotropic phase, at higher dodecane concentrations (>10 mol %), with domains in between where $L_{\alpha,}$ H_{II} and isotropic phases coexist. In previous studies, dodecane has only been added up to 2 mol dodecane : 1 mol pure phospholipid which is far below the dodecane concentration present in PAMPA. Our results at low dodecane concentrations are in line with the literature [43-45], however, we expanded our investigation to the dodecane : phospholipid ratio used in PAMPA (i.e. 33.5 mol dodecane : 1 mol POPC). Under these experimental conditions, essentially all lipids were organized in an isotropic phase, irrespective of whether or not cholesterol or water was added or whether a filter was used as support for the lipid mixture.

Thus we consider it a gross oversimplification when disregarding the presence of dodecane for interpreting PAMPA permeabilities. Specifically we consider it invalid to use the membrane fluidity assessed for bilayer liposomes as a correlate for the barrier fluidity and permeability in PAMPA [27].

4.1.2. The Influence of the Filter

The absence of bilayers in the PAMPA barrier may be surprising at the first moment since Thomspon et al. [40] provided evidence for the existence of micro BLM in the particular filter - lipid-solvent systems investigated. Much of Thompson's line of argument relied on the increase of conductivity upon addition of amphothericin, a peptide spanning exactly one leaflet of a membrane bilayer membrane. However, the filter used for these key experiments was polycarbonate, characterized by a highly uniform series of holes separated by smooth non - porous polymer [40]. In contrast, the AFM photograph (Fig. 1) of the PVDF filter applied in PAMPA demonstrates its rough surface which has been recognized as unfavorably for providing an aperture for BLMs.

In a series of screening experiments, Phung et al. [22] tested the ability of various filters to support BLMs for biosensors. He came to the conclusion that PVDF does not support bilayers which is in line with our results, even though Phung et al. used a different lipid - solvent mixture. The inability of PVDF to support BLM should not only be attributed to the roughness of the surface but also to the relative hydrophilicity of PVDF as compared to e.g. Teflon (PTFE). Ever since the pioneering work of Montal and Müller, hydrophobic surfaces have been preferred for the formation of BLM [6].

4.1.3. The Influence of the Lipid Composition

It has been known for a long time that highly purified lipids are of utmost importance for the stability of pore spanning membranes. In this light, crude egg yolk extract such as used in PAMPA must be considered unsuitable for the formation of BLM, which is confirmed by the isotropic phase observed by ^{31}P-NMR spectroscopy (Fig. 2I).

It is worth noting that the dodecane - lecithin systems investigated hitherto concerned pure lipid species (POPC; 1,2-dioleoyl-*sn*-glycero-3-phosphocholine [DOPC] [43, 44]) as distinct from crude extracts of egg yolk used for PAMPA (Roche). Our results demonstrated that crude egg lecithin bilayers are more prone to undergo the lamellar - to - isotropic phase transition as compared to pure POPC, pointing to the higher instability of the egg lecithin bilayer. In support of our results, alkane - spiked bilayers made up of purified phospholipids have been reported to equilibrate extremely slowly such that even after long - term storage (several month) phase equilibrium was not achieved. In contrast, it is well known that the dispersion of phospholipids (e.g. POPC, DOPC) in dodecane prior to the addition of water yields isotropic and hexagonal phases (see above [34, 44]). In case of the egg lecithin tested

in this study, the order of adding dodecane did not matter and a lamellar - to-isotropic phase transition was observed in each case.

4.1.4. A Proposal for the Structure of the PAMPA Barrier

In order to further characterize the isotropic phase we have measured self - diffusion coefficients for the individual components of the PAMPA-lipid solution. The diameters assessed for PC and PE as d = 6.9 nm and 4.6 nm, respectively (undiluted PAMPA solution), can be explained by the presence of reverse micelles. Phospholipids most likely orient themselves with the head group towards the residual water (maximal 2 %, according to Sigma) and the tails pointing towards the surrounding dodecane phase.

The high diffusion coefficient of dodecane suggests that the largest part of the solvent is not incorporated in the micelles but that bulk dodecane surrounds the lipid aggregates. Likewise, cholesterol appears not to be incorporated completely in the reverse micellar structure. This is indicated by the diffusion coefficient of cholesterol in the intermediate range between that of dodecane and PC/PE. Notably, the diffusion coefficients assessed are an average of the diffusion coefficients for the different physical states of a chemically defined species, weighted according to the relative proportion of that physical state. This means that the coexistence of monomers and lipid aggregates gives rise to an average diffusion coefficient and, in turn, an average estimate for the aggregate diameter. In the undiluted PAMPA lipid solution, the proportion of the monomeric form of phospholipids is the lowest which means that its influence on the diffusion coefficient is the smallest. Thus the diameter - estimate should approximate the diameter of the reverse micelle. However, the aggregate size is still only an approximate value since the non-linearity of the spin echo decays points to the presence of non - spherical particles. Using the Stokes Einstein equation for assessing the diameters of the diffusing lipid aggregates is therefore a simplification which we considered nevertheless useful for gaining an approximate aggregate size.

The presence of reverse micelles is in line with a large body of knowledge that has been acquired on the organization of amphiphiles (e.g. phospholipids) in non-polar organic solvents (best characterized solvent: cyclohexane) [46]. In qualitative terms, such system corresponds to the PAMPA mixture before its coating on a filter support. It is established that purified phospholipids assemble into spherical reverse micelles which transform into reverse tubular structures in the micrometer range upon addition of low amounts of water. These worm - like micelles are assumed to entangle and form continuous three - dimensional networks with pronounced gel properties [47-50]. The PAMPA lipid solution is not gel - like

which shows that a network of worm - like micelles is unlikely to be formed. The absence of which is in line with literature since it has been already recognized that purified but not crude soy lecithin dissolved in dodecane undergoes the liquid - to - gel transition. However, the presence of short worm - like micelles in the PAMPA lipid solution could explain the deviation from linearity of the spin echo decays.

The self - diffusion NMR experiments were conducted with the PAMPA lipid solution without using a filter support since the associated disturbance of the magnetic field is in conflict with high resolution NMR. We cannot exclude that the filter changes the size of the aggregates, however, the ^{31}P - NMR clearly demonstrated that the lipid aggregates tumble rapidly with respect to the time scale of NMR. Moreover, the size of the micelles (6.9 nm) is manifold smaller than the size of the pores in a PAMPA filter (0.45 μM) and therefore we assume that our results are applicable to the filter - phospholipid - solvent system.

4.2. The Function of the Lipids and a Proposed Permeation Mechanism

Our studies on the distribution of propranolol and diazepam showed that the higher the egg lecithin content in the PAMPA barrier, the higher the distribution coefficient which points to a carrier role of the phospholipids. For propranolol (cationic amphiphilic), the increase in the distribution coefficient was exceptionally high when increasing the egg lecithin content from 0 to 1 %. This indicates that the mechanism by which propranolol binds to the membrane changes in presence of egg lecithin, supposedly by micellar solubilization of the deprotonated drug. The data suggest that amphiphilic, hydrophilic molecules benefit more from the presence egg lecithin while lipophilic, barely amphiphilic solutes such as diazepam are already well solubilized in bulk dodecane.

Evidence for the binding of the charged species to the liquid - water interface is provided by the fact that the distribution coefficients for propranolol showed a concentration dependency. We suppose that not only amphiphilic drugs but also the phospholipids reside on the surface forming a monolayer. However, the ratio between the bulk lipid phase and the interface is approximately 1 : 3000 which explains that we could not verify the presence of a monolayer by means of ^{31}P-NMR. Both, the NMR studies and the $\log D'_{PAMPA}$ measurements, point to the proposed transport mechanism of solutes across the PAMPA barrier as summarized in Fig. 11.

Fig. 11

5. Conclusions

In summary, we have shown that in the bulk phase of the PAMPA-lipid solution (11.8 w t% egg lecithin in dodecane) egg lecithin particles are formed, however, the existence of multilamellar lipid bilayers or lipid hexagonal phases could not be verified. In fact, the addition of excess dodecane, such as used in PAMPA, to coarse dispersions of egg lecithin bilayers promotes a lamellar - to - isotropic phase transition. Likewise, pure egg lecithin - dodecane mixtures (PAMPA - lipid solution), whether or not spiked with cholesterol, adopted a non - bilayer phase in which isotropic motion occured. The isotropic phase also dominated when coating the PAMPA - lipid solution on a PVDF filter which was in contact with interfacial water. From the several lipid phases possibly giving rise to isotropic motion, inverted micelles are in best agreement with the low viscosity of the PAMPA - lipid solution and the lack of larger amounts of water (only moisture). Since the binding of cationic amphiphilic drugs to the PAMPA barrier strongly increases with a rise from 0 to 1 % egg lecithin, a change in the binding mechanism, specifically the formation of inverted drug - lipid mixed micelles, seems plausible. The generally stronger binding of drugs to the PAMPA-lipid barrier with increasing concentrations of egg lecithin demonstrates that the lipid acts as a carrier, rather than a barrier, for drug permeation. This distinguishes PAMPA from biological membranes. The size dependence, arising from attenuated insertion into densely packed biological membranes, is not observed in PAMPA and therefore we recommend considering effective PAMPA permeability values for bulky compounds as possibly too high.

Acknowledgements

We thank Marta Hidalgo for help with the preparation of the lipid samples.

6. Appendix

6.1. Background on Solid - State ^{31}P - NMR

^{31}P - NMR is a powerful tool to study the motion and average orientation of the phosphate head group of lipid dispersions [51]. The fact that different spectra are obtained for lipids incorporated into bilayer structures or in hexagonal and isotropic phases can be explained as follows: The magnetic field applied externally is reduced (shielded) by the electron cloud surrounding the phosphorous nuclei. Since the electron density is asymmetric, the chemical shielding is effective to a different extent depending on the orientation of the phosphate group with respect to the external magnetic field. This implies that the ^{31}P resonance frequencies and accordingly the chemical shifts (or shielding constants) vary with the molecular orientation giving rise to the so called chemical shielding anisotropy. The latter can be defined by the three principal components, σ_{11}, σ_{22} and σ_{33}, of the chemical shielding tensor, which correspond to the chemical shifts along the three principal directions. A ^{31}P - NMR spectrum is a probability - weighted superposition of all the chemical shifts that arise from the possible orientations of the phosphate head group in the magnetic field. In case of a randomly oriented sample, all orientations are populated and hence the spectrum is characterized by a broad line width (around 190 ppm) with a typical line shape (σ_{11} and σ_{33}define the shoulders and σ_{22} leads to a peak). If a phospholipid is incorporated into a lipid bilayer, rapid rotation of the phosphate group around the axis perpendicular to the bilayer surface partially averages out the chemical shielding anisotropy. The residual chemical shielding anisotropy, $\Delta\sigma$ (measured as the distance between the weak low-field and the intense high-field shoulder), amounts to ca. $\Delta\sigma$ = - 50 ppm for most of the yet studied bilayers (example: Fig. 2A). If the lipid is incorporated into a hexagonal phase, the line width is further reduced by a factor of two and the chemical shielding anisotropy has changed its sign (example: Fig. 2D). Finally, for small molecules or aggregates in solution, rapid tumbling (on the time scale of NMR) completely averages out the chemical shielding anisotropy and the NMR spectrum collapses to a single narrow resonance signal in the range of a few ppm. A variety of structures could give rise to a narrow (‘isotropic’) ^{31}P - NMR signal, such as micelles, inverted micelles, single walled vesicles and cubic phases [38].

6.2. Background on the Pulsed - Field Gradient NMR technique (^{1}H - NMR)

NMR spectroscopy allows estimating the self - diffusion coefficients (D) of objects in solution (molecules, micelles) by using magnetic field gradients [30]. Self - diffusion relates to the random translational motion of diffusing objects (Brownian motion) according to their size (Stokes - Einstein relation) and should not be confused with rotational diffusion.

As distinct from conventional NMR experiments, the sample is placed in a homogenous magnetic field (magnetic field strength B_0) upon which a magnetic field gradient (G) is imposed [52-54]. The strength of the field gradient varies linearly along the direction of B_0 (z-axis), i.e. along the long direction of the NMR tube. This means that also the Larmor frequency, which depends on the magnetic field strength, varies linearly along the direction of G and therefore depends on the location of the nucleus in the NMR tube. In other words, the magnetic field gradient can be used to encode (or label) the position of a nucleus in an indirect manner, i.e. through the Larmor frequency.

Accordingly, a change of position due to diffusion can be viewed as the effect on the resonant absorption (i.e. the NMR) signal. In self - diffusion experiments, the NMR signal observed is a so called spin echo which eliminates the effect of unwanted inhomogeneity in the static magnetic field (for details see basic NMR literature). Upon the 90° pulse involved in the generation of the spin echo, a gradient pulse is applied which encodes the position of the nuclei. Waiting for a short time after this first gradient pulse allows the nuclei to change their position. A second gradient pulse with the same duration (δ) and amplitude (g) is used to decode the position of the nuclei. If the nuclei did not undergo translational diffusion during the time span between the two gradient pulses (Δ), the effects of the two gradient pulses cancel each other out and the maximal spin echo will be observed. If, however, diffusion took place, a proportion of nuclei will not be in the same position with respect to the z - axis. Therefore, the net magnetization (i.e. the vector of the sum of the magnetic moments of all spins) will be changed which results in an attenuation of the NMR signal. The signal decay depends on the strength of the applied gradients (g), the time between the gradients (Δ), the gyromagnetic ratio of the nuclei (γ) and the diffusion coefficient (D); and therefore gives a measure of the motion of the particles (eq. see Materials and Methods).

TABLES

Table 1 Composition of egg lecithin 'powder' used for preparation of the PAMPA - lipid solution

Component	Fraction [wt %]
Phospholipids	min. 72
thereof	
Phosphatidylcholine[a]	min.59
Phosphatidylethanolamine	min. 6
Lyso-Phosphatidylcholine	max. 3
Other Phospholipids	min. 4
Triglycerides	max. 18
Cholesterol	max. 8
Water	max. 2

[a]for calculations phosphatidylcholine was taken as POPC.

Table 2 Diffusion coefficients and hydrodynamic radii of phosphatidylcholine (PC), phosphatidylethanolamine (PE) and cholesterol in the PAMPA lipid solution and a 1:4, 1:16 and 1:64 dilution thereof in dodecane - d26.

Conc. egg lecithin in dodecane [%]	Conc. cholesterol in dodecane [%]	Apparent Diffusion coefficient[a] 10^{-12} [M^2s^{-1}]			Apparent hydrodynamic diameter of the droplet [nm]		
		PC	PE	Cholesterol	PC	PE	Cholesterol
0.141	0.007	60.2	88.3	441.3	5.9	4.1	0.8
0.563	0.028	58.6	84.1	296.0	6.1	4.3	1.2
2.250	0.113	54.6	79.9	186.4	6.6	4.5	1.9
9.000	0.450	52.1	78.1	102.5	6.9	4.6	3.5

[a]The diffusion coefficient of dodecane ($D_{dodecane}$ = 915 10^{-12}m2s^{-1}) was used as a calibrant.

Table 3 Structure, $\log D_{oct}$ (pH 7.4), pK_a, fraction of ionized drug and the number of hydrogen bond donors and acceptors for the compounds investigated.

Compound	Structure	$\log D_{oct}$ pH 7.4)[a]	pK_a [b]	Fraction ionized (%)[c]	No. H-bond donors	No H-bond acceptors
Diazepam	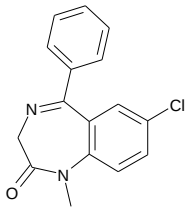	2.84	3.38	0	0	3
Propranolol	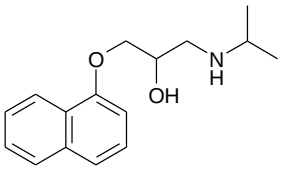	1.21	9.48	99.2	2	3

[a]in-house CAMDIS, [b]in-house potentiometric pK_a ; [c]calculated for pH 7.4 from measured pK_a using the Henderson-Hasselbalch equation.

Table 4 Charge class, pK_a values, molecular weights (desalted), cross sectional areas, A_D, calculated octanol/water partition coefficients, $c\log P$, octanol/water distribution coefficients, $\log D_{oct}$ (pH 7.4), and PAMPA-lipid solution - water distribution coefficients, $\log D_{PAMPA}$ (pH 7.4) for a representative set of drugs (n = 104).

No	Compound	Charge class[a]	pK_a (acid)[b]	pK_a (base)[b]	MW [g/mol]	A_D [c] [Å^2]	$c\log P$ [d]	$\log D'_{oct}$ (pH 7.4)[e]	$\log D'_{PAMPA}$ (pH 7.4)
1	Amitriptyline	B		9.49	277	55	4.85	2.77	2.34±0.09
2	Amoxapine	B		8.4/3.28	314	57	3.41	2.30	1.95±0.13
3	Atomoxetine	B		10.2	255	54	3.94	1.03	1.73±0.05
4	Bupropion	B		8.32	240	45	3.21	2.15	1.42±0.19
5	Buspirone	B		7.61	386	40	2.19	2.13	1.01±0.04
6	Caffeine	N			194	29	-0.04	-0.10	-0.27±0.00
7	Carbamazepine	N			236	60	2.38	1.58	0.17±0.77
8	Celecoxib	N	11.1		381	64	4.37	3.90	2.97±0.27
9	Chlorpromazine	B		9.38	319	48	5.30	3.23	2.61±0.23
10	Ciglitazone	A	6.88		333	37	5.07	3.96	2.51±0.34
11	Cimetidine	B		6.96	252	53	0.38	0.50	-0.27±0.00
12	Citalopram	B		9.52	324	62	3.13	1.40	1.52±0.02
13	Clozapine	B		7.68/3.9	327	53	3.71	2.73	2.19±0.06
14	Colchicine	N			399	89	1.20	0.95	0.05±0.28
15	Cyclobenzaprine	B		9.32	275	53	5.10	3.00	2.12±0.02
16	Desloratadine	B		9.78/4.57	311	52	3.83	1.20	1.88±0.10
17	Dexamethasone	N			392	73	1.79	1.79	1.34±0.17
18	Diazepam	N		3.38	285	58	2.96	2.84	1.77±0.09
19	Diclofenac	A	4.02		296	49	4.73	1.15	0.10±0.63
20	Ddigoxin	N			781	76	1.42	1.34	-0.27±0.00
21	Diphenhydramine	B		9.12	255	56	3.45	1.65	1.36±0.20
22	Diprenorphine	B	9.57	8.48	426	98	2.66	2.43	1.52±0.05
23	Donepezil	B		8.88	379	76	4.60	2.26	1.27±0.09
24	Doxepin	B		9.22	279	52	4.09	2.26	2.13±0.15
25	Doxorubicin	B	9.45	8.16	544	71	0.32	0.36	1.39±0.10
26	Eletriptan	B		9.59	383	61	3.36	0.84	1.64±0.09
27	Etoricoxib	N		4.53	359	64	2.35	2.23	1.32±0.29
28	Fallypride	B		8.22	364	57	3.18	2.02	1.22±0.21
29	Fentanyl	B		8.38	336	74	3.62	2.90	1.25±0.15
30	Flumazenil	N			303	53	1.29	1.08	-0.27±0.00
31	Fluoxetine	B		9.71	309	59	4.57	1.91	2.07±0.10
32	Fluphenazine	B		7.76/3.67	438	57	4.12	3.50	2.40±0.19
33	Flurbiprofen	A	4.03		244	36	3.75	0.87	-0.27±0.00
34	Fluvoxamine	B		9.11/5.82	318	55	3.03	1.56	1.76±0.09
35	Haloperidol	B		8.64	376	79	3.85	2.74	1.56±0.36
36	Hydrocodone	B		8.9	299	54	1.13	0.27	1.13±0.30
37	Hydroxyzine	B		7.51/2.66	375	63	4.00	3.09	1.99±0.03
38	Ibuprofen	A	4.45		206	34	3.68	0.95	0.24±0.89
39	Indinavir	N		5.77/4.01	614	125	3.68	2.97	0.87±0.11
40	Indometacin	A	4.43		358	51	4.18	0.79	0.91±0.04

No	Compound	Charge class[a]	pK_a (acid)[b]	pK_a (base)[b]	MW [g/mol]	A_D [c] [Å^2]	$c\log P$ [d]	$\log D'_{oct}$ (pH 7.4)[e]	$\log D'_{PAMPA}$ (pH 7.4)
41	Ketorolac	A	3.44		255	31	1.62	-0.58	-0.21±0.10
42	Lamotrigine	N		5.51	256	35	2.53	1.14	0.88±0.29
43	Loperamide	B		8.61	477	104	4.66	3.32	2.15±0.10
44	Loratadine	N		4.72	383	63	5.05	3.96	3.01±0.30
45	Loxapine	B		7.49/3.05	328	60	3.98	3.47	2.89±0.10
46	Maprotiline	B		10.2	277	54	4.52	1.47	1.92±0.16
47	MDL 100907	B		9.02	373	65	3.29	1.87	1.49±0.12
48	Mesoridazine	B		9.55	387	63	4.44	1.75	1.64±0.07
49	Methadone	B		9.26	309	69	4.17	1.60	1.72±0.04
50	Metoclopramide	B		9.36	300	40	2.23	0.22	0.66±0.24
51	Midazolam	N		5.71	326	63	3.42	3.32	1.68±0.06
52	Mirtazapine	B		7.79/3.59	265	48	2.81	2.52	1.65±0.10
53	Morphine	B	9.35	8.08	285	61	0.57	0.12	0.41±0.59
54	Naproxen	A	4.12		230	38	2.82	0.30	0.15±0.54
55	Naratriptan	B		9.43	335	63	1.70	-0.20	1.20±0.07
56	Nelfinavir	B	9.63	6.01	568	120	5.84	4.04	2.37±0.34
57	Norclozapine	B		8.56/4.13	313	54	3.14	1.62	1.95±0.15
58	Nortriptyline	B		10.13	263	52	4.32	1.59	2.06±0.02
59	Olanzapine	B		8.01/5.6	312	44	3.01	2.02	1.40±0.16
60	Paclitaxel	N			854	155	4.73	2.99	2.19±0.22
61	Paracetamol	N	9.45		151	35	0.49	0.22	-0.27±0.00
62	Paroxetine	B		9.7	329	59	4.24	1.63	2.15±0.03
63	Pemoline	N		3.08	176	29	0.46	0.15	-0.27±0.00
64	Pergolide	B		7.91	314	68	4.40	2.88	2.57±0.20
65	Perphenazine	B		7.86/3.7	404	54	3.81	3.39	2.57±0.01
66	Phenelzine	B		7.32	136	25	1.03	0.47	1.22±0.06
67	Phenytoin	A	8.18		252	55	2.09	2.29	1.66±0.06
68	Pioglitazone	A	6.6	5.7	356	41	3.53	2.94	2.13±0.07
69	PK 11195	N			353	73	4.62	3.79	2.28±0.04
70	Propoxyphene	B		9.06	339	68	5.21	2.39	1.95±0.04
71	Propranolol	B		9.48	259	48	2.75	1.14	1.72±0.02
72	Quetiapine	B		6.92/3.96	384	53	2.99	2.80	1.79±0.08
73	Quinidine	B		8.59/4.36	324	79	2.79	2.06	1.39±0.13
74	Ranitidine	B		8.38	314	70	0.67	-0.83	0.00±0.26
75	Risperidone	B		8.31/3.45	410	79	2.71	1.87	0.96±0.21
76	9-hydroxy-Risperidone	B		8.28/2.43	426	53	1.07	1.17	1.42±0.11
77	Ritonavir	N			721	121	4.94	4.41	2.29±0.12
78	Rizatriptan	B		9.59/1.77	269	48	1.18	-0.74	0.46±0.19
79	Rofecoxib	N			314	57	1.80	1.81	1.66±0.11
80	Rolipram	N			275	43	1.72	1.91	1.01±0.05
81	saquinavir	B		7/3	671	145	4.73	4.09	2.99±0.40
82	Selegiline	B		7.46	187	40	3.02	2.21	2.14±0.06
83	Sertraline	B		9.48	306	44	5.35	3.00	2.87±0.08
84	Spiperone	B		8.29	395	69	2.82	2.55	2.14±0.08
85	Sulpiride	B	10.01	9.01	341	65	1.11	-1.15	0.52±0.76

No	Compound	Charge class[a]	pK_a (acid)[b]	pK_a (base)[b]	MW [g/mol]	A_D [c] [Å^2]	$c\log P$ [d]	$\log D'_{oct}$ (pH 7.4)[e]	$\log D'_{PAMPA}$ (pH 7.4)
86	Sumatriptan	B		9.49	295	59	0.74	-1.15	0.62±0.24
87	Tacrine	B		9.81	198	37	3.27	-0.06	-0.27±0.00
88	Temazepam	N	9.14		301	63	2.34	2.10	1.51±0.09
89	Theobromine	N	9.79		180	30	-0.67	-0.72	0.46±0.33
90	Theophylline	A	8.51		180	30	-0.03	-0.15	-0.14±0.23
91	Thiopental	A	7.5		242	41	2.98	2.68	0.70±0.84
92	Thioridazine	B		9.68	371	60	6.00	3.59	2.84±0.15
93	Thiothixene	B		7.75/3.59	444	64	3.23	3.22	2.29±0.18
94	Trazodone	B		6.81	372	48	3.85	2.61	1.58±0.02
95	Trifluperazine	B		8.43/3.74	407	56	4.69	3.99	2.78±0.34
96	Triprolidine	B		9.47/3.75	278	54	3.63	1.84	0.50±0.68
97	Valdecoxib	N	9.69		314	50	1.83	2.43	2.27±0.01
98	Venlafaxine	B		9.62	277	63	3.27	0.64	1.12±0.06
99	Verapamil	B		8.8	455	86	4.47	2.54	1.81±0.05
100	WAY 100635	B		6.71	423	105	4.09	3.05	1.50±0.02
101	Zaleplon	N			305	52	1.44	1.24	0.23±0.19
102	Ziprasidone	B		6.57	413	76	4.21	2.80	1.77±0.07
103	Zolmitriptane	B		9.6	287	53	1.29	-1.00	-0.12±0.54
104	Zolpidem	B		6.47	307	61	3.03	2.29	0.77±0.12

[a]neutral (less than 3 % ionization at pH 7.4); A: acid pK_a < 8.9; B: base pK_a >6; Z: zwitterions with acid pK_a <8.9 and base pK_a >6; [b]in-house measured (potentiometric); [c]calculated at pH 7.4 as described elsewhere [55]; [d] clog P v4.71 Daylight; [e]in-house CAMDIS $\log D'_{oct}$ (buffer: 50mM Tris, 114mM NaCl, pH 7.4)

FIGURES

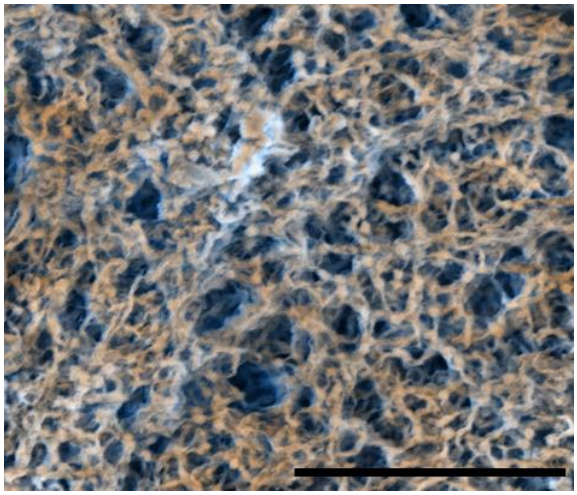

Figure 1 Scanning electron micrograph of the PAMPA membrane (polyvinylidendifluorid, Millipore, MAIPN, nominal pore size 0.45 μM, the length of the black line corresponds to 20 μM).

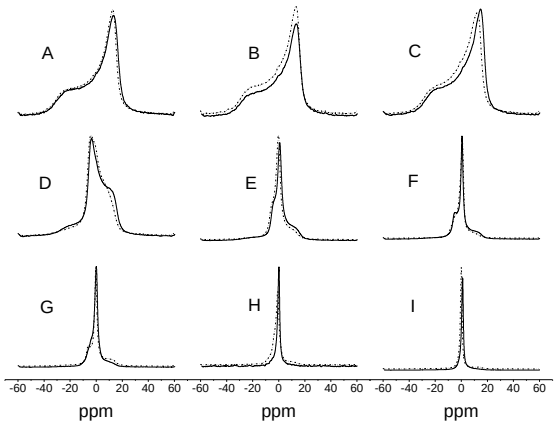

Figure 2 Experimental 162-MHz ^{31}P-NMR spectra (recorded at 25°C) of egg lecithin containing 45 mol H_2O per mol lipid and increasing amounts of n-dodecane: 0 (**A**), 0.25 (**B**), 0.5 (**C**), 1 (**D**), 2 (**E**), 3(**F**), 4(**G**), 5(**H**) and 33.5 (**I**) mol dodecane/mol lipid. Samples were prepared without (**—**) or with (**·····**) 10 % cholesterol (m/m lipid).

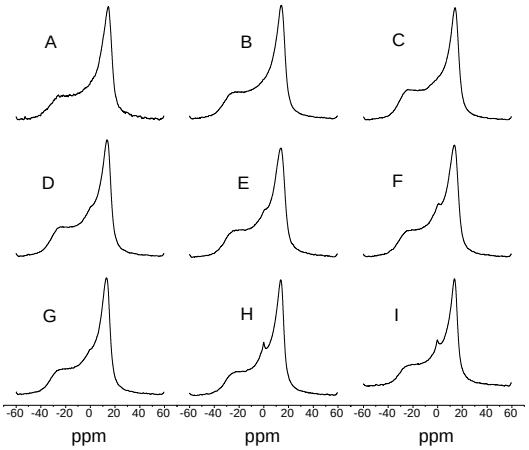

Figure 3 Experimental 162-MHz ^{31}P-NMR spectra (recorded at 25°C) of POPC containing 45 mol H_2O per mol lipid and increasing amounts of n-dodecane: 0 (**A**), 0.25 (**B**), 0.5 (**C**), 1 (**D**), 2 (**E**), 3(**F**), 4(**G**), 5(**H**) and 33.5 (**I**) mol dodecane/mol lipid.

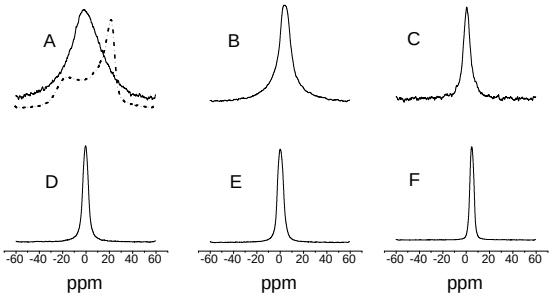

Figure 4 Experimental 162-MHz ^{31}P-NMR spectra (recorded at 25°C) of egg lecithin without additional H_2O and with increasing amounts of n-dodecane: 0 (**A**), 2 (**B**), 3 (**C**), 4 (**D**), 5 (**E**) and 33.5(**F**) mol dodecane/mol lipid. Samples were prepared with an "old" batch of egg lecithin stored for >3 month at 4-8°C (·····) in the fridge and, such as in the other series of experiments with a new batch (**—**). The data with the old and the new batch were not comparable up to 1 mol dodecane/mol lipid and therefore only higher dodecane/egg lecithin ratios are presented.

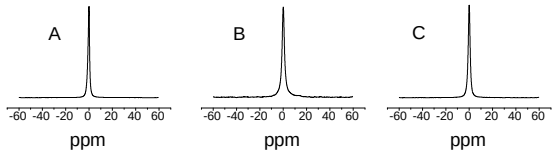

Figure 5 Experimental 162-MHz ^{31}P-NMR spectra (recorded at 25°C) of samples containing PAMPA lipid (10 % egg lecithin (m/V), 0.5 % cholesterol (m/V) in n-dodecane: (**A**) pure PAMPA lipid without filter device. (**B**) 40 stacks of hydrophobic PVDF filter devices (pore size 0.45 µm) impregnated with 4.5 µL of PAMPA lipid per filter. (**C**) according to (**B**) but each layer was separated by a hydrophilic PVDF filter device impregnated with 5 µL of H_2O.

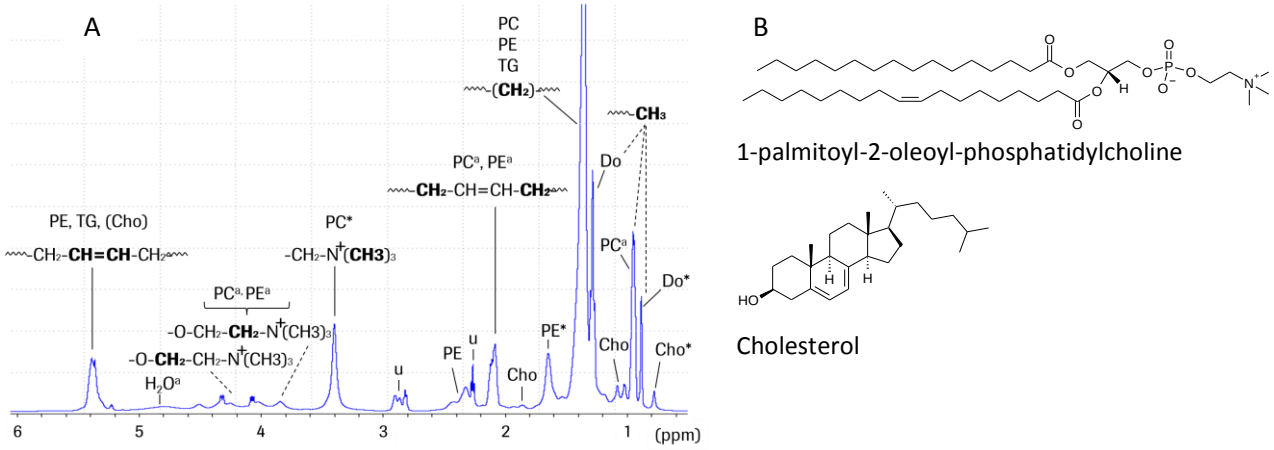

Figure 6 A: ^{1}H-NMR spectra of the PAMPA lipid solution (egg lecithin, 10 % (m/v) dissolved in n - dodecane-d-26). PC: phosphatidylcholine, PE: phosphatidylethanolamin, Cho: cholesterol, TG: triglycerides, Do: dodecane, u: unidentified, additional components present. **B:** Structures of the main components in the PAMPA lipid solution

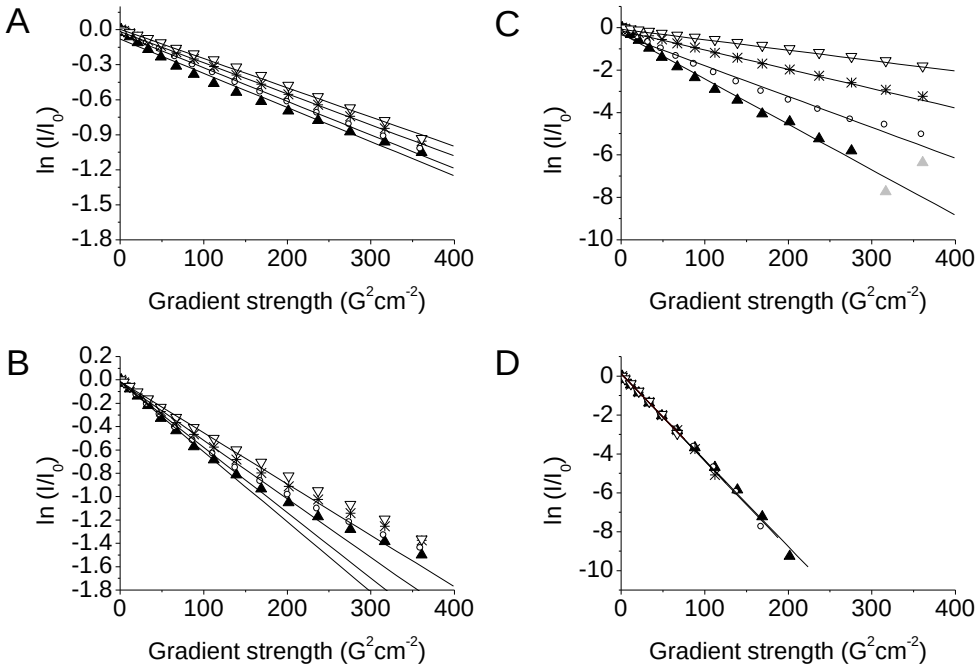

Figure 7 Echo attenuation of the ^{1}H resonances as a function of gradient strength. **A:** phosphatidylcholine (chemical shift 3.42 ppm), **B:** phosphatidylethanolamine (chemical shift 1.62 ppm), **C:** cholesterol (chemical shift 0.77 ppm) and **D:** dodecane (chemical shift 0.87 ppm). The concentration of egg lecithin in dodecane - d26 (m/v) was: 0.156 %(▲), 0.625 %(○), 2.5 % (✳) and 10 % (▽) corresponding to the PAMPA lipid solution and a 1:4, 1:16 and 1:64 dilution thereof in dodecane-d26. Lines are linear fits to the data. Grey symbols were not included in the fitting.

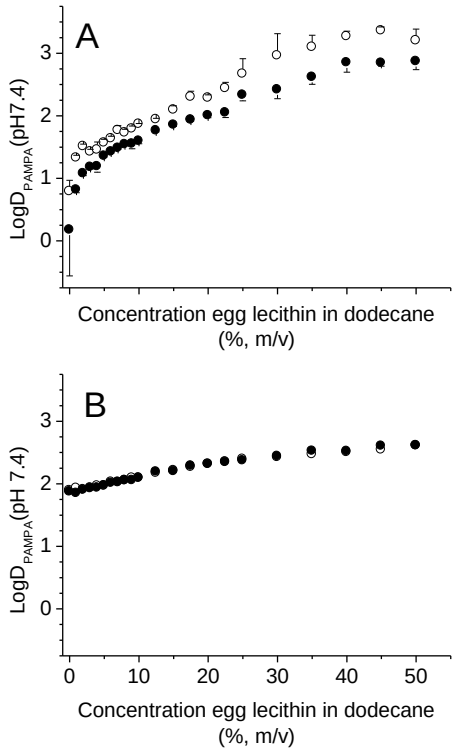

Figure 8 Egg-lecithin-dodecane/buffer distribution coefficients of (**A**) propranolol and (**B**) diazepam as a function of the amount of egg lecithin dissolved in dodecane. Distribution coefficients were measured at 25 µM (▲) and 100 µM (✳) initial drug concentrations. Only one direction for the standard deviation is shown in **A**. The standard deviation in B is not shown as it was smaller than the size of symbol.

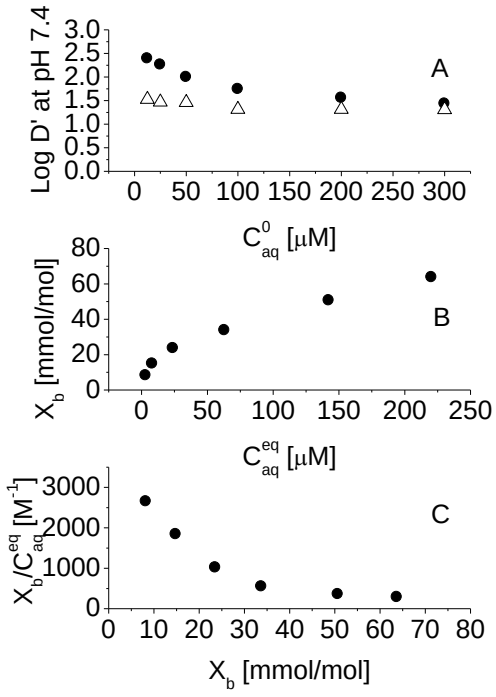

Figure 9 Binding data of propranolol. **A**: PAMPA lipid solution/buffer distribution coefficients (●) and octanol/buffer distribution coefficients (△) at pH 7.4 as a function of the total drug concentration (buffer : 50 mM Tris, 114 mM NaCl, pH 7.4). **B:** Adsorption isotherm. **C:** Scatchard plot.

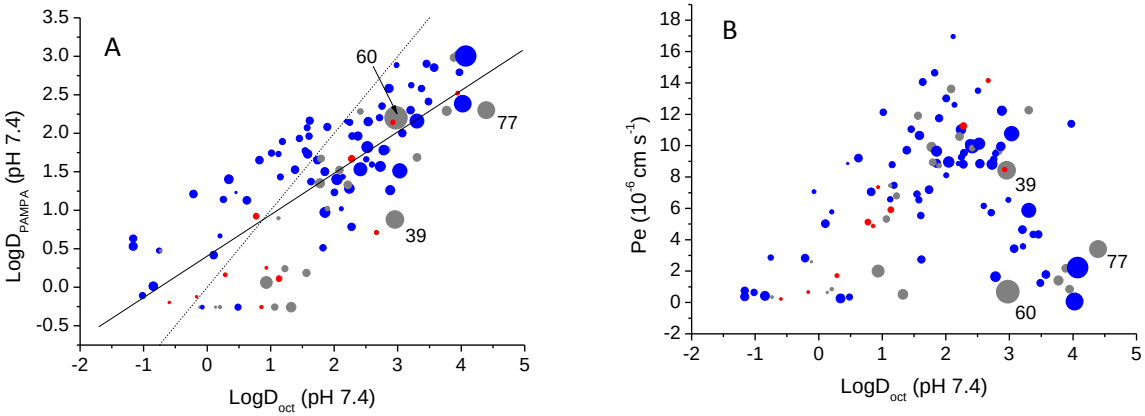

Figure 10 A: Relationship between the PAMPA - lipid solution/water distribution coefficients at pH 7.4 and the octanol/water distribution coefficients at pH 7.4 for a set of 104 structurally diverse drugs. (·····) line of identity, (**—**) linear regression line (correlation statistics: $\log D'_{PAMPA} = 0.538 \cdot \log D'_{oct} + 0.405$ (n = 104, $r^2 = 0.782$, SD = 0.571**). B:** Relationship between the effective permeability across the PAMPA barrier and $\log D'_{oct}$ for the same dataset. Colors according to charge class: nonionic (●), cationic (●), anionic (●); size according to the cross sectional area of the drug

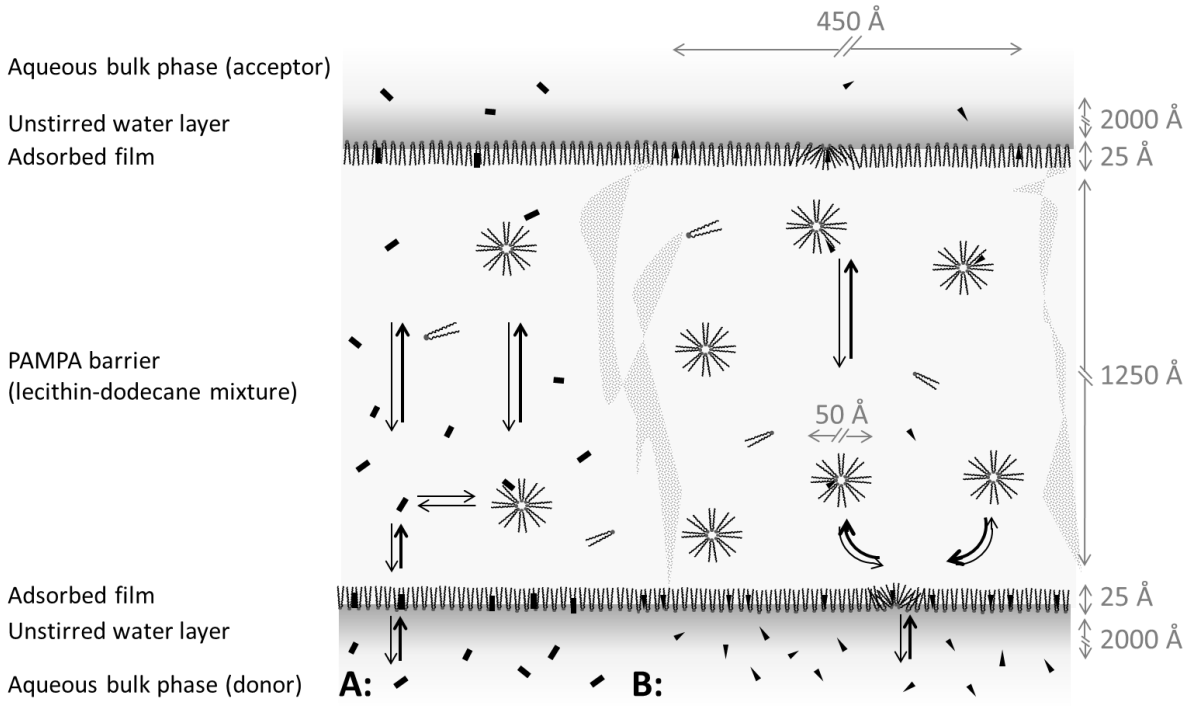

Figure 11 Hypothesized structure of the PAMPA barrier and two proposed mechanisms of transport. **A:** penetration across the PAMPA-lipid solution/water interface and transport via the continuous dodecane phase (light grey background). Once in the dodecane phase, the solute is also assumed to bind to and diffuse with the inverted micelles to the other liquid-liquid interface. The mechanism may play an important role for compounds with high solubility in dodecane. **B:** Direct transfer from the aqueous phase to the reverse micelles via the formation of a hemimicelle-like structure at the PAMPA-lipid solution/water interface. The drug-loaded reverse micelle detaches from the interface and diffuses to the other interface where the same mechanism takes place in a reverse order. Mechanism B is assumed to play a crucial role in the transport of amphiphilic drugs with low solubility in dodecane (black triangles). The irregular shaped regions denote the PVDF filter. Lipid in excess of the volume required to fill the pores is discounted.

Supporting Information

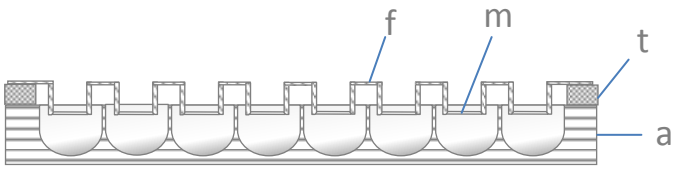

Figure S1 Assay construct for the measurement of distribution coefficients between the PAMPA-lipid solution and buffer. A 96 well filter plate (f) with a lipophilic membrane (m) fixed at the bottom of each single well was dipped into an acceptor Teflon plate (a) containing buffer spiked with the test compound. The filter membrane was pre-coated before with PAMPA-lipid solution. In order to avoid contact of the lipids with the borders of the acceptor plate, a Teflon frame (t) was constructed placed on top of the plane acceptor plate, carrying the filter plate and minimizing evaporation of the aqueous phase. The sandwich was left undisturbed for 22 h allowing the solute to distribute into the PAMPA-lipid solution. Afterwards the phases were separated by removal of the filter plate and the concentration in the aqueous phase was determined.

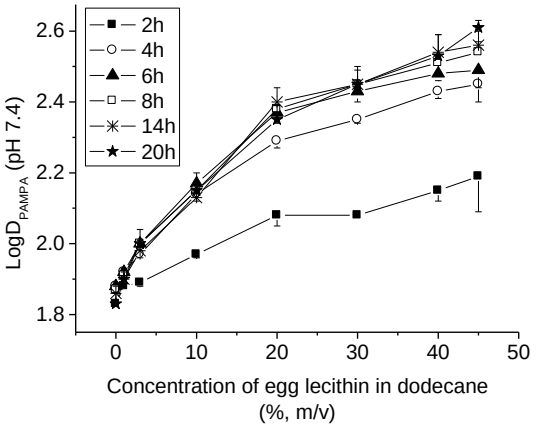

Figure S2 Apparent distribution coefficients of diazepam (C_{aq}^{0} = 100 µM) in the PAMPA - barrier/buffer system as measured for different contents of egg lecithin in dodecane. The $\log D'_{PAMPA}$ (pH 7.4) values were determined after 2 - 20 h incubation of both phases. Only one direction for the standard deviation is shown.

References

1. van de Waterbeemd, H., B. Testa, and Editors, *Drug Bioavailability; Estimation of Solubility, Permeability, Absorption and Bioavailability; Second, Completely Revised Edition. [In: Methods Princ. Med. Chem., 2009; 40]*2009. 623 pp.
2. Fischer, H., R. Gottschlich, and A. Seelig, *Blood-brain barrier permeation: molecular parameters governing passive diffusion.* J. Membr. Biol., 1998. **165**(3): p. 201-211.
3. Poole, S.K. and C.F. Poole, *Separation methods for estimating octanol-water partition coefficients.* J. Chromatogr., B: Anal. Technol. Biomed. Life Sci., 2003. **797**(1-2): p. 3-19.
4. Artursson, P. and J. Karlsson, *Correlation between oral drug absorption in humans and apparent drug permeability coefficients in human intestinal epithelial (Caco-2) cells.* Biochem. Biophys. Res. Commun., 1991. **175**(3): p. 880-5.
5. Kramer, S.D., et al., *Towards the predictability of drug-lipid membrane interactions: the pH-dependent affinity of propranolol to phosphatidylinositol containing liposomes.* Pharm. Res., 1998. **15**(5): p. 739-744.
6. Montal, M. and P. Mueller, *Formation of bimolecular membranes from lipid monolayers and a study of their electrical properties.* Proc. Nat. Acad. Sci. U. S. A., 1972. **69**(12): p. 3561-6.
7. Seydel, J.K., *Drug-membrane interaction and pharmacokinetics of drugs.* Methods Princ. Med. Chem., 2002. **15**: p. 141-215.
8. Leo, A., C. Hansch, and D. Elkins, *Partition coefficients and their uses.* Chem. Rev. , 1971. **71**(6): p. 525-616.
9. Qiu, X. and C. Pidgeon, *A phosphorus-31 NMR study of immobilized artificial membrane surfaces: structure and dynamics of immobilized phospholipids.* J. Phys. Chem., 1993. **97**(47): p. 12399-407.
10. Mensch, J., et al., *Novel generic UPLC/MS/MS method for high throughput analysis applied to permeability assessment in early Drug Discovery.* J. Chromatogr., B: Anal. Technol. Biomed. Life Sci., 2007. **847**(2): p. 182-187.
11. Gerebtzoff, G., et al., *Halogenation of drugs enhances membrane binding and permeation.* ChemBioChem, 2004. **5**(5): p. 676-684.
12. Anna Seelig, J.S., *Membrane Structure*. Encyclopedia of Physical Science and Technology. Vol. 9. 2002.
13. Boguslavsky, V., et al., *Effect of Monolayer Surface Pressure on the Activities of Phosphoinositide-Specific Phospholipase C-β1, -γ1, and -δ1.* Biochemistry, 1994. **33**(10): p. 3032-7.
14. Seelig, A., *The role of size and charge for blood-brain barrier permeation of drugs and fatty acids.* J. Mol. Neurosci., 2007. **33**(1): p. 32-41.
15. Xiang, T.-X. and B.D. Anderson, *Influence of chain ordering on the selectivity of dipalmitoylphosphatidylcholine bilayer membranes for permeant size and shape.* Biophys. J. , 1998. **75**(6): p. 2658-2671.
16. Gobas, F.A.P.C., et al., *A novel method for measuring membrane-water partition coefficients of hydrophobic organic chemicals: comparison with 1-octanol-water partitioning.* J. Pharm. Sci., 1988. **77**(3): p. 265-72.
17. Balon, K., B.U. Riebesehl, and B.W. Muller, *Drug liposome partitioning as a tool for the prediction of human passive intestinal absorption.* Pharm. Res., 1999. **16**(6): p. 882-888.
18. Kansy, M., F. Senner, and K. Gubernator, *Physicochemical high throughput screening: parallel artificial membrane permeation assay in the description of passive absorption processes.* J Med Chem, 1998. **41**(7): p. 1007-10.
19. Avdeef, A., *The rise of PAMPA.* Expert Opin. Drug Metab. Toxicol. , 2005. **1**(2): p. 325-342.

20. Tsinman, O., et al., *Physicochemical Selectivity of the BBB Microenvironment Governing Passive Diffusion-Matching with a Porcine Brain Lipid Extract Artificial Membrane Permeability Model.* Pharm. Res., 2011. **28**(2): p. 337-363.
21. Thompson, M., R.B. Lennox, and R.A. McClelland, *Structure and electrochemical properties of microfiltration filter-lipid membrane systems.* Anal. Chem., 1982. **54**(1): p. 76-81.
22. Phung, T., et al., *Porous materials to support bilayer lipid membranes for ion channel biosensors.* Int. J. Electrochem., 2011: p. 213107, 6 pp.
23. Wohnsland, F. and B. Faller, *High-Throughput Permeability pH Profile and High-Throughput Alkane/Water log P with Artificial Membranes.* J. Med. Chem., 2001. **44**(6): p. 923-930.
24. Sugano, K., et al., *High throughput prediction of oral absorption: Improvement of the composition of the lipid solution used in parallel artificial membrane permeation assay.* J. Biomol. Screening, 2001. **6**(3): p. 189-196.
25. Avdeef, A. and O. Tsinman, *PAMPA - A drug absorption in vitro model. 13. Chemical selectivity due to membrane hydrogen bonding: in combo comparisons of HDM-, DOPC-, and DS-PAMPA models.* Eur. J. Pharm. Sci., 2006. **28**(1-2): p. 43-50.
26. Sugano, K., et al., *Prediction of passive intestinal absorption using bio-mimetic artificial membrane permeation assay and the paracellular pathway model.* Int. J. Pharm., 2002. **241**(2): p. 241-251.
27. Seo, P.R., et al., *Lipid composition effect on permeability across PAMPA.* Eur. J. Pharm. Sci., 2006. **29**(3-4): p. 259-268.
28. Kansy, M., A. Avdeef, and H. Fischer, *Advances in screening for membrane permeability: high-resolution PAMPA for medicinal chemists.* Drug Discovery Today: Technol., 2004. **1**(4): p. 349-355.
29. Seelig, J., *Lipid polymorphism, reverse micelles, and phosphorus-31 nuclear magnetic resonance.* Reverse Micelles, [Proc. Eur. Sci. Found. Workshop], 4th 1984: p. 209-20.
30. Morris, K.F. and C.S. Johnson, Jr., *Resolution of discrete and continuous molecular size distributions by means of diffusion-ordered 2D NMR spectroscopy.* J. Am. Chem. Soc., 1993. **115**(10): p. 4291-9.
31. Stejskal, E.O. and J.E. Tanner, *Spin diffusion measurements: spin echoes in the presence of a time-dependent field gradient.* J. Chem. Phys., 1965. **42**(1): p. 288-92.
32. Wu, D., A. Chen, and C.S. Johnson, Jr., *An improved diffusion-ordered spectroscopy experiment incorporating bipolar-gradient pulses.* J. Magn. Reson., Ser. A, 1995. **115**(2): p. 260-4.
33. Holz, M., S.R. Heil, and A. Sacco, *Temperature-dependent self-diffusion coefficients of water and six selected molecular liquids for calibration in accurate 1H NMR PFG measurements.* Phys. Chem. Chem. Phys., 2000. **2**(20): p. 4740-4742.
34. Caudwell, D.R., et al., *The viscosity and density of n-dodecane and n-octadecane at pressures up to 200 MPa and temperatures up to 473 K.* Int. J. Thermophys., 2004. **25**(5): p. 1339-1352.
35. Avdeef, A., et al., *Drug absorption in vitro model: filter-immobilized artificial membranes. 2. Studies of the permeability properties of lactones in Piper methysticum Forst.* Eur J Pharm Sci, 2001. **14**(4): p. 271-80.
36. Nielsen, P.E. and A. Avdeef, *PAMPA--a drug absorption in vitro model 8. Apparent filter porosity and the unstirred water layer.* Eur J Pharm Sci, 2004. **22**(1): p. 33-41.
37. Armin Wendel, R.-P.R., *Lecithin*. Kirk-Othmer Encyclopedia of Chemical Technology., ed. Wiley.

38. Ruell, J.A. and A. Avdeef, *Absorption screening using the PAMPA approach.* Optim. Drug Discovery, 2004: p. 37-64.
39. Montal, M., *Formation of bimolecular membranes from lipid monolayers.* Methods Enzymol, 1974. **32**: p. 545-54.
40. Seelig, A., et al., *Binding of Substance P Agonists to Lipid Membranes and to the Neurokinin-1 Receptor*. Biochemistry, 1996. **35**(14): p. 4365-74.
41. Avdeef, A., *Absorption and drug development*2012: Wiley.
42. Nielsen, P.E. and A. Avdeef, *PAMPA-a drug absorption in vitro model 8. Apparent filter porosity and the unstirred water layer*. Eur. J. Pharm. Sci., 2004. **22**(1): p. 33-41.
43. Sjoelund, M., L. Rilfors, and G. Lindblom, *Reversed hexagonal phase formation in lecithin-alkane-water systems with different acyl chain unsaturation and alkane length.* Biochemistry, 1989. **28**(3): p. 1323-9.
44. Sjoelund, M., et al., *Hydrophobic molecules in lecithin-water systems. I. Formation of reversed hexagonal phases at high and low water contents.* Biophys. J., 1987. **52**(2): p. 145-53.
45. Kirk, G.L. and S.M. Gruner, *Lyotropic effects of alkanes and headgroup composition on the Lα-HII lipid liquid crystal phase transition: hydrocarbon packing versus intrinsic curvature.* J. Phys. (Les Ulis, Fr.), 1985. **46**(5): p. 761-9.
46. Luisi, P.L., B.E. Straub, and Editors, *Reverse Micelles: Biological and Technological Relevance of Amphiphilic Structures in Apolar Media*1984. 354 pp.
47. Schurtenberger, P., *Structure and dynamics of viscoelastic surfactant solutions - an application of concepts from polymer science.* Chimia, 1994. **48**(3): p. 72-8.
48. Angelico, R., et al., *Water Diffusion in Polymer-like Reverse Micelles. 2. Composition Dependence*. Langmuir, 1999. **15**(5): p. 1679-1684.
49. Ambrosone, L., et al., *Molecular diffusion in a living network.* Langmuir, 2001. **17**(22): p. 6822-6830.
50. Angelico, R., et al., *Structural investigation of lecithin/cyclohexane solutions.* Prog. Colloid Polym. Sci., 1999. **112**(Trends in Colloid and Interface Science XIII): p. 1-4.
51. Seelig, J., *31P nuclear magnetic resonance and the head group structure of phospholipids in membranes.* Biochim Biophys Acta, 1978. **515**(2): p. 105-40.
52. Price, W.S., *Pulsed-field gradient nuclear magnetic resonance as a tool for studying translational diffusion: Part 1. Basic theory.* Concepts Magn. Reson., 1997. **9**(5): p. 299-336.
53. Price, W.S., *Pulsed-field gradient nuclear magnetic resonance as a tool for studying translational diffusion: part II. experimental aspects.* Concepts Magn. Reson., 1998. **10**(4): p. 197-237.
54. Harmon, J., et al., *Determination of Molecular Self-Diffusion Coefficients Using Pulsed-Field-Gradient NMR: An Experiment for Undergraduate Physical Chemistry Laboratory*. J. Chem. Educ., 2012. **89**(6): p. 780-783.
55. Gerebtzoff, G. and A. Seelig, *In silico prediction of blood-brain barrier permeation using the calculated molecular cross-sectional area as main parameter.* J Chem Inf Model, 2006. **46**(6): p. 2638-50.

4.6 Evaluation of a Novel Lipid Membrane Binding Assay (LIMBA) for the Assessment of Brain Tissue Binding

Frauke Assmus, Anna Seelig, Holger Fischer

Author's Contributions:

Frauke Assmus	• Design of the study • Performing experiments and data analysis • Writing the manuscript
Anna Seelig	• Supervision of the work • Valuable discussions
Holger Fischer	• Idea of the study • Supervision of the work • Valuable discussions

ABSTRACT

The assessment of the unbound fraction of drug in brain, $f_{u,brain}$, is of major interest in CNS drug development in order to estimate active site, unbound drug concentrations from total drug exposure and moreover, to aid the understanding of pharmacokinetic/pharmacodynamics (PK/PD) relationships. Equilibrium dialysis with brain homogenate is commonly used to determine $f_{u,brain}$, however, relatively large amounts of brain tissue are required which hampers the application of the method for routine screening. In this study, we present a novel assay, referred to as Lipid Membrane Binding Assay (LIMBA), which enables the high-throughput measurement of brain tissue/ water distribution coefficients ($\log D_{brain}$) at minimal expense of animal tissue. LIMBA was validated on a set of 126 structurally diverse, marketed drugs with reported $f_{u,brain}$data obtained from equilibrium dialysis in rat and mouse. The accuracy of $f_{u,brain}$ predictions using LIMBA-$\log D_{brain}$ was evaluated in comparison with i) octanol/water distribution and partition coefficients ($\log D_{oct}$, $\log P$) and ii) fractions of drug retained in the permeation barrier of PAMPA. $LogD_{oct}$ and $\log P$ poorly described $f_{u,brain}$ (r^2 $\log D_{oct}$ = 0.23 , r^2 $\log P$ = 0.49), whereas an improved correlation was achieved with the membrane fraction in PAMPA (r^2= 0.61), provided that optimized lipid and buffer composition were used. LIMBA-$\log D_{brain}$ values yielded the best agreement with $f_{u,brain}$data (r^2= 0.74) and therefore we propose LIMBA as a viable alternative to equilibrium dialysis for the high throughput screening of brain tissue binding at significantly reduced consumption of animal tissue.

KEYWORDS

Brain tissue binding, Equilibrium dialysis, LIMBA

1. Introduction

One of the major challenges in CNS drug development is the design of compounds which are able to cross the blood brain barrier (BBB) with sufficient rate and extent [1-3] as a prerequisite for *in vivo* efficacy. Traditionally, the extent of brain penetration has been defined in terms of total brain to total plasma concentration ratios (K_p). However, according to the free drug hypothesis, unbound rather than total concentrations at the target site govern the pharmacological effect [4, 5] and hence it has been suggested to optimize compounds towards high unbound brain to unbound plasma concentrations ratios (K_{puu})[6]. Due to the presence of the blood brain barrier (BBB), constituted of endothelial capillary cells with tight junctions and active influx and efflux transporters, K_{puu}values in brain may significantly deviate from unity. In particular, P-glycorpotein (P-gp)-mediated efflux plays a crucial rule in the regulation and restriction of drug penetration into brain leading to unbound brain concentrations lower than those in plasma (K_{puu}<1) [7]. In order to derive the contribution of active transport at the BBB and to relate plasma to tissue pharmacokinetics, the measurement of plasma but also brain concentrations in the unbound state is required [3]. This may ultimately aid the understanding of dose-receptor occupancy relationships and allow for extrapolation of *in vitro* measurements to *in vivo* effects for the purpose of e.g. optimal dosing selection and compound prioritization.

Unbound drug concentrations in the interstitial fluid (ISF) in brain can experimentally be determined using *in vivo* microdialysis at steady state, however, the method is labor-intensive and not suitable for (mostly lipophilic) compounds adsorbing at the microdialysis equipment [6]. Alternatively, drug concentrations in the cerebrospinal fluid (CSF) from the cisterna magna have been used as surrogates for ISF, yet with limited value since the BBB and the blood-cerebrospinal fluid barrier (BCSFB) are separate barriers and concentrations in ISF and CSF may thus differ [3]. The measurement of total drug exposure in brain *in vivo* in combination with an *in vitro* method for the assessment of drug distribution within brain tissue provides a more viable and relevant approach for estimating unbound ISF drug levels [8].

The brain slice method is considered the gold standard *in vitro* method for measuring drug distribution in tissue because overall uptake including non-specific binding to phospholipid membranes and proteins, active uptake at the level of the brain parenchym as well as lysosomal trapping is quantified in terms of the volume of distribution of the unbound drug

($V_{u,brain}$) [9]. In contrast, the unbound fraction of drug in brain tissue ($f_{u,brain}$) available from equilibrium dialysis with brain homogenate reflects only the contribution of non-specific binding which, however, is the dominant factor of tissue distribution particularly for compounds with intermediate to high membrane affinity. Potential discrepancies between $f_{u,brain}$ and $V_{u,brain}$, associated with the disruption of subcellular compartments (e.g. acidic lysosomes) and the resulting depletion of intracellular pH gradients, can be corrected for by applying a mathematical pH partitioning model [8]. With the exception of compounds for which carrier-mediated cellular uptake may occur [8], equilibrium dialysis is therefore considered a reliable and more convenient alternative to the brain slice method which has found application in preclinical drug development programs.

A major drawback of the dialysis technique is, however, the requirement for relatively large amounts of tissue ($V_{\mathrm{homogenate}}$=150 µL) which limits the throughput of the method for ethical reasons. A high-throughput microemulsion electrokinetic chromatography (MEEKC) method working with lauric acid rather than biological tissue has been proposed for the prediction of drug distribution in brain tissue [10]. MEEKC retention factors showed a very good correlation with $f_{u,brain}$ on a set of 42 compounds, albeit, the correlation between retention factors and measured octanol-water partition coefficients ($\log P$) was likewise excellent. Thus, no general statement can be made of whether or not the MEEKC method is superior to measured $\log P$ regarding the prediction of tissue binding. Other authors [11] have used brain lipid membrane vesicles stabilized on silica beads (TRANSIL brain absorption), and membrane affinities have been correlated with $f_{u,brain}$ data showing a good agreement on a set of 65 drugs. Brain tissue obtained from porcine was still required for the preparation of the brain extract, yet only the lipid fraction was used for the preparation of membrane vesicles. It is also interesting to note that equilibrium dialysis with human embryonic kidney cells (HEK293) has recently been proposed as an inexpensive and easily available brain tissue surrogate resulting in binding data comparable with $f_{u,brain}$ values for a set of 46 drugs [12]. Importantly, system dependent differences in binding capacity had to be corrected for by deriving and applying a scaling factor which should accordingly be adjusted in other laboratories [12].

Certainly, all proposed methods based on brain tissue surrogates are valuable; nonetheless, the use of brain homogenate itself as the test tissue of interest may still be the closest approximation to the *in vivo* situation. The purpose of this study was to establish a novel *in*

vitro assay for the determination of non-specific binding of drugs to brain tissue. The assay, in the following referred to as Lipid Membrane Binding Assay (LIMBA), works with significantly reduced consumption of brain homogenate ($V_{homogenate}$=1.2 µL) as compared to equilibrium dialysis. We validated LIMBA on a set of 127 structurally diverse marketed drugs with reported $f_{u,brain}$ data obtained from equilibrium dialysis in rat and mouse. The accuracy of $f_{u,brain}$ predictions using LIMBA was evaluated in comparison with i) octanol/water distribution and partition coefficients ($\log D_{oct}$, $\log P$) available from a recently described Carrier Mediated Distribution System (CAMDIS) [13], and ii) fractions of drug retained in the permeation barrier of the parallel artificial membrane permeability assay (PAMPA). To the best of our knowledge, the membrane fraction in PAMPA has never been evaluated before in terms of the ability to predict drug distribution in tissue. A comparison between $f_{u,brain}$ prediction approaches based on CAMDIS $\log D_{oct}$ and $\log P$, the PAMPA membrane fraction as well as binding data measured with LIMBA is provided and results will be discussed in terms of the trade-off between prediction accuracy, practicability and the requirement for brain tissue.

2. Materials and Methods

2.1. Materials

Drugs were either available through our in-house Compound Depository Group as proprietary compounds or were purchased from ABX (Radeberg, Germany), AK Scientific (Mountain View, Ca), Acros Organics (Morris Plains, NJ), Aldrich (Milwaukee, WI), Bepharm Ltd. (Shanghai, China), Chem Pacific (Baltimore, MD), Fluka (Buchs, Switzerland), HRITIK Chemicals Cooperation (Mumbai, India), Molekula (Vaterstetten Germany), Sequoia (Pangbourne, UK), Socochim (Lausanne, Switzerland), TCI Europe (Zwijndrecht, Belgium), Tocris (Bristol, UK), TRC (Toronto, Canada) and Sigma (Steinheim, Germany).

Tris and sodium chloride were obtained from Fluka (Buchs, Switzerland). Tapso was obtained from AppliChem (Darmstadt, Germany). Mopso, octanol, glycocholic acid, egg yolk lecithin (60% TLC), cholesterol and dodecane were purchased from Sigma (Steinheim, Germany). Potassium hydrogen phthalate was obtained from Merck (Darmstadt, Germany). Brain polar and total lipid extract (porcine) were purchased from Avanti (Alabaster, AL). DMSO was obtained from Acros (Geel, Belgium). 2-propanol was purchased from Burdick & Johnson (Seelze, Germany). Buffer kits for CE- pK_a measurements were obtained from Advanced Analytical (Ames, IA). Water and acetonitrile for HPLC were supplied from Merck (Darmstadt, Germany) and were of HPLC-grade.

2.2. Compilation of a Validation Dataset

The literature was searched for compounds with reported $f_{u,brain}$ data as determined by means of equilibrium dialysis with brain homogenate. Since Wan et al. [14] demonstrated that species differences in drug binding to rat and mouse brain tissue can be neglected, $f_{u,brain}$ data measured in either or both species were included for the purpose of an extended dataset. However, if both rat and mouse data was reported within one single study [14], preference was given to rat data thus taking into account that LIMBA was conducted with rat brain homogenate. Drug binding to tissue was expressed as $\log((1-f_{u,brain})/f_{u,brain})$ and mean values from literature are reported.

2.3. Measurement of Brain Tissue/Water Distribution Coefficients with LIMBA

2.3.1. Experimental Setup

LIMBA is an *in vitro* assay for the measurement of the concentration ratio of a drug distributed between an aqueous phase and brain homogenate. The assay involves coating a filter support with brain homogenate and incubation of the coated filter with analyte-spiked aqueous phase as described in Fig. 1. The so formed sandwich can easily be disassembled to enable concentration analysis in the aqueous phase at steady state. The implementation in a 96 well plate format allows for the measurement of brain tissue/ water distribution coefficients ($\log D_{brain}$, see below) in a medium-to-high-throughput manner.

Fig. 1

2.3.2. Assay Protocol

Brain tissue (rat) /water distribution coefficients, $\log D_{brain}(pH\ 7.4)$, were determined with LIMBA as follows: On the day of the study, drug-naive female Wistar rats were sacrificed in a CO_2 chamber and the whole brain was sampled and immersed in assay buffer (50 mM TRIS/114 mM NaCl/ pH 7.4) to remove adherent blood. Experiments were conducted in accordance with the current Cantonal and Federal legislation on the welfare of experimental animals. The rat brain was weighted and homogenized on ice in 2 volumes (w/v) of n-dodecane using an ultrasonic probe (Branson sonifier, G. Heinemann, Schwäbisch Gmünd, Germany). A part of the fresh brain homogenate was used for the distribution experiments, and the rest was stored at 4°C for comparative purposes.

For the preparation of the aqueous phase, test compounds were introduced into the assay buffer (50 mM TRIS/114 mM NaCl/pH 7.4) as DMSO stock solutions (10 mM). The resulting aqueous drug solution (nominal concentration = 25 µM, DMSO content 0.25 %) was filtered (Millipore Deepwell Multiscreen Filter plate, MDRLN0410) into a 96-deep well receiver plate (NUNC, 278752) and aliquots of the filtrate (V_{aq} = 50 µL) were transferred into an in-house made Teflon plate. In parallel, the rat brain homogenate (V_{brain}=1.2 µL) was coated on a PVDF filter attached to the bottom of the customized and commercially available DIFI tubes (Weidmann Plastics Technology AG, Rapperswill, Switzerland, 23358) [15]. The pipetting of brain homogenate was conducted with a Hamilton robotic system using new

pipetting tips (10 µL disposable tips) for each coating step and a sealed 96 well PCR plate (Eppendorf) for the storage of brain homogenate. During the pipetting, the PCR plate was put on a shaker. The coated DIFI tubes were added on top of the Teflon plate pre-filled with aqueous drug solution thus forming a sandwich. The kit was sealed and allowed to shake at room temperature (RT) for 15 h. The incubation time was based on prior experiments showing that distribution equilibrium was achieved after 15 h. After removal of the DIFI tubes, the equilibrium drug concentration in the aqueous phase, C_{aq}^{eq}, was analyzed with HPLC - UV. A reference experiment was carried out in the same plate but without brain homogenate, to obtain the initial aqueous drug concentration, C_{aq}^{o}. $LogD_{brain}(pH7.4)$ values were obtained by mass balance according to,

$$LogD_{brain} = \frac{C_{aq}^{0} - C_{aq}^{eq}}{C_{aq}^{eq}} \cdot \frac{V_{aq}}{V_{brain}}, \quad (1)$$

All distribution experiments were performed in triplicate and mean $\log D_{brain}(pH7.4)$ values are reported.

2.4. Measurement of n-Octanol/Water Distribution Coefficients with CAMDIS

$LogD_{oct}(pH\,7.4)$ values were measured with CAMDIS, an in-house miniaturized shake flask assay based on the use of a filter-support for octanol as described above. Details about the validation of the assay are provided in our *accompanying manuscript 1* [13].

The assay protocol was very similar to LIMBA, however, the aqueous drug concentration of the filtrate was 100 µM (DMSO content 1 %, v/v) and the volume of the aqueous phase was V_{aq} = 150 µL. Different phase volume ratios were chosen to optimize CAMDIS and LIMBA in terms of applicability range. Drug concentrations in LIMBA were slightly lower as compared to CAMDIS to avoid saturation of binding sites (e.g. to phospholipids) in brain homogenate. In contrast to LIMBA; the filter support in CAMDIS was coated with octanol (V_{oct} = 1 µL and 15 µL; n = 3 for each volume) using of a Tecan robotic system. The octanol-coated DIFI tubes were incubated with the aqueous phase as described for LIMBA, however, the equilibration time was slightly longer in CAMDIS (16-22 h). $LogD_{oct}$ values were obtained by mass-balance according to the calculation of $LogD_{brain}$.

2.5. Measurement of PAMPA-Lipid Solution/Buffer Distribution Coefficients

Aqueous drug solutions (150 µM) were prepared by diluting DMSO stock solutions (10 mM) of the test compound in i) 50 mM MOPSO/0.5 % (m/v) glycocholic acid/ pH 6.5 ('Roche buffer'), ii) 50 mM MOPSO/pH 6.5 and iii) 50 mM Tris/114 mM NaCl/pH 7.4. The drug solution was filtered and a part of the filtrate (150 µL) was kept as a reference whereas another part (V_D = 320 µL) was transferred into a 96-well Teflon donor plate. The PAMPA membrane was formed by coating the filter (PVDF, pore size 0.45 µm) of a 96-well acceptor plate (Cat. 4550, Millipore, Billerica, MA) with a lipid-dodecane solution (10 %, m/v lipid: egg yolk lecithin, brain polar lipid or brain total lipids; V_M =4.5 µL). The acceptor filter plate and the donor plate were carefully assembled to form a sandwich. Blank assay buffer (V_A =280 µL, 50 mM Tris/114 mM NaCl/pH 7.4 or 50 mM MOPSO/pH 6.5) was added on top of the pre-coated filter plate. After 19.5 h incubation, the sandwich was separated and the amount of drug in the acceptor and donor compartment was determined by comparison with the UV spectra from the reference using a 96-well UV plate reader (Molecular Devices, model Spectra Max 190, Sunnyvale, CA and pION PSR4 p software). All measurements were performed in triplicate with an automated liquid handling system. Mass balance was used to determine the amount of drug remaining in the membrane barrier and the PAMPA-lipid solution/buffer distribution coefficient, $\log D_{PAMPA}$, was calculated according to:

$$LogD_{PAMPA} = \frac{C_M^{eq}}{C_A^{eq} + C_D^{eq}} \cdot \frac{V_D + V_A}{V_M}, \qquad (2)$$

where C_M^{eq}, C_D^{eq} and C_A^{eq} are the equilibrium drug concentrations in the PAMPA membrane, the donor and the acceptor compartment, respectively.

2.6. HPLC -MS Instrumentation and Chromatographic Conditions

Drug concentrations in aqueous solutions were quantified using an Agilent 1290 Infinity HPLC-MS system (Agilent Technologies, CA, USA) equipped with a DAD detector and an API single quadrupole mass spectrometer (Agilent 6140). An aliquot of each sample (5 µL) was injected onto a Kinetex 2.6 µm, 2.1 x 50 mm analytical column (Phenomenex, Germany) operated at 60°C. The mobile phase consisted of A (water) and B (acetonitril), both containing 0.1 % (v/v) formic acid. The gradient elution was performed as follows: initial 2 % B, 0 min - 0.35 min linear gradient from 2 % B to 95 % B, 0.35 min - 0.65 min 95 % B,

post time 0.5 min. After passing the DAD detector, the eluent was introduced into the electrospray interface maintaining the following source settings: capillary voltage + 3.5 kV, drying gas flow (N_2) 13 L/min, nebulizer pressure 60 psi, drying gas temperature 350°C. The integral of the pseudo - molecular ion intensity, $[M+H]^+$, was acquired in single reaction monitoring mode (SRM). Internal calibration for MS data analysis was accomplished by injection of 1, 3, and 5 µL of the sample solution. If UV sensitivity was sufficient, peak areas at appropriate wavelength were used for the calculation of $\log D_{oct}$ and $\log D_{brain}$.

2.7. Determination of Ionization Constants

Ionization constants (pK_a) were determined potentiometrically on a Gemini Profiler^{TM} (pION INC, Woburn, MA, USA). Solutions of cationic and non-charged compounds in KCL were pre-acidified to pH 1.8 - 3.5 with HCL and were titrated alkalimetrically with standardized KOH (0.5 M) to an appropriate pH (maximum pH 12.5). The measurement of acids started at pH 11 following titration with HCL (0.5 M). All measurements were carried out at 25°C, at constant ionic strength (0.15 M KCl), under Argon atmosphere. The initial pK_a - estimates, obtained from Bjerrum difference plots, were refined by a weighted non-linear least squares procedure [16] using the pS Data Refinement Program (pION, Version 3.2). The pK_a values of compounds which precipitated were obtained by extrapolation to about one pH unit outside the data range collected. The aqueous pK_a of thioridazine was obtained by Yasuda-Shedlovsky extrapolation of the pK_a values obtained in 35 - 65% (m/v) methanol. The pK_a of hydrocodone was determined by capillary electrophoresis (CE) on a pK_a Analyzer ProTM system as follows: sample solutions containing 0.25 mM test compound and 0.1 % DMSO as EOF (electroosmotic flow) marker were prepared in CE running buffer at 24 different pH values ranging from pH 1.8 -11. Aliquots of the filtrated sample solutions (10 nL) were injected into a 96-well fused–silica capillary device prefilled with aqueous running buffer. Separation followed after application of 3.5 kV and -0.2 psi. The effective mobility (µeff) was calculated at each pH from the migration time of DMSO and that of the test compound. The pK_a was derived from the inflection point in the µeff - pH plot.

2.8. ^{31}P-NMR Studies

Solid-state ^{31}P-NMR measurements were recorded on a Bruker Avance 400 spectrometer (Bruker AXS, Karlsruhe, Germany) operating at a phosphorous-31 frequency of 161 MHz and using a pulse-acquire sequence with broadband proton decoupling (400 MHz). The

recycling delay and the excitation pulse length was 6 s and 3 µs, respectively. A typical spectrum was obtained from 500 - 12.000 scans depending on the lipid content of the sample. The samples were prepared as follows: Drug-naive female wistar rats were sacrificed in a CO_2 chamber, the whole brain was sampled and immersed in assay buffer (50 mM Tris, 11 mM NaCl, pH 7.4). Brain tissue was homogenized on ice in i) 0.5, 1 and 2 volumes (w/v) of dodecane ii) in 2 volumes (w/v) of assay buffer(50 mM Tris, 114 mM NaCl, pH 7.4). The homogenates and undisrupted brain were transferred to in-house made glass tubes which were flame sealed (only the homogenate).

3. Results

3.1. Characterization of the Dataset

In order to test the predictive power of LIMBA for estimating drug binding to brain tissue, a dataset of 126 compounds with reported $f_{u,brain}$ data, obtained from equilibrium dialysis with brain homogenate (rat, mouse), was collated as described in Materials and Methods. The whole dataset was structurally diverse and included neutral, acidic, basic and zwitter-ionic compounds covering a broad physicochemical property space and a wide range of range of $f_{u,brain}$ (Table 1,2)

Table 1,2

For the stepwise optimization of LIMBA and PAMPA on a high quality dataset of reasonable size, a subset (Dataset 1) was selected with $f_{u,brain}$ data (rat or mouse) determined in at least two independent studies by means of equilibrium dialysis. Even though $f_{u,brain}$ data for theobromine and theophylline has only been determined within one equilibrium dialysis study, the compounds were included in Dataset 1 since $f_{u,brain}$ data obtained from equilibrium dialysis and the brain slice method were in excellent agreement. In contrast, caffeine, sumatriptan as well as NFPS were excluded due to high standard deviations (SD > 0.25 $f_{u,brain}$ units) between individual equilibrium dialysis studies (caffeine, sumatriptan) and between equilibrium dialysis and brain slice uptake data (NFPS), respectively. Dataset 1 was thus comprised of 35 drugs and covered a broad physicochemical property space, however with a smaller range in terms of lipophilicity and molecular weight (Table 1) as compared to the whole 126 compound dataset. The remaining compounds (n = 88), for which $f_{u,brain}$ data was available from only one equilibrium dialysis study, were assigned to Dataset 2.

3.2. Development of LIMBA

The basic concept of LIMBA was to facilitate the measurement of brain tissue/water distribution coefficients ($\log D_{brain}$) by immobilizing brain tissue on a filter support, thus preventing contamination of the aqueous phase with matrix components and allowing for convenient and complete phase separation after distribution equilibrium is achieved. As such, LIMBA can be considered a further development of CAMDIS, a recently described high-

throughput assay for the measurement of $\log D_{oct}$, which likewise involves the use of a filter support for the lipophilic phase [13]. Whilst octanol is used in CAMDIS, the filter in LIMBA is impregnated with brain tissue homogenized in a solvent. Various combinations of solvents and filter supports for the homogenization and immobilization of brain tissue, respectively, were investigated, including water and organic solvents as well as hydrophobic and hydrophilic filters materials. As outlined in the Supporting Information, dodecane in combination with a hydrophobic PVDF filter was most suitable since homogenates amenable for pipetting were obtained and contamination of the aqueous phase with brain tissue was prevented.

Details about the development of LIMBA in terms of equilibration time, selection of drug concentrations, influence of the presence of DMSO on tissue binding as well reproducibility are described in the Supporting Information. A summary of the selected experimental conditions is provided in Table 3.

Table 3

It is worth emphasizing that LIMBA is generally conducted with brain homogenate from rat, however, a comparison between LIMBA $\log D_{brain}$ values in rat and mouse, using a subset of compounds from Dataset 1, showed that species differences are negligible (Fig. S4, Supporting Information) which is in line with literature [14]. Therefore a comparative evaluation of LIMBA $\log D_{brain}$(rat) values and $f_{u,brain}$data (rat, mouse) collated from literature is valid and will be presented in the following along with results from other membrane surrogate systems, i.e. CAMDIS and PAMPA.

3.3. Comparative Evaluation of LIMBA, CAMDIS and PAMPA for the Prediction of Brain Tissue Binding (Dataset 1)

3.3.1 The Relationship between $\log D_{brain}$ (LIMBA) as well as $\log D_{oct}$ (CAMDIS) and Equilibrium Dialysis Data

The relationship between drug binding to brain tissue (equilibrium dialysis data), expressed as $\log((1-f_{u,brain})/f_{u,brain})$, and $\log D_{brain}$ (pH 7.4) measured with LIMBA is presented in Fig. 2A at the example of 27 test compounds from Dataset 1.

Fig. 2

Selegilin, carisoprodol and meprobamate were excluded due to poor analytics and only compounds within the applicability range of LIMBA ($\log D_{brain} > 0.4$) are shown, yielding the following correlation statistics:

$$\log((1 - f_{u,brain}) / f_{u,brain}) = 1.102 * \log D_{brain} \text{ (pH 7.4)} - 0.346 \quad (3)$$

($r^2 = 0.911$, n = 27)

The slope close to 1 and the intercept close to 0 indicate excellent agreement between LIMBA and equilibrium dialysis data for all compounds, however, it is important to note that Dataset 1 is dominated by neutral and basic compounds whereas only two weak acids were measured.

In contrast to LIMBA, $\log D_{oct}$ (pH 7.4) only poorly described $\log((1 - f_{u,brain}) / f_{u,brain})$ (Fig. 2B, $r^2 = 0.518$, n = 35), especially for lipophilic basic compounds whose tissue binding was under-predicted by $\log D_{oct}$. Interestingly, the correlation of $\log((1 - f_{u,brain}) / f_{u,brain})$ with $\log P$ rather than $\log D_{oct}$ (pH 7.4) yielded improved prediction accuracy ($r^2 = 0.827$, n = 35) due to less deviation of basic compounds from the correlation line. Note that 35 compounds could be measured with CAMDIS, however, when relying statistics on 27 compounds amenable for measurement with LIMBA, the ranking of surrogate systems according to their correlation with equilibrium dialysis data remained the same (LIMBA $\log D_{brain} > \log P >$ CAMDIS $\log D_{oct}$) (Table 4).

Table 4

3.3.2 The Optimization of PAMPA and the Relationship between $\log D_{PAMPA}$ and Equilibrium Dialysis Data

PAMPA has been introduced as a more physiologically relevant system for the screening of passive permeability as compared to preceding methods largely based on organic solvent/water partitioning [17]. The permeation barrier in PAMPA usually consists of synthetic or natural phospholipids (e.g. egg yolk lecithin, exception Novartis: 100 % hexadecane) dissolved in excess organic solvent (e.g. n - dodecance) and coated on a filter support (e.g. (PVDF). The permeation of test compounds from an aqueous donor

compartment across the so formed membrane into an aqueous acceptor compartment can be measured and is corrected for the fraction of drug retained in the membrane. A drug's membrane retention is therefore a side product which we evaluated in terms of its surrogate properties for the prediction of drug binding to brain tissue.

It is worth noting that considerable efforts have been put into optimization of PAMPA, towards improved predictability of e.g. gastrointestinal drug absorption and BBB permeation. Every individual component has been varied including the organic solvent (*e.g. dodecane* [17], *hexadecane* [18], *1,7 octadiene* [19], the lipid (*1-palmitoyl-2-oleoyl-phosphatidylcholine (POPC), soy lecithin* [20], *brain polar lipids, biomimetic lipid mixtures* [21]), the filter unit (*PVDF* [17], *polycarbonate* [18]) as well as the buffer composition [22]. In this study, the PAMPA setup routinely applied at Roche was investigated and used as a starting point for the optimization towards improved predictive power for brain tissue binding. The modification of the buffer and lipid composition was thereby inspired by previously reported optimization strategies with regard to the prediction of *in vivo* permeability (a summary of experimental conditions used in this study is provided in Table 4).

Fig. 3A-F show the correlation between literature $\log((1-f_{u,brain})/f_{u,brain})$ data obtained from equilibrium dialysis and $\log D_{PAMPA}$ at the example of 32 test compounds from Dataset 1 (same exclusion criteria like for CAMDIS $\log D_{oct}$, in addition carisoprodol, meprobamat and selegiline were excluded due to poor UV absorption), and for the different setups investigated. The standard Roche setup (donor and acceptor: pH 6.5; donor spiked with glycocholic acid; membrane: 10% (m/v) egg lecithin in dodecane) yielded poor correlation statistics ($r^2 = 0.521$) and high standard deviations (Fig. 2A), however, both parameters improved when omitting glycocholic acid from the donor compartment (Fig. 2B). Lower standard deviations in absence of glycocholic acid indicate that the solubilizer distorts the integrity of the PAMPA membrane. Moreover, $\log D_{PAMPA}$ (pH 6.5) values in presence of glycocholic acid were lower for 27 of 32 compounds than in its absence which can be explained by the shift in distribution equilibria towards drug solubilized in glycocholic acid micelles (exceptions are the acid theophylline, the weak bases zolpidem and trazodone, as well as hydrocodone and methylphenidate (both showing poor UV absorption)). The effect of solubilization is missing in literature equilibrium dialysis studies, and even though drug binding to plasma proteins *in vivo* might occur, it adds an undesired layer of complexity to the *in vitro* data and leads to a prediction bias towards underestimated drug binding to brain

tissue, in particular for lipophilic basic drugs (see deviation of correlation line at $\log((1-f_{u,brain})/f_{u,brain}) > 1.8$).

Apart from the effect of glycocholic acid, the pH in the Roche setup (pH 6.5) also deviates from the pH in brain ISF (pH 7.3 [8]) giving rise to higher ionized fractions of drugs with a basic pK_a and, in turn, a decrease of drug retention in the PAMPA membrane. In order to conduct measurements at physiological conditions, $\log D_{PAMPA}$ values were measured at pH 7.4 (absence of glycocholic acid) leading to increased binding of basic drugs with intermediate to high lipophilicity and further improved correlation with $\log((1-f_{u,brain})/f_{u,brain})$ (Fig. 2C, $r^2 = 0.791$). However, the trend towards increased binding was not observed for all basic drugs.

In the next step, the optimized buffer composition was adopted (pH 7.4, no glycocholic acid) and the effect of lipid composition on the performance of tissue binding prediction with PAMPA was investigated. Due to the large excess of dodecane in the egg lecithin-solvent mixture (10% (m/v) egg lecithin) applied above, the question as to the relevance of phospholipids for the extent of membrane retention arises. Fig. 2D shows that omitting egg lecithin from the lipid mixture and performing experiments with pure dodecane drastically decreases the correlation with $\log((1-f_{u,brain})/f_{u,brain})$ ($r^2 = 0.326$), and increases the trend towards under-prediction of brain tissue binding, in particular for lipophilic basic drugs. However, a reduction in membrane retention in absence of egg lecithin was not evident for all drugs (e.g. chlorpromazine) and further research is required to understand the nature of the binding process (*accompanying manuscript 5*)

In contrast to egg lecithin, brain tissue is relatively rich in acidic phospholipids (between 9.4 and 20.8 % of total phospholipids) as estimated from the phospholipid composition in brain tissue reported for rat [23]. In order to remain as close as possible to the *in vivo* situation, it would be preferable to use the brain homogenate applied in LIMBA for the formation of a permeation barrier in PAMPA, however, the addition of an aqueous acceptor phase on top of the coated filter distorted the barrier integrity. In contrast, lipids extracted from porcine brain and dissolved in dodecane (10% (m/v) lipid) yielded stable membranes in presence of the acceptor phase which allowed for the measurement of $\log D_{PAMPA}$ values with commercially available i) brain total lipid (BTL) extract and ii) brain polar lipid (BPL) extract. An inspection of the lipid composition (Table 5) reveals that both brain extracts contain higher amounts of negatively charged phospholipids (egg lecithin < BTL < BPL) and lower amounts

of net neutral phosphatidylcholine as compared to egg lecithin used in the standard PAMPA setup at Roche.

Table 5

Fig. 3C, E, F shows the correlation between $\log((1 - f_{u,brain}) / f_{u,brain})$ (equilibrium dialysis data) and $\log D_{PAMPA}$ (pH 7.4) values derived from experiments with egg lecithin (Fig. 3C, r^2=0.791), BTL extract (Fig. 3E, r^2=0.800) and BPL extract (Fig. 3F, r^2=0.850). Only minor differences between $\log D_{PAMPA}$ (pH 7.4) from the different setups were observed with slightly more pronounced binding of hydrophilic basic compounds to membranes formed from BPL and egg lecithin as compared to BTL. Since a major part of the lipid extracts was uncharacterized, further research is required to understand the rather good agreement between BPL and egg lecithin data despite the higher content of negatively charged phospholipids in BPL extract. From a theoretical point of view, the presence of negatively charged phospholipids should lead to electrostatic attraction of basic compounds, and. in turn, an increase of drug binding to BPL. The best overall correlation statistics was, albeit, obtained with BPL extract (r^2 = 0.850) which we therefore used for further investigation on an extended dataset, along with the egg lecithin-dodecane mixture for comparative purposes. More information about the optimization of PAMPA is provided in the Supporting Information showing 1:1 correlations of $\log D_{PAMPA}$ data obtained with the various experimental conditions (Figure S5).

3.4. Comparative Evaluation of CAMDIS, Optimized PAMPA, LIMBA and Equilibrium Dialysis on an Extended Dataset

The correlations shown in Section 3.2 were based on high quality $f_{u,brain}$ data reported in at least two independent studies showing that LIMBA $\log D_{brain}$(pH 7.4) values were in best agreement with equilibrium dialysis data. Good correlation statistics were also obtained with $\log D_{PAMPA}$ available from the optimized PAMPA setup (pH 7.4, no glycocholic acid, membrane formed of BPL in dodecane) as well as measured $\log P$ data, even though in the latter case previous literature reports suggest that a considerable scatter in the correlation may be encountered [14, 24]. However, the physicochemical property space of Dataset 1 was limited and dominated by neutral and basic compounds.

In order to test the predictive power of LIMBA $\log D_{brain}$(pH 7.4) in comparison with i) $\log D_{oct}$ (pH 7.4), ii) $\log P$ (CAMDIS) and iii) $\log D_{PAMPA}$ (pH 7.4, optimized setup) on an extended dataset, compounds from Dataset 2 were measured in each assay allowing for the evaluation of assay performances on the complete 126 compound dataset. Fig. 4A-F show the correlations between $\log((1-f_{u,brain})/f_{u,brain})$ and the various surrogate parameters confirming poor predictive power of $\log D_{oct}$ (pH 7.4) (Fig. 4A, r^2=0.564, n = 112, for exclusion criteria see Fig. 4) as already observed with Dataset 1.

Fig. 4

It was also confirmed that predictions of brain tissue binding based on measured and calculated $\log P$ data improved the correlation statistics (r^2=0.606 and r^2=0.649, respectively, n = 112) however, a considerable scatter of the data was still evident (Fig. 4B,C). It is worth noting that brain tissue binding of acidic compounds tend to be under-predicted by measured $\log P$, and to a minor degree by calculated $\log P$ values , which can be explained by i) electrostatic repulsion of acidic compounds from negatively charged phospholipids present in brain tissue but not in octanol, and ii) by the disregard of ion partitioning when extrapolating $\log P$ data from measured $\log D_{oct}$ (pH 7.4) and pK_a using the Hendersson-Hasselbalch equation. The resulting overestimation of $\log P$ is the higher, the higher the discrepancy between pH = 7.4 and the pK_a, which explains the pronounced deviation from the correlation line for compounds with low acidic pK_a values.

With respect to the performance of $\log D_{PAMPA}$ (pH 7.4) (optimized PAMPA setup), improved correlation statistics were obtained as compared to prediction approaches based on $\log D_{oct}$ (pH 7.4) and $\log P$. More specifically, it was confirmed that drug distribution into membranes constituted of egg lecithin (Fig. 4D) and BPL extract (Fig.4 E) was similar and resulted in the same trend towards generally reasonable correlations with $\log((1-f_{u,brain})/f_{u,brain})$. However, brain tissue binding for compounds with $\log((1-f_{u,brain})/f_{u,brain}) > 2.5$ was underestimated.

Among all investigated surrogate systems, LIMBA $\log D_{brain}$(pH 7.4) was in best agreement with brain tissue binding available from equilibrium dialysis (Fig. 4F, r^2=0.741, n = 73), however, a trend towards underestimation of $\log((1-f_{u,brain})/f_{u,brain})$ for acidic and zwitterionic compounds was evident in both PAMPA and LIMBA. A strong outlier,

ziprasidone (base), was observed in each surrogate assay, which, may thus be explained by experimental variability in the equilibrium dialysis study (only one reported $f_{u,brain}$ value was available).

3.5. The Influence of Dodecane on the Lipid Organization in LIMBA

As outlined above and in the Supporting Information, dodecane was used for the homogenization of brain tissue, which may have an influence on the organization of phospholipids (e.g. formation of hexagonal and iotropic phases) as reported for other lipid-organic solvent-water systems [25-27]. Therefore, we investigated the phospholipid organization in brain tissue as well as brain tissue homogenized in i) water and ii) dodcane, at a constant tissue:solvent ratio (1:2 (m/v), Fig. 5A), and at increasing concentrations of dodecane (Fig.5B).

Fig. 5A shows typical bilayer NMR spectra for undisrupted brain tissue and brain tissue homogenized in water, which, however, were superimposed by an isotropic phase in presence of dodecane that becomes the more pronounced the higher the dodecane content. At the tissue:dodecane ratio used in LIMBA (1:2 (m/v)), a portion of bilayer was still present, yet with a not further quantified portion of isotropic phase pointing to the formation of reversed micelles.

Fig. 5

4. Discussion

Equilibrium dialysis is a standard method for the measurement of tissue binding, however, the requirement for relatively large amounts of animal tissue limits the throughput of the technique and alternative assays relying on lower or less consumption of animal tissue were investigated during the course of this study. In particular, we have developed a novel Lipid Membrane Binding Assay (LIMBA) for the assessment of drug binding to brain tissue, which was evaluated in comparison with other membrane surrogate systems, i.e. CAMDIS and PAMPA, in terms of their agreement with $f_{u,brain}$ data available from equilibrium dialysis.

The poor correlation between $\log D_{oct}$ (pH 7.4) (CAMDIS) and $\log((1-f_{u,brain})/f_{u,brain})$ (equilibrium dialysis) confirms results from previous studies on smaller datasets [28] and can partly be explained by the higher contribution of ionized species to overall membrane binding as compared to drug distribution into octanol dominated by the non-ionized form [22]. Moreover, the presence of negatively charged phospholipids in tissue but not octanol gives rise to electrostatic attraction of cationic drugs resulting in increased membrane binding. For instance, Yata et al. showed that the extent of tissue binding is positively correlated to the content of negatively charged phosphatidylserine [29] as observed for a range of different tissues and drugs. Accordingly, it can be explained that the underestimation of brain tissue binding by $\log D_{oct}$ (pH 7.4) for basic compounds is less pronounced when relying prediction approaches on $\log P$ leading to improved overall correlation statistics. Yet, octanol lacks the anisotropy and asymmetry of a biological membrane [7], and therefore it is not surprising that $\log D_{PAMPA}$ (PAMPA), reflecting drug distribution into reverse micelles formed from phospholipids in dodecane (*accompanying manuscript 5*), showed better agreement with $\log((1-f_{u,brain})/f_{u,brain})$. It is important to note that reasonable correlation statistics were only obtained with an optimized PAMPA setup (pH 7.4, no solubilizer, BPL membrane) whereas the default setup at Roche performed poorly due to the non-physiological pH (with respect to brain) and membrane composition as well as the disturbance of the membrane integrity in presence of solubilizers.

From all surrogate systems investigated, $\log D_{brain}$ (pH 7.4) values measured with LIMBA were in best agreement with equilibrium dialysis data, reflecting the fact that brain tissue homogenized in dodecane is the closest approximation of the *in vivo* situation with respect to surrogate systems tested within this study. The miniaturized format of LIMBA allows working with minute amounts of brain homogenate (V_{brain} = 1.2 µL), which is optimized for

the characterization of compounds with intermediate to high tissue binding ($\log D_{brain} > 0.4$) matching the typical physicochemical property space encountered in drug development programs. A trend towards under-prediction of brain tissue binding was observed for anionic and zwitterionic compounds in both LIMBA and PAMPA which might be explained by the negative surface potential of the PVDF filter support for the tissue surrogate, giving rise to reinforced electrostatic repulsion of compounds with an acidic pK_a. However, cationic and non-ionic compound predominate in most drug discovery programs.

The good agreement between LIMBA $\log D_{brain}$ and equilibrium dialysis data for this majority of compounds demonstrates that preparing tissue homogenate in dodecane (rather than aqueous buffer) does not change the ranking between the two tissue binding scales, with respect to the chemical space investigated. In this regard, it is important to note that compounds with a high likelihood for adsorption to Teflon (predominantly large and lipophilic compounds, for prediction model see *accompanying manuscript 2*) were excluded from the dataset to avoid experimental artifacts. However, the NMR spectra showed that dodecane disrupts the phospholipid bilayer of undisrupted brain tissue in favor of an isotropic phase suggesting the formation of reverse micelles. Since the insertion into densely packed bilayers requires more energy than the insertion into isotropic systems [7], a deviation from the good agreement between LIMBA and equilibrium dialysis data for larger compounds is thus likely. Further research is required to address this question.

5. Conclusions

In summary, we have demonstrated on a large dataset that octanol is only a poor surrogate for brain tissue binding ($\log((1-f_{u,brain})/f_{u,brain})$ measured with equilibrium dialysis, even though slightly improved prediction accuracy was achieved when using $\log P$ rather than $\log D_{oct}$ (pH 7.4). The correlation with equilibrium dialysis data further improved when using the fraction of drug retained in the PAMPA membrane, provided that experiments were conducted under optimized experimental conditions in terms of buffer and lipid composition (brain polar lipids). The best agreement with equilibrium dialysis data was yielded when relying predictions on $\log D_{brain}$ values available through the novel LIMBA assay, albeit tissue binding for acidic and zwitter-ionic compounds was slightly under-predicted. With this limitation, LIMBA may provide a useful alternative to equilibrium dialysis for the medium-to-high throughput screening of drug binding to brain tissue, at significantly reduced consumption of brain homogenate.

Acknowledgements

The authors thank Björn Wagner for excellent help with the $\log D_{oct}$ measurements.

TABLES

Table 1 Key molecular properties of the complete dataset and the subset (Dataset 1) used for the development and comparative evaluation of CAMDIS, PAMPA and LIMBA.

Parameter	Range	
	n = 126, whole dataset	n = 36, Dataset 1
$f_{u,brain}$ [%]	0.009 - 100	0.078 - 83%
Molecular weight [g/mol]	146 - 875	151 - 477
Highest basic pK_a - lowest acidic pK_a	10.59 - 1.94	10.13 - 1.94
$c\log P$ [a]	-2.5 - 6.1	-0.67 - 5.35
$\log D_{oct}$ at pH 7.4 (shake flask)	-2.0 - 5.4	-1.15 - 3.32

[a] $c\log P$ v4.71 Daylight

Table 2 Physicochemical properties of the compounds investigated (n=126) along with CAMDIS, PAMPA, LIMBA data as well as literature fraction unbound brain data obtained from homogenate dialysis.

			Ionization state			Calculated Properties			CAMDIS		PAMPA	LIMBA	Equilibrium Dialysis	
No.	Compound[a]	Data set[b]	Charge class[c]	pK_a (acid)[d]	pK_a (base)[d]	MW [e] [g/mol]	A_D [f] [Å^2]	$c\log P$ [g]	$m\log P$ [h]	$\log D_{oct}$ (pH 7.4) ± SD	$\log D_{PAMPA}$ (pH 7.4) [i] ± SD	$\log D_{brain}$ (pH 7.4) ± SD	$f_{u,brain}$ [%] ±SD	Reference
1	Buspirone	1	B		7.61	386	39.5	2.19	2.55	2.13±0.03	1.20±0.04	1.10±0.05	19.0±4.2	[1, 2]
2	Caffeine[a1]	1	N		<2	194	28.6	-0.04	-0.10	-0.10±0.04	-0.05±0.38	<0.4	81.0±41.0	[1, 3]
3	Carbamazepine	1	N			236	59.8	2.38	1.58	1.58±0.04	0.34±0.54	0.70±0.10	12.1±2.9	[1, 2, 4, 5]
4	Carisoprodol	1	N			260	61.2	2.34	2.16	2.16±0.03	[j]	<0.4[j]	28.1±11.2	[1, 2]
5	Chlorpromazine	1	B		9.38	319	47.8	5.30	5.21	3.23± 0.02	2.41±0.18	2.97±0.13	0.1±0.1	[1, 2, 4]
6	Citalopram	1	B		9.52	324	62.0	3.13	3.52	1.40±0.01	1.37±0.03	1.70±0.02	3.6±0.9	[1, 2, 4, 5]
7	Clozapine	1	B		7.68/3.9	327	53.3	3.71	3.19	2.73±0.01	1.90±0.02	2.23±0.09	1.0±0.1	[1, 2, 4]
8	Cyclobenzaprine	1	B		9.32	275	53.2	5.10	4.93	3.00±0.03	2.16±0.05	2.47±0.11	0.7±0.1	[1, 2]
9	Diazepam	1	N		3.38	285	57.9	2.96	2.84	2.84±0.05	1.68±0.11	1.60±0.03	4.3±0.7	[1, 2, 4]
10	Fluoxetine	1	B		9.71	309	58.9	4.57	4.22	1.91±0.05	2.07±0.04	2.67±0.04	0.2±0.1	[1-4]
11	Fluvoxamine	1	B		9.11/5.82	318	55.3	3.03	3.29	1.56±0.02	1.70±0.06	2.40±0.07	0.8±0.0	[1, 2]
12	Haloperidol	1	B		8.64	376	78.9	3.85	4.00	2.74±0.04	1.76±0.06	2.16±0.05	0.9±0.2	[1, 2, 4]
13	Hydrocodone	1	B		8.9	299	54.1	1.13	1.78	0.27±0.01	0.14±0.71	0.50±0.06	53.5±2.1	[1, 2]
14	Hydroxyzine	1	B		7.51/2.66	375	62.7	4.00	3.45	3.09±0.04	1.82±0.08	1.97±0.07	1.2±0.2	[1, 2, 6]
15	Lamotrigine	1	N		5.51	256	35.0	2.53	1.15	1.14±0.06	1.12±0.04	0.64±0.10	24.8±2.7	[1, 2, 4]
16	Loperamide	1	B		8.61	477	103.6	4.66	4.56	3.32±0.05	1.90±0.08	2.40±0.12	0.7±0.3	[6, 7]
17	Meprobamate	1	N			218	42.6	0.92	0.73	0.73±0.03	[j]	<0.4[j]	69.9±8.6	[1, 4]
18	Methylphenidate	1	B		8.96	233	51.9	2.56	2.14	0.57±0.04	1.37±0.15	0.83±0.03	24.5±3.5	[1, 2]
19	Metoclopramide	1	B		9.36	300	40.2	2.23	2.18	0.22±0.07	0.20±0.51	0.93±0.06	33.9±2.4	[1, 2, 4, 5]
20	Midazolam	1	N		5.71	326	62.8	3.42	3.33	3.32±0.02	1.69±0.07	1.61±0.05	2.5±0.2	[1, 2, 4]
21	Morphine	1	B	9.35	8.08	285	60.8	0.57	0.88	0.12	0.19±0.79	< 0.4	45.5±6.4	[1, 6]

No.	Compound[a]	Data set[b]	Ionization state			Calculated Properties			CAMDIS		PAMPA	LIMBA	Equilibrium Dialysis	
			Charge class[c]	pK_a (acid)[d]	pK_a (base)[d]	MW [e] [g/mol]	A_D [f] [Å^2]	$c\log P$ [g]	$m\log P$ [h]	$\log D_{oct}$ (pH 7.4) ± SD	$\log D_{PAMPA}$ (pH 7.4) [i] ± SD	$\log D_{brain}$ (pH 7.4) ± SD	$f_{u,brain}$ [%] ±SD	Reference
22	NFPS[a2]	1	Z	1.94	9.57	393	67.3	3.99		2.82±0.03	2.15±0.15	1.74±0.06	0.2	[3]
23	Nortriptyline	1	B		10.13	263	52.5	4.32	4.32	1.59±0.04	1.80±0.02	2.59±0.03	0.4±0.1	[1, 2]
24	Paracetamol	1	N	9.45		151	34.9	0.49	0.22	0.22±0.04	-0.12±0.25	<0.4	83.3±0.0	[7, 8]
25	Paroxetine	1	B		9.7	329	59.1	4.24	3.93	1.63±0.03	2.06±0.08	2.54±0.04	0.3±0.1	[1, 2]
26	Phenytoin	1	A	8.18		252	54.8	2.09	2.36	2.29±0.08	1.25±0.15	0.81±0.01	8.2±0.1	[1, 4]
27	Propranolol	1	B		9.48	259	47.8	2.75	3.22	1.14±0.08	1.65±0.04	2.02±0.02	2.8±1.1	[2, 3]
28	Quinidine	1	B		8.59/4.36	324	79.2	2.79	3.28	2.06±0.03	1.54±0.05	1.60±0.03	3.8±0.1	[3, 5, 6]
29	Risperidone	1	B		8.31/3.45	410	78.9	2.71	2.83	1.87±0.04	1.17±0.05	1.47±0.01	9.3±3.1	[1, 2, 4, 5, 8]
30	Rizatriptan	1	B		9.59/1.77	269	48.2	1.18	1.45	-0.74	0.35±0.13	<0.4	32.1±3.9	[4, 6]
31	Selegiline	1	B		7.46	187	39.8	3.02	2.54	2.21±0.03	[j]	[j]	6.8±1.0	[1, 2, 4]
32	Sertraline	1	B		9.48	306	43.8	5.35	5.08	3.00±0.02	2.76±0.02	2.79±0.11	0.1±0.0	[1, 4]
33	Sumatriptan[a3]	1	B		9.49	295	59.0	0.74	0.94	-1.15	0.91±0.04	<0.4	54.2±25.7	[4, 6]
34	Theobromine	1	N	9.79		180	30.5	-0.67	-0.72	-0.72	-0.27±0.00	<0.4	61.0	[3]
35	Theophylline	1	A	8.51		180	29.8	-0.03	-0.12	-0.15±0.03	0.24±0.47	<0.4	39.0	[3]
36	Trazodone	1	B		6.81	372	48.3	3.85	2.71	2.61±0.02	1.46±0.12	1.38±0.02	4.9±0.6	[1, 2, 4]
37	Venlafaxine	1	B		9.62	277	63.0	3.27	2.86	0.64±0.05	0.89±0.49	0.98±0.04	21.5±0.5	[1, 2, 4]
38	Zolpidem	1	B		6.47	307	61.2	3.03	2.34	2.29±0.03	0.76±0.20	0.71±0.07	18.5±2.1	[1, 2]
39	Alfentanil	2	B		6.46	417	59.3	2.13	2.25	2.20±0.04	0.54±0.49	0.71±0.04	29.7±3.7	[6]
40	Amantadine	2	B		10.46	151	37.4	2.00	2.74	-0.32	[j]	[j]	32.0	[4]
41	Amitriptyline	2	B		9.49	277	55.1	4.85	4.86	2.77±0.03	2.34±0.08	2.57±0.04	23.3	[4]
42	Amoxapine	2	B		8.4/3.28	314	57.5	3.41	3.34	2.30±0.03	1.82±0.12	2.59±0.02	0.9	[4]
43	Amprenavir	2	N			506	105.6	3.29	2.46	2.46±0.01	-0.27±0.00	<0.4	1.0	[6]
44	Atomoxetine	2	B		10.2	255	54.4	3.94	3.83	1.03±0.01	1.68±0.07	2.06±0.08	9.1	[4]

No.	Compound[a]	Data set[b]	Ionization state: Charge class[c]	Ionization state: pK_a (acid)[d]	Ionization state: pK_a (base)[d]	Calculated Properties: MW [e] [g/mol]	Calculated Properties: A_D [f] [Å^2]	Calculated Properties: $c\log P$ [g]	CAMDIS: $m\log P$ [h]	CAMDIS: $\log D_{oct}$ (pH 7.4) ± SD	PAMPA: $\log D_{PAMPA}$ (pH 7.4) [i] ± SD	LIMBA: $\log D_{brain}$ (pH 7.4) ± SD	Equilibrium Dialysis: $f_{u,brain}$ [%] ±SD	Reference
45	Bupropion	2	B		8.32	240	44.5	3.21	3.12	2.15±0.04	1.52±0.14	1.33±0.11	1.9	[4]
46	Celecoxib	2	N	11.1		381	64.0	4.37	3.90	3.90±0.03	2.77±0.34	1.72±0.04	17.1	[8]
47	Cetirizine	2	Z	2.86	7.997	389	63.4	2.08		1.28±0.05	1.04±0.20	0.46±0.06	0.3	[6]
48	Ciglitazone	2	A	6.88		333	37.0	5.07	4.07	3.96±0.13	[j]	[j]	7.2	[8]
49	Cimetidine	2	B		6.96	252	53.1	0.38	0.63	0.50±0.08	0.17±0.41	<0.4	0.03	[6]
50	Colchicine	2	N			399	89.4	1.20	0.95	0.95±0.04	0.16±0.41	<0.4	53.0	[9]
51	Desloratadine	2	B		9.78/4.57	311	52.3	3.83	3.58	1.20±0.03	1.75±0.06	2.42±0.03	2.4	[6]
52	Dexamethasone	2	N			392	73.2	1.79	1.79	1.79±0.01	0.44±0.36	<0.4	0.7	[6]
53	Diclofenac	2	A	4.02		296	48.7	4.73	4.53	1.15±0.08	-0.27±0.00	0.40±0.06	9.8	[8]
54	Digoxin*	2	N			781	76.5	1.42	1.34	1.34±0.05	[j]	<0.4	5.5	[6]
55	Diphenhydramine	2	B		9.12	255	56.1	3.45	3.38	1.65±0.11	1.54±0.13	1.50±0.08	1.6	[6]
56	Diprenorphine	2	B	9.57	8.48	426	97.8	2.66	3.54	2.43±0.01	1.28±0.07	1.00±0.04	5.8	[7]
57	Donepezil	2	B		8.88	379	76.1	4.60	3.75	2.26±0.02	1.32±0.18	1.49±0.08	30.8	[4, 8]
58	Doxepin	2	B		9.22	279	52.1	4.09	4.09	2.26±0.03	2.17±0.04	2.15±0.04	11.4±1.7	[4]
59	Doxorubicin *	2	B	9.45	8.16	544	71.4	0.32	1.19	0.36	1.18±0.06	0.99±0.05	2.5	[6]
60	Eletriptan	2	B		9.59	383	61.1	3.36	3.03	0.84±0.04	1.19±0.14	1.54±0.05	0.1	[6]
61	Ergotamine	2	B		6.4	582	102.6	4.66	0.04	instable	instable	instable	5.5	[4]
62	Ethosuximide	2	N	9.25		141	31.7	0.40	0.37	0.36±0.12	[j]	[j]	1.3	[4]
63	Etoricoxib	2	N		4.53	359	64.3	2.35	2.23	2. 23±0.02	0.53±0.69	0.88±0.03	73.0	[8]
64	Fallypride	2	B		8.22	364	57.3	3.18	2.90	2.02±0.03	1.18±0.05	1.20±0.03	15.0	[7]
65	Fentanyl	2	B		8.38	336	74.3	3.62	3.92	2.90±0.03	1.63±0.01	1.40±0.04	23.9	[6]
66	Fexofenadine	2	Z	4.21	9.68	502	66.6	1.96		1.95±0.44	0.23±0.23	<0.4	7.0	[6]
67	Flumazenil	2	N		<2	303	53.2	1.29	1.08	1.08±0.09	-0.27±0.00	<0.4	7.7	[7]

No.	Compound[a]	Data set[b]	Ionization state			Calculated Properties			CAMDIS		PAMPA	LIMBA	Equilibrium Dialysis	
			Charge class[c]	pK_a (acid)[d]	pK_a (base)[d]	MW [e] [g/mol]	A_D [f] [Å^2]	$c\log P$ [g]	$m\log P$ [h]	$\log D_{oct}$ (pH 7.4) ± SD	$\log D_{PAMPA}$ (pH 7.4) [i] ± SD	$\log D_{brain}$ (pH 7.4) ± SD	$f_{u,brain}$ [%] ±SD	Reference
68	Fluphenazine	2	B		7.76/3.67	438	56.8	4.12	4.02	3.50±0.05	2.13±0.28	2.52±0.17	83.5	[4]
69	Flurbiprofen	2	A	4.03		244	35.5	3.75	4.24	0.87±0.01	-0.27±0.00	<0.4	0.1	[8]
70	Gabapentin	2	Z	3.68	10.59	171	34.0	-0.66		-1.12	[j]	<0.4	12.9	[4]
71	Ganciclovir	2	N	9.23	2.1	255	46.5	-2.55	-1.94	-1.95	[j]	<0.4	78.2	[5]
72	Ibuprofen	2	A	4.45		206	34.1	3.68	3.90	0.95±0.01	-0.27±0.00	<0.4	85.5	[8]
73	Indinavir*	2	N		5.77/4.01	614	124.6	3.68	2.98	2.97±0.03	0.38±0.13	<0.4	29.6	[6]
74	Indometacin	2	A	4.43		358	50.7	4.18	3.76	0.79±0.06	0.00±0.29	<0.4	10.0	[8]
75	Isocarboxazid	2	N			231	42.1	0.99	1.40	1.40±0.03	[j]	[j]	5.9	[4]
76	Ivermectin	2	N			875	167.0	5.39	5.39	5.39	[j] not measured	[j] not measured	21.1	[6]
77	Ketorolac	2	A	3.44		255	31.1	1.62	3.38	-0.58	0.10±0.35	<0.4	0.01	[8]
78	Loratadine	2	N		4.72	383	63.4	5.05	3.96	3.96±0.09	[j]	[j]	48.5	[6]
79	Loxapine	2	B		7.49/3.05	328	59.5	3.98	3.82	3.47±0.07	2.71±0.27	2.48±0.05	0.2	[4]
80	Maprotiline	2	B		10.2	277	54.0	4.52	4.27	1.47±0.02	1.80±0.07	2.79±0.09	1.1	[4]
81	MDL 100907	2	B		9.02	373	65.2	3.29	3.50	1.87±0.04	1.50±0.06	not measured	0.6	[7]
82	Meperidine	2	B		8.68	247	41.4	2.23	2.56	1.26±0.04	1.46±0.10	0.97±0.01	10.8	[6]
83	Mesoridazine	2	B		9.55	387	63.4	4.44	3.90	1.75±0.03	1.35±0.16	1.91±0.05	13.0	[4]
84	Methadone	2	B		9.26	309	69.0	4.17	3.47	1.60±0.06	1.72±0.14	1.89±0.04	1.6	[6]
85	Mirtazapine	2	B		7.79/3.59	265	48.0	2.81	3.06	2.52±0.04	1.73±0.01	1.78±0.07	2.9	[4]
86	Naproxen	2	A	4.12		230	37.5	2.82	3.58	0.30±0.04	0.19±0.92	<0.4	8.0	[8]
87	Naratriptan	2	B		9.43	335	62.6	1.70	1.83	-0.20	1.00±0.11	0.43±0.04	54.2	[6]
88	Norclozapine	2	B		8.56/4.13	313	54.0	3.14	2.81	1.62±0.06	1.84±0.08	2.52±0.02	23.0	[5]
89	Nelfinavir*	2	B	9.63	6.01	568	120.2	5.84	4.06	4.04±0.06	2.52±0.03	[j]not measured	0.6	[6]
90	Olanzapine	2	B		8.01/5.6	312	43.9	3.01	2.73	2.02±0.03	0.96±0.16	1.31±0.06	0.1	[4]

No.	Compound[a]	Data set[b]	Ionization state			Calculated Properties			CAMDIS		PAMPA	LIMBA	Equilibrium Dialysis	
			Charge class[c]	pK_a (acid)[d]	pK_a (base)[d]	MW [e] [g/mol]	A_D [f] [Å^2]	$c\log P$ [g]	$m\log P$ [h]	$\log D_{oct}$ (pH 7.4) ± SD	$\log D_{PAMPA}$ (pH 7.4) [i] ± SD	$\log D_{brain}$ (pH 7.4) ± SD	$f_{u,brain}$ [%] ±SD	Reference
91	Paclitaxel*	2	N			854	155.3	4.73	2.99	2.99±0.12	2.10±0.16	not measured	3.4	[6]
92	Pemoline	2	N		3.08	176	29.2	0.46	0.15	0.15±0.03	-0.07±0.35	<0.4	0.3	[4]
93	Pergolide	2	B		7.91	314	68.4	4.40	3.51	2.88±0.04	2.39±0.06	2.22±0.04	55.8	[4]
94	Perphenazine	2	B		7.86/3.7	404	53.7	3.81	3.98	3.39±0.06	2.38±0.12	2.63±0.14	2.7	[4]
95	Phenelzine	2	B		7.32	136	25.2	1.03	0.73	0.47±0.11	1.69±0.09	not measured	0.4	[4]
96	Pioglitazone	2	A	6.6	5.7	356	41.3	3.53	3.81	2.94±0.02	1.86±0.17	1.22±0.06	7.6	[8]
97	PK 11195	2	N			353	73.0	4.62	3.79	3.79±0.06	2.34±0.19	2.12±0.05	2.3	[7]
98	Primidone	2	N			218	44.0	0.88	0.74	0.74±0.04	0.89±0.03	<0.4	1.6	[4]
99	Propoxyphene	2	B		9.06	339	68.3	5.21	4.06	2.39±0.04	2.08±0.09	1.85±0.01	62.2	[1]
100	Quetiapine	2	B		6.92/3.96	384	52.9	2.99	2.92	2.80±0.04	1.55±0.09	1.55±0.06	3.3	[4]
101	Raclopride	2	Z	5.95	9.46	347	44.1	4.06		1.13±0.04	1.09±0.07	1.05±0.04	2.5	[7]
102	Ranitidine	2	B		8.38	314	69.8	0.67	0.19	-0.83±0.16	0.68±0.33	<0.4	13.0	[6]
103	9-hydroxy-risperidone	2	B		8.28/2.43	426	52.8	1.07	2.10	1.17±0.01	1.45±0.04	1.29±0.06	96.0	[1, 5]
104	Ritonavir*	2	N			721	120.6	4.94	4.41	4.41±0.01	1.85±0.04	1.52±0.03	8.1±0.7	[6]
105	Rofecoxib	2	N			314	57.0	1.80	1.81	1.81±0.01	1.33±0.07	1.15±0.05	1.1	[7]
106	Rolipram	2	N			275	43.5	1.72	1.91	1.91±0.05	1.01±0.08	0.44±0.14	27.5	[7]
107	Saquinavir*	2	B		7/3	671	144.7	4.73	4.24	4.09±0.04	2.55±0.31	not measured	0.2	[6]
108	Spiperone	2	B		8.29	395	68.6	2.82	3.49	2.55±0.04	2.17±0.05	2.18±0.02	3.7	[7]
109	Sulpiride	2	B	10.01	9.01	341	65.3	1.11	0.47	-1.15	-0.27±0.00	<0.4	63.0	[1]
110	Tacrine	2	B		9.81	198	36.7	3.27	2.35	-0.06±0.09	-0.27±0.00	1.21±0.05	12.4	[4]
111	Temazepam	2	N	9.14		301	62.7	2.34	2.11	2.10±0.05	1.37±0.11	0.97±0.10	5.4	[4]
112	Terfenadine	2	B		8.6	472	101.8	6.07	5.19	3.96±0.01	[j]	[j]	0.1	[10]
113	Thiopental	2	A	7.5		242	41.2	2.98	2.93	2.68±0.08	0.81±0.19	0.45±0.14	12.2±3.4	[1, 5]

No.	Compound[a]	Data set[b]	Ionization state			Calculated Properties			CAMDIS		PAMPA	LIMBA	Equilibrium Dialysis	
			Charge class[c]	pK_a (acid)[d]	pK_a (base)[d]	MW [e] [g/mol]	A_D [f] [Å^2]	$c\log P$ [g]	$m\log P$ [h]	$\log D_{oct}$ (pH 7.4) ± SD	$\log D_{PAMPA}$ (pH 7.4) [i] ± SD	$\log D_{brain}$ (pH 7.4) ± SD	$f_{u,brain}$ [%] ±SD	Reference
114	Thioridazine	2	B		9.68	371	60.4	6.00	5.87	3.59±0.05	2.63±0.30	2.98±0.07	0.1	[4]
115	Thiothixene	2	B		7.75/3.59	444	63.6	3.23	3.73	3.22±0.03	[j]	[j]	0.3	[4]
116	Tiagabine	2	Z	3.1	9.02	376	65.7	2.78		1.23±0.06	0.55±0.49	0.76±0.03	4.0	[4]
117	Trifluperazine	2	B		8.43/3.74	407	56.4	4.69	5.06	3.99±0.05	[j]	[j]	0.1	[4]
118	Triprolidine	2	B		9.47/3.75	278	53.8	3.63	3.91	1.84±0.04	1.21±0.06	1.34±0.01	9.2	[6]
119	Valdecoxib	2	N	9.69		314	50.1	1.83	2.43	2.43±0.02	1.81±0.09	1.26±0.08	3.4	[8]
120	Valproate	2	A	4.5		144	39.6	2.76	3.14	0.24±0.04	[j] not measured	[j] not measured	100.0	[10]
121	Verapamil	2	B		8.8	455	86.0	4.47	3.96	2.54±0.02	1.65±0.03	1.87±0.04	3.3	[6]
122	Vinblastine*	2	B		7.4/5.4	811	116.3	5.23	3.41	3.11±0.05		1.79±0.20	0.5	[6]
123	WAY 100635	2	B		6.71	423	105.5	4.09	3.13	3.05±0.03	1.39±0.13	1.39±0.06	14.1	[7]
124	Zaleplon	2	N			305	51.8	1.44	1.24	1.24±0.09	0.15±0.38	<0.4	47.1	[4]
125	Ziprasidone	2	B		6.57	413	75.6	4.21	2.85	2.80	1.74±0.01	1.76±0.02	0.1	[4]
126	Zolmitriptane	2	B		9.6	287	53.3	1.29	1.20	-1.00	0.20±1.14	<0.4	54.0	[6]

[a1-a3] compounds excluded from the correlation due to high SD of $f_{u,brain}$ data obtained from literature. * predicted drug adsorption to Teflon > 5% (excluded from correlation)

[b] dataset1: at least two independent measures of $f_{u,brain}$ with the homogenate dialysis technique, dataset 2: only one $f_{u,brain}$ estimate from literature

[c] neutral (less than 3 % ionization at pH 7.4); A: acid pK_a < 8.9; B: base pK_a >6; Z: zwitterions with acid pK_a <8.9 and base pK_a >6;

[d] in-house measured (potentiometric);

[e] desalted form

[f] calculated at pH 7.4 as described elsewhere [11];

[g] clog P v4.71 Daylight;

[h] calculated from measured $\log D_{oct}$ and measured pK_a values using Henderson Hasselbalch equation.

[i] PAMPA performed with optimized experimental conditions: pH 7.4, brain polar lipids, no solubilizer

[j] poor UV and MS peak or impure compound

Table 3 Summary of optimized experimental conditions and applicability domain of LIMBA.

Experimental conditions	**Specification**
Phase volume ratios[a]	V_{aq}=50µL; V_{brain}=1.2µL (homogenate)
Initial aqueous drug concentration	C_{aq}^{0}=25 µM
DMSO content in the aqueous phase	0.25% (v/v)
Filter support	hydrophobic PVDF (DiFi tubes)
Equilibration time	15 h
Applicability range	$Log\,D_{brain}$= 0.4 to maximal 4.2[b]

[a] solvents used in this study: 50 mM TRIS/114 mM NaCl/pH 7.4, rat brain homogenized in 2 volumes (w/v) of n-dodecane.

[b] upper $Log\,D_{brain}$limited by the sensitivity of HPLC-UV/MS and by drug adsorption of basic compounds to the filter-supported interface as described in *our accompanying manuscript 1*.

Table 4 Surrogate systems evaluated in terms of their ability to predict drug binding to brain tissue. Correlation statistics obtained from linear fits of $\log D_{oct}$, $\log P$ (CAMDIS), $\log D_{PAMPA}$ (PAMPA) and $\log D_{brain}$(LIMBA) with $\log((1-f_{u,brain})/f_{u,brain})$ (equilibrium dialysis data) for Dataset 1 and an extended Dataset (1+2).

Surrogate System		Statistics (r^2)	
Assay	Specification	Dataset 1 (n=27)[a]	Whole Dataset (n=73)[b]
Octanol			
CAMDIS $\log D_{oct}$ (pH 7.4)		0.370	0.232
'measured' $\log P$	derived from measured $\log D_{oct}$ and pK_a	0.796	0.493
calculated $\log P$	clog P v4.71 Daylight	0.786	0.495
PAMPA barrier			
PAMPA 01 *(default at Roche)*	pH 6.5, egg lecithin, donor spiked with 0.5% glycocholic acid	0.375	not tested
PAMPA 02	pH 6.5, egg lecithin	0.564	not tested
PAMPA 03	pH 7.4, egg lecithin	0.710	0.572
PAMPA 04	pH 7.4, dodecane	0.290	not tested
PAMPA 05	pH 7.4, brain total lipids	0.812	not tested
PAMPA06	pH 7.4, brain polar lipids	0.805	0.612
Brain homogenate			
LIMBA $\log D_{brain}$ (pH 7.4)	pH 7.4, brain homogenate in dodecane	0.911	0.741

[a]from the initial set of 38 compounds with $f_{u,brain}$data reported in two independent studies (details see Section 3.1), caffeine, sumatriptan and NFPS were excluded due to high standard deviation of the $f_{u,brain}$data. Moreover, carisoprolol, meprobamat and selegiline were excluded due to poor UC absorption. LIMBA $\log D_{brain}$values could only be determined at $\log D_{brain}$> 0.4 and statistics for the other surrogate systems refer to the same subset of compounds (n = 27). [b]statistics refer to the same subset that was measured with LIMBA (for exclusion criteria see Fig. 4).

Table 5 Lipid composition of egg lecithin, brain total lipids and brain polar lipids

% Lipid (m/m)	Pampa Standard (egg lecithin)[a]	Brain Total Lipids[b]	Brain Polar Lipids[b]
Phosphatidylethanolamine	5.7	16.7	33.1
Phosphatidylserine (acidic)		10.6	18.5
Phosphatidylcholine	59.0	9.6	12.6
Phosphatidic acid (acidic)		2.8	0.8
Phosphatidylinositol (acidic)		1.6	4.1
Cholesterol	12.4		
Triglyceride	17.1		
Sphingomyelin			
Cerebroside			
Sulfatides			
Other	5.7	58.7	30.9

[a]product information provided by the supplier; [b]as reported on http://avantilipids.com/

FIGURES

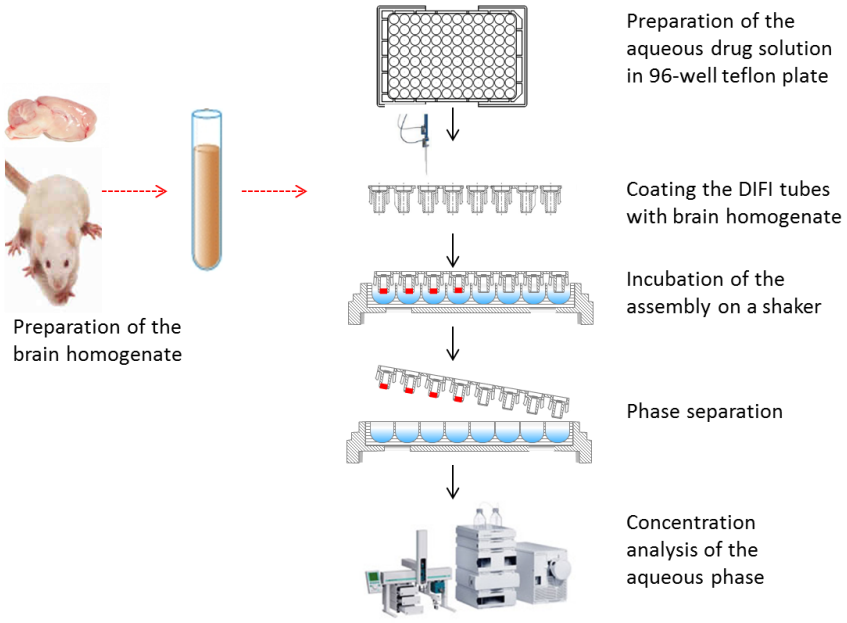

Figure 1 Work flow for determining brain tissue / water distribution coefficients, $\log D_{Brain}$ (pH 7.4), with LIMBA.

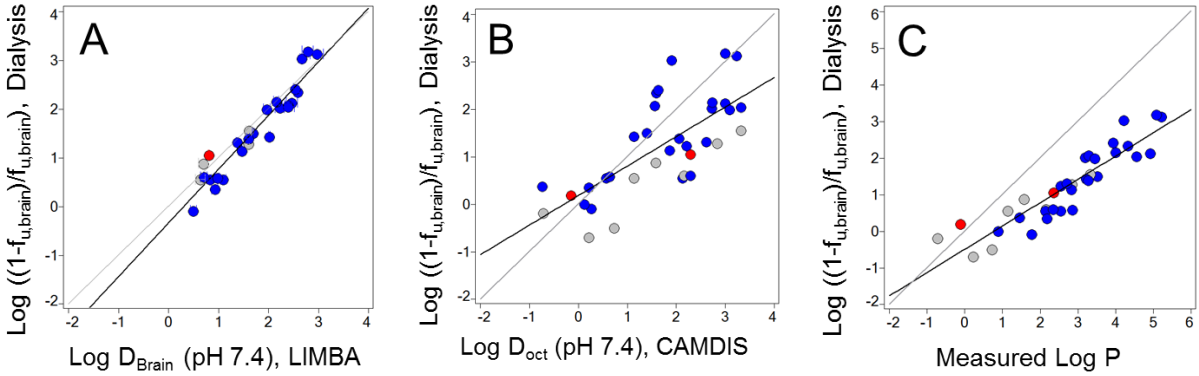

Figure 2 Relationship between drug binding to brain tissue (equilibrium dialysis data), expressed as $\log((1-f_{u,brain})/f_{u,brain})$, and **A:** $\log D_{Brain}$ (pH 7.4) measured with LIMBA (r^2=0.911, n = 27), **B:** $\log D_{oct}$ (pH 7.4) measured with CAMDIS (r^2=0.518, n=35) and **C:** $\log P$ derived from measured $\log D_{oct}$ and measured pK_a (r^2=0.827, n = 35). Data in **B** and **C** is shown for n=35 compounds from Dataset 1 (caffeine, sumatriptan, NFPS were excluded due to high standard deviation of the $f_{u,brain}$data). The same exclusion criteria were applied for the LIMBA data (**A**), however selegiline, meprobamate and carisoprodol was excluded due to poor analytics, and only the applicability range, i.e. $\log D_{Brain} > 0.4$, is presented. Colors according to charge class: nonionic (●), cationic (●), anionic (●). Black lines are fits to the experimental data, grey lines are lines of identiy.

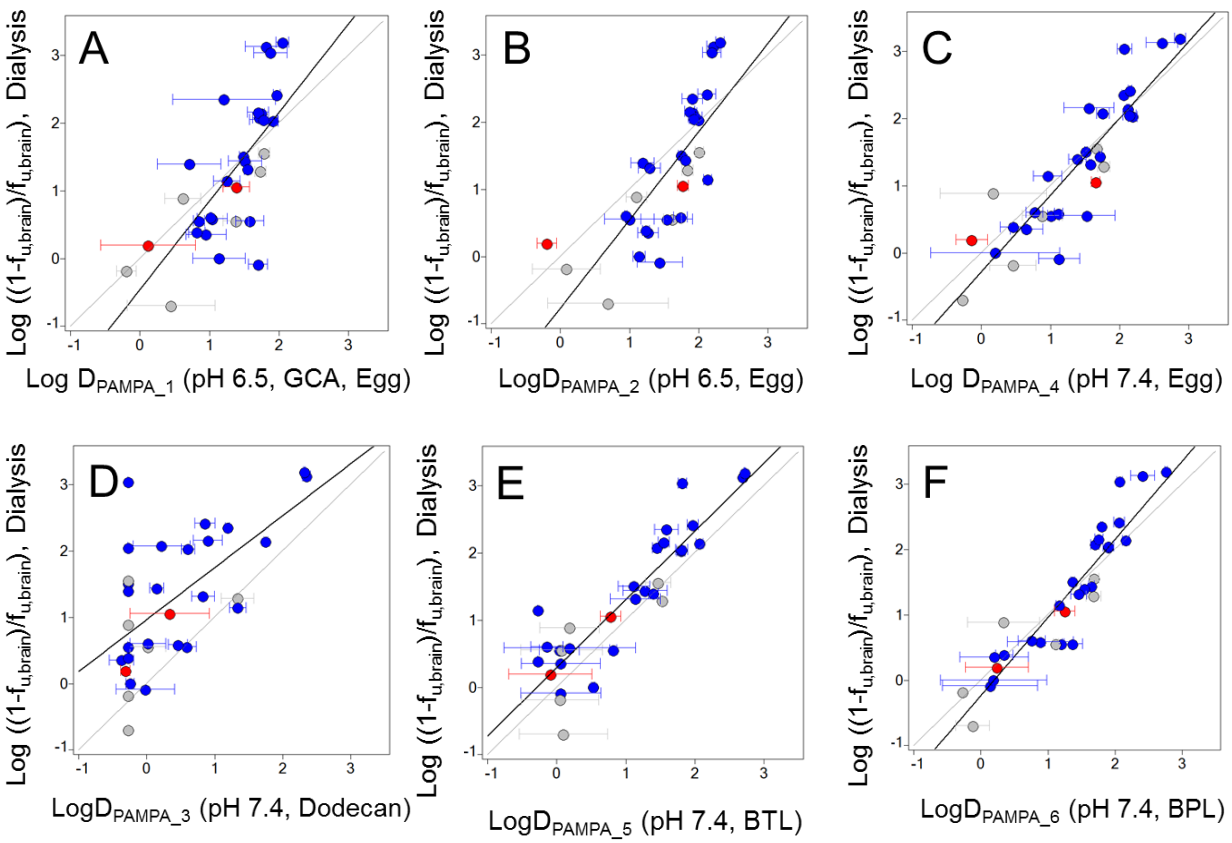

Figure 3 Relationship between $\log((1-f_{u,brain})/f_{u,brain})$, obtained from equilibrium dialysis, and membrane retention in PAMPA, expressed as $\log D_{PAMPA}$, for n = 32 compounds from Dataset 1 (exclusion criteria as described in Fig. 2). Different experimental conditions in PAMPA are shown (A - F) with details provided in Table 3. Correlation statistics (n = 32): **A:** PAMPA 1 (default setup at Roche, r^2=0.521); **B:** PAMPA 2 (r^2=0.597); **C:** PAMPA 4 (r^2=0.791); **D:** PAMPA 3 (r^2=0.326); **E:** PAMPA 5 (r^2=0.800); **F:** PAMPA 6 (r^2=0.850). Colors according to charge class: nonionic (●), cationic (●), anionic (●). Black lines are fits to the experimental data, grey lines are lines of identiy.

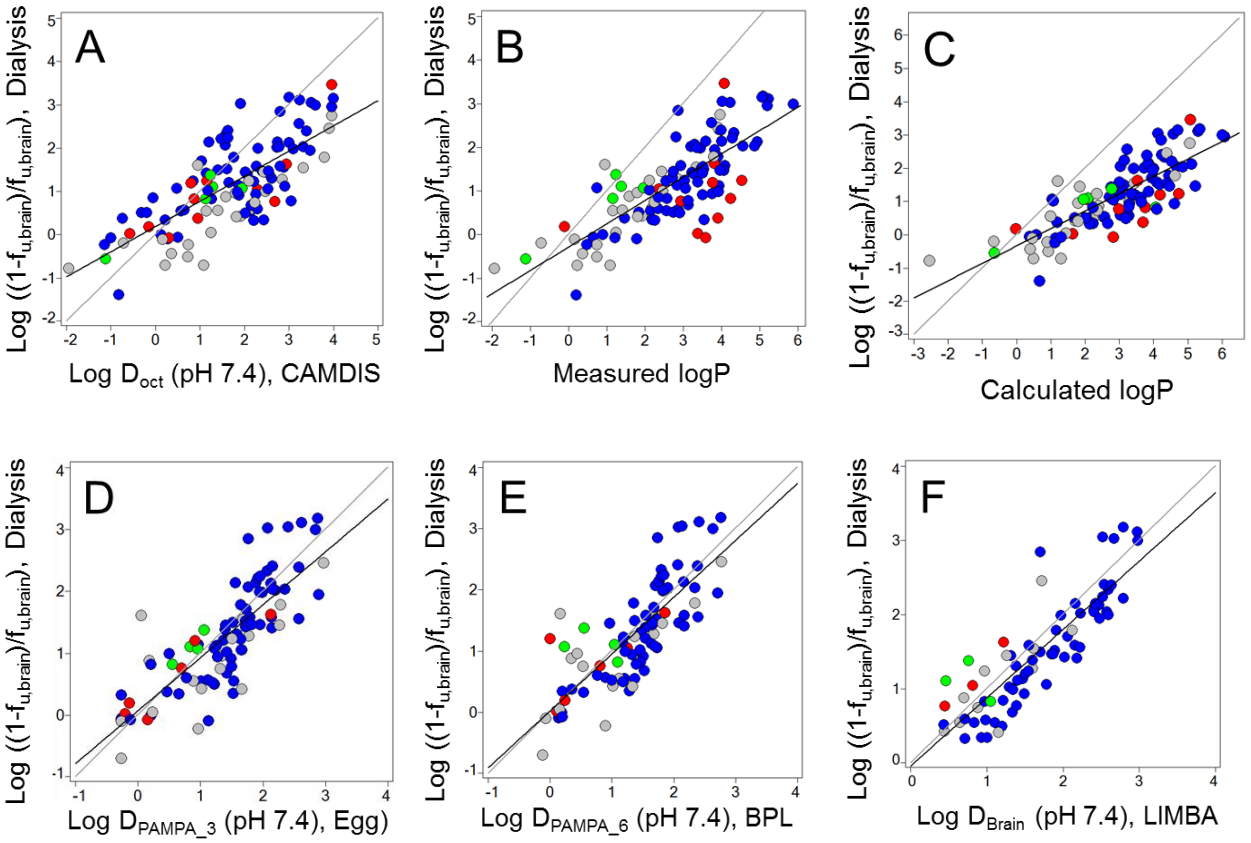

Figure 4 Relationship between $\log((1-f_{u,brain})/f_{u,brain})$, obtained from equilibrium dialysis, and **A:** $\log D_{oct}$ (pH 7.4) measured with CAMDIS (r^2=0.564, n=112); **B:** $\log P$ derived from measured $\log D_{oct}$ and pK_a (r^2=0.606, n = 112); **C:** calculated $\log P$ (r^2=0.649, n = 112); **D:** $\log D_{PAMPA}$ (pH 7.4, membrane formed from egg lecithin, r^2=0.607, n = 90); **E:** $\log D_{PAMPA}$ (pH 7.4, membrane formed from BPL r^2=0.6, n = 90) and **F:** $\log D_{Brain}$ (pH 7.4) measured with LIMBA (r^2=0.741, n = 73). Statistics without acidic and zwitterionic compounds and without ziprasidone (outlier in all assays): r^2=0.824, n = 66.The following compounds were excluded from the correlation: caffeine, sumatriptan, NFPS (high standard deviation of the $f_{u,brain}$data); ergotamine (instable); doxorubicin, digoxin, indinavir, paclitaxel, vinblastine, ritonavir, saquinavir, nelfinavir adsorption to Teflon (> 5%) as predicted by a PLS model described in our *accompanying manuscript 2*. In addition, only compounds within the applicability range of PAMPA ($\log D_{PAMPA}$ > -0.27) and LIMBA ($\log D_{Brain}$ > 0.4) are shown in D/E and F, respectively. Since no access to the HPLC/MS system was possible at the time of LIMBA measurements, only compounds with good analytics in HPLC/UV are shown in F. Likewise, PAMPA was measured with a UV (platereader) and therefore compounds with poor UV absorption were excluded (carisoprodol, meprobamat, selegiline). Colors according to charge class: nonionic (●), cationic (●), anionic (●), zwitter-ionic (●). Black lines are fits to the experimental data, grey lines are lines of identiy.

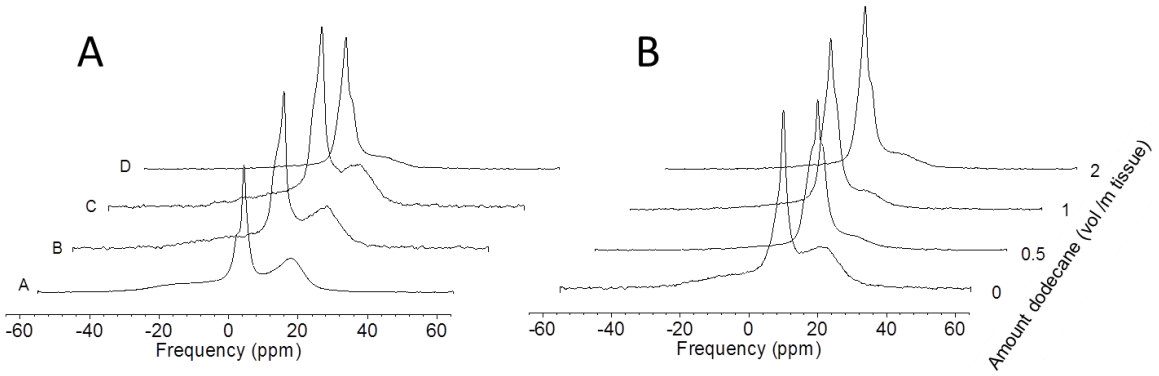

Figure 5A: Experimental 162-MHz ^{31}P-NMR spectra of brain tissue in the form of (A) undisrupted tissue, (B) homogenate in aqueous buffer (2:1, v/m, buffer:50 mM Tris, 114 mM NaCl, pH 7.4) at 25°C, (C) same like (B) but at 37°C and (D) homogenized in dodecane (2:1, v/m). **B:** ^{31}P-NMR spectra recorded from brain tissue homogenized with increasing amounts of dodecane.

Supporting Information

S1. LIMBA - Assay Development

Data provided in the following was obtained from preliminary series of experiments with LIMBA not conducted with a liquid handling system. Therefore, the data may deviate slightly from the data from the validation setup provided in the main manuscript and obtained from the optimized LIMBA setup.

S1.1. Selection of the Filter-Solvent System

The basic concept of LIMBA was to facilitate the measurement of brain tissue/water distribution coefficients ($\log D_{brain}$) by immobilizing brain tissue on a filter support thus preventing contamination of the aqueous phase and allowing for convenient and complete phase separation after distribution equilibrium is achieved. Since LIMBA was designed as a medium - to - high throughput assay, brain homogenate (rather than undisrupted brain tissue) was used which can be dispensed with a robotic liquid handling system.

Various combinations of solvents and filter supports for the homogenization and immobilization of brain tissue, respectively, were investigated, including water and organic solvents as well as hydrophobic and hydrophilic filters materials. For the preparation of the homogenates, mouse brain was homogenized on ice in 2 volumes (w/v) of solvent by means of an ultrasonic probe. In order to detect a potential contamination of the aqueous phase with matrix components from brain tissue, the UV absorbance in the aqueous phase before and after incubation with tissue-coated filter was measured.

Water would clearly be preferable for homogenization in order to remain as close as possible to the *in vivo* situation and, in particular, to maintain the bilayer structure of brain tissue. However, phase separation was not achieved when coating aqueous homogenate on a hydrophilic filter, and vice versa, a hydrophobic filter was not wetted which would thus prevent solute partitioning. Among the organic solvents investigated (Table S1), octanol and other alcohols as well as olive oil were generally unsuitable since mixtures with brain tissue flocculated. Short chain alkanes (e.g. hexane) yielded homogenates, but their fast evaporation complicates the application. Moreover, the UV check revealed that organic solvents of medium - to - high polarity (e.g. 1,9-decadien) in combination with hydrophilic filter materials (e.g. hydrophilic PVDF) are unsuitable since phase separation was incomplete. Only long chain, saturated alkanes prevented a contamination of the aqueous phase with brain

homogenate, irrespective of whether a hydrophilic (polycarbonate) or a lipophilic filter (PVDF) was used. Tissue - hexadecane mixtures were too viscous for pipetting and the addition of hexane was required with the drawback of introducing variability due to evaporation of hexane. The combination of a hydrophobic filter (PVDF) and dodecane, showing low solubility in water, and allowing for the preparation of homogenates amenable for pipetting, was considered the most suitable setup which was further applied for the development and validation of LIMBA. It is worth noting that also homogenization of brain tissue in dodecane and coating of a hydrophilic polycarbonate filter would be feasible, however, the absorption capacity of the PVDF filter investigated was higher (thickness = 125 μM, PVDF vs. 10 μM, polycarbonate) and therefore PVDF was preferred.

Table S1 Solvents tested for the homogenization of brain tissue and their properties with respect to the applicability for LIMBA.

Solvent	Homogenisation achieved?	Hydrophobic filter wettable?[a]	Phase separation achieved (hydrophobic filter ?[b]
Water	yes	no	filter not wettable
Alcohols			
- Octanol, butanol, 1,6-heptadienol	no	not tested	not tested
Unsaturated alkanes			
- 1,7-octadien, 1,8-nonadiene, 1,9-decadien	yes	filter opalescent	no
Saturated alkanes			
Short chain: pentane, hexane, heptane	yes	yes, but evaporation	no
Long chain: dodecane, hexadecane	**yes**	**yes**	**yes**
Other			
2-n-octyloxynitrobenzen	no	not tested	not tested
Olive oil	no	not tested	not tested

[a]assessed by visual check whether or not the filter (hydrophobic PVDF) was transparent; [b]assessed by measurement of the UV absorption of the aqueous phase before and after incubation with a tissue-coated PVDF filter

S1.2. Equilibration Time

In order to determine the time required to reach distribution equilibrium in LIMBA, $\log D_{brain}$ (pH 7.4) values were measured in a time dependent manner for two test compound with different lipophilicity, namely cyclobenzaprine ($\log D_{oct}$ = 3; $\log D_{brain}$ = 2.47) and risperidone ($\log D_{oct}$ = 1.87; $\log D_{brain}$ = 1.47). Fig. S1 shows that distribution equilibrium for cyclobenzaprine and risperidone was reached after t = 10 h and t = 15 h, respectively. In the

following, aqueous drug solutions were incubated for t = 15 h with brain tissue before determining $\log D_{brain}$.

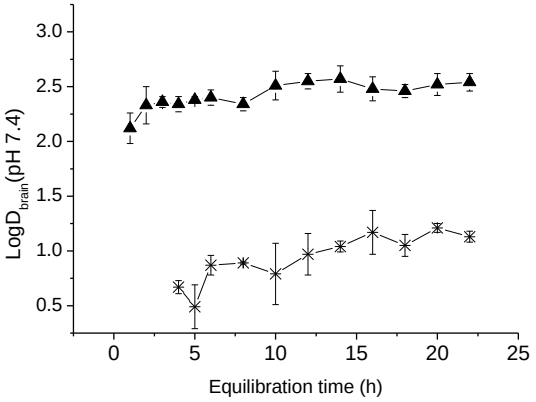

Figure S1 Kinetics of drug distribution in the brain tissue - filter - buffer system for cyclobenzaprine and riserpidone (25µM in 50mM Tris/114mM NaCl/pH 7.4). The $\log D_{brain}$ were measured with LIMBA using 1.2 µL brain homogenate (solvent: dodecane) and a lipophilic PVDF filter.

S1.2. Concentration Dependency of Tissue Binding and the Selection of Optimal Drug Concentrations

LIMBA $\log D_{brain}$ (pH 7.4) values were measured as a function of drug concentration (C_{drug}) at the example of three test compounds with different lipophilicity and charge state, namely risperidone ($\log D_{oct}$ = 1.87, cationic), cyclobenzaprine ($\log D_{oct}$ = 3, cationic) and carbamazepine ($\log D_{oct}$ = 1.58, neutral). An inspection of the $\log D_{brain}$ - C_{drug} profiles (Fig. S2) reveals that $\log D_{brain}$ values for the neutral test compound (carbamazepine) were insensitive to variations in drug concentration. In contrast, a trend towards lower $\log D_{brain}$ values at higher concentrations of cationic compounds was evident. A similar trend was also observed when determining CAMDIS $\log D_{oct}$ values by mass balance (*accompanying manuscript 1*), i.e. when only initial and equilibrium aqueous drug concentrations were analyzed, and drug concentrations in the octanol phase were estimated by difference. Drug adsorbed to the filter-supported octanol/water interface is then wrongly assigned to the octanol phase leading to an overestimation of $\log D_{oct}$. The same effect likely explains the overestimation of LIMBA, $\log D_{brain}$ at low drug concentrations.

During the optimization of CAMDIS it became clear that drug adsorption to the filter can be neglected at higher drug concentrations (C_{drug} = 100 µM), however, drug concentrations in

LIMBA should also be selected such that saturation of the brain lipids is avoided. As a compromise, we selected C_{drug} = 25 µM as the default drug concentration applied in LIMBA.

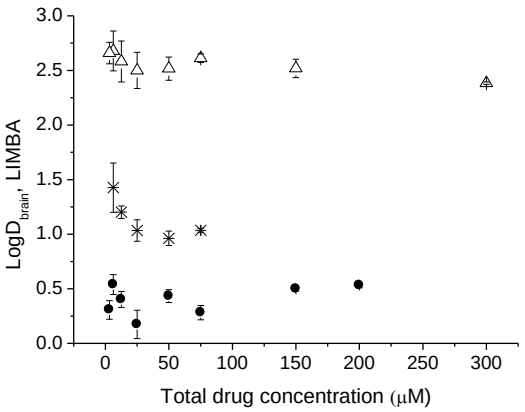

Figure S2 LIMBA $\log D_{brain}$ (pH 7.4) values as a function of drug concentration at the example of carbamazepine (▲), risperidone (✳) and cyclobenzaprine (△).

S1.3. The Influence of DMSO on Tissue Binding

In LIMBA, test compounds are introduced into the aqueous phase as DMSO stock solutions which simplifies the assay automation as a requirement for a screening assay. In order to test whether the presence of DMSO affects the extent of tissue binding, $\log D_{brain}$ (pH 7.4) values were measured as a function of the DMSO content (C_{DMSO} = 0.125 - 3%) using risperidone and cyclobenzaprine as representative test compounds.

Fig. S3 shows that the influence of DMSO on $\log D_{brain}$ (pH 7.4) was negligible, however, a slight trend towards lower $\log D_{brain}$ values with increasing concentrations of DMSO (above 1%) was evident for cyclobenzaprine, which is the compound with the higher affinity for brain tissue. In the following, LIMBA $\log D_{brain}$ values were determined at C_{DMSO} < 0.25 % where the influence of DMSO was negligible.

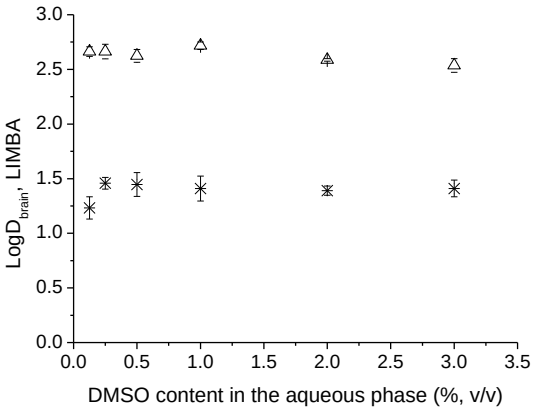

Figure S3 The $\log D_{brain}$ values of cyclobenzaprine (△) and risperidone (✳) as a function of the DMSO content in the aqueous drug solution.

S1.4. Reproducibility of LIMBA

Intraday reproducibility of LIMBA was assessed by filling each well of a 96 well plate with an aqueous solution of the same test compound followed by measurement of $\log D_{brain}$ values for the whole plate. More precisely, a filtrate containing the test compound was prepared for 6 wells, of which 3 were incubated with brain tissue and 3 were used as a reference for the assessment of the initial drug concentrations. Thus, 16 $\log D_{brain}$ values were measured on a 96 well plate at the example of cyclobenzaprine ($\log D_{oct}$=3; $\log D_{brain}$ 2.47) and risperidone ($\log D_{oct}$=1.87; $\log D_{brain}$ 1.47). Slightly better reproducibility was achieved for the compounds with the higher $\log D_{brain}$ value (cyclobenzaprine, SD = 0.08 $\log D_{brain}$ units) as compared to risperidone (SD = 0.10) which can be explained by the phase volume ratio (V_{brain} = 1.2µL, V_{aq} = 50 µL) optimized for lipophilic compounds.

S1.5. Species Differences in Brain Tissue Binding

For practical and ethical reasons, LIMBA was conducted with brain homogenate from rat since higher yields of tissue per animal can be gained as compared to the other most commonly used pre-clinical species, i.e. mouse. However, since LIMBA was validated with equilibrium dialysis data from both rat and mouse brain, we were interested whether species differences in tissue binding become evident in LIMBA. To this purpose, LIMBA $\log D_{brain}$ values were determined with brain homogenate from both rat and mouse, using a small subset of compounds from Dataset 1 (n = 21) with good analytical properties. The

species comparison of LIMBA $\log D_{brain}$ values (Fig. S4) demonstrates that differences in drug binding to rat and mouse brain tissue assessed with LIMBA are negligible which is in line with equilibrium dialysis data [14].

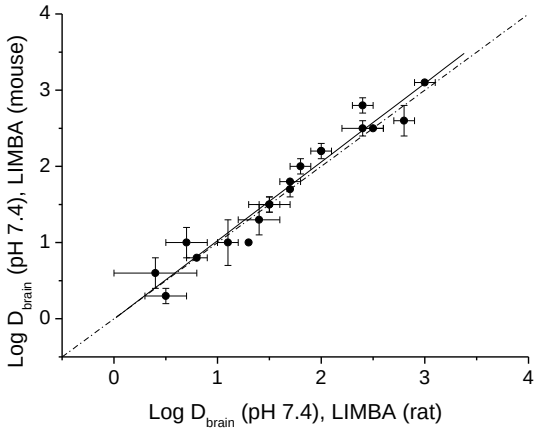

Figure S4 LIMBA $\log D_{brain}$ (pH 7.4) values determined from brain homogenate of mouse and rat on a 21-compound dataset: Buspirone, Carbamazepine, Chlorpromazine, Citalopram, Clozapine, Cyclobenzaprine, Diazepam, Fluoxetine, Fluvoxamine, Methylphenidate, Metoclopramide, Midazolam, Nortriptyline, Paroxetine, Propanolol, Quinidine, Risperidone, Trazodone, Venlafaxine. Correlation statistics: LIMBA $\log D_{brain}$ (mouse) = 1.031*LIMBA $\log D_{brain}$ (mouse) -0.005, r^2 = 0.975.

S2. Optimization of PAMPA

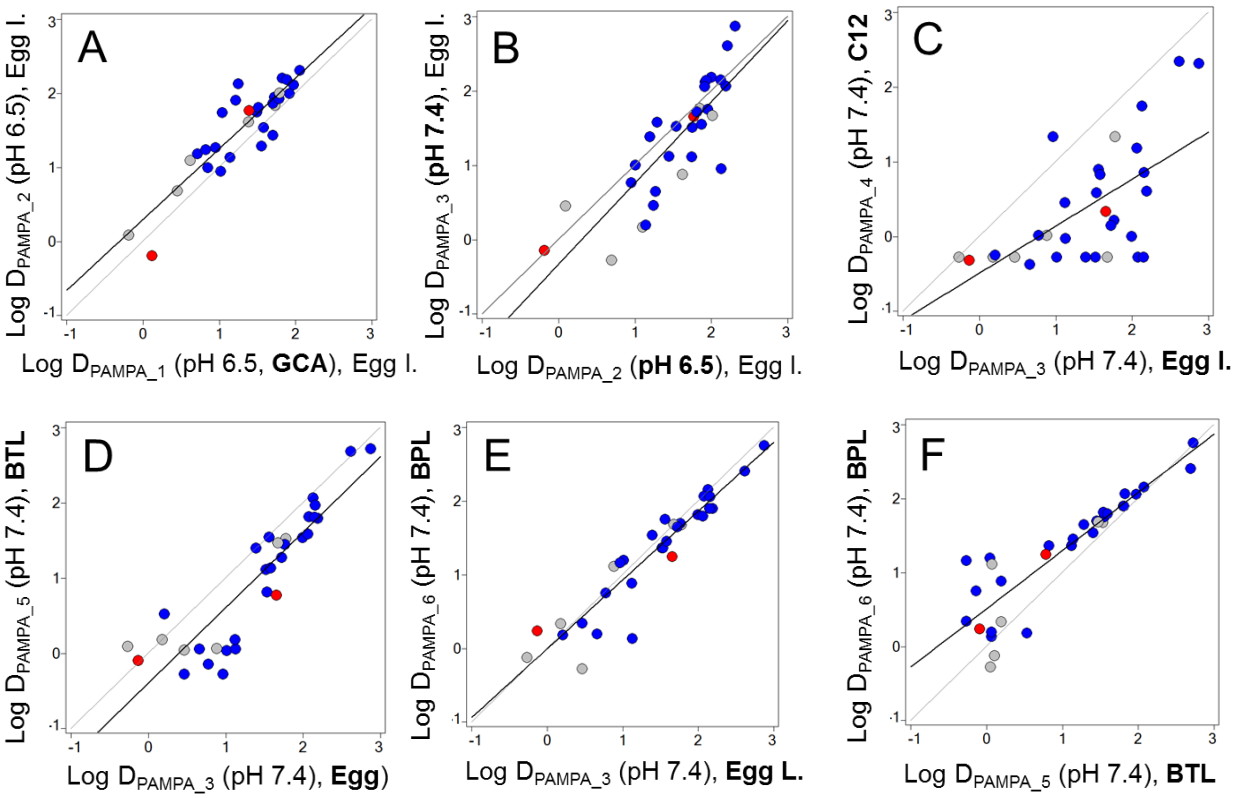

Figure S5 Membrane retention in PAMPA, expressed as $\log D_{PAMPA}$, for n = 32 compounds from Dataset 1 using different experimental setups showing **A:** the influence of glycocholic acid, GCA; **B:** the influence of pH; **C:** the effect of the presence of egg lecithin (egg l.) in excess dodecane **D:** the comparison between drug distribution in membranes formed from egg lecithin and brain total lipid (BTL) extract as well as **E:** brain polar lipid (BPL) extract. Moreover, **F:** the comparison between drug distribution in BPL and BTL membranes is shown. Colors according to charge class: nonionic (●), cationic (●), anionic (●). Black lines are fits to the experimental data, grey lines are lines of identiy.

References

1. Liu, X. and C. Chen, *Strategies to optimize brain penetration in drug discovery.* Curr Opin Drug Discov Devel, 2005. **8**(4): p. 505-12.
2. Reichel, A., *Addressing central nervous system (CNS) penetration in drug discovery: basics and implications of the evolving new concept.* Chem Biodivers, 2009. **6**(11): p. 2030-49.
3. Hammarlund-Udenaes, M., et al., *On the rate and extent of drug delivery to the brain.* Pharm Res, 2008. **25**(8): p. 1737-50.
4. Watson, J., et al., *Receptor occupancy and brain free fraction.* Drug Metab Dispos, 2009. **37**(4): p. 753-60.
5. Hammarlund-Udenaes, M., *Active-site concentrations of chemicals - are they a better predictor of effect than plasma/organ/tissue concentrations?* Basic Clin Pharmacol Toxicol, 2010. **106**(3): p. 215-20.
6. Hammarlund-Udenaes, M., U. Bredberg, and M. Friden, *Methodologies to assess brain drug delivery in lead optimization.* Curr Top Med Chem, 2009. **9**(2): p. 148-62.
7. Seelig, A., *The role of size and charge for blood-brain barrier permeation of drugs and fatty acids.* J Mol Neurosci, 2007. **33**(1): p. 32-41.
8. Friden, M., et al., *Measurement of unbound drug exposure in brain: modeling of pH partitioning explains diverging results between the brain slice and brain homogenate methods.* Drug Metab Dispos, 2011. **39**(3): p. 353-62.
9. Friden, M., et al., *Development of a high-throughput brain slice method for studying drug distribution in the central nervous system.* Drug Metab Dispos, 2009. **37**(6): p. 1226-33.
10. Wan, H., M. Ahman, and A.G. Holmen, *Relationship between brain tissue partitioning and microemulsion retention factors of CNS drugs.* J Med Chem, 2009. **52**(6): p. 1693-700.
11. Longhi, R., et al., *Brain tissue binding of drugs: evaluation and validation of solid supported porcine brain membrane vesicles (TRANSIL) as a novel high-throughput method.* Drug Metab Dispos, 2011. **39**(2): p. 312-21.
12. Mateus, A., P. Matsson, and P. Artursson, *A high-throughput cell-based method to predict the unbound drug fraction in the brain.* J Med Chem, 2014. **57**(7): p. 3005-10.
13. Wagner, B., et al., *Carrier Mediated Distribution System (CAMDIS): A new approach for the measurement of octanol/water distribution coefficients.* Eur J Pharm Sci, 2014. **68C**: p. 68-77.
14. Wan, H., et al., *High-throughput screening of drug-brain tissue binding and in silico prediction for assessment of central nervous system drug delivery.* J Med Chem, 2007. **50**(19): p. 4606-15.
15. Fischer, H., M. Kansy, and B. Wagner, *Determination of high lipophilicity values.*, 2006.
16. Avdeef, A., *pH-metric log P. II: Refinement of partition coefficients and ionization constants of multiprotic substances.* J Pharm Sci, 1993. **82**(2): p. 183-90.
17. Kansy, M., F. Senner, and K. Gubernator, *Physicochemical high throughput screening: parallel artificial membrane permeation assay in the description of passive absorption processes.* J Med Chem, 1998. **41**(7): p. 1007-10.
18. Wohnsland, F. and B. Faller, *High-throughput permeability pH profile and high-throughput alkane/water log P with artificial membranes.* J Med Chem, 2001. **44**(6): p. 923-30.
19. Sugano, K., et al., *High throughput prediction of oral absorption: improvement of the composition of the lipid solution used in parallel artificial membrane permeation assay.* J Biomol Screen, 2001. **6**(3): p. 189-96.
20. Avdeef, A. and O. Tsinman, *PAMPA--a drug absorption in vitro model 13. Chemical selectivity due to membrane hydrogen bonding: in combo comparisons of HDM-, DOPC-, and DS-PAMPA models.* Eur J Pharm Sci, 2006. **28**(1-2): p. 43-50.

21. Sugano, K., et al., *Prediction of passive intestinal absorption using bio-mimetic artificial membrane permeation assay and the paracellular pathway model.* Int J Pharm, 2002. **241**(2): p. 241-51.
22. Avdeef, A., *Absorption and Drug Development: Solubility, Permeability, and Charge State*2012.
23. Rodgers, T., D. Leahy, and M. Rowland, *Tissue distribution of basic drugs: accounting for enantiomeric, compound and regional differences amongst beta-blocking drugs in rat.* J Pharm Sci, 2005. **94**(6): p. 1237-48.
24. Summerfield, S.G., et al., *Central nervous system drug disposition: the relationship between in situ brain permeability and brain free fraction.* J Pharmacol Exp Ther, 2007. **322**(1): p. 205-13.
25. Sjolund, M., et al., *Hydrophobic molecules in lecithin-water systems. I. Formation of reversed hexagonal phases at high and low water contents.* Biophys J, 1987. **52**(2): p. 145-53.
26. Kirk, G.L. and S.M. Gruner, *Lyotropic effects of alkanes and headgroup composition on the lα -Hii lipid liquid crystal phase transition : hydrocarbon packing versus intrinsic curvature.* J. Phys. France 1985. **46**: p. 761-769.
27. Luisi, P.L. and B.E. Straub, eds. *Reverse Micelles: Biological and Technological Relevance of Amphiphilic Structures in Apolar Media*. 1984.
28. Jiang, Z., et al., *A rapid vesicle electrokinetic chromatography method for the in vitro prediction of non-specific binding for potential PET ligands.* J Pharm Biomed Anal, 2011. **54**(4): p. 722-9.
29. Yata, N., et al., *Phosphatidylserine as a determinant for the tissue distribution of weakly basic drugs in rats.* Pharm Res, 1990. **7**(10): p. 1019-25.
30. Maurer, T.S., et al., *Relationship between exposure and nonspecific binding of thirty-three central nervous system drugs in mice.* Drug Metab Dispos, 2005. **33**(1): p. 175-81.
31. Becker, S. and X. Liu, *Evaluation of the utility of brain slice methods to study brain penetration.* Drug Metab Dispos, 2006. **34**(5): p. 855-61.
32. Liu, X., et al., *Unbound drug concentration in brain homogenate and cerebral spinal fluid at steady state as a surrogate for unbound concentration in brain interstitial fluid.* Drug Metab Dispos, 2009. **37**(4): p. 787-93.
33. Kalvass, J.C., T.S. Maurer, and G.M. Pollack, *Use of plasma and brain unbound fractions to assess the extent of brain distribution of 34 drugs: comparison of unbound concentration ratios to in vivo p-glycoprotein efflux ratios.* Drug Metab Dispos, 2007. **35**(4): p. 660-6.
34. Summerfield, S.G., et al., *Toward an improved prediction of human in vivo brain penetration.* Xenobiotica, 2008. **38**(12): p. 1518-35.
35. Summerfield, S.G., et al., *Improving the in vitro prediction of in vivo central nervous system penetration: integrating permeability, P-glycoprotein efflux, and free fractions in blood and brain.* J Pharmacol Exp Ther, 2006. **316**(3): p. 1282-90.
36. Zhao, R., J.C. Kalvass, and G.M. Pollack, *Assessment of blood-brain barrier permeability using the in situ mouse brain perfusion technique.* Pharm Res, 2009. **26**(7): p. 1657-64.
37. Kielbasa, W., J.C. Kalvass, and R. Stratford, *Microdialysis evaluation of atomoxetine brain penetration and central nervous system pharmacokinetics in rats.* Drug Metab Dispos, 2009. **37**(1): p. 137-42.
38. Gerebtzoff, G. and A. Seelig, *In silico prediction of blood-brain barrier permeation using the calculated molecular cross-sectional area as main parameter.* J Chem Inf Model, 2006. **46**(6): p. 2638-50.

4.7 Label-Free Assay for the Assessment of Non-specific Binding of Positron Emission Tomography Tracer Candidates

Frauke Assmus, Anna Seelig, Holger Fischer

Author's Contributions:

Frauke Assmus	• Design of the study • Performing the experiments • Data mining • Evaluation of *in vivo* PET data • Writing the manuscript
Anna Seelig	• Supervison of the work • Valuable discussions •
Holger Fischer	• Idea of the study • Supervision of the work • Valuable discussions

ABSTRACT

Positron emission tomography (PET) is a valuable technique for the visualization of drug tissue distribution and receptor occupancy at the target site in living animals and men. Many potential PET tracers, however, fail due to an unfavorably high non-specific binding to non-target proteins and phospholipid membranes which compromises the sensitivity of PET. Hence, there is a high demand to assess the extent of non-specific binding as early as possible in the PET tracer development process, preferentially before labeling of the ligand and elaborate autoradiography studies. The purpose of this study was to establish a Lipid Membrane Binding Assay (LIMBA) for estimating non-specific binding in brain tissue. To test LIMBA we used i) 30 tracers characterized with *in vitro* autoradiography (rat, mouse) and ii) 10 tracers investigated with *in vivo* PET (literature data, human). Rat brain tissue/water distribution coefficients, $\log D_{brain}(pH7.4)$, of the unlabeled test compounds were measured with LIMBA which allows for medium-throughput screening at minimal expense of animal tissue. With respect to the autoradiography data, good prediction accuracy was achieved ($r^2 \geq 0.87$) whereas octanol/water distribution coefficients, $\log D_{oct}(pH7.4)$ were less predictive). Moreover, LIMBA yielded $\log D_{brain}(pH7.4)$ values in good agreement with non - specific binding estimates derived from PET studies, pertaining to tracers classified as non - substrates of P-glycoprotein. In conclusion, LIMBA provides a fast and reliable tool for identifying compounds with unfavorably high non-specific binding in brain tissue. The data may be used in conjunction with other image-determining parameters like permeability, target affinity and receptor density for predicting the likely development success of potential PET tracers.

KEYWORDS

Nonspecific binding, Tissue binding, Positron emission tomography, Lipophilicity, PET tracer

1. Introduction

Positron Emission Tomography (PET) has emerged as a valuable tool in the drug development process to study the biodistribution and receptor occupancy of drug candidates at the target site in living animals and men [1]. The value of PET as a non-invasive imaging technique is of particular interest in the field of CNS drug discovery where large discrepancies may arise between plasma and biophase pharmacokinetics and, moreover, where animal models may not adequately reflect the complexity of human disease [2]. The study of dose-receptor occupancy relationships by means of PET allows not only for optimal dosing selection to achieve maximal target vs. off target responses but may also improve our understanding of the relationship between receptor occupancy and pharmacodynamics, both in healthy and in diseased state. The advancement of small animal PET cameras has furthermore paved the way for PET studies in preclinical species with great promise to bridge the gap between preclinical and clinical drug discovery [3].

In order to exploit the full potential of PET for drug development, drug candidates and the corresponding PET tracer for the target site of interest should ideally be developed in parallel. Notably, there is still a lack of suitable PET tracers for many targets, and their innovation is challenging given the large number of sometimes conflicting requirements to be fulfilled, particularly for imaging agents that bind to specific targets in the brain [4, 5]. A high binding sites density is desirable and only the unmetabolized radiotracer should pass the blood-brain barrier (BBB) to bind with high affinity and specificity to the target site of interest (specific binding, SB) [6]. In contrast, non-specific binding (NSB) to non-target proteins and lipids should be low to ensure a high SB to NSB ratio. The higher the ratio, the higher the sensitivity of PET to monitor changes of the available binding sites due to drug-related receptor occupancy [4, 7]. Radiotracers should achieve SB/NSB ratios in the range 3-10 to be successfully applied *in vivo* [7, 8], and [4] stressed that ”most of the failures in ligand development result from an unfavorable combination of target density, ligand affinity and nonspecific binding”.

The full characterization of a PET tracer is time-consuming, expensive and requires expert knowledge of a radiotracer imaging team as well as special technical facilities [9]. To concentrate resources only on the most promising candidates, preliminary and less resource demanding assays are applied for selecting radiotracers with the desired properties. *Ex vivo* autoradiography studies, for example, can be performed to image the *in vivo* distribution of radiotracers throughout the entire body, without the need to incorporate positron emitting

nuclei into the ligands. Autoradiography studies performed *in vitro* (i.e. incubation of radioligands with tissue slices) can further accelerate the pace by which images of SB and NSB can be obtained and quantified. Even though pharmacokinetic aspects such as the presence of permeation barriers as well as drug clearance and distribution across different organs are disregarded, a primary measure of the SB/NSB ratio becomes available. Tracers are rejected when e.g. a major part of the total binding (TB=SB+NSB) in the brain region of interest (ROI) is originating from an unfavorably high NSB, as assessed in a reference region (R_{REF}) devoid of receptors. Yet, failing at this point of the tracer development process is costly given that autoradiography studies are time-consuming, require radiolabeling of the ligand and the sacrifice of animals.

To provide a faster and less resource-intensive estimation of NSB, *in vitro* methods working with the unlabeled compound are highly desirable. The octanol/water distribution coefficient, $\log D_{oct}$ (pH 7.4) is the commonly used parameter for assessing the NSB of potential PET tracers, albeit with limited prediction accuracy for structurally unrelated compounds [4, 10]. The unbound fraction of a ligand in brain, $f_{u,brain}$, available from equilibrium dialysis with brain homogenate, provides a physiologically more relevant NSB-estimate which has successfully been applied for the parameterization of a comprehensive radiotracer kinetic model [11]. The dialysis technique has found entry in many laboratories as a higher throughput alternative to measure tissue binding [12-14] when compared to the brain slice uptake technique [15, 16]. Potential experimental errors in $f_{u,brain}$, associated with the disruption of tissue and the resulting depletion of intracellular pH gradients, can be corrected by a pH partitioning model [17]. However, a drawback of the homogenate dialysis is the high consumption of tissue which impedes the screening of larger datasets at reasonable expense of laboratory animals. Recently, a vesicle electrokinetic chromatography (VEKC) method working with an artificial anionic detergent (Sodium bis(2-ethylhexyl) sulfosuccinate, AOT) has been developed for the prediction of NSB showing a good correlation between chromatographic retention factors and *in vitro* NSB derived from equilibrium dialysis. The VEKC method has also been shown to provide a useful tool for the classification of either successful or terminated PET ligands tested *in vivo*, however, on a qualitative level only [18].

Quantitative *in vivo* NSB estimates, expressed as the volume of distribution of non-specifically bound tracer in brain, $V_{NS,F}$, have been derived from kinetic analysis of PET scans and were used for the validation of a computational NSB prediction method. A good correlation with calculated drug-lipid interaction energy and $V_{NS,F}$ was found [10, 19], yet, the

ab initio quantum mechanical method was computationally expensive and relied on the interaction of the ligand with 1,2-dioleoyl-sn-glycero-3-phosphorylcholine (DOPC) neglecting the full complexity of a biological membrane.

The purpose of the present study was to test whether a novel *in vitro* assay, referred to as Lipid Membrane Binding Assay (LIMBA), proves useful for estimating the NSB of potential PET tracers. LIMBA relies on the use of rat brain tissue, albeit requires only small amounts thereof for the label-free assessment of tissue binding. The medium-throughput assay was recently developed in our laboratory and yields brain tissue/water distribution coefficients, $\log D_{brain}$ in excellent agreement with $f_{u,brain}$ (homogenate dialysis) [20], even when brain tissue was replaced by a microemulsion of brain polar lipids [21]. In the course of this study, we evaluated LIMBA on a set of i) 30 publicly available and proprietary tritiated radioligands for which NSB-estimates in brain were available from *in vitro* autoradiography studies (in-house data, in rat and mouse), and ii) 10 PET tracers for which NSB data was retrieved from *in vivo* PET studies (literature data, in human). The ability of LIMBA for predicting NSB was evaluated in comparison with $\log D_{oct}$ (pH 7.4), and outliers for the $V_{NS,F}$ prediction are discussed by taking into account the effect of P-glycoprotein (P-gp), an important efflux transporter protein present at the BBB [22]. In addition, we investigated whether a threshold-NSB value can be assessed above which the likelihood of a sufficient TB/NSB ratio in autoradiography is low and the rejection of compounds for later-stage *in vivo* studies indicated.

2. Materials and Methods

2.1. Drugs and Chemicals

Fallypride and 3-amino-4-[2-[(di(methyl)amino)methyl]phenyl]sulfanylbenzonitrile (DASB) were purchased from ABX (Radeberg, Germany). Diprenorphine, SCH 23390 and SR 222200 were obtained from Tocris (Bristol, UK). Flumazenil and raclopride·tartrat were purchased from Sigma (Steinheim, Germany). All other drugs were available through our in-house Compound Depository Group as proprietary compounds. TRIS, TAPSO and sodium chloride were obtained from Fluka (Buchs, Switzerland). Octanol and dodecane were purchased from Sigma (Steinheim, Germany). DMSO was obtained from Acros (Geel, Belgium). Water and acetonitrile for HPLC were supplied from Merck (Darmstadt, Germany) and were of HPLC-grade.

2.2. Determination of n-Octanol/Water Distribution Coefficients

Unless otherwise stated, $\log D_{oct}\,(pH\,7.4)$ values were measured with a miniaturized shake flask technique. In brief, a DMSO stock solution of the test compound (0.5 mM) was dispensed in aqueous buffer (50 mM TAPSO /pH 7.4, final DMSO content 5 %) which was pre-saturated with octanol. The aqueous drug solution (25 µM) was filtrated and an aliquot of the filtrate was transferred to a 96-well PCR plate (Eppendorf). After adding buffer-saturated octanol on top of the filtrate, the PCR plate was sealed and incubated for two hours at room temperature (RT), while shaking. The plate was left undisturbed overnight and was then centrifuged for 10 min at 3000 rpm (Eppendorf, Centrifuge 5810R). The aqueous drug solution was sampled with a robotic pipetting system (Tecan) and the equilibrium aqueous drug concentration, C_{aq}^{eq}, was determined with a UV plate reader (SpectraMax). In parallel, a reference experiment was carried out under the same conditions but without octanol in order to obtain the initial aqueous drug concentration, C_{aq}^{0}. $LogD_{oct}\,(pH\,7.4)$ values were obtained by mass balance according to

$$\log D_{oct} = \log\left(\frac{\left(C_{aq}^{0} - C_{aq}^{eq}\right)\cdot V_{aq}}{C_{aq}^{eq}\cdot V_{oct}}\right), \qquad (1)$$

where V_{aq} and V_{oct} denote the volume of the aqueous and the octanol phase, respectively.

2.3. Determination of Brain Tissue/Water Distribution Coefficients (LIMBA)

Brain tissue (rat) /water distribution coefficients, $\log D_{brain}(pH\,7.4)$, were determined with the in-house LIMBA assay as described below. Briefly, drug-naive female Wistar rats were sacrificed in a CO_2 chamber and the whole brain was sampled and immersed in assay buffer (50 mM TRIS/114 mM NaCl/ pH 7.4) to remove adherent blood. The rat brain was weighted and homogenized on ice in 2 volumes (w/v) of n-dodecane using an ultrasonic probe (Branson sonifier, G. Heinemann, Schwäbisch Gmünd, Germany). Experiments were conducted in accordance with the current Cantonal and Federal legislation on the welfare of experimental animals. For the preparation of the aqueous phase, test compounds were introduced into the assay buffer (50 mM TRIS/114 mM NaCl/pH 7.4) as DMSO stock solutions (10 mM). The resulting aqueous drug solution (25 µM, DMSO content 0.25 %) was filtrated (Millipore Multiscreen plates, MDRLN0410) and aliquots of the filtrate (V_{aq} = 50 µL) were transferred into an in-house made Teflon plate. In parallel, rat brain homogenate (V_{br} =1.2 µL) was coated on a PVDF filter attached to the bottom of the customized and commercially available DIFI tubes (Weidmann Plastics Technology AG, Rapperswill, Switzerland, 23358) [23]. The pipetting was conducted with a Hamilton robotic system using new pipetting tips (disposable, 10 µL) for each coating step and a sealed 96 well PCR plate (Eppendorf) for the storage of brain homogenate, which was put on a shaker. The coated DIFI tubes were added on top of the Teflon plate pre-filled with aqueous drug solution thus forming a sandwich. The kit was sealed and allowed to shake at RT for 15 h. The incubation time was based on prior experiments showing that distribution equilibrium was achieved after 15 h. After removal of the DIFI tubes, the equilibrium drug concentration in the aqueous phase, C_{aq}^{eq}, was analyzed with HPLC - UV/MS. A reference experiment was carried out in the same plate but without brain homogenate. $LogD_{brain}(pH7.4)$ values were obtained by mass balance according to the assessment of $\log D_{oct}(pH\,7.4)$. All distribution experiments were performed in triplicate and mean $\log D_{brain}(pH7.4)$ values are reported.

2.4. HPLC-MS Instrumentation and Chromatographic Conditions

Drug concentrations in aqueous solutions were quantified using an Agilent 1290 Infinity HPLC-MS system (Agilent Technologies, CA, USA) equipped with a DAD detector and an API single quadrupole mass spectrometer (Agilent 6140). An aliquot of each sample (5 µL) was injected onto a Kinetex 2.6 µm, 2.1 x 50 mm analytical column (Phenomenex, Germany)

operated at 60 °C. The mobile phase consisted of A (water) and B (acetonitril), both containing 0.1 % (V/V) formic acid. The gradient elution was performed as follows: initial 2 % B, 0 - 0.35 min linear gradient from 2 % B to 95 % B, 0.35 min - 0.65 min 95 % B, post time 0.5 min. After passing the DAD detector, the eluent was introduced into the electrospray interface maintaining the following source settings: capillary voltage + 3.5 kV, drying gas flow (N_2) 13 L/min, nebulizer pressure 60 psi, drying gas temperature 350 °C. The integral of the pseudo - molecular ion intensity, $[M+H]^+$, was acquired in single reaction monitoring mode. Internal calibration for MS data analysis was accomplished by injection of 1, 3, and 5 µL of the sample solution. Peak areas at appropriate wavelength (UV) or mass responses (if UV sensitivity was insufficient) were used for the calculation of $\log D_{brain}$.

2.5. Determination of [^{3}H]-Radioligand Binding in Brain by *in vitro* Autoradiography

A dataset of 30 tritiated radioligands was comprised from our in-house database and included radioligands with known NSB data from *in vitro* autoradiography studies in brain. Autoradiography studies were performed as follows and as described elsewhere in more detail [24]. Laboratory animals (mice, gerbil, rats) were housed at controlled temperature (20 – 22°C) and 12 h light/dark cycle. All animals were allowed *ad libitum* access to food and water. The animals were killed by decapitation and the brains were rapidly removed from the skull and immediately frozen on dry ice. Sections (10 - 20 µm) from brain were cut in a cryostat and thaw-mounted onto silane-coated microscope slides (HistoBond, Paul Marienfeld GmbH, Lauda-Königshofen, Germany). Brain sections (n = 10) were dried at RT and stored at -20 °C until the day of the autoradiography measurements. Brain sections (n = 5) were first pre-incubated (10 - 20 min) in assay buffer (in most cases TRIS/pH 7.4) and then in assay buffer containing the tritium-labeled ligand (concentration of the ligand: 0.08 - 23.5 nM; incubation time: 12 - 120 min; RT or 37 °C). NSB was measured using five additional brain sections incubated in presence of a non-radiolabeled compound that compete with the radioligand for the same binding site (concentration of the antagonist: 1 - 100 µM). Brain sections were subsequently rinsed in ice-cold assay buffer (washing time t_{wash}= 2 - 10 min) and dipped briefly (n = 1 - 3) in distilled water at 4 °C to remove buffer salts. The brain sections were dried at RT and exposed, together with a tritium microscale (RPA-510, GE Healthcare, Glattbrugg, Switzerland), to tritium-sensitive imaging plates (BAS-TR 2025, Fujifilm, Dielsdorf, Switzerland) for 5 - 6 days. The imaging plate was scanned in a Fujifilm high-resolution plate scanner (BAS-5000, Bucher Biotec AG, Basel,

Switzerland) and images were quantified with an MCID M2 image analysis system (Imaging Research Inc., St. Catherines, Ontario, Canada). The total amount of radioligand bound in the ROI and in the reference region devoid of receptors (NSB) was expressed as fmol of bound radioligand per mg of protein (total binding = TB). A quantitative estimate of NSB was also obtained after blocking the receptors with an unlabeled molecule. The nominal tracer concentration for the determination of NSB was 3 nM, and the measured radioactivity was corrected for the real concentration. The experimental conditions (buffer, incubation temperature, animal species, length of incubation/rinsing) used for quantification of receptor binding and NSB were notably optimized for each tracer and are enclosed in detail in the Supplementary Information. The following selection criteria for the inclusion of compounds in our dataset were applied: i) presence of an unlabeled ligand for blocking of specific binding sites and allowing for the assessment of NSB ii) agreement of results for the extent of NSB at two different radioligand concentrations and iii) a exposure time of the brain slices to a washing solution (after incubation with the assay buffer) of $t_{wash} \leq 10\text{min}$.

2.6. Compilation of NSB Data from *in vivo* PET Studies

A database of 10 radioligands was compiled from literature and, if not otherwise stated, included PET tracers investigated with *in vivo* PET in living man. Different tracer kinetic models [25], e.g. one tissue and two tissue compartmental models, have been used in the reported studies for the analysis of radioligand - time activity curves in PET. The volume of distribution of the non-specifically bound radioligand in a reference region with respect the total plasma concentration (V_{NS}) was extracted from the published kinetic PET data and was expressed with respect to the free plasma concentration ($V_{NS,F}$) according to:

$$V_{NS,F} = \frac{V_{NS}}{f_p} = \frac{V_{ND}}{f_p} - 1 = \frac{K_1^{'}}{f_p k_2^{'}} - 1, \qquad (2)$$

where V_{ND} is the is volume of distribution of the non-displaceable radioligand (free +non-specifically bound) with respect to the total plasma concentration in a reference region, and f_p is the unbound fraction of radioligand in plasma reported in literature (for references see Table 3). $K_1^{'}$ and $k_2^{'}$ denote the rate constants for the transfer of radioligand from plasma into the brain and vice versa, respectively. The term $V_{NS,F}$ reflects the extent of NSB in brain,

provided that a radioligand passes the BBB by passive diffusion [26]. Further details regarding the derivation of Eq.2 including relevant background information about compartmental analysis and tracer kinetic modelling are provided in the Supplementary Information. Eq. 2 is similar to that derived by [10], however, for clarity we distinguish V_{NS} (distribution volume related to the total plasma concentration) from $V_{NS,F}$ (distribution volume related to the free plasma concentration). No $V_{NS,F}$ - data from *in vivo* PET studies in human brain was available for rolipram and therefore data from PET studies in porcine brain was used for regression analysis.

3. Results and Discussion

A high NSB of radiotracers to membranes and non-target proteins affects the accuracy with which the specific binding to a target site (receptor occupancy) can be measured by means of PET. Many PET tracers fail due to an unfavorable combination of low receptor density, low receptor affinity and, in particular, high NSB [4]. In order to enhance the confidence in the likely quality of a tracer, we have evaluated the ability of a novel medium-throughput assay (LIMBA) to predict the extent of NSB of the unlabeled compound, as well as the likelihood to achieve sufficient TB/NSB ratios. The results are shown and discussed below in comparison with $\log D_{oct}\,(pH\,7.4)$, using the example of radioligands characterized with i) *in vitro* autoradiography and ii) *in vivo* PET.

3.1. Characterization of the *in vitro* Autoradiography Dataset

A dataset of 30 radiotracers with known NSB-estimates in brain sections (rat, mouse), available from *in vitro* autoradiography studies, was compiled as described in Materials and Methods. The larger body of NSB autoradiography data as compared to PET data allowed us to form a structurally diverse database covering a wide physicochemical property space. The dataset was comprised of both publicly disclosed and proprietary radiotracers in the tritium-labelled form, yet, the measurement of $\log D_{oct}$ and $\log D_{brain}$ was performed with the unlabelled ligands. The structures for 13 ligands, for which no potential conflict of interest might prevent publication, are disclosed in the Supplementary Information. Key physicochemical properties (molecular weight, pK_a, $c\log P$, $\log D_{oct}$(pH 7.4)) of all 30 compounds are provided in Table 1 along with NSB data obtained from *in vitro* autoradiography. The dataset included neutral, basic, and zwitter-ionic compounds covering a broad range of $\log D_{oct}$ values ($\log D_{oct}$(pH 7.4) = -0.64 - 4.35) and NSB-estimates (NSB = 7.6 - 3151.1 fmol/mg protein).

Table 1

It is important to note that the NSB-estimates provided in Table 1, and used for comparison with $\log D_{oct}$(pH 7.4) and $\log D_{brain}$ (pH 7.4), refer to the TB in a reference region in presence of a receptor blocker. From a theoretical point of view, an NSB-estimate may also be obtained under non-blocking conditions from the TB in a reference region which is, by

definition, devoid of receptors and should therefore solely reflect NSB. However, the presence of specific binding sites cannot *a priori* be excluded. This is supported by the example of the NK3 receptor antagonist [^{3}H]-SR222200 (No. 11) for which *in vitro* autoradiographs in absence and in presence of a blocker (osanetant) are shown in Fig. 1A1 and Fig. 1A2, respectively.

Fig. 1

The TB in the reference region (hippocampus) in absence of the unlabeled blocker was approximately twice as high as the NSB in the same region under blocking conditions. A saturation of NSB sites (phospholipid lipid membranes, non-target proteins) with the unlabeled receptor blocker is unlikely considering the excess of lipids relative to the concentration of the receptor blocker ($C_{blocker}$ = 10 μM). Since SR222200 is non-charged, it is also safe to exclude that electrostatic repulsion of the ligand by the cationic blocker leads to a decrease of NSB. The higher TB in the reference region in absence of a blocker may rather be explained by the presence of low - but not zero - levels of NK3 receptors [27] in the hippocampus, which has historically been considered as reference region.

The TB in a reference region in absence and in presence of a blocker was further assessed for the complete autoradiography dataset (Fig. 2) revealing a higher TB under non-blocking conditions for 11 of the 30 ligands tested, which confirmed the trend observed for [^{3}H]-SR222200.

Fig. 2

The autoradiographs under non-blocking conditions were also analyzed in terms of TB in a ROI in order to retrieve the TB/NSB binding ratios which are provided in Table 1 (for discussion see Section 3.4). Contrary to [^{3}H]-SR222200 (Fig. 1A), the dopamine D2 receptor antagonist [^{3}H]-raclopride (No. 16) is an example for a tracer with an excellent signal to noise (TB/NSB) ratio, irrespective of whether or not a dopamine receptor blocker was employed for determining NSB (Fig. 1B).

3.2. The Relationship between Non-specific Binding in Brain (Autoradiography Data) and $LogD_{oct}$

$LogD_{oct}$ (pH 7.4) is the most commonly used parameter for estimating the NSB of potential PET tracers, however, the datasets investigated hitherto were rather small and a trend between $\log D_{oct}$ and NSB was only observed when structurally similar ligands were compared [4]. In order to evaluate the predictive ability of $\log D_{oct}$ (pH 7.4) on a larger and structurally diverse set of compounds, we compared the NSB-estimates from the *in vitro* autoradiography dataset (in presence of a blocker) with measured $\log D_{oct}$ (pH 7.4) values.

At this point it should be noted that the times brain slices were exposed to a washing solution in autoradiography were slightly different and optimized for the individual tracers. Longer washing times are likely associated with a reduction in NSB (see below) and are therefore desirable to yield higher signal-to-noise ratios (TB/NSB) for more reliable quantification of receptor densities and affinities. However, in order to analyse the relationship between $\log D_{oct}$ (pH 7.4) and NSB, it was necessary to analyse NSB autoradiography data at different washing times (subsets: t_{wash}= 2 - 4 min and t_{wash} = 7 - 10 min) separately as shown in Fig. 3A.

Fig. 3

The correlation statistics for the two subsets based on binned washing times are summarized in Table 2 showing improved, but still unsatisfactory fits to the experimental NSB data as compared to the correlation based on the whole dataset. A clear trend was evident towards lower NSB at longer incubation times of brain slices with the washing buffer. The discrepancy in NSB is reflected by the intercepts of the linear regression lines which are more than one log unit apart. Due to the scatter of the data, no clear trend in terms of the predictive power of $\log D_{oct}$ (pH 7.4) for different charge classes can be drawn. However, for the less scattered subset at washing times t_{wash}=7 - 10 min, an underestimation of NSB by $\log D_{oct}$ (pH 7.4) is evident for the most hydrophilic basic compound (No. 25), while the remaining basic and neutral compounds roughly cluster.

With respect to the rather poor correlation between $\log D_{oct}$ (pH 7.4) and NSB, it is worth to note that even though octanol is widely considered as a surrogate for lipid bilayer membranes, it lacks the anisotropy of a bilayer and the charge of a phospholipid head group

[28]. Depending on the charge state, the binding of drugs to phospholipid membranes may be driven by both hydrophobic and electrostatic interactions. At the example of propranolol and other bases, it has been shown that neutral and cationic species of a basic drug can bind to a net neutral phospholipid membrane with a relatively large contribution of the ionized species to the overall extent of membrane binding [29, 30]. The minor contribution of ionized species to the partitioning into octanol (here observed for compound No.25) may accordingly reflect the difference between bulk phase partitioning (octanol) and drug binding in an anisotropic amphiphilic environment in which charged drugs can bind to a membrane surface. The presence of negatively charged phospholipids (e.g. phosphatidylserine (PS), phosphatidylinositol (PI), phopshatidylglycerol (PG), phosphatidic acid (PA)) in a biological membrane may further enhance the membrane affinity of basic drugs by electrostatic interactions with the acidic phospholipid head groups. Pronounced distribution of basic drugs into tissues containing high concentration of negatively charged phospholipids is well documented [31-33], and in particular the presence of PS has been identified as a main determinant of interorgan variation in tissue distribution [34]. Notably, brain tissue is relatively rich in acidic phospholipids (between 9.4 and 20.8 % of total phospholipids) as estimated from the phospholipid composition in brain tissue reported for rat: 50 mg of lipid phosphorous / g of tissue, thereof 0.23-5.9 mg/g PS, 2.79 mg/g PI, 1.10 mg/g PG and 0.6 mg/g PA [32].

3.3. The Prediction of NSB in Brain (Autoradiography Data) Using LIMBA

$Log\,D_{brain}$ (pH 7.4) values for the complete autoradiography dataset were measured with a novel *in vitro* assay, LIMBA, as described in Materials and Methods. As opposed to the octanol shake flask technique, LIMBA works with minimal consumption of brain homogenate in dodecane (here: rat) which more likely resembles the composition and properties of brain tissue (see Section 3.2). The assay has been optimized for compounds with intermediate to high tissue binding, allowing the measurement of $\log D_{brain}$ (pH 7.4) values in the range of $\log D_{brain}$(pH 7.4) = 0.35 - 4. This range applied to 27 of the 30 compounds tested for which the results are presented in Table 1.

Fig. 3B shows the correlation and the linear regression lines between NSB and $\log D_{brain}$ (pH 7.4) for the different times brain slices were exposed to the washing solution. An inspection of the correlation statistics (Table 2) in comparison with those obtained with $\log D_{oct}$(pH 7.4)

reveals a higher statistical certainty (r^2 = 0.87 - 0.91) in the estimates of NSB when using $\log D_{brain}$ (pH 7.4).

Table 2

No clear outliers for compounds of different charge classes were observed indicating that the applied brain homogenate provides a fairly good surrogate for brain tissue, despite the presence of dodecane. It is interesting to note that alkanes (e.g. dodecane) have been shown to change the membrane fluidity and, at higher concentrations, the long range order of phospholipids in a membrane [35-38]. The effect of high concentrations of dodecane (as used herein) on the membrane structure has been investigated in great detail in our laboratory and further details will be published separately [39].

3.4. The Relationship between TB/NSB Ratios and NSB in Brain

We could show that the NSB in rodent brain, derived from autoradiography experiments, can reliably be predicted using LIMBA, however, NSB should not be considered in isolation from the TB in a ROI; the ratio between both (i.e. TB/NSB) determines the image quality and therefore the likely development success, or failure, of potential PET tracers [4]. Both parameters (TB/NSB and NSB) are closely related, however their relationship is not trivial. On the one hand, high NSB obscures the TB in the ROI and therefore reduces the sensitivity of PET to changes in receptor occupancy. On the other hand, pronounced NSB (i.e. high affinity for lipid membranes and non-target proteins) may also be associated with a higher affinity for the target site. It would therefore be interesting to proof whether a limit with respect to NSB exists above which the probability to obtain sufficient TB/NSB ratios is low. A correlation between TB/NSB and NSB for the complete autoradiography dataset is shown in Fig. 4A and may be used as a classification map.

Fig. 4

According to [8] the signal-to-background noise ratio (SB/NSB) in a PET scan should be at least 4, which corresponds to a TB/NSB ratio of at least 5. At NSB values > 3, none of the radioligands (n=3; No. 13, 14, 15) fulfilled the requirement for the suggested TB/NSB limit (Fig. 4A). It is important to note that those compounds with sufficient TB/NSB ratios were

exposed for longer incubation times to the washing solution (open symbols) leading to artificially high TB/NSB ratios (see Section 3.5).

3.5. Identification of Radioligands with Inadequate TB/NSB Ratios using LIMBA

In the next step, we investigated whether ligands with a TB/NSB ratio < 5 at high NSB values can be identified with a classification map that is based on LIMBA $\log D_{brain}$ (pH 7.4) values rather than on NSB *in vitro* autoradiography data (Fig. 4B). All three critical compounds identified in Fig. 4A matched those in the corresponding TB/NSB - $\log D_{brain}$ (pH 7.4) classification map (Fig. 4B), provided that the threshold value was set to $\log D_{brain}$(pH) = 2.1. However, two compounds (No. 28, 29) with TB/NSB > 5 showed $\log D_{brain}$ values > 2.1, and were thus misclassified in LIMBA as likely to fail. It is important to note that brain slices for both misclassified compounds were exposed for relatively long times to a washing solution (t = 10 min), which leads to a decrease in NSB and, in turn, an artificial increase in the TB/NSB ratio. A reduction of washing times would accordingly shift both misclassified compounds to the lower right corner of the classification map, which would then agree with the high $\log D_{brain}$(pH 7.4) values. All compounds for which shorter washing times (t = 2-4 min) were applied, and for which the specified $\log D_{brain}$ (pH 7.4) threshold was exceeded, were correctly classified by LIMBA (No. 13, 14, 15). The classification map may thus be used as a guideline for optimizing potential PET tracers with undesirably high NSB values, without the need for autoradiography studies and prior to radioactive labelling. Whether or not compounds below the critical NSB or $\log D_{brain}$(pH 7.4) threshold yield sufficient TB/NSB ratios depends on the target affinity and the receptor density which are available from classical receptor binding studies and/or from literature.

It is worth to reiterate that long washing procedures of brain slices in autoradiography might be desirable to maximize TB/NSB ratios, however, the situation *in vivo* lacks the benefit of washing. Therefore, we propose limiting the exposure times of brain slices to washing solutions to maximal 4 minutes to achieve the elimination of buffer salts, yet, without reducing NSB in an unphysiological manner. Likewise, a non-washing procedure as proposed by other authors may be applied [40], as long as a uniform protocol is used for all ligands of interest.

3.6. Predicting Non-specific Binding in PET using LIMBA

Hitherto, we have based the analysis of prediction methods for radioligand bindig in brain on autoradiography data which was more readily available as compared to PET studies and therefore beneficial for the explanatory power of the validation. Moreover, it was advantageous that NSB-estimates available from *in vitro* autoradiography were not confounded by active transport mechanisms at the BBB because brain slices were directly exposed to the radioligand incubation medium. However, we have shown that results obtained from the autoradiography experiments were sensitive to the assay conditions.

In order to test the applicability of LIMBA for predicting *in vivo* NSB observed by PET, a database of 10 well characterized PET tracers studied in living human was compiled from literature and comprised tracers acting on a variety of molecular targets in the CNS (Table 3). Rate constants governing the transfer from plasma into brain and vice versa (K_1' and k_2', respectively) have been reported and were used to infer the volume of distribution for non-specifically bound tracer with reference to the unbound plasma concentration ($V_{NS,F} = V_{NS} / f_p$, Eq.2). Provided that radioligands pass the BBB by passive diffusion, the term $V_{NS,F}$ can be considered as an expression for NSB [26], and could therefore be used to investigate the suitability of LIMBA - $\log D_{brain}$(pH 7.4) for the prediction of NSB *in vivo*. Measured LIMBA-$\log D_{brain}$(pH 7.4) values as well as $\log V_{NS}$ and f_p data for the investigated PET tracers are provided in Table 3, along with some key physicochemical properties including the cross-sectional areas, A_D.

Table 3

It is well known that compounds with A_D > 70Å^2 are associated with reduced brain uptake as a result of reinforced efflux by P-gp [28, 41]. This would notably lead to $V_{NS,F}$ levels below those reflecting only passive drug-tissue distribution under steady state. The relationship between $V_{NS,F}$ and $\log D_{brain}$(pH 7.4) for compounds with A_D values below and above the critical A_D threshold is shown in Fig. 4.

Fig. 4

Linear regression analysis demonstrated excellent correlation statistics (r^2=0.94, SD=0.21) for compounds with $A_D \leq 70$ Å^2, which we classified as non-substrates for P-gp based on A_D. In contrast, $V_{NS,F}$ values observed for compounds with $A_D > 70$ Å^2 (fallypride, PK 11195 and WAY 100635) were generally lower than $V_{NS,F}$ values predicted by $\log D_{brain}$(pH 7.4). In this regard, it is important to note that LIMBA is only capable of assessing drug distribution governed by passive mechanisms since active transport proteins are not functional in the brain homogenate due to the presence of dodecane and the absence of ATP. Accordingly, any active efflux (influx) transport processes present *in vivo* will translate into an overestimation (underestimation) of $V_{NS,F}$ values by LIMBA, as observed for fallypride, PK 11195 and WAY 100635. All three compounds have experimentally been identified as substrates [42, 43] or modulators (PK 11195, [44]) of the efflux transport protein P-gp which is in line with our classification based on A_D. With regard to the PET tracers with $A_D \leq 70$ Å^2, literature supported our classification as non-P-gp substrates in case of rolipram [45], diprenorphine [46] , raclopride [47] and DASB (no literature with contrary information was found). For Spiperone, a borderline compound in terms of A_D (A_D = 70 Å^2), efflux by P- gp was reported [48] and a slightly, but not significant overestimation of $V_{NS,F}$ by $\log D_{brain}$(pH 7.4) was observed (Fig. 4). Active efflux *in vivo* in rodents was reported for flumazenil [47, 49], which is in contrast to our classification. Notably, *in vitro* transport studies using MDCKII cells transfected with human multidrug resistance (MDR1) genes suggested that flumazenil cannot be considered as substrate of human P-gp. Since the $\log D_{brain}$(pH 7.4) value for flumazenil was below the applicability range of LIMBA a direct comparison between $\log D_{brain}$(pH 7.4) and the $V_{NS,F}$ data could not be made. Further research is therefore required to address this question, however, it is worth noting that the classification of whether or not a compound is a substrate of P-gp is heavily dependent on the compound concentration [50]. Even though the A_D-based classification gives only a first indication for the likelihood of active efflux, the size restriction of the BBB is well documented [51, 52] and we considered our classification useful for rationalizing the relationship between $V_{NS,F}$ and $\log D_{brain}$(pH7.4). In summary, LIMBA-$\log D_{brain}$(pH 7.4) values were highly predictive for *in vivo* $V_{NS,F}$ data -estimates in human brain with respect to compounds classified as non-P-gp substrates ($A_D \leq 70$ Å^2). This is in line with the results obtained from *in vitro* autoradiography experiments showing

excellent performance of LIMBA for predicting the NSB in rodent brain for tritium-labelled compounds.

3.7. Limitations and Future Perspectives

The likely development success of potential PET tracers depends on a multitude of factors apart from NSB. The list of requirements is long and includes e.g. sufficient target density and affinity, target selectivity, low protein binding, brain permeability, resistance to rapid metabolism and absence of brain penetrant metabolites [6]. The aim for achieving low NSB, on the one hand, and a high affinity for the target site as well as high brain permeability, on the other hand, are potentially conflicting and thus the need for balancing lipophilicity cannot be overemphasized [53].

For future applications, $\log D_{brain}$ (pH 7.4) values available through LIMBA should therefore not be considered in isolation but rather within the framework of an integrative strategy. Recently, a bio-mathematical modelling approach has been successfully applied to predict the image quality in PET by integrating the properties of both, the tracer candidate and the biological system, into one prediction model [11]. An important input parameter was the unbound fraction of PET tracers in brain, as determined by equilibrium dialysis. An estimate for $f_{u,brain}$, or in other terms NSB, can now be derived at higher throughput and with lower consumption of brain homogenate by using LIMBA, which we propose as a novel assay for estimating NSB in brain.

4. Conclusions

In summary, the novel LIMBA assay yields $\log D_{brain}$ (pH 7.4) values in excellent agreement with NSB-estimates in brain, as demonstrated on a large dataset studied with *in vitro* autoradiography. Moreover, good prediction accuracy was achieved for the estimation of NSB in *in vivo* PET, provided that tracers are not classified as P-glycoprotein substrates. The weaker statistical performance of $\log D_{oct}$ (pH 7.4) shows that bulk octanol is rather a poor surrogate for brain tissue. Since LIMBA works with minimum consumption of brain homogenate (1.2 μL) and, moreover, does not require radioactive labeling, reliable NSB-estimates can be obtained at higher throughput as compared to autoradiography and equilibrium dialysis studies. Tracer candidates with an unfavourably high NSB can be identified with LIMBA, however, other factors such as brain permeability as well as sufficient receptor density and target affinity are equally important for the success of a PET tracer. $Log\, D_{brain}$ (pH 7.4) values may thus be used in conjunction with other physiological and physicochemical parameters to predict the image quality in PET by means of tracer kinetic modelling and simulation. Therefore, LIMBA holds much promise to accelerate the optimization of novel PET tracers in order to exploit the full potential of PET neuroimaging for drug discovery and development.

Acknowledgements

The authors thank Patrizia Glaentzlin for providing the autoradiography data and Luca Gobbi for valuable discussion.

Table 1 Target sites, key physicochemical properties (including $\log D_{oct}$ and $\log D_{brain}$ at pH 7.4) and *in vitro* autoradiography binding data for the ligands investigated. The compounds are listed below according to washing time, t_{wash}, and within each class in increasing order of NSB.

		Physicochemical properties						Autoradiography data			
No.	Target	MW	Charge class[a]	pK_a [b]	clogP[c]	$logD_{oct}$ (pH 7.4)[d]	LIMBA $logD_{brain}$ (pH 7.4)	NSB (blocking)	t_{wash}	TB (ROI) / NSB (blocking)	ROI
		[g/mol]						[fmol/mg]	[min]		
1	M1 recpetor	351.4	B	10.7[b1]/7.73[b1]	-0.35	-0.64[d1]	<0.35	7.6 ± 2.4	2	367.6	Hippocampus
2	D3 receptor	221.3	B	9.47/7.31	2.12	1.66	0.57 ± 0.16	13.9 ± 0.7	4	4.1	Striatum
3	NK3 recpetor	559.7	N	4.67[b2]	2.82	2.99[d2]	0.43 ± 0.02	46.4 ± 11.1	4	11.8	Cortex
4	GABA(A) receptor	362.4	N	4.97	1.61	1.94	0.70 ± 0.02	64.3 ± 5.0	4	4.1	Hippocampus
5	D3 receptor	388.5	B	9.14[b2]	3.14	1.71	0.35 ± 0.08	65.8 ± 17.6	4	2.2	Striatum
6	D3 receptor	367.5	B	8.79	2.47	0.95	<0.35	70.2 ± 11.4	4	1.8	Striatum
7	GABA(A) receptor	326.3	N		2.00	1.39	0.80 ± 0.07	75.2 ± 9.6	4	28.6	Hippocampus
8	GABA(A) receptor	351.4	N		3.12	3.35	1.70 ± 0.02	119.6 ± 11.1	4	3.8	Hippocampus
9	NK 3 receptor	447.9	N		2.56	2.73	1.23 ± 0.12	214.1 ± 17.1	4	1.5	Cortex
10	NK3 recpetor	582.5	B	7.98	3.77	2.55	<0.35[c1]	405.2 ± 14.0	4	1.9	Cortex
11	NK3 recpetor	380.5	N	3.89[b3]	6.26	4.35	2.08 ± 0.01	590.7 ± 150.1	4	1.3	Cortex
12	NK3 recpetor	458.9	N		3.25	3.09	1.93 ± 0.12	957.8 ± 108.3	4	2.4	Cortex
13	NK3 recpetor	602.5	B	8.49[b2]	5.33	3.92[d2]	2.45 ± 0.11	2249.7 ± 158	4	2.8	Cortex
14	NK3 recpetor	475.3	N		3.89	1.88	2.16 ± 0.04	3151.1 ± 385.3	4	1.8	Cortex
15	mGluR5 receptor	343.8	N	4.15[b3]	4.86	3.78	2.54 ± 0.03	1560.2 ± 220.2	7	1.8	Striatum
16	D2 receptor	347.2	Z	5.95/9.46	4.06	1.10[d2]	1.06 ± 0.06	15.8 ± 1.9	10	82.5	Striatum
17	OX2 receptor	454.5	N	4.54	3.43	2.27	1.19 ± 0.03	16.8 ± 0.6	10	6.4	Hippocampus

No.	Target	MW	Charge class[a]	pK_a [b]	clogP[c]	$logD_{oct}$ (pH 7.4)[d]	LIMBA $logD_{brain}$ (pH 7.4)	NSB (blocking)	t_{wash}	TB (ROI) / NSB (blocking)	ROI
18	GlyT1 transporter	468.0	N	3.71	2.05	2.26	0.92 ± 0.11	22.1 ± 1.3	10	162.8	Colliculus
19	confidential	401.0	N	5.12	3.41	2.66	0.87 ± 0.03	22.7 ± 1.6	10	1.4	Lateral septal
20	confidential	409.9	N	5.2	3.59	2.51	1.03 ± 0.12	24.9 ± 3.1	10	3.0	Lateral septal
21	NMDA 2B receptor	339.5	B	10.27/9	4.30	2.23[d3]	1.13 ± 0.10	37.3 ± 12.0	10	53.2	Hippocampus
22	GlyT1 transporter	500.4	N	3.75[b3]	3.15	3.16[d2]	1.13 ± 0.63	46.9 ± 5.3	10	167.7	Colliculus
23	GlyT1 transporter	350.5	B	8.3	4.70	2.61[d2]	1.53 ± 0.08	50.4 ± 4.4	10	64.8	Colliculus
24	GlyT1 transporter	497.5	N		2.92	2.52	1.22 ± 0.19	55.5 ± 5.8	10	70.7	Pons
25	D1 receptor	287.8	B	9.26/7.73	4.02	1.82	1.39 ± 0.02	61.8 ± 15.3	10	95.3	Striatum
26	PDE-10 enzyme	388.4	N	5.74	1.37	2.61	1.46 ± 0.05	79.6 ± 17.7	10	173.3	Striatum
27	PDE-10 enzyme	402.4	N		2.92	2.48	1.18 ± 0.00	93.1 ± 5.0	10	82.9	S.nigra
28	GlyT1 transporter	472.5	N		3.30	3.18[d2]	2.22 ± 0.02	155.8 ± 22.3	10	22.8	Colliculus
29	GlyT1 transporter	428.5	N		3.71	3.45[d2]	2.41 ± 0.00	180.4 ± 34.8	10	16.8	Colliculus
30	PDE-10 enzyme	394.4	N		4.00	3.17	2.05 ± 0.01	787.7 ± 214.2	10	41.0	S.nigra

[a] N: neutral (less than 3 % ionization at pH 7.4); A: acid with $ApK_a < 8.9$; B: base $BpK_a > 6$; Z: zwitterions with $ApK_a < 8.9$ and $BpK_a > 6$.

[b] If not otherwise stated, the pK_a was measured potentiometrically as described elsewhere [54]). The first pK_a is the acidic pK_a, the second is the basic pK_a. If only one value is given, this is the basic pK_a.

[b1] Potentiometric pK_a in 13% methanol; [b2] Calculated pK_a (Moka); [b3] In-house SGA pK_a in 10% methanol.

[c] ClogP v4.71 Daylight.

[d] Measured in-house with a miniaturized shake flask assay (50mM TAPSO, 5% (v/v) DMSO, pH 7.4).[d1] large-scale shake flask, [d2] CAMDIS-$logD_{oct}$ (in-house assay, 50mM TAPSO, 1% (v/v) DMSO, pH 7.4), [d3] pH-metric

[e1] Compound probably precipitated

Table 2 Correlation statistics for the data shown in Fig. 3.A and Fig.3B.

t_{wash}	$LogD_{oct}$ (pH 7.4)			$LogD_{brain}$ (pH 7.4)		
[min]	Regression equation (n=27)	r^2	sd	Regression equation (n=27)	r^2	sd
2-4	$logNSB=0.36*logD_{oct}+1.33$	0.48	0.69	$logNSB=0.88*logD_{brain}+1.15$	0.91	0.34
7-10	$logNSB=0.65*logD_{oct}+0.13$	0.74	0.39	$logNSB=0.92*logD_{brain}+0.47$	0.87	0.29

Table 3 Target sites, key physicochemical properties (including $\log D_{oct}$ and LIMBA - $\log D_{brain}$ at pH 7.4) and *in vivo* PET data for the ligands investigated.

Compound	No.	Target	Physicochemical properties								PET data			
			MW [g/mol]	A_D[a] [Å^2]	Charge class	pK_a [b]	clogP	$logD_{oct}$ (pH 7.4)[c]	LIMBA $logD_{brain}$ (pH 7.4)	f_p[d]	Log V_{NS} [ml plasma/ g tissue]	Reference region	Model	Reference
DASB	1	SERT transporter	283.4	65	B	8.73[b1]	3.21	2.52±0.03	1.72 ± 0.04	0.094	2.00	Cerebellum[e1]	1TC model	[55]
Diprenorphinee	2	Opiate receptor	425.6	70	B	9.57/8.48	2.66	2.43±0.01	1.00 ±0 .04	0.300	1.14	Blocking[e2]	2TC model	[56]
Fallypride	3	D_2/D_3 receptor	364.5	90	B	8.22	3.18	2.02±0.03	1.20 ± 0.03	0.070	0.95	Cerebellum[e3]	1TC model	[57]
Flumazenil	4	GABA(A) recpetor	303.3	55	N		1.29	1.08±0.09	<0.35	0.049	-0.41	Blocking[e4]	2TC model	[58]
MDL-100907	5	5-HT_{2A} receptor	373.5	56	B	9.02	3.29	1.87±0.04	1.22 ± 0.05	0.305[d1]	1.74	Blocking[e5]	2TC model	[59]
PK 11195	6	TSPO receptor	352.9	76	N		4.62	3.79±0.06	2.12 ± 0.05	0.012[d1]	1.43	Cortex[e6]	2TC model	[60]
Raclopride	7	D2 recpetor	347.2	65	Z	5.95/9.46	4.06	1.13±0.04	1.05 ± 0.04	0.0344	1.08	Cerebellum[e7]	Ratio method	[61]
Rolipram	8	PDE-4 enzyme	275.3	43	N		1.72	1.91±0.05	0.44 ± 0.14	0.265	0.92	Blocking[e8]	Logan method	[62]
Spiperone	9	D2 recpetor	395.5	70	B	8.29	2.82	2.55±0.04	2.18 ± 0.02	0.045	2.22	Cerebellum[e9]	1TC model	[63]
WAY-100635	10	5-HT_{1A} receptor	422.6	98	B	6.71	4.09	3.05±0.03	1.39 ± 0.06	0.066	0.87	Cerebellum[e10]	Extrapolation	[64]

[a] Cross sectional area at pH 7.4 calculated as described by [65]
[b] if not otherwise stated, the pK_a was measured potentiometrically. The first pK_a is the acidic pK_a, the second is the basic pK_a. If only one value is given, this is the basic pK_a.[b1]calulated pKa (Moka).
[c] CAMDIS-$logD_{oct}$ (in-house assay, 50mM TAPSO, 1% (v/v) DMSO, pH 7.4)
[d]fraction unbound in plasma taken from [66]
[e1]from mean reported V_T estimate [e2]from regional values for K_1,k_2,k_5 and k_6, mean value from 18 brain regions, [e3]from reported V_{ND} estimate (baseline scan), [e4]from mean reported f_{ND} estimate (unbound fraction of tracer in brain) across volunteers (grey matter), [e5]from reported V_{ND} (mirtazapine scan) , [e6]from reported K_1 and k_2 estimates [e7]from reported V_2 estimates, [e8]from reported V_{ND}(F+NS), mean from 6 brain regions, porcine brain, [e9]from mean reported f_{ND} estimate; [e10]from reported V_{WM} (volume in cerebral white matter).

FIGURES

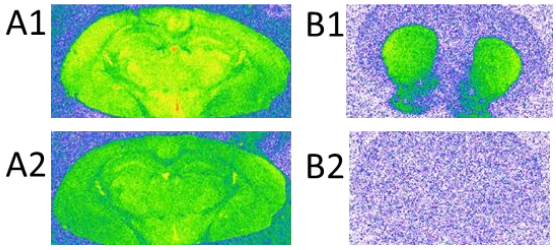

Figure 1 *In vitro* autoradiographs of [^{3}H]-radioligands in absence (Fig. A1, B1) and in presence (Fig. A2, B2) of an unlabeled receptor blocker. **A:** [^{3}H]-SR222200 (NK3 receptor antagonist) at C=2.49 nM. The total binding in the Region of interest (cortex) and in the reference region (hippocampus) under non-blocking conditions was 776 and 809 fmol/mg protein, respectively (Fig. A1). The total binding in the reference region under blocking conditions (NSB, presence of osanetant at C=10 µM) was 591 fmol/mg protein (Fig. A2). **B:** [3H]-raclopride (D2 receptor antagonist) at C=3 nM. The total binding in the region of interest (striatum) was 1307 fmol/mg protein under non-blocking conditions (Fig. B1). The total binding in the reference region under blocking and non-blocking conditions (NSB, presence of butaclamol at C=10µM) was 7 fmol/mg protein, respectively (Fig. B1,2).

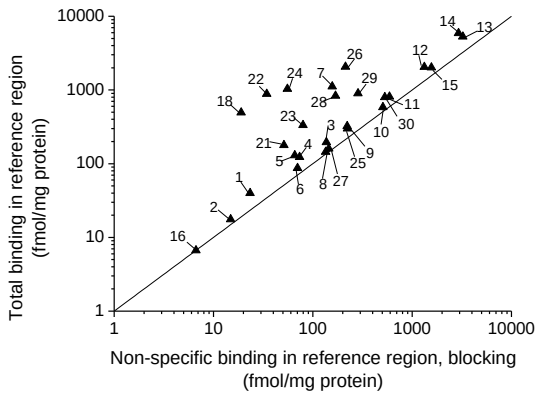

Figure 2 Comparison between non-specific binding measurements: total binding in the reference region vs. non-specific binding in the same reference region after blocking the targets with cold ligand.

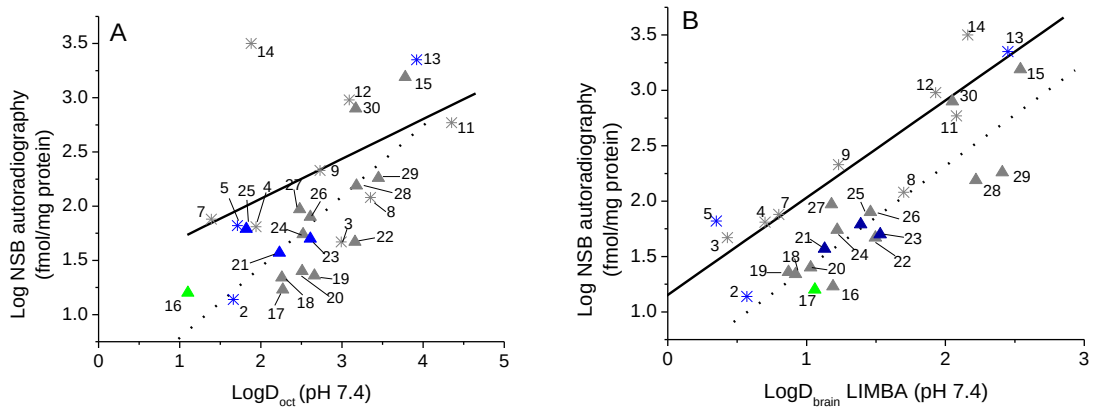

Figure 3 Nonspecific binding (autoradiography data) as a function of **A:** the octanol/water distribution coefficient, $\log D_{oct}$ (pH 7.4), and **B:** the brain tissue/water distribution coefficient, $\log D_{brain}$ (pH 7.4), measured with LIMBA. The color and the shape of the symbols correspond to the charge class of the compounds (neutral:✳▲; basic: ✳▲; zwitter-ionic: ✳▲) and the exposure time of brain slices to a washing solution after incubation with the tritiated tracer (t_{wash}=2-4 min:✳; t_{wash}=7 - 10 min:▲).

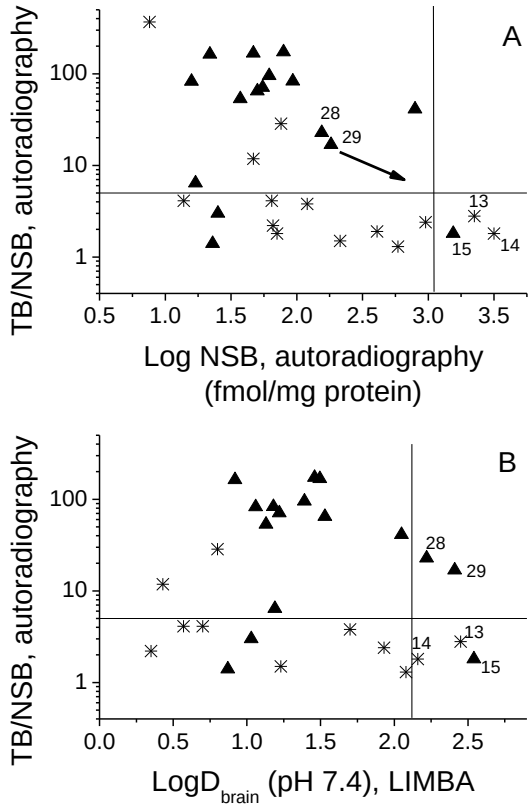

Figure 4 Signal-to-noise ratio (i.e. total binding in a region of interest / non-specific binding in a reference region) for a representative set of radioligands as a function of A: non-specific binding measured with in vitro autoradiography (n=30) and B: brain tissue /water distribution coefficients, (pH 7.4), measured with LIMBA (n=27). Shape of the symbols according to exposure times of brain slices to a washing solution (t=2-4 min:✳; t=7-10 min:▲).

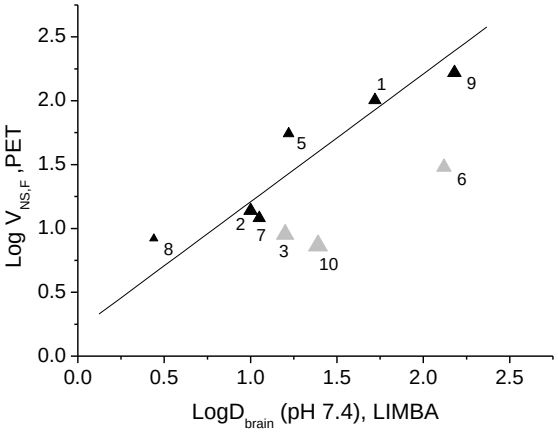

Figure 5 *In vivo* non-specific binding in PET (expressed as the volume of distribution of non-specifically bound radiotracer in the non-displaceable compartment) as a function of the brain tissue /water distribution coefficient, $\log D_{brain}$ (pH 7.4), for 10 PET tracers (Table 3). Size of the symbols according to the cross-sectional area, A_D, of the ligands; compounds with $A_D > 70\text{Å}^2$ (▲) and $A_D \leq 70\text{Å}^2$ (▲) have a high likelihood to be apparent P-gp substrates and to be non-substrates for P-gp, respectively. Correlation statistics: $\text{LogV}_{NS,F}$ (PET)= 0.83 * logD_{brain} (LIMBA) + 0.46 (r^2=0.94, SD = 0.21).

Supporting Information

S1 Tracer kinetic modeling and the estimation of volumes of distribution

PET experiments seek to derive quantitative information on target binding in terms of 'binding potential' (BP_F) which equals the equilibrium concentration ratio between specifically bound (C_S) and free ligand in the tissue (C_{FT}) [4, 25, 26, 67, 68]. At tracer doses, such that $C_{FT} \ll K_D$ and C_S is a negligible fraction of the receptor density available to bind ligand (B_{avail}), BP_F reflects the product of B_{avail} and affinity ($1/K_D$).

$$BP_F = \frac{C_S}{C_{FT}} = \frac{B_{avail}}{K_D} \quad . \tag{S1}$$

The recorded PET data represent a composite of all tissue and blood components. In order to isolate the various signals, a mathematical framework relating the observed time activity curve in the region of interest (ROI) to the time activity curve in the arterial plasma is required. Most approaches rely on compartmental modeling in which binding and transport are expressed as a combination of rate constants (K_1, k_2, k_3, k_4) that govern the transfer between the different compartments. In a target region, three compartments correspond to the concentrations of unmetabolized radioligand in plasma (C_p), free plus nonspecifically bound radioligand in brain (C_{ND}, nondisplaceable compartment) and radioligand specifically bound to receptors (C_S) (Fig.S1). The concept of free fraction arises from the underlying assumption that the transfer between free and nonspecifically bound ligand is rapid compared to receptor binding and thus the free fraction in brain, f_{ND}, denotes the fraction of total tracer in C_{ND} in the unbound state. In addition, it is assumed that only the unbound concentration is available for receptor binding and similarly that only the free fraction in plasma (f_p) can cross the blood brain barrier. Then, BP_F can be expressed as

$$BP_F = \frac{C_S}{f_{ND}C_{ND}} = \frac{k_3}{f_{ND}k_4}, \tag{S2}$$

where the rate constants derived from fitting the three-compartmental model are entering the equation. Since f_{ND} measurements in human are limited to post-mortem studies, a more practical derivation of BP_F is given by equation S3, which is valid at equilibrium state and if transport across the blood brain barrier is passive, such that $f_{ND}C_{ND} = f_pC_p$, and

$$BP_F = \frac{C_S}{f_p C_p} = \frac{K_1 k_3}{f_p k_2 k_4}. \quad \text{(S3)}$$

While it is mathematically feasible to find estimates of all four rate constants, the most reliable outcome measure is the total volume of distribution V_T. It refers to the sum of binding in the individual compartments as a ratio to the total plasma concentration, such that

$$V_T = \frac{C_T}{C_p} = V_{ND} + V_S = V_{FT} + V_{NS} + V_S, \quad \text{(S4)}$$

where $V_{ND} = C_{ND} / C_p$ and $V_S = C_S / C_p$ and. $V_{NS} = C_{NS} / C_p$.

In a region with specific binding , V_T (ROI) is the sum of V_{ND} (nondisplaceable compartment) and V_S (specific binding). V_{ND} is the sum of the volume of distribution of the non-specifically bound radiotracer (V_{NS}) and the volume of distribution of free radiotracer in tissue, V_{FT}. Assuming equal nonspecific binding characteristics in all brain regions, V_T in a reference region devoid of receptors (V_S=0) gives an estimate of V_{ND} in the ROI. BP_F will then be obtained as follows:

$$BP_F = \frac{V_S}{f_p} = \frac{V_T(ROI) - V_{ND}(R_{REF})}{f_p}, \quad \text{(S5)}$$

where

$$V_T(ROI) = \frac{K1}{k_2}\left(1 + \frac{k_3}{k_4}\right), \quad \text{(S6)}$$

and

$$V_{ND}(R_{REF}) = \frac{K_1^{'}}{k_2^{'}} = \frac{1}{f_{ND}} \quad . \quad \text{(S7)}$$

Since the expression levels of transporters (e.g. P-glycoprotein) in the ROI may be different from those in the reference region, the rate constant governing the transport of tracer across the blood brain barrier in the reference region is indicated as $K_1^{'}$.

V_{NS} may be expressed as:

$$V_{NS} = V_{ND}^{\cdot\cdot} - V_{FT} = \frac{K_1^{'}}{k_2} - \frac{C_{FT}}{C_P} \quad \text{(S8)}$$

At equilibrium state, and if no active transport takes place ($C_{FT} = f_p C_p$), the volume of distribution of non-specifically bound drug in relation to the free plasma concentration can be inferred from the rate constants and f_p such that:

$$V_{NS,F} = \frac{V_{NS}}{f_p} = \frac{V_{ND}}{f_p} - 1 = \frac{K_1^{'}}{f_p k_2^{'}} - 1 \qquad \text{(S9)}$$

Equation S9 equals equation. 2 in the main manuscript. From equation S5 it becomes obvious that the signal reflecting receptor binding will be lowered by non-specific binding, which is embraced in the term $V_{NS,F}$. An estimate of $V_{NS,F}$ *in vitro* may be obtained by assessment of the brain tissue/water distribution coefficients available through LIMBA.

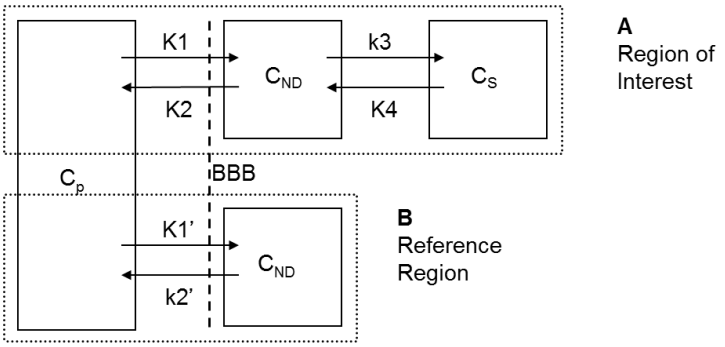

Figure S1 Classical three-compartmental model used to quantify PET data. C_p is the total concentration of tracer in plasma, C_{ND} is the sum of free and non-specifically bound tracer (non-displceable concentration), and C_S is the concentration of tracer specifically bound to the target site in the region of interest. K_1 ($K_1^{'}$) and k_2 denote the rate constants for the transfer from plasma into and out of the brain, respectively, and k_3 and k_4 describe association and dissociation to and from the receptors, respectively.

Table S1 Experimental conditions used for *in vitro* autoradiography experiments.

No.	Species	Blocker	C blocker [uM]	Assay buffer	Buffer additives	Exposure time [d]	Wash time pre-incubation [min]	Wash time incubation [min]	Wash time after incubation [min]	Dips in water	Incubation temp. [°C]
1	Mouse	Atropine	100	Na-phosphate,1mM,pH7.4	-	5	20	60	2	3	RT
2	Rat	Spiperone	10	TRIS,50mM,pH7.4	1mM EDTA	5	15	120	4	3	RT
3	Gerbil	Osanetant	10	TRIS,50mM,pH7.4	3mM MnCl2, 0.02% BSA, antibiotics	5	15	90	4	1	RT
4	Rat	L655708	1	Na-phosphate,1.47mM,pH7.4	146.5mM NaCl, 2.7mM KCl,1.2mM CaCl2, 0.85mM MgCl2, 0.1% ascorbic acid	5	20	60	4	3	37
5	Rat	Spiperone	10	TRIS,50mM,pH7.4	120mM NaCl, 1.5mM CaCl2, 5mM MgCl2, 1mM EDTA	6		120	4	3	RT
6	Rat	Spiperone	10	TRIS,50mM,pH7.4	120mM NaCl, 1.5mM CaCl2, 5mM MgCl2, 1mM EDTA			12	4	3	RT
7	Rat	L655,708	1	TRIS,50mM,pH7.4	120mM NaCl, 5mM KCl, 2mM CaCl2, 1mM MgCl2	5	20	60	4	3	37
8	Rat	Proprietary	10	TRIS,50mM,pH7.4	120mM NaCl, 5mM KCl, 2mM CaCl2, 1mM MgCl2	5	20	60	4	3	37
9	Gerbil	Osanetant	10	TRIS,50mM,pH7.4	3mM MnCl2, 0.02% BSA, antibiotics	5	15	90	4	1	RT
10	Gerbil	SR142801	10	Na-phosphate,1.47mM,pH7.4	146.5mM NaCl, 2.7mM KCl,1.2mM CaCl2, 0.85mM MgCl2, 0.1% ascorbic acid	5	15	90	4	1	RT
11	Gerbil	SR142801	10	TRIS,50mM,pH7.4	0.02 % BSA, antibiotics	5	15	90	4	1	RT
12	Gerbil	SR142801		Na-phosphate,1.47mM,pH7.4	146.5mM NaCl, 2.7mM KCl,1.2mM CaCl2, 0.85mM MgCl2, 0.1% ascorbic acid	5	15	90	4	1	RT
13	Gerbil	SR142801	10	Na-phosphate,1.47mM,pH7.4	146.5mM NaCl, 2.7mM KCl,1.2mM CaCl2, 0.85mM MgCl2, 0.1% ascorbic acid	5	15	90	4	1	RT
14	Gerbil	Proprietary	10	TRIS,50mM,pH7.4	3mM MnCl2, 0.02% BSA, antibiotics	5	15	90	4	1	RT
15	Rat	MPEP	10	TRIS,15mM,pH7.4	120mM NaCl, 1.25mM KCl, 1.25mM CaCl2, 1.25mM MgCl2, 10mM EDTA	5	20	60	7	3	37
16	Mouse	Butaclamol	10	Na-phosphate,1.5mM,pH7.4	146.5mM NaCl, 2.7mM KCl,1.2mM CaCl2, 0.85mM MgCl2, 0.1% ascorbic acid	6	20	45	10	3	RT

No.	Species	Blocker	C blocker	Assay buffer	Buffer additives	Exposure time	Wash time pre-incubation	Wash time incubation	Wash time after incubation	Dips in water	Incubation temp.
17	Rat	Proprietary	10	Hepes,25mM,pH7.4	-	5	20	60	10	3	RT
18	Rat	Proprietary	1	TRIS,50mM,pH7.4	120mM NaCl, 5mM KCl, 2mM CaCl2, 1mM MgCl2	5	10	60	10	3	37
19	Rat	Proprietary	40	TRIS,50mM,pH7.4	5mM MgCl2, 0.1 % BSA, antibiotics	5	10	60	10	1	RT
20	n.p.	n.p.	10	TRIS,50mM,pH7.4	5mM MgCl2, 0.1 % BSA, antibiotics	5		60	10	1	RT
21	Mouse	Proprietary	10	TRIS,50mM,pH7.4	10mM EDTA	5	20	90	10	3	RT
22	Rat	Org24598	1	TRIS,50mM,pH7.4	120mM NaCl, 5mM KCl, 2mM CaCl2, 1mM MgCl2	5	10	60	10	3	37
23	Rat	Org24598	1	TRIS,50mM,pH7.4	120mM NaCl, 5mM KCl, 2mM CaCl2, 1mM MgCl2	5	10	60	10	3	37
24	Rat	Org24598	1	Na-citrat,50mM,pH6.1	50mM NaCl	5	10	60	10	3	RT
25	Mouse	Pifluthixol	1	TRIS,50mM,pH7.4	120mM NaCl, 5mM KCl, 2mM CaCl2, 1mM MgCl2	6	20	60	10	3	RT
26	Rat	Proprietary	1	TRIS,50mM,pH7.4	120mM NaCl, 5mM KCl, 2mM CaCl2, 1mM MgCl2	5		60	10	2	RT
27	Rat	Proprietary	10	TRIS,50mM,pH7.4	120mM NaCl, 5mM KCl, 2mM CaCl2, 1mM MgCl2	5		60	10	2	RT
28	Rat	Pifluthixol	1	TRIS,50mM,pH7.4	120mM NaCl, 5mM KCl, 2mM CaCl2, 1mM MgCl2	5	10	60	10	3	37
29	Rat	Pifluthixol	1	TRIS,50mM,pH7.4	120mM NaCl, 5mM KCl, 2mM CaCl2, 1mM MgCl2	5	10	60	10	3	37
30	Rat	Proprietary	10	TRIS,50mM,pH7.4	120mM NaCl, 5mM KCl, 2mM CaCl2, 1mM MgCl2	5		60	10	2	RT

n.p. not provided

Structures not provided at the moment.

Figure S2 Structures of the radioligands tested with *in vitro* autoradiography (unlabeled form).

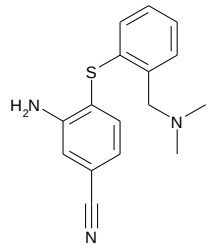

DASB (1)

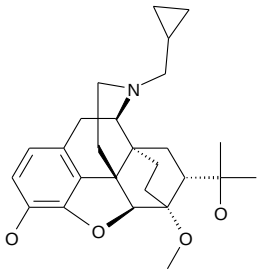

Diprenorphine (2)

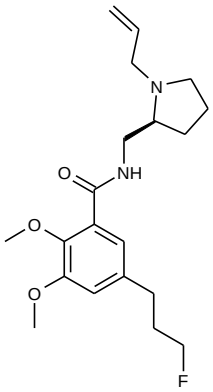

Fallypride (3)

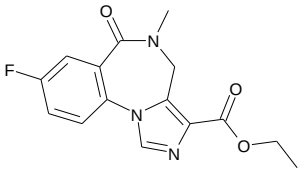

Flumazenil (4)

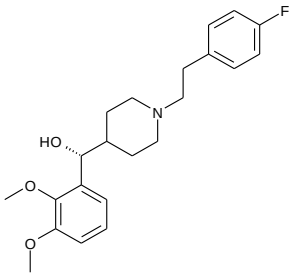

MDL-100907 (5)

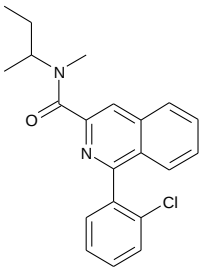

PK 10095 (6)

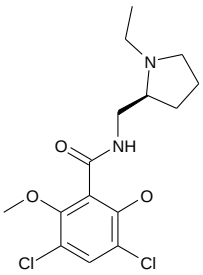

Raclopride (7)

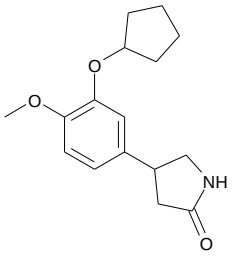

Rolipram (8)

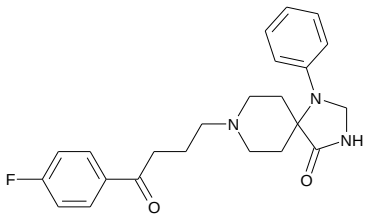

Spiperone (9)

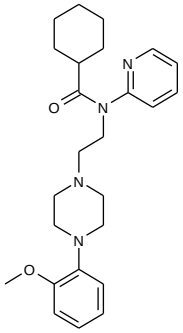

WAY 100635 (10)

Figure S3 Structures of the PET tracers characterized *in vivo* (literature data)

References

1. Fernandes, E., et al., *Positron emitting tracers in pre-clinical drug development.* Current Radiopharmaceuticals, 2012. **5**(2): p. 90-98.
2. Danhof, M., et al., *Mechanism-based pharmacokinetic-pharmacodynamic modeling: biophase distribution, receptor theory, and dynamical systems analysis.* Annual Review of Pharmacology and Toxicology, 2007. **47**: p. 357-400.
3. Aboagye, E.O., *Positron emission tomography imaging of small animals in anticancer drug development.* Mol Imaging Biol, 2005. **7**(Copyright (C) 2014 U.S. National Library of Medicine.): p. 53-8.
4. Laruelle, M., M. Slifstein, and Y. Huang, *Relationships between radiotracer properties and image quality in molecular imaging of the brain with positron emission tomography.* Molecular imaging and biology, 2003. **5**(6): p. 363-75.
5. Honer, M., et al., *Radioligand development for molecular imaging of the central nervous system with positron emission tomography.* Drug Discovery Today, 2014(Copyright (C) 2014 American Chemical Society (ACS). All Rights Reserved.): p. Ahead of Print.
6. Ametamey, S.M. and P.A. Schubiger, *PET radiopharmaceuticals for neuroreceptor imaging.* Nuclear Science and Techniques, 2006. **17**(3): p. 143-147.
7. Pike, V.W., *Positron-emitting radioligands for studies in vivo-probes for human psychopharmacology.* J Psychopharmacol, 1993. **7**(2): p. 139-58.
8. McCarthy, D.J., et al., *Chapter 24 Discovery of Novel Positron Emission Tomography Tracers.* Annual Reports in Medicinal Chemistry, 2009. **44**: p. 501-513.
9. Wong, D.F. and M.G. Pomper, *Predicting the success of a radiopharmaceutical for in vivo imaging of central nervous system neuroreceptor systems.* Mol Imaging Biol, 2003. **5**(6): p. 350-62.
10. Dickson, C.J., et al., *Further evaluation of quantum chemical methods for the prediction of non-specific binding of positron emission tomography tracers.* Phys Chem Chem Phys, 2011. **13**(48): p. 21552-7.
11. Guo, Q., M. Brady, and R.N. Gunn, *A biomathematical modeling approach to central nervous system radioligand discovery and development.* Journal of Nuclear Medicine, 2009. **50**(10): p. 1715-1723.
12. Kalvass, J.C. and T.S. Maurer, *Influence of nonspecific brain and plasma binding on CNS exposure: implications for rational drug discovery.* Biopharmaceutics & Drug Disposition, 2002. **23**(8): p. 327-338.
13. Liu, X., et al., *Unbound drug concentration in brain homogenate and cerebral spinal fluid at steady state as a surrogate for unbound concentration in brain interstitial fluid.* Drug metabolism and disposition: the biological fate of chemicals, 2009. **37**(4): p. 787-93.
14. Summerfield, S.G., et al., *Central nervous system drug disposition: the relationship between in situ brain permeability and brain free fraction.* J Pharmacol Exp Ther, 2007. **322**(1): p. 205-13.
15. Loryan, I., M. Friden, and M. Hammarlund-Udenaes, *The brain slice method for studying drug distribution in the CNS.* Fluids Barriers CNS, 2013. **10**(Copyright (C) 2014 U.S. National Library of Medicine.): p. 6.
16. Friden, M., et al., *Development of a high-throughput brain slice method for studying drug distribution in the central nervous system.* Drug Metab. Dispos., 2009. **37**(Copyright (C) 2014 American Chemical Society (ACS). All Rights Reserved.): p. 1226-1233.

17. Friden, M., et al., *Measurement of unbound drug exposure in brain: modeling of pH partitioning explains diverging results between the brain slice and brain homogenate methods.* Drug Metabolism and Disposition, 2011. **39**(3): p. 353-362.
18. Jiang, Z., et al., *A rapid vesicle electrokinetic chromatography method for the in vitro prediction of non-specific binding for potential PET ligands.* J Pharm Biomed Anal, 2011. **54**(4): p. 722-9.
19. Rosso, L., A.D. Gee, and I.R. Gould, *Ab initio computational study of positron emission tomography ligands interacting with lipid molecule for the prediction of nonspecific binding.* J Comput Chem, 2008. **29**(14): p. 2397-405.
20. Assmus, F., A. Seelig, and H. Fischer, *Evaluation of a Novel Lipid Membrane Binding Assay (LIMBA) for the Assessment of Brain Tissue Distribution*, Manuscript in preparation.
21. Belli, S., et al., *Methodology and in vivo application of a partitioning assay with brain polar lipid microemulsion for the estimation of drug binding to brain tissue.* Manuscript in preparation.
22. Schinkel, A.H., *P-Glycoprotein, a gatekeeper in the blood-brain barrier.* Adv. Drug Delivery Rev., 1999. **36**(Copyright (C) 2014 American Chemical Society (ACS). All Rights Reserved.): p. 179-194.
23. Fischer, H., M. Kansy, and B. Wagner, *Determination of high lipophilicity values.*, 2006.
24. Borroni, E., et al., *Pre-clinical characterization of [(11)C]R05013853 as a novel radiotracer for imaging of the glycine transporter type 1 by positron emission tomography.* NeuroImage, 2011.
25. Slifstein, M. and M. Laruelle, *Models and methods for derivation of in vivo neuroreceptor parameters with PET and SPECT reversible radiotracers.* Nuclear Medicine and Biology, 2001. **28**(5): p. 595-608.
26. Innis, R.B., et al., *Consensus nomenclature for in vivo imaging of reversibly binding radioligands.* Journal of Cerebral Blood Flow & Metabolism, 2007. **27**(9): p. 1533-1539.
27. Kulkarni, S.K. and M.K. Ticku, *Chronic benzodiazepine antagonist treatment and its withdrawal upregulates components of GABA-benzodiazepine receptor ionophore complex in cerebral cortex of rat.* Brain Research, 1990. **519**(1-2): p. 6-11.
28. Seelig, A., *The role of size and charge for blood-brain barrier permeation of drugs and fatty acids.* Journal of Molecular Neuroscience, 2007. **33**(1): p. 32-41.
29. Avdeef, A., et al., *pH-metric logP 10. Determination of liposomal membrane-water partition coefficients of ionizable drugs.* Pharm. Res., 1998. **15**(Copyright (C) 2014 American Chemical Society (ACS). All Rights Reserved.): p. 209-215.
30. Balon, K., B.U. Riebesehl, and B.W. Muller, *Drug liposome partitioning as a tool for the prediction of human passive intestinal absorption.* Pharm. Res., 1999. **16**(Copyright (C) 2014 American Chemical Society (ACS). All Rights Reserved.): p. 882-888.
31. Obach, R.S., F. Lombardo, and N.J. Waters, *Trend analysis of a database of intravenous pharmacokinetic parameters in humans for 670 drug compounds.* Drug Metab. Dispos., 2008. **36**(Copyright (C) 2014 American Chemical Society (ACS). All Rights Reserved.): p. 1385-1405.
32. Rodgers, T., D. Leahy, and M. Rowland, *Tissue distribution of basic drugs: Accounting for enantiomeric, compound and regional differences amongst β-blocking drugs in rat.* J. Pharm. Sci., 2005. **94**(Copyright (C) 2014 American Chemical Society (ACS). All Rights Reserved.): p. 1237-1248.
33. Rodgers, T., D. Leahy, and M. Rowland, *Physiologically based pharmacokinetic modeling: Predicting the tissue distribution of moderate-to-strong bases.* J. Pharm. Sci., 2005.

94(Copyright (C) 2014 American Chemical Society (ACS). All Rights Reserved.): p. 1259-1276.

34. Yata, N., et al., *Phosphatidylserine as a determinant for the tissue distribution of weakly basic drugs in rats.* Pharm. Res., 1990. **7**(Copyright (C) 2014 American Chemical Society (ACS). All Rights Reserved.): p. 1019-25.
35. Pope, J.M. and D.W. Dubro, *The interaction of n-alkanes and n-alcohols with lipid bilayer membranes: a deuterium NMR study.* Biochim. Biophys. Acta, Biomembr., 1986. **858**(Copyright (C) 2014 American Chemical Society (ACS). All Rights Reserved.): p. 243-53.
36. Kirk, G.L. and S.M. Gruner, *Lyotropic effects of alkanes and headgroup composition on the Lα-HII lipid liquid crystal phase transition: hydrocarbon packing versus intrinsic curvature.* J. Phys. (Les Ulis, Fr.), 1985. **46**(Copyright (C) 2014 American Chemical Society (ACS). All Rights Reserved.): p. 761-9.
37. Pope, J.M., L.W. Walker, and D. Dubro, *On the ordering of n-alkane and n-alcohol solutes in phospholipid bilayer model membrane systems.* Chem. Phys. Lipids, 1984. **35**(Copyright (C) 2014 American Chemical Society (ACS). All Rights Reserved.): p. 259-77.
38. Sjolund, M., et al., *Hydrophobic molecules in lecithin-water systems. I. Formation of reversed hexagonal phases at high and low water contents.* Biophys J, 1987. **52**(Copyright (C) 2014 U.S. National Library of Medicine.): p. 145-53.
39. Assmus, F., H. Fischer, and A. Seelig, *31P and 1H-NMR studies on the molecular organization of lipids in the PAMPA permeation barrier*, Manuscript in preparation.
40. Patel, S., et al., *An in vitro assay for predicting successful imaging radiotracers.* Mol Imaging Biol, 2003. **5**(Copyright (C) 2014 U.S. National Library of Medicine.): p. 65-71.
41. Fischer, H., R. Gottschlich, and A. Seelig, *Blood-brain barrier permeation: molecular parameters governing passive diffusion.* Journal of Membrane Biology, 1998. **165**(3): p. 201-211.
42. Elsinga, P.H., et al., *Positron emission tomography studies on binding of central nervous system drugs and P-glycoprotein function in the rodent brain.* Mol Imaging Biol, 2005. **7**(1): p. 37-44.
43. Piel, M., et al., *Evaluation of P-glycoprotein (abcb1a/b) modulation of [(18)F]fallypride in MicroPET imaging studies.* Neuropharmacology, 2014. **84**: p. 152-8.
44. Walter, R.B., et al., *PK11195, a peripheral benzodiazepine receptor (pBR) ligand, broadly blocks drug efflux to chemosensitize leukemia and myeloma cells by a pBR-independent, direct transporter-modulating mechanism.* Blood, 2005. **106**(10): p. 3584-3593.
45. Fujita, M., et al., *Downregulation of brain phosphodiesterase type IV measured with 11C-(R)-rolipram positron emission tomography in major depressive disorder.* Biol Psychiatry, 2012. **72**(7): p. 548-54.
46. Hassan, H.E., et al., *Differential involvement of P-glycoprotein (ABCB1) in permeability, tissue distribution, and antinociceptive activity of methadone, buprenorphine, and diprenorphine: in vitro and in vivo evaluation.* J Pharm Sci, 2009. **98**(12): p. 4928-40.
47. Ishiwata, K., et al., *In vivo evaluation of P-glycoprotein modulation of 8 PET radioligands used clinically.* J Nucl Med, 2007. **48**(1): p. 81-7.
48. Xue Y., et al., *Prediction of P-Glycoprotein Substrates by a Support Vector Machine Approach.* Journal of Chemical Information and Modeling, 2004. **44**: p. 1497-1505.
49. Froklage, F.E., et al., *[11C]Flumazenil brain uptake is influenced by the blood-brain barrier efflux transporter P-glycoprotein.* EJNMMI Res, 2012. **2**: p. 12.

50. Li-Blatter, X., P. Nervi, and A. Seelig, *Detergents as intrinsic P-glycoprotein substrates and inhibitors.* Biochim. Biophys. Acta, Biomembr., 2009. **1788**(Copyright (C) 2014 American Chemical Society (ACS). All Rights Reserved.): p. 2335-2344.
51. Fischer, H., R. Gottschlich, and A. Seelig, *Blood-brain barrier permeation: molecular parameters governing passive diffusion.* J. Membr. Biol., 1998. **165**(Copyright (C) 2014 American Chemical Society (ACS). All Rights Reserved.): p. 201-211.
52. Seelig, A., *The role of size and charge for blood-brain barrier permeation of drugs and fatty acids.* J. Mol. Neurosci., 2007. **33**(Copyright (C) 2014 American Chemical Society (ACS). All Rights Reserved.): p. 32-41.
53. Wong Dean, F. and G. Pomper Martin, *Predicting the success of a radiopharmaceutical for in vivo imaging of central nervous system neuroreceptor systems.* Molecular imaging and biology, 2003. **5**(6): p. 350-62.
54. Bendels, S., et al., *PAMPA Excipient Classification Gradient Map.* Pharmaceutical Research, 2006. **23**(11): p. 2525-2535.
55. Frankle, W.G., et al., *Estimation of serotonin transporter parameters with 11C-DASB in healthy humans: reproducibility and comparison of methods.* Journal of Nuclear Medicine, 2006. **47**(5): p. 815-826.
56. Jones, A.K.P., et al., *Quantitation of [11C]diprenorphine cerebral kinetics in man acquired by PET using presaturation, pulse-chase and tracer-only protocols.* Journal of Neuroscience Methods, 1994. **51**(2): p. 123-34.
57. Slifstein, M., et al., *Striatal and extrastriatal dopamine release measured with PET and [18F] fallypride.* Synapse (Hoboken, NJ, United States), 2010. **64**(5): p. 350-362.
58. Price, J.C., et al., *Measurement of benzodiazepine receptor number and affinity in humans using tracer kinetic modeling, positron emission tomography, and [11C]flumazenil.* Journal of Cerebral Blood Flow and Metabolism, 1993. **13**(4): p. 656-67.
59. Hinz, R., et al., *Validation of a tracer kinetic model for the quantification of 5-HT2A receptors in human brain with [11C]MDL 100,907.* Journal of Cerebral Blood Flow & Metabolism, 2007. **27**(1): p. 161-172.
60. Kropholler Marc, A., et al., *Evaluation of reference tissue models for the analysis of [11C](R)-PK11195 studies.* Journal of cerebral blood flow and metabolism, 2006. **26**(11): p. 1431-41.
61. Mawlawi, O., et al., *Imaging human mesolimbic dopamine transmission with positron emission tomography: I. Accuracy and precision of D2 receptor parameter measurements in ventral striatum.* Journal of Cerebral Blood Flow and Metabolism, 2001. **21**(9): p. 1034-1057.
62. Parker, C.A., et al., *Behaviour of [11C]R(-)- and [11C]S(+)-rolipram in vitro and in vivo, and their use as PET radiotracers for the quantificative assay of PDE4.* Synapse (Hoboken, NJ, United States), 2005. **55**(4): p. 270-279.
63. Perlmutter, J.S., et al., *Decreased [18F]spiperone binding in putamen in idiopathic focal dystonia.* Journal of Neuroscience, 1997. **17**(2): p. 843-850.
64. Giovacchini, G., et al., *Using cerebral white matter for estimation of nondisplaceable binding of 5-HT1A receptors in temporal lobe epilepsy.* Journal of nuclear medicine, 2009. **50**(11): p. 1794-800.
65. Gerebtzoff, G. and A. Seelig, *In silico prediction of blood-brain barrier permeation using the calculated molecular cross-sectional area as main parameter.* Journal of Chemical Information and Modeling, 2006. **46**(6): p. 2638-2650.
66. Summerfield, S.G., et al., *Toward an improved prediction of human in vivo brain penetration.* Xenobiotica, 2008. **38**(12): p. 1518-1535.

67. Mintun, M.A., et al., *A quantitative model for the in vivo assessment of drug binding sites with positron emission tomography.* Annals of Neurology, 1984. **15**(3): p. 217-27.
68. Frankle, W.G., et al., *Neuroreceptor imaging in psychiatry: theory and applications.* Int Rev Neurobiol, 2005. **67**: p. 385-440.

5 Summary

PET has found ever growing interest in the pharmaceutical industry as a non-invasive imaging modality with great potential to accelerate the development of novel therapeutics, particularly of CNS-active drugs [1]. However, the availability of innovative PET tracers for imaging the brain is currently the limiting factor to exploit the full potential of PET for the drug discovery and development process [2]. Many potential radioligands fail due to an imbalance between specific binding at the target site and NSB to non-target proteins and lipid membranes [3]. Since NSB reduces the sensitivity of PET to the specific binding, radioligands showing extensive NSB are unlikely to be successful, particularly in combination with low receptor density and/or low receptor affinity. Estimating the extent of NSB at an early stage in the PET tracer development process is therefore highly desirable and was the main purpose of the thesis. Specifically, we explored whether compounds with unfavorably high NSB can be identified prior to radioactive labeling and with reduced animal testing as compared to yet existing methods (autoradiography, equilibrium dialysis).

In pursuit of our aim, we have evaluated the predictive power of three membrane-mimicking systems and their corresponding miniaturized assays (in brackets), namely i) octanol (CAMDIS), ii) phospholipids dissolved in dodecane (PAMPA), and iii) brain homogenate prepared in dodecane (LIMBA).

It was essential to translate the measurement of each surrogate parameter into a miniaturized format (if not yet available) in order to be in line with our ambition for higher-throughput and minimal consumption of samples, reagents and animal tissue. At the beginning of this thesis, only PAMPA was already established as a screening method [4] while CAMDIS and LIMBA have been developed and validated as entirely new assays. However, also PAMPA required the optimization of experimental conditions in terms of compatibility with mass spectrometry and lipid as well as buffer composition.

In the following, we summarize the major contributions of this thesis pertaining to the development and optimization of the individual assays. The thorough validation of the assays was the precondition for evaluating the assays with respect to their ability to predict NSB.

As a strategy to identify the model system which yields the most reliable NSB - estimates, we first evaluated the simplest artificial membrane-mimicking system, namely octanol. However, our data indicated that octanol (CAMDIS) is only a poor surrogate for NSB which brought us to the next more complex artificial membrane-mimicking system, namely the PAMPA

barrier. Since the predictive power of the membrane fraction was still unsatisfactory, we tested whether the use of brain homogenate (LIMBA) provides more reliable NSB - estimates which could justify using animal tissue over artificial membrane-mimicking systems. The abovementioned order of increasing complexity is maintained in the following summary of our research.

5.1 CAMDIS - Development of a Novel Assay for the Measurement of Octanol/Water Distribution Coefficients

Related Manuscripts:

Manuscript 1	Carrier Mediated Distribution System (CAMDIS): A Novel Approach for the Measurement of Octanol/Water Distribution Coefficients
Manuscript 2	The Impact of Drug Adsorption on the Accuracy of $LogD_{oct}$
Manuscript 3	Drug Adsorption to Teflon and Excipient-Aided Drug Recovery

It is worth to recall that octanol/water distribution coefficients ($\log D_{oct}$) have already been used for NSB prediction, albeit with varying success depending on the structural similarity of the test compounds [3]. The major advantage of $\log D_{oct}$ is certainly the fact that many laboratories routinely measure this key physicochemical parameter, e.g. for the prediction of a drug candidate's ADMETox profile [5]. Provided that the $\log D_{oct}$ yields reliable NSB-estimates, the characterization of potential PET tracers could thus be implemented in the available screening platforms without the need for additional facilities.

However, the value of $\log D_{oct}$ for the prediction of tissue binding was ambiguous due to i) the small datasets characterized hitherto and ii) the reliance on *indirect* lipophilicity data derived from reversed phase chromatography [6]. On the one hand, there was a broad consensus that tissue binding and lipophilicity ($\log D_{oct}$) are unrelated except for compounds within a given structural family [3]. On the other hand, remarkably good correlations between tissue binding and calculated octanol/water partition coefficient ($c\log P_{oct}$) have been reported, yet an evaluation on the basis of *measured* $\log P_{oct}$ data was missing [7]. The lack of directly measured lipohilicity data is supposedly a consequence of several difficulties encountered with the traditional shake flask technique, i.e. high consumption of reagents in

addition to tedious, time-consuming and error-prone phase separation associated with a low throughput.

One of the original contributions of this work is a novel miniaturized $\log D_{oct}$ assay (CAMDIS) in which the drawbacks of the traditional shake flask technique have been overcome. We could demonstrate that a filter support for octanol facilitates the phase separation and thus considerably reduces the net manpower hours required for the assessment of $\log D_{oct}$

The concern as to whether adsorption to the filter-supported interface disturbs the accuracy of $\log D_{oct}$ was addressed in *manuscript 1* along with the question under which experimental conditions adsorption does not significantly compromise the accuracy of $\log D_{oct}$. Our data indicated that amphiphilic, cationic compounds adsorb at the octanol/water interface irrespective of whether or not a filter support is used. While the filter matrix is inert to adsorption, the spreading of octanol across the filter area increases the extent of interfacial drug enrichment, simply by enlarging the boundary surface between octanol and water. We could demonstrate that the interface effect does not manifest itself as experimental artifact, except for the rare case that several unfavourable conditions coincide, namely i) the presence of a positive charge, and ii) low lipophilicity of the test compound, iii) low volume of octanol and iv) low drug concentrations. Under these conditions, few drug molecules enter the octanol phase, and, in turn, drug adsorption to the octanol/water interface cannot be neglected. The related overestimation of $\log D_{oct}$ could be counteracted by an appropriate choice of experimental conditions (total drug concentration: 100µM, volume of octanol depending on the $\log D_{oct}$ range) and a clear definition of the applicable $\log D_{oct}$ range (- 0.5 - maximal 4.2).

In miniaturized $\log D_{oct}$ assays it is also important to consider that the surface formed between the well plate and the aqueous phase is much more prominent as compared to large scale experiments. Whether and to what extent adsorption to the assay construct (Teflon) affects the accuracy of $\log D_{oct}$ was studied in *manuscript 2* along with the problem of drug aggregation / precipitation as a potential source of experimental artifact. We could demonstrate that the compounds which are most susceptible to adsorption (lipophilic, high molecular weight compounds) are not the compounds for which a major error in $\log D_{oct}$ occurs: The reason is that the distribution of lipophilic drugs into octanol (non-saturable) outweighs the adsorption to the well plate (saturable) and the associated violation of the mass

balance equation. Exceptions are lipophilic *and* sparingly soluble drugs (e.g. paclitaxel) which precipitate during the time course of the experiment giving rise to erroneously low $\log D_{oct}$ values. The same trend towards an underestimation of $\log D_{oct}$ was observed for drugs which have a high tendency for adsorption despite being hydrophilic. The latter pattern is typical for large and coplanar compounds carrying many hydrogen-bond donors and forming multilayers presumably by stacking interactions. While adsorption-related artifacts for the hydrophilic compounds could be counteracted by increasing the volume of octanol (or the drug concentration), this is not a viable option for the lipophilic, sparingly soluble drugs. Under these conditions hardly any drug would be left in the aqueous phase and the limits of detection would soon be reached.

These considerations raised the question of another strategy for correcting erroneous $\log D_{oct}$ values. The most obvious possibility was the recovery of drug residing at the Teflon surface, however, this required an excipient which is both effective and compatible with the method used for detecting the analyte, i.e. HPLC-ESI/MS. In this regard it is important to note that excipients may disturb the concentration analysis with ESI/MS by suppressing the ionization efficiency of the analyte of interest (matrix effect) [8]. Previous studies on excipient-aided drug recovery have focused on case studies or small datasets, however, since structurally diverse compounds are encountered in screening assays such as CAMDIS, strategies are required that work for most and at best all types of analytes. Moreover, and contrary to our results, Teflon is often considered as inert to adsorption and accordingly no efforts have been made before towards recovery of adsorbed drugs by means of excipient. Therefore, we studied the sorption of a set of structurally diverse compounds to a Teflon well plate, followed by the study of excipient-aided drug recovery. The test dataset (n=24) covered a wide physicochemical property space and included acidic, basic, neutral and zwitterionic compounds. Various classes of excipients were investigated, namely i) detergents of different charge states (sodium dodecyl sulfate [SDS], CTAB [cetyltrimethylammonium bromide], Polyoxyethylene lauryl ether [Brij 35], Na· 3-[(3-Cholamidopropyl) dimethylammonio]-1-propanesulfonate **[**CHAPS], taurocholic acid) ii) organic solvents (DMSO, 2-propanol, acetonitrile) and iii) 2,6-di-O-methyl-β-cyclodextrin. We could demonstrate that micellar concentrations of SDS most effectively reversed the adsorption of drugs, more precisely the adsorption of cationic drugs. This indicates that not only solubilization but also charge effects play a major role for drug recovery. Our data suggests that electrostatic repulsion between SDS enriched at the Teflon surface and SDS incorporated in the drug-loaded micelles (net

negatively charged) facilitates desorption. However, since SDS and all other excipients except 2-propanol disturbed the concentration analysis in ESI/MS, we recommend using SDS for data analysis with UV and 2-propanol whenever MS compatibility is required. Except for doxorubicin, 2-propanol could completely recover all compounds and therefore we consider the solvent a good compromise between efficiency and compatibility with mass spectrometry. Accordingly, 2-propanol was used in pursuit of our goal to improve the accuracy of the CAMDIS - $\log D_{oct}$ values which were affected by drug precipitation and/or adsorption to the well plate (*manuscript 2*). At the example of paclitaxel we demonstrated that the corrected CAMDIS - $\log D_{oct}$ value was indeed in better agreement with the gold standard value obtained from a traditional shake flask experiment (1L glass flask). The remaining slight discrepancy may be explained by the presence of drug aggregates in CAMDIS and the supposedly different distribution coefficient as compared to the drug monomer. The example shows that 2-propanol may be used for recovering a drug and correcting the mass balance equation, however, it cannot correct for changes in the distribution behavior of a compound due to formation of aggregates.

With the optimized experimental conditions and the knowledge gained from the adsorption studies, we validated CAMDIS on an extended 52 compound dataset with known shake flask $\log D_{oct}$ values (*manuscript 1*). Excellent agreement of the CAMDIS- $\log D_{oct}$ values with the shake flask data (gold standard) was obtained ($r^2 = 0.996$, standard error of estimate, SEE = 0.111), and therefore we propose CAMDIS as a high throughput alternative to the traditional shake flask technique. This enabled the rapid and accurate characterization of a larger set of compounds and in turn a higher level of statistical certainty with respect to the prediction of NSB (see below).

5.2 PAMPA - Optimization towards MS Compatibility, Study on the PAMPA Membrane Structure

Related Manuscripts:

Manuscript 4	Evaluation and Management of Excipient-Related Matrix Effects in HPLC-ESI/MS Analysis of PAMPA-Permeability
Manuscript 5	^{31}P and ^{1}H-NMR Studies on the Molecular Organization of Lipids in the PAMPA Permeation Barrier

PAMPA is a well - established primary screen for passive permeability [9], however, the permeation barrier has only been used as a means to regulate permeability[7] [10]. As an original contribution, we studied whether the fraction of drug retained in the PAMPA membrane can be used for estimating the non-specific binding of drugs in brain. We started our study with the experimental conditions applied in Roche (pH 6.5; membrane: 10% egg lecithin in dodecane) and optimized them in the course of this thesis. The optimization concerned two aspects, namely i) the use of HPLC-ESI/MS as a more sensitive and specific detection method as compared to UV and ii) the search for a chemical composition (membrane, donor, acceptor) that is better predictive for brain tissue binding.

With respect to the first aspect, we investigated whether the excipients used in PAMPA cause matrix effects in ESI/MS, and if so, how it is feasible to avoid or correct associated artifacts. We focused on glycocholic acid (GCA) because it is used as a solubilizer in the Roche PAMPA setup and is as such of direct interest for our research project. Since matrix-related excipients effects are a matter of general concern, we also studied excipients which have been applied in PAMPA as model formulation agents, namely hydroxypropyl-β-cyclodextrin (HP - β - CD), propylene glycol (PG) and N-methyl-2-pyrrolidone (NMP) [11]. Finally, the simulated gastrointestinal fluid in the fasted state (FaSSIF) and in the fed state (FeSSIF), respectively, were included in our study due to their relevance for predicting food-induced changes in permeability and solubility [12]. As revealed by surface activity measurements,

[7] An exception is the method proposed by Faller et al. for deriving octanol/water partition coefficients from apparent permeability values. However, the Faller approach suffers from reduced accuracy in the $\log P_{oct}$ range 0 - 2, requires knowledge of the pK_a and is an indirect method. Moreover, the authors have applied octanol as the permeation barrier rather than a mixture of phospholipids in an organic solvent.

matrix effects were most pronounced for excipients favoring the air-water interface (GCA, the FaSSIF/FeSSIF media), and/or forming multiply-charged ions (HP - β - CD). PG caused the least matrix effects which moreover only became evident for hydrophilic compounds coeluting with PG close to the solvent front. The non-uniform presence of ion-suppressing excipients in the PAMPA sandwich resulted in erroneous concentration measurements and accordingly in invalid estimates of permeability and membrane retention. To obtain accurate results, the excipient concentrations in the donor and acceptor compartment should be adjusted to the same level prior to injecting aliquots of each compartment into the HPLC-MS system. If the purpose of the excipient was only to increase a compound's solubility, replacement of the frequently used GCA by PG is suggested. Provided that the sensitivity of the mass spectrometer is sufficiently high for detecting sparingly soluble analytes, it is also feasible to perform PAMPA measurements without the aid of a solubilizer. As will be outlined below, the presence of GCA resulted in very poor NSB predictions and highly variable data than in its absence, and therefore we abstained from applying solubilizers. The second aspect, the optimization of the chemical composition towards better capability to predict tissue binding, will be summarized in chapter 5.3 in the framework of a comparative evaluation of all assays. At this point we would like to remind that each model including PAMPA can never be more than an approximation to the reality (i.e. non-specific tissue binding in living animals and humans). In order to assess the scope and the limitations of model it is of utmost importance to understand its structure and the properties associated with it. At the beginning of this thesis, the PAMPA membrane was a black box and all previous attempts to shed light in it, e.g. by means of fluorescence anisotropy measurements, had failed [13]. As a novel approach to resolving the question, we applied different nuclear magnetic resonance (NMR) techniques which are well established in classical membrane science [14]. In contrast to the nature of a classical membrane (phospholipid-water dispersion), the PAMPA barrier is formed from a phospholipid - dodecane mixture[8] which is immobilized on a filter that is dipped into an aqueous phase. By means of ^{31}P-NMR, we could demonstrate that the lipids in the PAMPA barrier are organized in an 'isotropic' phase contradicting speculations as to the presence of micro-bilayers and hexagonal phases. Pulsed field gradient NMR (PFGNMR) [15] experiments further revealed that the 'isotropic' motion corresponds to the diffusion of small aggregates which have a diameter in the order of d = 4 - 7 nm. In addition to the NMR studies, the distribution coefficients of diverse drugs

[8] Roche setup: 9% egg lecithin (m/v) and 0.45 % cholesterol (m/v) dissolved in dodecane

between the PAMPA-lipid solution and buffer, $\log D_{PAMPA}$ (pH7.4), were measured in order to link the structure of the PAMPA barrier with its function. The binding of cationic amphiphilic drugs to the PAMPA barrier strongly increased with a rise from 0 to 1% egg lecithin in dodecane indicating a change in the binding mechanism. The results from both series of experiments could most likely be explained by the presence of reverse micelles which act as a carrier rather than as a barrier particularly for cationic amphiphilic compounds. This distinguishes PAMPA from biological membranes. The size cutoff, arising from attenuated insertion into densely packed biological membranes [16], was not observed in PAMPA and therefore we recommend considering effective PAMPA permeability values for bulky compounds as possibly too optimistic.

5.3 LIMBA - Development of a Novel Assay for the Measurement of Brain Tissue/Water Distribution Coefficients, Comparative Evaluation of CAMDIS, PAMPA and LIMBA

Related Manuscripts:

Manuscript 6	Evaluation of a Novel Lipid Membrane Binding Assay (LIMBA) for the Assessment of Brain Tissue Binding

5.3.1 Development and Validation of LIMBA

So far, we have summarized the optimization of miniaturized *in vitro* assays which rely on artificial membrane-mimicking models (i.e. octanol and the PAMPA membrane) and whose ability to predict brain tissue binding was supposed to be tested (see below). We are aware of the fact that membrane models are always oversimplifications of the *in vivo* situation (see above) and it goes without saying that making brain tissue itself the test system of interest is the closest approximation thereof. Accordingly, the unbound fraction of drug in brain homogenate ($f_{u,brain}$) measured by equilibrium dialysis is considered a reliable surrogate for brain tissue binding [17]. However, the high consumption of animal tissue hampers the throughput of the assay and limits its application for routine screening purposes. We therefore developed a novel assay (LIMBA = Lipid Membrane Binding Assay) in which the advantage

of the equilibrium dialysis technique, i.e. the close resemblance to the *in vivo* situation, is combined with the high throughput and low reagent consumption of CAMDIS. The conceptual idea of LIMBA is borrowed from CAMDIS and involves the measurement of drug distribution in a 2-phase system (tissue surrogate and water) and the use of a filter to facilitate the phase separation. The two systems differ in the nature of the tissue surrogate, namely octanol in CAMDIS and brain homogenized in dodecane in LIMBA. Homogenization of the tissue was mandatory since automation requires the supply of brain tissue in the form of an easily dispensable liquid. Although it would be clearly preferable to use aqueous buffer as dispersing agent (like in equilibrium dialysis), a long chain organic solvent (dodecane) was necessary to avoid mutual mixing of the two phases. The miniaturized format of LIMBA allows working with minute amounts of brain tissue which is particularly suitable for the characterization of compounds with extensive tissue binding. Notably these are the compounds which should be identified prior to radioactive labeling since they are unlikely to be successfully applied in PET.

At the example of 126 structurally diverse drugs, we could demonstrate that the brain tissue/water distribution coefficients ($\log D_{brain}$) available through LIMBA are in good agreement with $f_{u,brain}$ values available through equilibrium dialysis. Exceptions are anionic and zwitterionic compounds for which the extent of tissue binding was underestimated by LIMBA, possibly due to electrostatic repulsion at the negatively polarized filter support. However, cationic and non-ionic compound predominate in most drug discovery programs including the development of PET tracers. The good agreement between $\log D_{brain}$ (LIMBA) and $f_{u,brain}$ for this majority of compounds demonstrates that preparing tissue homogenate in dodecane (instead of aqueous buffer) does not change the ranking between the two tissue binding scales, with respect to the chemical space investigated. In this regard, it is important to note that large and hydrophobic drugs for which non-specific binding to Teflon has been predicted as > 5% (*manuscript 2*) was excluded from the dataset to avoid artifacts (drug recovery by addition of 2 - propanol was not established yet at the time of the assay development). We could show by means of ^{31}P-NMR that dodecane disrupts the phospholipid bilayer of undisrupted brain tissue in favor of an isotropic phase (not further specified). A deviation from the good agreement between LIMBA and the equilibrium dialysis technique for larger compounds is thus expected since it is well known that the insertion into densely packed bilayers requires more energy than the insertion into a more unordered structure. Nevertheless, good agreement between LIMBA and the equilibrium dialysis method was

obtained ($r^2 = 0.74$ (n = 73 drugs of the 126 compound dataset, for exclusion criteria see *manuscript 6*), $r^2 = 0.91$ for a high quality dataset).

It is important to note that the experience gained from CAMDIS in terms of management of adsorption - related artifacts was applied in LIMBA in order to aid the selection of optimized experimental conditions and the interpretation of outliers (compounds for which adsorption - related artifacts and drug precipitation are likely or have been observed were excluded from the validation dataset.).

5.3.2 Comparative Evaluation of CAMDIS, PAMPA and LIMBA

So far, we have summarized i) the development of CAMDIS, ii) the optimization of PAMPA with respect to the compatibility with mass spectrometry and iii) the development and validation of LIMBA. We have analyzed and eliminated potential artifacts and indicated for which compounds the assays are applicable. These investigations are the necessary precondition for answering the key question as to which assay should be used for predicting the NSB of potential PET tracers in brain. For obvious ethical reason it would be preferable to rely on artificial surrogate systems, i.e. either octanol (CAMDIS) or phospholipids dissolved in dodecane (PAMPA). But we also raised the question whether the predictive power of LIMBA is considerably better as compared to CAMDIS and PAMPA - which may justify the use of minute amounts of animal tissue.

For validation purposes, we compared the $\log D_{oct}$, $\log D_{PAMPA}$ and $\log D_{brain}$ values obtained from CAMDIS, PAMPA and LIMBA, respectively with the $f_{u,brain}$ values (= industrial gold standard) available through equilibrium dialysis.

The poor correlation between $\log D_{oct}$ (pH 7.4) and $f_{u,brain}$ confirms what has been observed before by other authors on much smaller datasets, the weakness of $\log D_{oct}$ for predicting tissue binding [6]. Nevertheless, it is interesting to note that the measured octanol/water partition coefficient of the unionized drug ($\log P$ [9]) was in much better agreement with the $f_{u,brain}$ data as compared to $\log D_{oct}$. This has also been recognized before but only on the basis of calculated $\log P$ values [7]. Using the fraction of drug retained in the PAMPA membrane (expressed as $\log D_{PAMPA}$), the prediction of $f_{u,brain}$ was better reliable as compared to CAMDIS (r^2(PAMPA) = 0.61 vs. r^2(CAMDIS) = 0.23), provided that the assay was

[9] Measured $\log P$ values were calculated from measured $\log D_{oct}$ (pH 7.4) values and the measured pK_a using the Henderson - Hasselbalch equation. The transformation is not applicable to zwitter-ionic compounds which were therefore excluded from the dataset.

conducted under optimized experimental conditions (brain polar lipids (BPL), pH 7.4, no solubilizers). In contrast, the PAMPA method as used in Roche was unsuitable to predict tissue binding ($r^2 = 0.38$). However, tissue binding as determined by means of equilibrium dialysis ($f_{u,brain}$) was best described by the brain tissue/water distribution coefficients ($\log D_{brain}$) available through LIMBA ($r^2 = 0.74$ (n=73, see above). Table 1 summarizes the comparative evaluation of the *in vitro* assays.

Table 1 Overview of assays investigated.

Assay	**Surrogate system for tissue binding**	**Predictive ability for NSB (n=73)**[b]	**Applicability range**	**Demand for brain tissue**	**Model system**
CAMDIS (novel assay)	Octanol	Poor (r^2=0.23, $\log D_{oct}$ (pH 7.4))	Non-ionic compounds	None	Reverse octanol micelles
PAMPA (optimized assay)	BPL-dodecane mixture, no excipients[a]	Good (r^2=0.61)	Non-ionic and cationic compounds	None	Reverse phospholipid micelles
LIMBA (novel assay)	Brain homogenized in dodecane	Very good (r^2=0.74)	Non-ionic and cationic compounds	Low	Bilayer and isotropic phase
Equilibrium dialysis (established)	Brain homogenized in buffer	Gold standard	All charge classes	High	Bilayer

[a]The standard Roche PAMPA setup (egg lecithin in dodecane, presence of glycocholic acid in the donor, pH 6.5) was inappropriate (correlation statistics with the dialysate method: r^2=0.375). [b]statistics for all charge classes and based on the subset of compounds which could be measured with LIMBA.

5.4 NSB in Autoradiography and in PET

Related Manuscripts:

Manuscript 7	Label-Free Assay for the Assessment of Non-specific Binding of Positron Emission Tomography Tracer Candidates

5.4.1 NSB Asessment with LIMBA

Hitherto, the predictive power of CAMDIS, PAMPA and LIMBA has been tested by comparison with the equilibrium dialysis method. The strategy has been pursued because a high number of compounds had been characterized with the dialysis method and the interpretation of the data was not complicated by active transport mechanisms (the goal was to develop an assay for the assessment of passive tissue binding). This enabled an unambiguous comparison of the assays and a high statistical certainty level (n=126 compounds). However, the brain homogenate used in equilibrium dialysis is also just an *in vitro* surrogate for intact brain tissue which could differ by e.g. the packing density of the lipids.

Therefore, our next objective was to test whether the assay which was in best agreement with equilibrium dialysis, namely LIMBA, is also predictive for the binding of drugs and PET tracers to undisrupted brain tissue. To this purpose, $\log D_{brain}$ values available through LIMBA were compared with i) NSB quantified with *in vitro* autoradiography (30 marketed and proprietary compounds, in-house data) and ii) estimates of the volume of distribution of non-specifically bound drug characterized with PET (10 marketed tracers, *in vivo* literature data). Moreover, we compared the predictive power of $\log D_{brain}$ (LIMBA) with that of the traditional lipophilicity parameter, i.e. $\log D_{oct}$. The *in vitro* autoradiography data was used for validation purposes since a larger number of compounds was available than from PET (literature data) - which we considered beneficial for the explanatory power of a prediction model. Moreover, it was advantageous that *in vitro* autoradiographs are not confounded by active transport mechanisms at the blood brain barrier since brain slices rather than intact brain imbedded in adjacent compartments were used. In contrast, the volume of distribution obtained from *in vivo* PET is a more complex parameter and e.g. efflux transport at the BBB may complicate the unambiguous data interpretation. Our data showed that the brain

tissue/water distribution coefficients ($\log D_{brain}$) available through LIMBA are more predictive for NSB (*in vitro* autoradiography data) than $\log D_{oct}$ (r^2 (LIMBA) = 0.87 - 0.91 depending on the assay protocol, see below). The analysis further showed that the time brain slices were exposed to a washing solution after incubation with tracer matters for the determination of NSB. A clear trend towards lower binding at longer washing times was observed. Therefore correlations between *in vitro* assays (LIMBA,CAMDIS) and NSB have to be performed on the basis of the same assay protocol and washing procedure in autoradiography. Regarding the *in vivo* PET data, LIMBA was suitable to predict the NSB for tracers which are considered non-Pgp substrates.

5.4.2 Identification of PET Tracer Candidates with a High Probability of Attrition

So far, we have shown that the extent of NSB of potential PET tracers can be predicted with LIMBA, which works with the unlabeled compound and which requires considerably reduced animal testing as compared to other assays (equilibrium dialysis, autoradiography). However, NSB in the reference region should not be contemplated in isolation from total binding (TB) in the region of interest. The ratio between both (i.e. TB/NSB) determines the image quality and therefore the likely development success or failure of a potential PET tracer (see introduction). It was stressed that PET tracer candidates with low TB/NSB ratios are unlikely to be successful [3].

We could show that a plot of TB/NSB vs. NSB can be used as classification map for the identification of inappropriate PET tracer candidates: None of the compound tested with NSB > 3 fmol/mg protein reached a TB/NSB ratio > 5. The key question was whether the compounds with inappropriately high NSB can also be identified by using the $\log D_{brain}$ value available through LIMBA. Provided that the brain slices in autoradiography were exposed for maximal 4 min to the washing solutions, LIMBA was indeed suitable to identify the problematic compounds. This means that compounds with undesirably high NSB and a low probability of a sufficient TB/NSB ratio can be identified without the need for autoradiography and prior to radioactive labelling.

5.5 Conclusions

In conclusion, we have shown that the NSB of potential PET tracers in brain can be estimated with a novel miniaturized *in vitro* assay, LIMBA, which requires only minute amounts of brain homogenate prepared in dodecane (1.2 µL). Neither octanol nor the phospholipid-dodecane mixture used in PAMPA could mimic the binding of drugs to brain tissue with the same accuracy. In comparison to the equilibrium dialysis technique, the consumption of animal tissue could be considerably reduced and therefore we recommend favouring LIMBA when brain tissue binding data is requested. Since LIMBA works with unlabelled compounds, PET tracers with inappropriately high NSB can be identified prior to resource - intensive autoradiography studies. We have developed LIMBA as a semi-automated screening assay which requires similar efforts in terms of time and technical facilities as compared to other physicochemical screening assays. The implementation of LIMBA in the existent platforms for eADME screening experiments is therefore viable without much additional expenditures. LIMBA may accelerate the selection of PET tracers with appropriate NSB characteristics and the rejection of compounds with undesirable high background noise (= NSB). This may enhance the confidence in the likely development success of a PET tracer and reduce the attrition rate in the late and more costly stages. The availability of innovative PET tracers for studying the functioning of brain may ultimately advance the expansion of PET for the drug discovery process in pursuit of a higher efficiency and lower attrition rate.

5.6 Limitations and Outlook into Future Research

In the course of this thesis, the ability of LIMBA to estimate the NSB of drugs and PET tracers in tissue has been demonstrated at the example of brain tissue, however, it would also be of great value to test the applicability of LIMBA to other tissues. The sum of all tissue/water distribution coefficients could be utilized to calculate a drug's volume of distribution, one of the key pharmacokinetic parameters required for rational dosing selection [18]. Moreover, tissue/water distribution coefficients available through LIMBA could be used to parameterize physiologically-based pharmacokinetic (PBPK) models which are frequently applied to predict a test compound's pharmacokinetic profile in different animal species [19]. Until now, drug tissue distribution is predicted by mechanistic equations integrating compound lipophilicity (octanol/water or oil/water distribution coefficients), the binding of compound to proteins and phospholipids and the levels of protein, lipids and water in plasma and tissue [20]. As will be demonstrated in an additional manuscript (unpublished results, the

work is not included in the thesis), LIMBA yields more reliable estimates for brain tissue binding as compared to the mechanisms-based model implemented in Gastroplus®[10]. The inferior predictive power may be attributed to the fact that the models rely on the assumption that the properties of phospholipids can be resembled by a mixture water and octanol, which is a severe oversimplification of the reality.

Even though LIMBA enables the assessment of NSB at considerably reduced amounts of brain tissue, artificial membrane mimicking systems would still be preferable. Hitherto we have only compared egg lecithin and porcine lipids, but it would also be interesting to perform a design of experiments with phospholipid mixtures of different charge state and chain length, to simulate the lipid composition of human brain and other tissues. Rather than relying on the PAMPA setup, we recommend using the assay construct of CAMDIS and LIMBA since the latter is specifically designed to measure distribution coefficients. It should be mentioned that measuring permeability and membrane retention at the same time is an advantage of PAMPA but also complicates the analysis of the data: We could demonstrate that PAMPA lipid/water distribution coefficients are concentration dependent owing to charge repulsion and probably saturation at the interfaces. The presence of two liquid-water interfaces in PAMPA enhances the concentration dependency and the difficulty to correct the effect by the choice of appropriate experimental conditions. The determination of membrane binding constants would then require concentration dependent measurements and an interpretation of the obtained binding isotherms by means of the Gouy-Chapman theory [21].

Finally, we would like to stress that NSB should not be considered as an isolated parameter. Other factors such as permeability across the blood brain barrier, receptor density and target affinity are equally important for the success of an imaging agent [22]. Recently, a bio-mathematical modelling approach has been successfully applied to predict a PET tracer's image quality by integrating the properties of both the drug and of the biological system into a prediction model [23]. An important input parameter was the unbound fraction of tracer in brain which had been measured with the equilibrium dialysis technique but which could be assessed by using LIMBA with less brain tissue.

[10] Test date: June 2012. The Rodgers model was tested at the example of the 126-compound used also for the validation of LIMBA. The $f_{u,brain}$ values obtained from equilibrium dialysis were considered the gold standard. Model input parameters: measured $\log D_{oct}$ values.

References

1. Fernandes, E., et al., *Positron emitting tracers in pre-clinical drug development.* Curr. Radiopharm., 2012. **5**(2): p. 90-98.
2. Schwaiger, M. and H.-J. Wester, *How many PET tracers do we need?* J. Nucl. Med., 2011. **52**(Suppl. 2): p. 36S-41S.
3. Laruelle, M., M. Slifstein, and Y. Huang, *Relationships between radiotracer properties and image quality in molecular imaging of the brain with positron emission tomography.* Mol Imaging Biol 2003. **5**(6): p. 363-75.
4. Kansy, M., F. Senner, and K. Gubernator, *Physicochemical High Throughput Screening: Parallel Artificial Membrane Permeation Assay in the Description of Passive Absorption Processes.* J. Med. Chem., 1998. **41**(7): p. 1007-1010.
5. Poole, S.K. and C.F. Poole, *Separation methods for estimating octanol-water partition coefficients.* J. Chromatogr., B: Anal. Technol. Biomed. Life Sci. , 2003. **797**(1-2): p. 3-19.
6. Jiang, Z., et al., *A rapid vesicle electrokinetic chromatography method for the in vitro prediction of non-specific binding for potential PET ligands.* J. Pharm. Biomed. Anal., 2011. **54**(4): p. 722-729.
7. Wan, H., et al., *High-throughput screening of drug-brain tissue binding and in silico prediction for assessment of central nervous system drug delivery.* J. Med. Chem., 2007. **50**(19): p. 4606-4615.
8. Taylor, P.J., *Matrix effects: the Achilles heel of quantitative high-performance liquid chromatography-electrospray-tandem mass spectrometry.* Clin. Biochem., 2005. **38**(4): p. 328-334.
9. Avdeef, A., *The rise of PAMPA.* Expert Opin. Drug Metab. Toxicol., 2005. **1**(2): p. 325-342.
10. Wohnsland, F. and B. Faller, *High-Throughput Permeability pH Profile and High-Throughput Alkane/Water log P with Artificial Membranes.* J. Med. Chem., 2001. **44**(6): p. 923-930.
11. Bendels, S., et al., *PAMPA-Excipient Classification Gradient Map.* Pharm. Res., 2006. **23**(11): p. 2525-2535.
12. Kostewicz, E.S., et al., *Forecasting the oral absorption behavior of poorly soluble weak bases using solubility and dissolution studies in biorelevant media.* Pharm. Res., 2002. **19**(3): p. 345-349.
13. Seo, P.R., et al., *Lipid composition effect on permeability across PAMPA.* Eur. J. Pharm. Sci., 2006. **29**(3-4): p. 259-268.
14. Seelig, J., *Lipid polymorphism, reverse micelles, and phosphorus-31 nuclear magnetic resonance.* Reverse Micelles, [Proc. Eur. Sci. Found. Workshop], 4th, 1984: p. 209-20.
15. Morris, K.F. and C.S. Johnson, Jr., *Resolution of discrete and continuous molecular size distributions by means of diffusion-ordered 2D NMR spectroscopy.* J. Am. Chem. Soc. , 1993. **115**(10): p. 4291-9.
16. Seelig, A., *The role of size and charge for blood-brain barrier permeation of drugs and fatty acids.* J. Mol. Neurosci., 2007. **33**(1): p. 32-41.
17. Kalvass, J.C. and T.S. Maurer, *Influence of nonspecific brain and plasma binding on CNS exposure: implications for rational drug discovery.* Biopharm. Drug Dispos., 2002. **23**(8): p. 327-338.
18. Poulin, P. and F.-P. Theil, *Prediction of pharmacokinetics prior to in vivo studies.: II. Generic physiologically based pharmacokinetic models of drug disposition.* J. Pharm. Sci. , 2002. **91**(5): p. 1358-1370.

19. Lave, T., et al., *Challenges and opportunities with modelling and simulation in drug discovery and drug development.* Xenobiotica, 2007. **37**(10/11): p. 1295-1310.
20. Rodgers, T., D. Leahy, and M. Rowland, *Tissue distribution of basic drugs: Accounting for enantiomeric, compound and regional differences amongst β-blocking drugs in rat.* J. Pharm. Sci., 2005. **94**(6): p. 1237-1248.
21. Beck, A., et al., *On the Interaction of Ionic Detergents with Lipid Membranes. Thermodynamic Comparison of n-Alkyl-+N(CH3)3 and n-Alkyl-SO4.* J. Phys. Chem. B, 2010. **114**(48): p. 15862-15871.
22. Ametamey, S.M. and P.A. Schubiger, *PET radiopharmaceuticals for neuroreceptor imaging.* Nucl. Sci. Tech., 2006. **17**(3): p. 143-147.
23. Guo, Q., M. Brady, and R.N. Gunn, *A biomathematical modeling approach to central nervous system radioligand discovery and development.* J. Nucl. Med., 2009. **50**(10): p. 1715-1723.

6 Acknowledgements

This work was carried out in the physicochemical screening group of the Nonclinical Safety Department at F. Hoffmann-La Roche Ltd. Basel, Switzerland and in the laboratories of Prof. Dr. Anna Seelig and Prof. Dr. Joachim Seelig in the Department of Biophysical Chemistry at the Biozentrum of the University of Basel, Switzerland.

I would like to express my thanks to my supervisors Prof. Anna Seelig (Biozentrum) and Dr. Holger Fischer (Roche) who showed me manifold insights into the worlds of academic and industrial research. They were always encouraging, sometimes demanding, and they did never forget about the human behind the Ph.D. student. I am thankful for their willingness to pass their tremendous expert knowledge about biophysical chemistry without being patronizing.

I wish to thank Dr. Manfred Kansy who was always supportive and for sure without his encouragement I would have never had the possibility for such an interesting Ph.D. thesis. Particularly, I would like to thank him for leaving oneself the freedom in shaping the project.

I would also wish to thank Prof. J. Seelig for a lot of valuable suggestions and the impression that research is fun when an impressive body of scientific knowledge and analytical skills is combined with a bit of irony.

I would also like to acknowledge the work of Prof. Beat Ernst as a referee and thank him for reading and evaluating this thesis.

Thanks a lot to my collegues of the former structure-property/effect relationship group for their friendly welcome and their open attitude. Thanks Björn Wagner, Stefanie Bendels, Alexander Hillebrecht, Viriginie Micallef, Isabelle Parrilla, Severin Wendelspiess, Gergori Gerebtzoff, Wolfgang Muster and Allessandro Brigo ! My special gratitude goes to Björn Wagner for technical, scientific and last but not least moral support whenever there was demand. For the same reasons and for the steady support with self-made cakes I would like to thank Stefanie Bendels. And thanks for rescuing me from the coffee machine and the printer

in the hallway! Alex, I thank you for becoming a friend in between burgers, discussions and computational advice.

I am gratefully indepted to Dr. Alfred Ross for helping me with the self-diffusion NMR studies and Dr. Andreas Stämpfli for giving me advice in the field of mass spectrometry.

Many thanks also to Marta Hidalgo for the funny moments in lab and a million thanks to James Zimmerman for help with formatting the manuscript in the very last minute.

I really enjoyed also the nice, friendly, uncompetitive atmosphere of the research groups of Prof. A. and J. Seelig. Many thanks to all of you Caro, Cinzia, Christine, Estefania, Gabi, Susanna, Therese, Xiachum, Andre, Christian, Fabian, Matthias and Reto.

Finally I would like to thank my family and friends for reminding me of what life is about apart from science.

7 Curriculum Vitae

Personal Data

Name	Frauke Assmus
Date of birth	28/12/1982
Nationality	German
Profession	Pharmacist

University Education and Training

04/2009 - 03/2013	Preparation of PhD thesis in the former Structure/Property Effect Relationships group, Non-Clinical Safety *F. Hoffmann-La Roche Ltd., Basel, Switzerland* Research topic: Development and comparative evaluation of *in vitro* and *in silico* membrane binding models for the prediction of nonspecific binding of potential PET tracers Cooperation with the biophysical institute, doctoral adviser Prof. A. Seelig *Biozentrum, University of Basel, Switzerland*
02/2008	Licensure as pharmacist
05/2007 - 10/2007	Pre-reg pharmacist *Schlehen Pharmacy, Leipzig, Germany*
10/2006 - 04/2007	Industrial internship in the QSAR group, *F. Hoffmann-La Roche Ltd., Basel, Switzerland* Research topic: Assay for determining the binding constant of high affinity compounds to proteins (patented)
02/2002 and 07/2003	Medical clerkship *Antoinetten Pharmacy, Dessau, Germany*
10/2002 - 09/2006	Undergraduate studies in pharmacy *University of Leipzig, Germany* Grade 2nd state examination: 1.4

1993 - 2002	Abitur (university entrance examination) *Fürst-Franz Gymnasium, Dessau, Germany* Grade: 1.1

Professional experience

04/2010 - 07/2010	Temporary employee for routine passive permeability screening (PAMPA) *F. Hoffmann-La Roche Ltd., Basel, Switzerland*
03/2008 - 04/2009	Research assistent at the institute of pharmacy, biopharmacy department *University of Halle/Saale, Germany*

Skills

Strong background in analytical chemistry, biophysical chemistry and pharmacy

Laboratory expertise	HPLC-ESI/MS, capillary electrophoresis, physicochemical profiling, assay development and automation, NMR
Data mining	(Q)SAR, multivariate data analysis, design of experiments
Computational skills	MS-Office, Origin, SIMCA, MODDE
Language	German (native), English (fluent), French (basic), Spanish (basic), Latin (basic)